



University
of Glasgow

Gheorghiu, Delia Mihaela (2012) *Testing climate synchronicity between Scotland and Romania since the last glacial maximum*. PhD thesis.

<http://theses.gla.ac.uk/3362/>

Copyright and moral rights for this thesis are retained by the author

A copy can be downloaded for personal non-commercial research or study, without prior permission or charge

This thesis cannot be reproduced or quoted extensively from without first obtaining permission in writing from the Author

The content must not be changed in any way or sold commercially in any format or medium without the formal permission of the Author

When referring to this work, full bibliographic details including the author, title, awarding institution and date of the thesis must be given

Testing climate synchronicity between Scotland and Romania since the Last Glacial Maximum

Delia Mihaela Gheorghiu

Thesis submitted for the degree of Doctor of Philosophy (Ph.D.)

University of Glasgow

School of Geographical & Earth Sciences

2012

To my parents

Abstract

This thesis develops a chronology of ice retreat in the Monadhliath Mountains (Scotland) and Rodna Mountains (Romania) during the late Pleistocene using glacial geomorphology and surface exposure dating with cosmogenic ^{10}Be .

In the Monadhliath Mountains, ^{10}Be exposure ages indicate deglaciation of the Last Devensian ice sheet at 15.1 ka ($n = 2$). Boulders from moraines in three Monadhliath cirques yielded exposure ages between 11.8 ka and 9.8 ka (470 – 600 m), suggesting that a Late Glacial readvance occurred during the Younger Dryas stadial ($n = 9$). The limited extent of these YD glaciers in the Monadhliath Mountains is explained in terms of the drier climate experienced by the eastern part of the Central Highland ice cap, but also in terms of local factors such as topography and snow blow. The resulting glacial reconstruction largely confirms that a SW to NE precipitation gradient dominated Scotland during the Younger Dryas.

In the Romanian Carpathians, located at the southern periphery of the NW European ice sheet, there was only limited coverage of ice, mostly at higher elevations in the form of mountain glaciers. Field evidence suggests that during the last local maximum glaciation ice reached lower elevations than previously suggested in the Rodna Mountains. Glacially transported boulders were abandoned at 37.2 – 26.6 ka ($n = 4$) at an elevation of ~900 m. Glacial erratics and bedrock samples ($n = 27$) provide a consistent chronology for deglaciation during the Lateglacial, suggesting that ice retreated towards higher ground between 18.3 – 13.2 ka (1100 – 1800 m altitude). Final deglaciation took place at 12.5 – 11.2 ka ($n = 9$).

These new chronologies are compared to other climate archives in Europe and the climatic oscillations recorded in the North Atlantic region. This analysis increases our understanding of past atmospheric circulation across Europe, and gives insights into the climatic forcing mechanisms during the last maximum extent of ice sheets and glaciers. During the last glacial episodes, the pattern of climate cooling from the western high latitudes towards the eastern mid latitudes was complicated, triggering different responses in local climates that appear to have been out of phase with the broader north-western European trend. Located in the NW Europe, Scotland was influenced by the wetter and colder conditions from the Atlantic which led to the expansion of the British Ice sheet during the global Last Glacial Maximum (LGM). However, smaller ice masses located

further southwards and south-eastwards of the European ice sheet responded faster to the climatic oscillations in the North Atlantic region. During the LGM, the southward repositioning of the Polar Front and the presence of the ice sheet changed the atmospheric circulation across Europe. There was limited supply of moisture to the Rodna Mountains, especially because of blocking by the eastern Siberian high pressure system, and the glaciers experienced a slow retreat in a very cold and dry environment. However, a more synchronous Younger Dryas is likely to have occurred due to a more northern position of the Polar Front. This allowed for stronger wet and cold westerly winds to reach most of Europe at the same time.

Table of contents

Abstract.....	i
Table of contents.....	iii
List of figures.....	vi
List of tables.....	vii
Acknowledgements.....	viii
Declaration.....	x
Abbreviations.....	xi
Chapter 1. Introduction and aims.....	1
1.1 Rationale	2
1.2 Objectives of the thesis	3
1.3 Outline of the thesis	4
Chapter 2. Geographical & climatological context.....	5
2.1 Geographical context	6
2.1.1 Scotland.....	6
2.1.2 Romania	8
2.2 Climatological context	10
2.2.1 Last glaciation in Europe	10
2.2.2 Last glacial maximum (LGM)	12
2.2.2.1 Last maximum glaciation in Scotland.....	16
2.2.2.2 Last maximum glaciation in Romania	19
2.2.3 Younger Dryas (YD).....	20
2.2.3.1 Younger Dryas in Scotland	22
2.2.3.2 Younger Dryas in Romania.....	24
2.3 Outline of missing information.....	25
Chapter 3. Methods	26
3.1 Introduction	27
3.2 Remote sensing	27
3.3 Field mapping	28
3.4 Surface exposure dating	29
3.4.1 Cosmic radiation	29
3.4.1.1 Primary cosmic rays.....	30
3.4.1.2 Secondary cosmic rays.....	30
3.4.2 Scaling factors and production rates	33
3.4.2.1 Scaling factors.....	33
3.4.2.2 Shielding factors.....	34
3.4.2.3 Production rates.....	36
3.4.3 <i>In situ</i> cosmogenic ¹⁰ Be production	40
3.4.4 Sampling considerations and limitations	40
3.4.5 Exposure ages.....	41
3.5 ELA reconstruction for the palaeoglaciers.....	44
Chapter 4. Scotland	46
4.1 Introduction	47
4.2 Monadhliath Mountains	48
4.2.1 Geographical position	48
4.2.2 Climate	48
4.2.3 Geology	49

4.2.4	Earlier investigations in the Monadhliath Mountains	50
4.2.5	Study area	50
4.3	Geomorphology	52
4.4	Regional Glaciation.....	52
4.5	Valley glaciation	56
4.5.1	Glen Lochain.....	56
4.5.2	Glen Ballach.....	58
4.5.3	Glen Fionndrigh	60
4.5.4	Glen Chaorainn	62
4.6	Surface exposure ages	63
4.7	Discussion	66
4.7.1	The pattern of Late Devensian deglaciation in the SE Monadhliath Mountains.....	66
4.7.2	Younger Dryas	72
4.8	Younger Dryas ELA reconstruction and palaeoclimatic implications.....	75
4.9	A plateau ice field in the Monadhliath Mountains during the YD?.....	76
4.10	Conclusions	79
Chapter 5. Romania.....		81
5.1	Introduction	82
5.2	Rodna Mountains	83
5.2.1	Geographical position	83
5.2.2	Climate	83
5.2.3	Geological structure	84
5.2.4	Earlier investigations in the Rodna Mountains	85
5.3	Study area.....	87
5.4	Geomorphology of the study area	88
5.4.1	Zănoaga Mare cirque.....	90
5.4.2	Iezer cirque.....	92
5.4.3	Pietroasa and Șarampin valleys.....	96
5.4.4	Buhăiescu cirque complex	99
5.4.4.1	Tăuri cirque	99
5.4.4.2	Curmătura (- Buhăiescu) cirque	100
5.4.4.3	Rebra cirque	101
5.4.4.4	Buhăiescu Mare cirque.....	102
5.4.5	Buhăiescu Valley	104
5.4.5.1	Repede Valley	105
5.5	Surface exposure ages	106
5.5.3	Discussion	112
5.5.3.1	Pattern of deglaciation in the study area	112
5.5.3.2	Glacial and climatic implications in the study area	116
5.5.3.3	ELA reconstruction and palaeoclimatic implications	116
5.5.3.4	Comparison with the palaeoclimate records in the Romanian mountains.....	119
5.5.4	Conclusions	122
Chapter 6. Synthesis.....		123
6.1	Introduction	124
6.2	Ice sheets and climate in the North Atlantic	124
6.3	Timing and extent of Late Devensian glaciation in Europe.....	126
6.3.1	North-western Europe	126
6.3.2	South and south-eastern Europe.....	127
6.4	Palaeoclimatic implications	129

6.4.1	Glacial-climate relationships in the Scottish Highlands	129
6.4.2	Glacial-climate relationships in the Romanian Carpathians	130
6.5	Comparison in the context of global climate records.....	131
6.5.1	Middle Devensian (60-30 ka)	132
6.5.2	Global LGM (30-19 ka)	134
6.5.3	LGM deglaciation (21-15 ka)	139
6.5.4	Lateglacial (14.7-12.9 ka)	141
6.5.5	Younger Dryas (12.9-11.7 ka)	142
6.6	Equilibrium Line Altitudes (ELA).....	144
6.7	Summary	146
Chapter 7. Conclusions.....		148
7.1	Conclusions.....	149
7.2	Future considerations.....	151
Appendixes.....		153
Appendix A. Laboratory procedure.....		154
Appendix B. Sample details.....		178
Monadliath Mountains.....		179
Rodna Mountains.....		180
Appendix C. Maps.....		182
Monadliath Mountains.....		183
Rodna Mountains.....		185
References.....		187

List of figures

Figure 2.1. Digital elevation model of Scotland.....	7
Figure 2.2. Digital Elevation Model of Romania.....	9
Figure 2.3. The reconstructed limits of the Eurasian ice sheet at the Last Glacial Maximum	13
Figure 2.4. Digital elevation model of Europe.....	16
Figure 2.5. The reconstructed environment of the NW European ice sheet at 30–25 ka BP	18
Figure 2.6. Model of maximum ice extent in Scotland during the Younger Dryas episode	23
Figure 3.1. Cosmic ray cascade in the atmosphere and lithosphere.....	31
Figure 3.2. Diagram showing how to determine topographic shielding for a sampled surface	35
Figure 3.3. Exponential decrease of the ^{10}Be production rate.....	38
Figure 3.4. Concentration of <i>in situ</i> cosmogenic nuclides reaches secular equilibrium in case of constant production rates.....	39
Figure 4.1. Position of the Monadhliath Mountains in the Scottish Highlands.....	47
Figure 4.2. Monadhliath Mountains.....	48
Figure 4.3. Geological map of the study area in the Monadhliath Mountains.....	49
Figure 4.4. Digital elevation model of the study area in the south-eastern part of the Monadhliath Mountains.	51
Figure 4.5. Geomorphological map of the study area.....	53
Figure 4.6. Glacifluvial assemblages at the south end of Glen Chaorainn	54
Figure 4.7. Esker in the eastern part of Glen Banchor.....	54
Figure 4.8. South-western view of Glen Banchor.....	55
Figure 4.9. Glen Lochain, south view towards Glen Banchor.....	56
Figure 4.10. Glen Lochain and landform assemblages at Loch Dubh.....	57
Figure 4.11. Kettled blocky till on the plateau above Loch Dubh.....	58
Figure 4.12. Lake deposit complex in Glen Ballach.....	59
Figure 4.13. Moraine ridges in Glen Ballach.....	60
Figure 4.14. Outwash levels in Glen Fionndrigh.....	61
Figure 4.15. Hummocky deposits in upper Glen Fionndrigh.....	61
Figure 4.16. South view of Glen Chaorainn	62
Figure 4.17. The plateau edge above Glen Chaorainn.....	63
Figure 4.18. Till mounds on the interfluvium between Glen Ballach and Glen Fionndrigh....	66
Figure 4.19. Surface exposure ages plotted on the geomorphological map.....	68
Figure 4.20. Schematic representation of the glaciation pattern in the Monadhliath Mountains.....	71
Figure 4.21. Monadhliath Mountains. ^{10}Be exposure ages plotted against the GRIP ice core and other Scottish dates.....	74
Figure 5.1. Position of the Rodna Mountains in the Romanian Carpathians.....	82
Figure 5.2. Position of the field area in the NW part of Rodna Mountains	83
Figure 5.3. The geological map of the Rodna Mountains.....	85
Figure 5.4. Orthophotomap of the study area overlaid on a 3D surface.....	87
Figure 5.5. Geomorphological map of the study area.....	89
Figure 5.6. Zănoaga Mare cirque	90
Figure 5.7. The lower moraine and part of the upper moraine in Zănoaga Mare cirque	91
Figure 5.8. Iezer cirque	92
Figure 5.9. Roches moutonnées in the upper part of the Iezer cirque.....	93
Figure 5.10. Geomorphological map of the NW part of the study area.....	94
Figure 5.11. Glacially abraded surfaces.....	95

Figure 5.12. Glacially moulded bedrock above the lower step at Iezer cirque.....	95
Figure 5.13. Longitudinal profile of the cirques in the study area.....	96
Figure 5.14. Medial moraine between Pietroasa and Șarampin valleys	97
Figure 5.15. Lateral moraine on the western side of the Pietroasa valley.	97
Figure 5.16. Geomorphological map of the SE part of the study area.....	98
Figure 5.17. View of the Tăuri cirque from the east.....	99
Figure 5.18. Tăuri cirque with the Lakes Buhăiescu and moraine ridges.....	100
Figure 5.19. Curmătura & Rebra cirques of Buhăiescu glacial complex.....	101
Figure 5.20. Distal slope of the moraine in the Curmătura (- Buhăiescu) cirque	102
Figure 5.21. Buhăiescu glacial complex	103
Figure 5.22. Glacially striated surface at the lower end of the Buhăiescu Mare cirque	104
Figure 5.23. Glacial landforms on the Buhăiescu Valley	105
Figure 5.24. Surface exposure ages plotted on the geomorphological map.....	109
Figure 5.25. Surface exposure ages of the boulders and bedrock samples from the study area plotted on the 3D images of the orthophotomaps.....	114
Figure 5.26. The pattern of deglaciation in the NW part of the Rodna Mountains between 37-17 ka.....	117
Figure 5.27. Rodna Mountains. ¹⁰ Be exposure ages plotted against the GRIP ice core and other Romanian dates.....	121
Figure 6.1. Atmospheric circulation pattern during the Last Glacial Maximum in Europe.....	135
Figure 6.2. Distribution of loess deposits across Europe.....	138
Figure 6.3. Late Quaternary chronostratigraphy (Monadhliath & Rodna Mountains) and their correlation with Marine Isotope Stages and Greenland ice core data.....	140
Figure 6.4. Equilibrium Line Altitudes in Europe.....	143

List of tables

Table 2.1. Terminology used across the Northern Hemisphere.....	11
Table 3.1. Spallogenic production rates of ¹⁰ Be.....	38
Table 3.2. Target element and half-life of the commonly used cosmogenic nuclides in the geosciences.....	39
Table 4.1. Sample information and surface exposure ages in the Monadhliath Mountains.....	65
Table 4.2. Reconstructed equilibrium line altitudes (ELA) for the YD glaciers in the Monadhliath Mountains.....	76
Table 5.1. Sample characteristics, ¹⁰ Be concentrations and calculated surface exposures ages in the Rodna Mountains.....	110
Table 5.2. The equilibrium line altitudes (ELA) for the Last Glacial Maximum and YD glaciers in the Rodna Mountains.....	118

Acknowledgements

Firstly I would like to thank the institutions that made this research possible. This study was funded by a University of Glasgow Ph.D. studentship award, with additional financial support from the SUERC AMS consortium (East Kilbride) for sample measurement and from the School of Geographical & Earth Sciences to attend international conferences. Many thanks go to the Rodna Mountains National Park for enabling access to the study area. All of whom are gratefully acknowledged.

Clearly this work would not have been possible without the constant support and guidance of my supervisors: Dr. Derek Fabel and Dr. Jim Hansom.

I would like to express special thanks to Derek for his initial interest in this project and for making it possible. He always believed in me, he taught me the fundamentals of scientific work and treated me with great patience when things seemed difficult. I am grateful for all the lab and teaching opportunities, and also for conference support. Subsequently, it was his extra motivation and genuine enthusiasm that kept me going through all the highs and lows of my Ph.D. life. Thank you, Derek!

Sincere thanks also go to Jim for his invaluable support with this thesis. His thoughtful comments into some of the details were greatly appreciated and posed many questions that stimulated further reflection. I especially thank him for pushing me for further clarity on certain ideas and also for reviving my enthusiasm for coastal environments. His sense of humour and kindness were always welcomed.

I am also indebted to numerous people for their considerable assistance with all aspects of this research over the last four years. I would like to thank Maria Miguens-Rodriguez and Dr. Henriette Linge for their assistance during sample processing at SUERC. I'm most grateful to Mike Shand for his endless support with GIS and Illustrator, and I have also appreciated the assistance of Anca Brişan, Katie Whitbread and Miguel Castillo. Many thanks go to Anca Brişan and Claudiu Onea for helping me with the Rodna orthophotomaps. I am very grateful to Dr. John Gordon for allowing access to the aerial photographs of the Monadhliath Mountains and I thank Lorant Czarán for sharing the 30 m DEM of the Rodna Mountains. Dr. Ramona Bălc is also gratefully acknowledged for joining me in Rodna.

Particular thanks are extended to my colleagues and friends Alessa, Hannah, Helen, and Katie who have made time in the EQ enjoyable and cheered me up in the bleak PhD days. I also benefited immensely from our scientific discussions and I would like to thank

Hannah for taking the time to read parts of the thesis. I am especially grateful to Alessa for assisting me in the field, both in Rodna and Monadhliath Mountains, most of the time at her own expense, for her advice and comments on all aspects of this work and for being there whenever I needed.

I have also appreciated the immense help from Morag Armstrong and Eoghainn Maclean, Hilary and Mark Wilson, Alison and Mathew Lee, Josephine Armstrong and Keith Ingham, Virginia Braid and David Shearer, both before and during my Ph.D. You will always have a special place in my heart.

I would like to thank Mihaela Trelea-Newton since it was her initial encouragement that convinced me to start this project. Thank you for introducing me to the beautiful glacial landscape of the Rodna Mountains and for your support throughout the years.

Mr. Traian Timiș-Ponțiu will always be remembered for his love and care for the Rodna Mountains and its wildlife. Thank you for always providing me a shelter in your home, even when I was an unexpected guest. Thank you for being there and for sharing your stories with us.

I owe many thanks to soon to be Dr. Luminița Zaharia who has been my field assistant, geology adviser, proof reader, and, most of all, my friend, as we shared tears of joy and sorrow during our Ph.D. lives.

I am indebted to Adela, Ana and Ruxandra for their continued friendship, for giving up their free time to answer my countless phone calls and for their constant words of encouragement.

My ultimate inspiration in life comes from my lovely parents, Lia and Iancsi. I will never be able to thank them enough for always believing in me, for continuously encouraging and supporting me emotionally and financially in whatever crossed my mind. Their guidance, patience and their endless help have brought me where I am today. Thank you for sharing with me the beauty of the mountains and for making my 2009 Rodna fieldtrip another wild adventure.


Finally, my thanks go to Clau for his never-ending support and patience, and for maintaining my mental health during the stresses and strains of the last four years. His calm and wisdom have brought so much light into my life and work. Thank you for giving up your summer holidays to assist me on fieldwork in Rodna and never missing an opportunity to come to Monadhliath. Words are useless to show you my love and gratitude.

Thank you all.

Declaration

The material presented in this thesis is the result of the research undertaken by myself between October 2007 and October 2011. This work was supervised by Dr. Derek Fabel and Dr. Jim Hansom.

I declare that, except where explicit reference is made to the contribution of others, that this dissertation is the result of my own work and has not been submitted for any other degree at the University of Glasgow or any other institution.

Signature 

Printed name GHEORGHIU

Date Apr 2012

Delia M. Gheorghiu

Apr 2012

Abbreviations

AMS	– Accelerator Mass Spectrometre
ANCPI	– Agenția Națională de Cadastru și Publicitate Imobiliară, România
AABR	– Area Altitude Balance Ratio
AAR	– Accumulation Area Ratio
AWMA	– Area Weighted Mean Altitude
ASTER	– Advanced Spaceborn Thermal Emission and Reflection Radiometer
BIIS	– British-Irish Ice Sheet
CR	– Cosmic Radiation
DEM	– Digital Elevation Model
DIMAP	– Digital Maps, Hungary
DTM	– Direcția Topografică Militară, România
IRSL	– Infra-red Stimulated Luminiscence
EIS	– European Ice Sheet
FIS	– Fennoscandian Ice Sheet
ELA	– Equilibrium Line Altitude
LGM	– Last Glacial Maximum
LLGM	– Last Local Glacial Maximum
NAO	– North Atlantic Oscillation
NASA	– National Aeronautics and Space Administration
OSL	– Optically Stimulated Luminiscence
OS	– Ordonance Survey
PCR	– Primary Cosmic Rays
PNMR	– Parcul Național Munții Rodnei
RCAHMS	– Royal Commission on the Ancient and Historical Monuments of Scotland
SCR	– Secondary Cosmic Rays
SED	– Surface Exposure Dating
SLHL	– Sea Level and High Latitude
SRTM	– Shuttle Radar Topography Mission
SUERC	– Scottish Universities Environmental Research Center
TCN	– Terrestrial Cosmogenic Nuclide
THC	– Thermohaline Circulation
U/Th TIMS	– Thermo-Ionisation Mass Spectrometry
YD	– Younger Dryas

Chapter 1

Introduction and aims

1.1 Rationale

Identifying the glacial extent and dynamic behaviour of past glaciers is a key factor in understanding climate change and its influence over a wide area. There exist several studies of the role of continental ice sheets and their indirect influence on less glaciated areas. However, understanding the way in which modern ice masses will react to climate change and vice versa, is currently missing critical palaeoenvironmental information. Generally, glaciers respond relatively quickly to variations in local climatic conditions and are therefore excellent proxies for climate change. Glacial extent can be determined based on field evidence, while surface exposure dating can be used to constrain the timing of glacial events. Used together, these two methods clarify both the spatial and temporal reconstruction of ice sheets and mountain glaciers and help to increase our knowledge of ice mass behaviour under general climate forcing mechanisms and local environmental conditions.

Until recently, information on climatic and environmental conditions in Europe during the Late Devensian glaciation (here taken as 40 – 11.5 ka) has been provided mainly from research studies in western and northern Europe, with only fragmentary evidence from regions situated in eastern and/or south-eastern Europe. The climatic variability towards the end of the last glaciation has been well documented in the Greenland ice core records and terrestrial and marine archives from other regions. Often the climatic oscillations are assumed to have been synchronous over wide areas of Europe but this has not been widely tested. There is a growing body of evidence indicating that the glacial advances and retreats due to the abrupt climatic changes in the North Atlantic region at the end of the Devensian glaciation occurred at different times and magnitudes across Europe. For example, while wetter north-western areas (closer to the North Atlantic Ocean) were covered by the European ice sheet, the Carpathians were influenced by a drier continental climate, allowing only limited coverage of ice and mostly at higher elevations as mountain glaciers.

The main aim of this thesis is to test the existence of climate synchronicity at the end of the Devensian glaciation. To achieve this two formerly glaciated, but very different areas are compared, the Rodna Mountains, Romania (high altitude, mid latitude) and Monadhliath Mountains, Scotland (low altitude, high latitude) (Figure 1.1). The style and pattern of Late Devensian glaciation in Scotland has been extensively investigated; however, there has

been only limited study of the Lateglacial history of the Monadhliath Mountains and an absolute glacial chronology has never been established. Similarly, in northern Romania, it is known that the Rodna Mountains were glaciated in the past, but there are no constraints on the timing, extent and dynamics of these glaciations.

To fully understand the magnitude and distribution of ice masses in Europe at the close of the Devensian glaciation, it is essential to establish the style, dynamics and timing of glaciation in both the Monadhliath and Rodna Mountains. The comparison between the central Highlands of Scotland, which were subjected to continental glaciation, and the Romanian Carpathians, which were affected by alpine glaciers, should provide new insights into past climatic gradients across Europe and clarify the critical role of ice sheets in influencing local, regional, and continental environmental conditions.

The climatic changes which took place across Europe during the Late Devensian are not simply embodied by the development and decay of the large European ice sheet. The presence of this ice sheet caused a significantly more complex translation of climate cooling from the western high latitudes towards eastern mid latitudes, resulting in a series of feedbacks that triggered different responses in local climates. Since the Romanian Carpathians were not subject to continental glaciation they may preserve a distinctive and independent palaeoclimatic record. Hence, the Romanian Carpathians could be central to understanding the hemispheric transmission of the climate change.

1.2 Objectives of the thesis

This thesis aims to:

1. Determine the glacial extents and dynamics in each of the study areas during the Last Maximum Glaciation and the Younger Dryas.
2. Temporally constrain the timing of the Devensian deglaciation in both areas using surface exposure dating.
3. Evaluate the differences in the advance and retreat pattern between the Carpathians and the north-western part of Europe.

4. Assess the dominant influences on the spatial and temporal asymmetry in the deglaciation histories of Scotland and Romania.

1.3 Outline of the thesis

This thesis comprises seven chapters.

Chapter 1 is an overview of this research study and introduces the aims of the thesis.

Chapter 2 provides a review of the termination of the Devensian glaciation in Europe, specifically the Last Glacial Maximum and the Younger Dryas glacial advances. Each glacial period is reviewed separately for both study areas.

Chapter 3 introduces the methods used for reconstructing the glacial extent and dynamics in the study areas, with an emphasis on the principles of surface exposure dating using the *in situ* terrestrial cosmogenic nuclide ^{10}Be , as the main dating tool to constrain the glacial events.

Chapter 4 outlines the glacial history of the Monadhliath Mountains using mapping and landform evidence temporally constrained using surface exposure dating.

Chapter 5 examines the glacial advances and retreats in the Rodna Mountains and introduces the first surface exposure ages from the northern part of the Romanian Carpathians.

Chapter 6 discusses the results obtained in the Monadhliath and Rodna Mountains set within a wider context by relating them to the role of ice sheets in regional climate change and the implications of the ocean-ice-atmosphere system.

Chapter 7 summarizes the aims, methods and main conclusions drawn from this study, with the intention of providing an overview of the thesis as a whole and its role in providing a better understanding of the last Quaternary glaciation of Europe as well as highlighting potential future research directions.

Chapter 2

Geographical & climatological context

2.1 Geographical context

2.1.1 Scotland

Scotland occupies the northernmost part of the British mainland and extends between 55° and 60° N latitude and 1.7° and 6° W longitude (Figure 2.1). It is bounded to the east by the North Sea and to the north and west by the Atlantic Ocean. In the south, the English border lies between the Solway Firth and the Tweed valley.

The Scottish landscape is divided into three distinct geographical areas: the Highlands and Islands, the Central Lowlands and the Southern Uplands (Figure 2.1). The Highlands refer to the two thirds of Scotland to the north and west of the Highland Boundary Fault which crosses Scotland's mainland (Figure 2.1). This area comprises of the Northwest Highlands and the Grampian Mountains and is characterized by a variety of both large wide valleys (straths) and steep, narrow valleys (glens). These two mountain ranges are separated by the Great Glen Fault (Figure 2.1), a long over deepened glacial trough. Hundreds of islands are spread along the northwest and north Scottish coast. The Hebrides lie off the northwest coast of Scotland, whilst the Orkney and Shetland Islands lie north of the mainland and form the boundary between the North Sea and the Atlantic Ocean.

The Scottish climate is a moderate temperate one, with the mean July temperature of ca. 15°C and the mean January temperature of ca. 5°C. The general climatic influence comes from the transit of oceanic air from the west. Western Scotland receives the maximum rainfall (4577 mm) whilst the eastern part is more continental, cooler and with less precipitation (550 mm) (Met Office, 2011). Scotland owes its moderate climate to the effect of warm Atlantic Ocean currents, important components of the global thermohaline circulation. Transiting from tropical latitudes to higher, colder latitudes, the North Atlantic Drift is a branch of the Gulf Stream and is responsible for a warming influence across Scotland. This leads to wet and mild winters, but also cooler and wetter summers.

In spite of Scotland's high latitude location, the mild winters are the reason why there are currently no glaciers in Scotland, although semi-permanent snow beds can survive in sheltered spots at high altitudes. The summit of Ben Nevis in the Western Grampians is the highest mountain in the British Isles (1334 m), whilst further to the east the Cairngorms comprise the highest mountain plateau in the British Isles, incised by glens from all sides. The Scottish mountains have been repeatedly glaciated in the past, including the south-

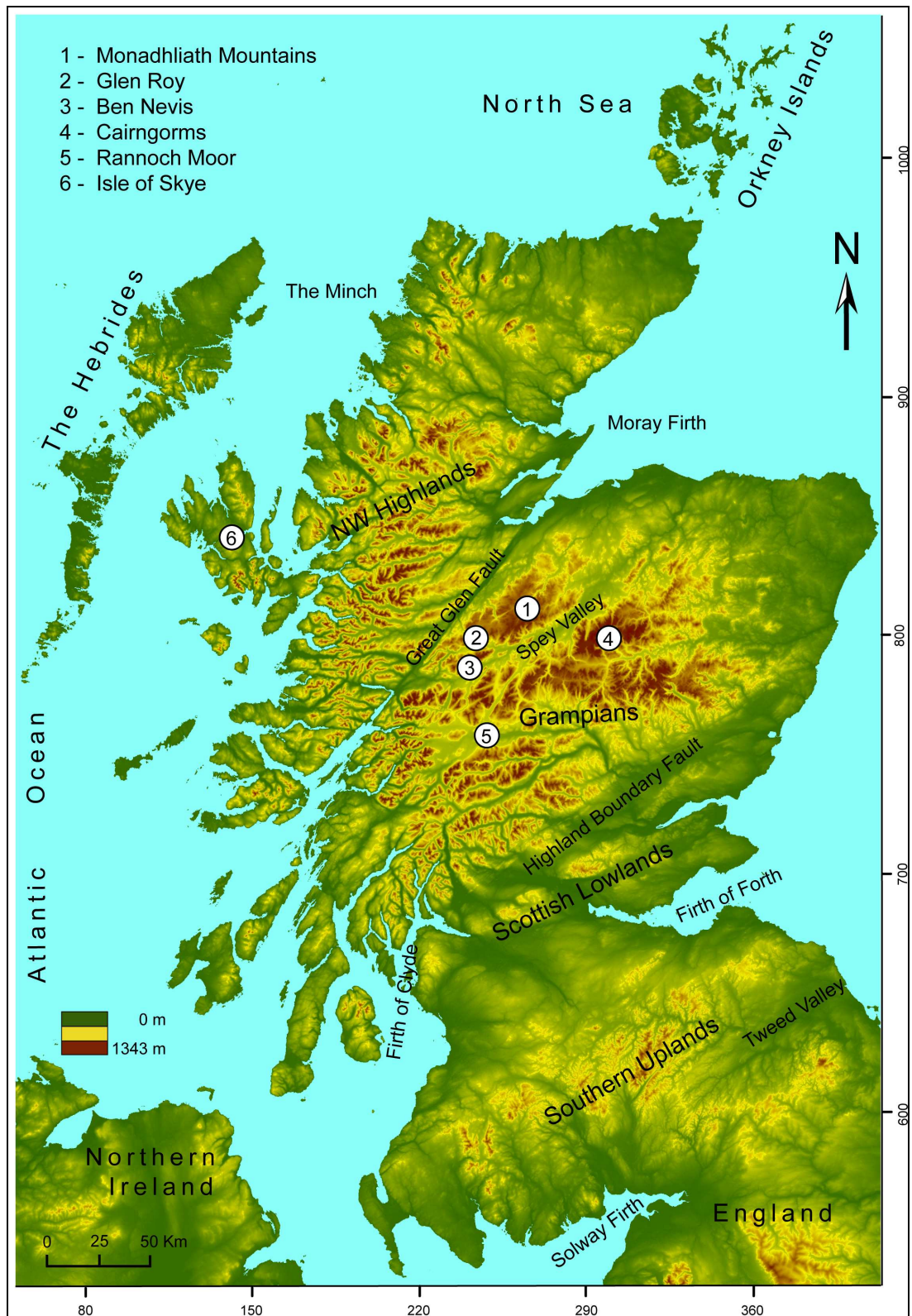


Figure 2.1. Digital elevation model of Scotland (SRTM, NASA 2004).

eastern Grampians which are lower in altitude, producing a spectacular landscape with deep valleys and high rugged mountains. The last British ice sheet erased any previous geomorphological record while the last glacial advance overprinted new glacial landform assemblages. A steep west-east precipitation gradient had been noticed in the different distribution of ice during glacial periods, but more pronounced than at present.

2.1.2 Romania

The Romanian Carpathians are situated in the south-eastern part of the Carpathian Mountains, occupying a central position within the temperate climate limits between ca. 44° and 48° N latitude and 21° and 26° E longitude. More than half of the Carpathians are located in Romanian territory, extending approximately 900 km in length (Figure 2.2).

Part of the Alpine-Himalayan orogenic system, the Romanian Carpathians are comprised of a series of orographically and geologically distinct subdivisions. They comprise a triangular block of high mountains with varied landscape that surrounds the Transylvanian basin (Figure 2.2), and can be separated into the Eastern, the Southern and the Western Carpathians. The Eastern Carpathians stretch approximately 400 km NW-SE from the Ukrainian border to the Prahova Valley where they curve westwards continuing into the high Southern Carpathians for approx 250 km towards the Timiș-Cerna Couloir in the West (Figure 2.2). Both the Eastern and the Southern Carpathians display parallel ridges running NW – SE and E – W, respectively. The Western Carpathians stretch from the Bărcău Valley in the north to the Danube River in the south (Figure 2.2).

The geographical position of the Romanian Carpathians results in particular climatic influences. From the south, the Mediterranean influences the Retezat – Godeanu Group (Figure 2.2), with a milder climate; in the west, oceanic air masses from the Atlantic (restricted by the barrier of the Apuseni Mountains) bring milder winters and heavier rainfall; in the north the cold air of the Baltic influences the Rodna – Maramureș Mountains; and in the east and the south-east, continental air brings frosty winters and less rain, mainly to the eastern side of the Eastern Carpathians (Atlas of Romania, 1979). The transition climate from the colder and wetter climates of the N and W respectively, to the more arid east creates a diverse climatic environment, and the influence of the north Atlantic should decline towards the east.

Similar to all mountain environments, the Carpathian climate is subject to local variations, for example slope aspect, with colder and wetter air on the northern parts and sunny and drier southern slopes. The mean annual temperature varies with altitude between ~8°C at the foothills and -2°C on the highest peaks. Mean annual precipitation is between 750 mm and 1200 mm, depending on the altitude and slope orientation (Atlas of Romania, 1979).

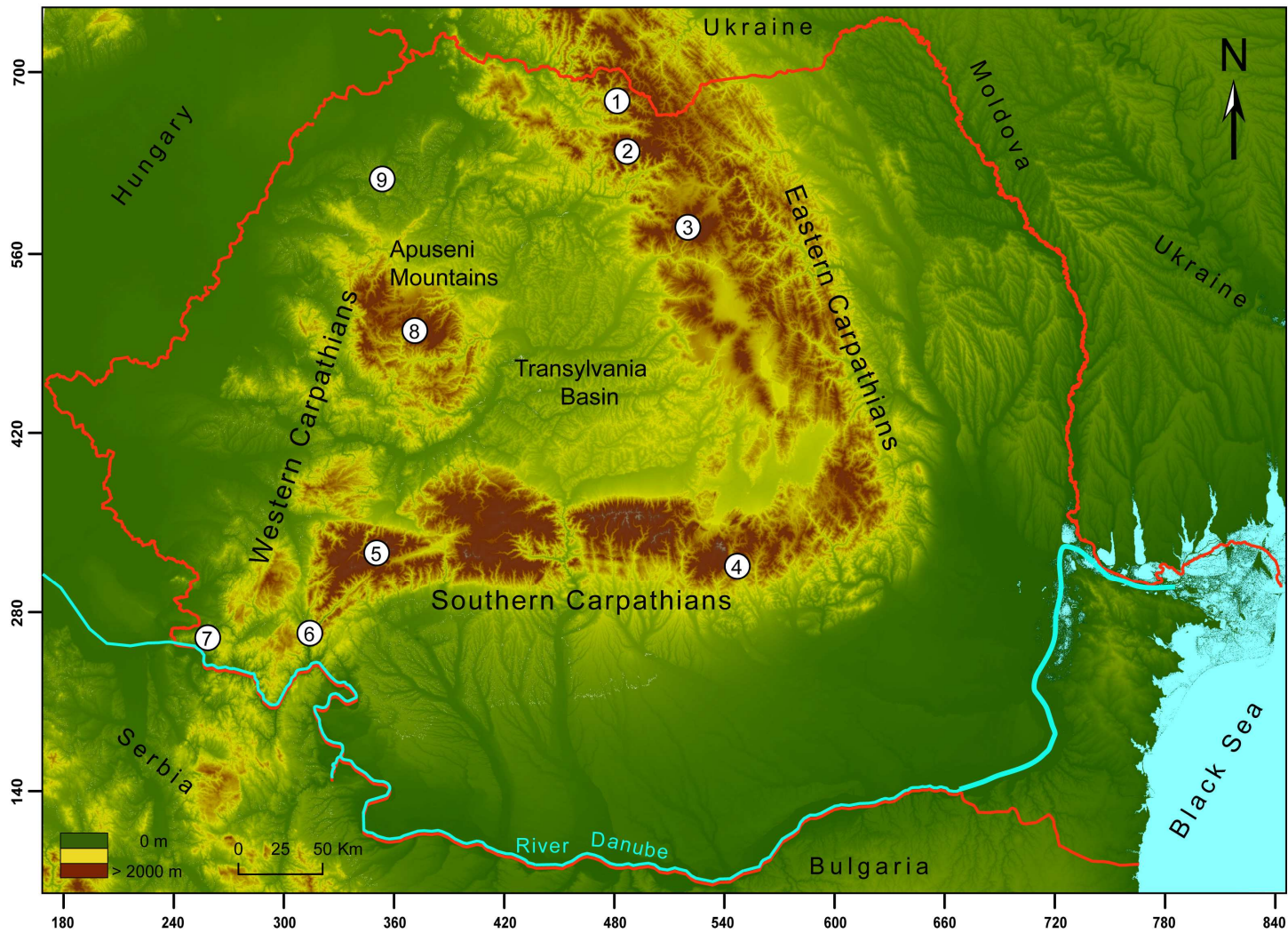


Figure 2.2. Digital Elevation Model of Romania (SRTM, NASA 2004):

- 1 - Maramureş Mountains;**
- 2 - Rodna Mountains;**
- 3 - Călimani Mountains;**
- 4 - Prahova Valley;**
- 5 - Retezat & Godeanu Mountains;**
- 6 - Timiş-Cerna Couloir;**
- 7 - Poleva Cave;**
- 8 - Bihor Mountains;**
- 9 - Barcău Valley.**

In spite of the high altitudes of the Romanian Carpathians no glaciers exist today, but various landforms provide evidence of previous glaciations and they are an excellent natural laboratory for the study of landscape evolution. The highest and the most massive mountain range is the Southern Carpathians, with altitudes over 2000 m in 10 of its massifs, offering the best conditions for cirque, plateau and valley glaciers to develop, especially at their western end due to precipitation from the Mediterranean Sea. In the Apuseni Mountains, slightly above 1800 m, humid Atlantic climatic characteristics prevail and few glacial features can be found (Figure 2.2).

The Eastern Carpathians are lower in altitude and have only three mountain massifs that formerly held ice, specifically the Rodna, Maramureş and Călimani ranges. The combination of altitude and low temperatures in this northern part of the country appears to have provided suitable accumulation areas where ice was able to survive during the Quaternary.

2.2 Climatological context

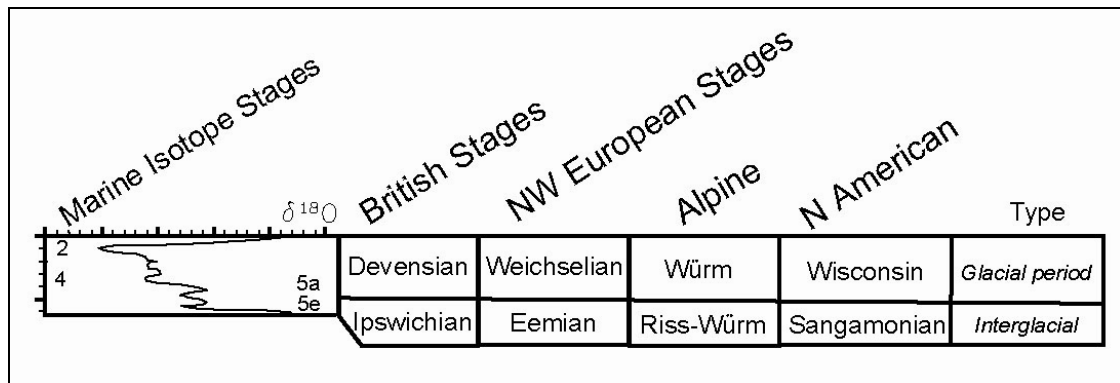
2.2.1 Last glaciation in Europe

The Quaternary period of the last 2.6 Ma was a time of critical importance in Earth history since a series of dramatic climatic and environmental changes occurred during this time. The frequent ~40 ka climate cycles that occurred from 2.6 – 0.9 Ma, changed to ~100 ka cycles after 0.7 Ma (Clark et al., 2006; Williams et al., 1998). This means that the Earth's climate changed from cold to warm, specifically from slow and uneven cooling periods with ice covered land (glacials) followed by rapid warming, during shorter intervals (interglacials). These climatic oscillations have been recorded by the $\delta^{18}\text{O}$ variations in the Greenland ice cores and various other archives from Europe (e.g. Dansgaard et al., 1993; Johnsen et al., 2001).

The last glaciation of the high latitude regions in the northern hemisphere lasted from the last interglacial (~125 ka ago; Ipswichian or Eemian) to the present one (11.7 ka – present; Holocene). It comprised of a series of glacial advances (stadials) due to continued cooling episodes until mid-latitude areas were in full glacial conditions resulting in a low global sea-level. This last maximum glaciation terminated in an abrupt warming period, glacier

contraction and the re-advance of forest vegetation towards the high latitudes and higher elevations. The last glaciation has various names, according to the geographical location of field evidence (Table 2.1). In this study, the last glaciation is referred to as the Devensian Glaciation. The Devensian glaciation was the last time when ice sheets grew over Europe but previous Quaternary glaciations occupied larger areas during their maximum extent.

Table 2.1. Terminology used across the Northern Hemisphere.



According to Lundqvist (1986) and Mangerud (1991), the European ice sheet maintained its existence throughout all of the Devensian glaciation, ice retreating towards northern Fennoscandia during interstadials. Others describe the ice sheet maximum occurring towards the end of the Devensian glaciation (Punkari, 1984; Punkari & Forsström, 1995). It is generally agreed that three distinct ice sheet advances occurred during the Devensian glaciation: 90-80 ka (Early Devensian), 60-50 (Middle Devensian) and 20-15 (Late Devensian) with the ice sheets that developed over Scandinavia extending eastwards towards NW Russia and ice sheets from the Barents sea spreading southwards (Svendsen et al., 2004). Reconstructed ice sheet limits suggest that the Scandinavian ice sheet was much smaller during the Early Devensian than the late Devensian (Andersen & Mangerud, 1989; Mangerud, 2004; Svendsen et al., 2004).

Most researchers focus on studies of the Late Devensian glaciation since this is the most recent period and the maximum extent of Late Devensian ice removed much of the geomorphological record of earlier glaciations. The ice extent and, implicitly, climatic oscillations during the last Devensian glaciation had different impacts across the continents in the Northern Hemisphere. For example, the massive Laurentide ice sheet developed progressively over North America but nearby smaller ice masses behaved independently, reaching their maximum glacial extent at different times (e.g. the Innuitian ice sheet; Dyke et al., 2002). Precipitation was drastically reduced in Japan, Taiwan, Karakorum and

Himalaya during the global last glacial maximum (LGM) as opposed to earlier glaciations (Ono et al., 2004, 2005). Other areas in Europe experienced a maximum extent of ice in the mid-Devensian with a more restricted coverage during the Late Devensian (see below).

In northern Europe, the Late Devensian glaciation is thought to have been caused by an imbalance in the thermohaline circulation (THC) which transported less warm waters towards the North Atlantic causing ice to advance southwards (Ruddiman & McIntyre, 1981; Clark et al., 2002). Subsequent warming of the climate caused a slow retreat of ice from its maximum extent after ~19 ka (Lambeck et al., 2000), with deglaciation occurring at different times across the European continent, and triggering rapid sea level rise and glacial isostasy between 17–15 ka BP in most areas (Wohlfarth et al., 2008; Svendsen et al., 2004). During the Lateglacial period of 14.7 – 11.7 ka (Lowe et al., 2008) the climate experienced several abrupt fluctuations from warm to cold and vice versa following the wastage of the Last Glacial Maximum (LGM) until the beginning of the Holocene. The short warm period after ice deglaciation was interrupted by the Older Dryas event (14.5 - 13.7 ka) (Lowe et al., 2008). A repositioning of the North Atlantic Polar Front towards southern latitudes caused a short-term ice re-advance, still-stand or ice margin fluctuations depending on local factors, and led to the formation of landform assemblages often superimposed on the LGM features. The latest advance of glacial ice in the Devensian glaciation occurred during the Younger Dryas stadial (12.9 – 11.7 ka BP; Lowe et al., 2008). Based on the timing and magnitude of this event, Lotter et al. (1992) argue that this was the most important climatic oscillation of the whole Lateglacial period.

2.2.2 Last Glacial Maximum (LGM)

Last glacial maximum (LGM) refers to the period when ice masses reached their last maximum position and when sea level was at a minimum level. According to terrestrial and marine proxy records, the LGM was different from one continent to another. Moreover, it also varied from place to place on the same continent due to the variations in the dominant controlling factors (precipitation, temperature). To determine the synchronicity between various regions, several local climatic and environmental factors have to be considered that may act independently of the general climatic influences.

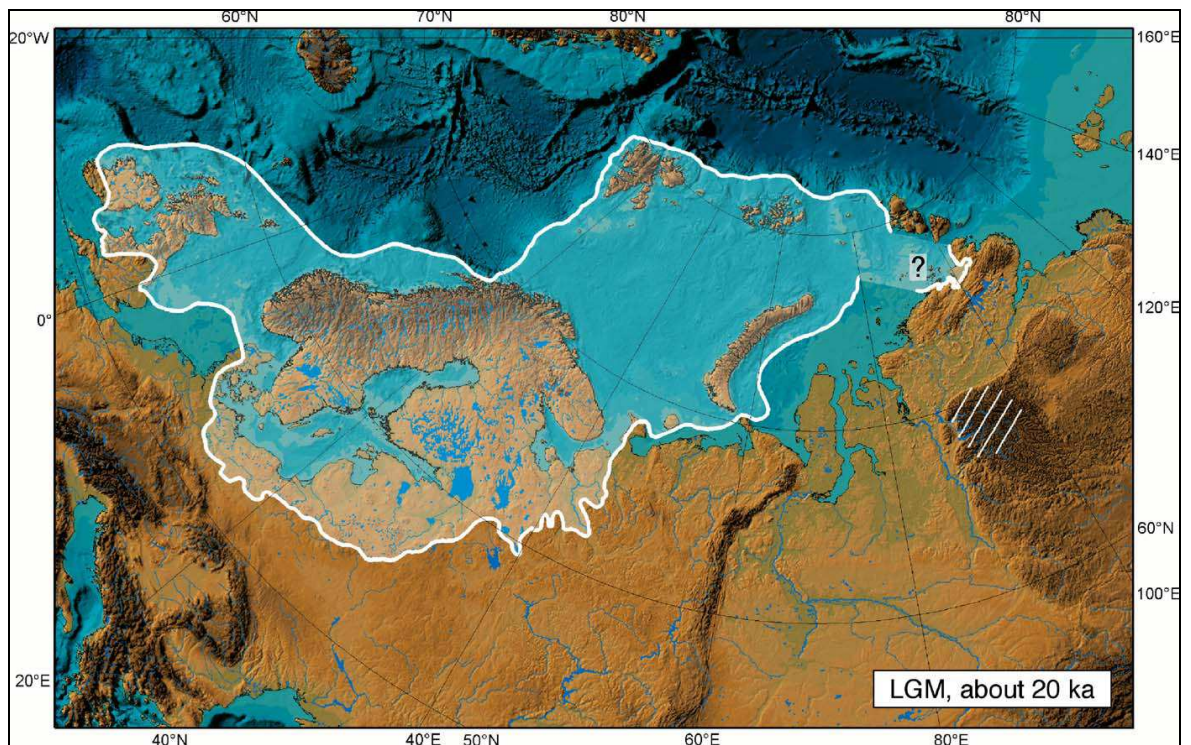


Figure 2.3. The reconstructed limits of the Eurasian ice sheet at the Last Glacial Maximum (Svendsen et al., 2004).

According to Peltier and Fairbanks (2006) the LGM occurred between 26–21 ka. However, it is unlikely that the global LGM took place at the same time everywhere, and various places experienced a maximum glaciation at different times as a result of the varied behaviour of different parts of the ice-sheets. This is supported by a series of reconstructions across the globe which contradicts the concept of the LGM as a global synchronous event (see below). Therefore, the local maximum advance of ice in our study areas will be treated as the Last Local Glacial Maximum (LLGM).

Full glacial conditions were reached by the north-western European ice sheet (EIS) towards the close of the Devensian glaciation (Figure 2.3). The EIS started with the growth and the southern expansion of the Fennoscandian Ice Sheet (FIS) and across the western Norwegian continental shelf, later coalescing with the British Irish ice-sheet (BIIS), and then expanding over northern Europe as far south as Denmark and the northern plains of Germany (Mangerud, 2004). Ice sheet lobes from the main Baltic ice stream, controlled by topography, invaded Poland, Lithuania and north-western Belarus (Boulton et al., 2001; Marks, 2002, 2010) and spread in SW-NE direction, blocking pre-existing drainage system and forming proglacial lakes, which later catastrophically discharged. The continental ice sheet also extended eastwards across the NW Russian plains and the White Sea to meet the Barents Ice Sheet and the Kara Ice Sheet, all together forming the Eurasian ice sheet (Svendsen et al., 2004).

The growth of these massive ice sheets across the globe locked up some of the sea water, lowering the sea surface to ~120 m below its present level (Peltier & Fairbanks, 2006) and exposing wide areas of continental shelf. The start of the ice sheet growth occurred as a result of climate deterioration but the location, extent and morphology of the accumulation areas was driven by topographical conditions (Boulton et al., 1985; 2004). The ice front reached its maximum extent at different points on its perimeter and at various times as the ice lobes behaved differently. These variations were due to the differences in temperature and elevation gradients and in the moisture availability of each area (Ono et al., 2004).

The deglaciation history of the European ice sheet has been reconstructed by various authors based on the geomorphological evidence of glacial landforms: moraines, long eskers, massive deposits (Ehlers & Gibbard, 2004), whose pattern and distribution does not suggest a uniform deglaciation. For example, the rapid sea level rise at ~19 ka initially affected the western part of the Scandinavian ice sheet, leading to de-coupling of the eastern ice streams which probably took a long time to completely disappear (Boulton et al., 2001; Rinterknecht et al., 2007). Deglaciation from the maximum advance of the ice sheet in Belarus and Lithuania occurred at 19.0 ± 1.6 ka (Rinterknecht et al., 2008). According to Marks (2010), ice lobes in Poland extended independently towards their maximum limits between 24-19 ka with the last deglaciation phase at 16-17 ka. Ice thickness over Scandinavia at about 15 ka was >2.5 km (Svendsen et al., 2004). Ice lobes of the European ice sheet retreated from Belarus at 17.7 ± 2.0 ka with the final deglaciation at 13.1 ± 0.5 ka (Rinterknecht et al., 2007, 2008). Other deglaciation ages (^{36}Cl) from the Pomeranian moraine in Poland suggest a deglaciation at 14.4 ± 1.0 and 14.7 ± 0.9 ka, indicating a long response of the Scandinavian ice sheet to climate change (Dzierzek & Zreda, 2007).

Although northern Europe was covered by a massive ice sheet (Figure 2.3), the southern and eastern part of the continent was affected by more restricted mountain glaciation or small ice caps, specifically in south Germany, the Pyrenees, the Alps, the Vosges and Jura Mountains, the Carpathians and the Ural mountains (Ehlers & Gibbard, 2004). The Alpine ice cap drained through several ice streams that occupied the main valleys, forming the largest glacial system beyond the southern limits of the massive ice sheet (Florineth & Schlüchter, 2000). Other smaller ice caps formed in the Massif Central, Vosges and Jura Mountains (Gillespie & Molnar, 1995). The glaciers in the eastern Alps attained their maximum position as piedmont glaciers between 24-21 ka, rapidly decaying afterwards

with occasional short time ice oscillations and stillstands (~16 ka) followed by re-advances during the Older Dryas event (van Husen, 1997; Reitner, 2007).

Although the established chronology in the Alps suggests a simultaneous maximum advance of ice with the Northern European ice sheet (Reitner, 2007), other areas do not appear to experience a synchronous LGM, likely due to precipitation starvation (Gillespie & Molnar, 1995). OSL (optically stimulated luminescence) dating in Denmark constrained the LGM at about 35-32 ka (Houmark-Nielsen, 2008, 2010) consistent with an IRSL-date (infra-red stimulated luminescence) of sediments of 32.4 ± 9.4 ka in the Bavarian Forest just between the southern margins of the Scandinavian ice sheet and the north flowing piedmont glaciers of the Alps (Raab & Völkel, 2003). The LLGM in the Cantabrian Mountains has been dated to a smaller extent than a previous maximum advance of ice which occurred at ca. 48-32 ka (Jalut et al., 2010). Moreover, the LLMG in the Pyrenees occurred between 70-50 ka, much earlier than the maximum extent of the European ice sheet, with glaciers slowly diminishing to valley glaciers by the time of the global LGM ice advance (Jalut et al., 1992; Gibbons & Moreno, 2002; Garcia-Ruiz et al., 2003; Calvet, 2004). Other high altitude areas towards the east experienced a LGM at an earlier time. The reconstructed mountain glaciated environment in the Carpathians, using different proxies, suggests that the LGM in the Tatra Mountains occurred at 32-30 ka (Lindner et al., 1990, 2003). The LGM in the Southern Carpathians was inferred from relative chronology of moraine deposits as asynchronous to global climate records (Reuther et al., 2007). In Greece, preliminary uranium-series dating of glacial sediments places the maximal glacial advance to an earlier period in the Devensian glaciation and suggests that the last maximum glacial advance was less extensive (Woodward et al., 2004). The LLGM was also assumed to have occurred earlier in the last glaciation in other regions: Massif Central, Iberia and the Albanian Alps (Straus, 1992, cited by Allen et al., 2008; Gillespie & Molnar, 1995; Marjanac & Marjanac, 2004; Milivojević et al., 2008). Glacial landforms assemblages in the high altitude Caucasus Mountains suggest another restricted glaciation with cirque and valley glaciers of up to 70 km length during the Late Devensian glaciation (Gobejishvili, 2004). The LLGM in the Ural Mountains occurred at ca. 50-60 ka and during the global LGM glaciers were restricted to higher areas, only 1 km down valley from the present ice limits (Dolvik et al., 2002 cited by Svendsen et al., 2004; Mangerud et al., 2008). Although connected to the NW European Ice Sheet during the Devensian glaciation, a different response was recorded by the Barents-Kara (Siberian) ice sheet which reached its maximum extent at ca. ~90-80 ka. After successive advances, it became progressively smaller in size towards the LGM when the European ice sheet increased

(Svendsen et al., 2004). Due to an extremely cold climate, the eastern part of the Northern ice sheet retreated from Arctic Siberia before the global LGM (Siegert & Marsiat, 2001) leaving only corrie and valley glaciers during this time (Astakhov, 1997; Svendsen et al., 2004; Hubberten et al., 2004).

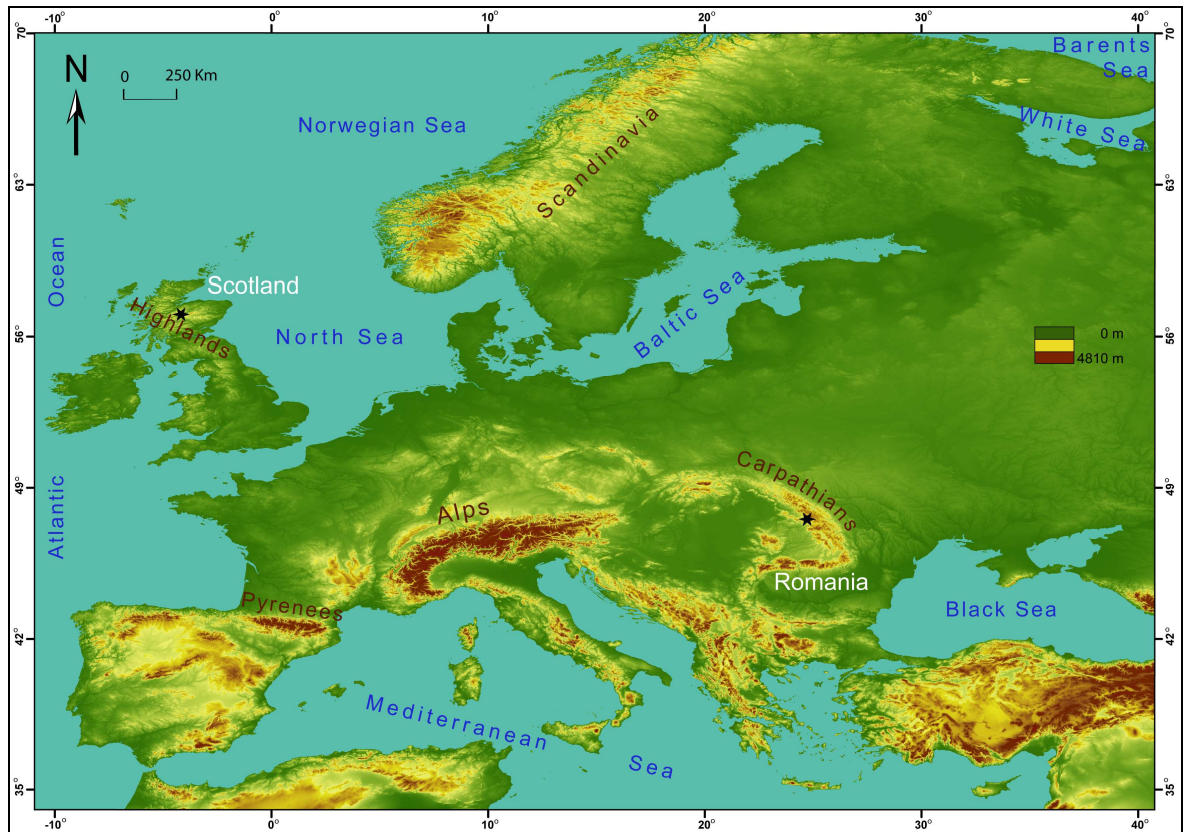


Figure 2.4. Digital elevation model of Europe (SRTM). The areas considered in this study are located in the Scottish Highlands (★= Monadhliath Mountains) and the Romanian Carpathians (★= Rodna Mountains).

2.2.2.1 Last maximum glaciation in Scotland

A major imprint on Britain's landscape was left by the Late Devensian glaciation that immersed much of the country under a massive ice sheet. The extent and timing of this ice sheet has been the subject of a long scientific debate in the last decades, with glacial geomorphology and advances in absolute dating techniques unveiling some of the Late Devensian glacial histories.

During the LGM of Scotland, Rannoch Moor (Figure 2.1) was a major ice accumulation centre (Barrow et al., 1913; Sissons, 1974; Golledge & Hubbard, 2005; Golledge, 2006; Lowe & Walker, 1976). At this time, ice also spread from various upland areas in Britain.

Ice streams flowed outwards from Rannoch Moor across the valleys (Sutherland, 1984; Thorp, 1987; Gordon & Sutherland, 1993), this clearly evidenced by deposits of grey Rannoch granite erratics and ice moulded landforms showing former ice directions (Young, 1978; Sutherland, 1984). Tributaries of the Minch palaeo-ice stream drained the NW part of the Scottish Highlands (Figure 2.5), extending to the continental shelf beyond the present coast and calving into the Atlantic Ocean (Bradwell et al., 2008b). The Spey ice stream flowed along the present upper Spey Valley (Figure 2.1), draining a considerable part of the south-eastern Grampians and modifying the underlying bedrock by grooving and breaching (Barrow et al., 1913; Young, 1978). Ice with a thickness of at least 700 m is thought to have flowed northeast, covering the entire landscape. Long meltwater channels associated with this ice configuration were cut across cols towards the lowlands of the Moray Firth (Young, 1978). Several united ice streams in the NE part of the BIIS coalesced with the FIS (Figure 2.5), which drained the northern part of the North Sea basin westwards and pushed the Scottish ice to flow towards the NNW (Boulton et al., 1977; Sutherland, 1984; Bradwell, 2008b; Hubbard, 2009). The maximum extent of the BIIS is interpreted to have occurred somewhere between ca. 26–21 ka (Ballantyne, 2010). Away from the mainland, the coalesced ice streams left much evidence across the continental shelves and the islands of Orkney and Shetland in the form of subglacial tunnel valleys and moraines (Bradwell et al., 2008b).

Subsequent sea-level rise caused de-coupling of ice masses and a punctuated retreat, forcing each ice stream to re-organize in terms of flow direction and dynamics (Bradwell et al., 2008b). By ~16 ka the BIIS had retreated to the coastline (Hubbard, 2009), with a variety of geomorphological features marking its offshore stillstands and oscillations. As more retreat and thinning occurred, the regional evidence of meltwater channels, eskers, roches moutonnées, striations and parallel recessional moraines show that the ice was dynamically active, although topographically constrained with flow mostly within the main troughs (Sissons, 1973; Mitchell & Merritt, 2004). As the ice sheet collapse was generally rapid (Bradwell et al., 2008b), its eroded meltwater channels produced extensive glacifluvial deposits whose location and orientation assist in the interpretation of the deglaciation pattern. However, recent studies provide geomorphological evidence of stillstands during the time of deglaciation (Charlesworth, 1956; Young, 1974; Brazier et al., 1998; Gollledge, 2002) with stagnant ice masses and ice-dammed lakes formed by meltwater in topographically suitable locations, such as between the lobes of the major ice streams and local retreating glaciers. Deglaciation was also punctuated by several minor readvances of ice which created push moraines (Merritt, 1998). These readvances

generally occurred due to the increasing warmth brought by the North Atlantic Current which then increased the amount of snowfall (Clapperton, 1997). Deglaciation of the BIIS occurred at different times across Scotland. In the eastern part of Scotland, the Cairngorms and adjacent Spey valley experienced deglaciation before ca. 14.5 ka (Ballantyne, 2010). The timing of deglaciation obtained from readvancing moraines in NW Scotland occurred at ca. 14.0 ka (Ballantyne, 2010). However, the NW sector of the ice sheet did not experience a complete deglaciation during the Lateglacial (14.5–12.9 ka), ice being maintained in favourable locations until after 14.0 ka (Sutherland, 1984; Bradwell et al., 2008a; Lukas & Bradwell, 2010).

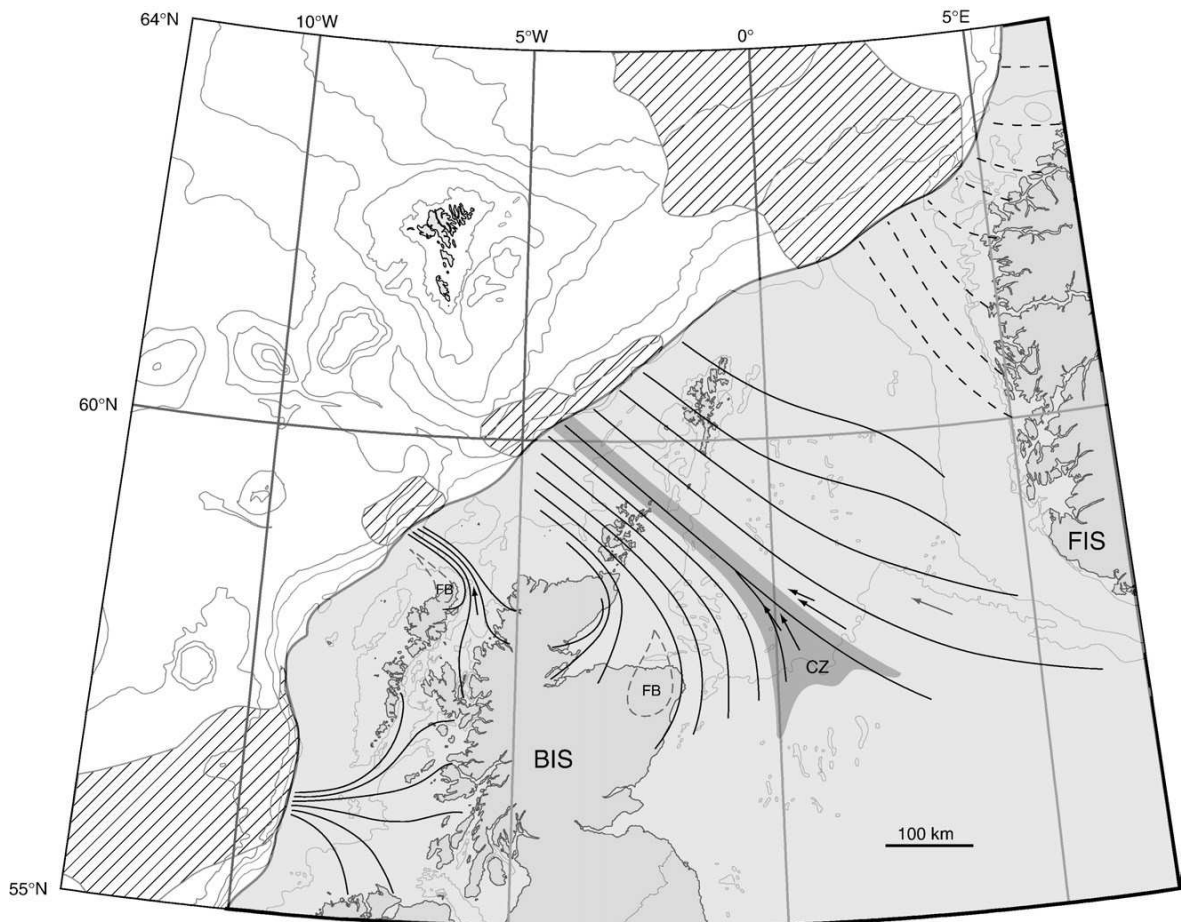


Figure 2.5. The reconstructed environment of the NW European ice sheet at 30–25 ka BP. Dark grey shading represents the zone of confluence (CZ) between the BIS & FIS (Bradwell et al., 2008b).

In terms of ice sheet thickness in Scotland, there was a general confidence that nunataks were protruding through the ice during the maximum glaciation in Scotland and that the upper limit of the ice sheet was marked by trimlines on the valley sides between the glacially moulded lower surfaces and the periglacially-weathered upper surfaces and summits (Ballantyne, 2002). More recently, it has been shown that non-glacial features can survive under cold-based ice masses which have limited erosional interaction with the underlying substrate (Fabel et al., 2002).

2.2.2.2 Last maximum glaciation in Romania

Although separated from the NW European ice sheet, the Romanian Carpathians (Figure 2.4) experienced multiple glacial advances throughout the Quaternary and there is evidence of past glaciations in all the three mountain ranges. Local geographic conditions influenced the glacier dynamics resulting in different glacial morphologies. To date there is limited knowledge about the timing of the last glaciations and intervening interglacials in the Carpathians, with existing glacial reconstructions based on a relative chronology reliant mainly on glacial landforms.

The Quaternary glaciations in the Romanian Carpathians have been researched since the end of the 19th century, with the pioneering work of H. Zapalowicz (1886), Lehman (1885), Czirbusz (1896), de Martonne (1924), Munteanu-Murgoci (1898), Athanasiu (1899), Szadeczky (1905, 1906) and Sawicki (1909, 1911), Kräutner (1930), Bleahu (1957), Sârcu (1963), Morariu (1981). On the basis of geomorphological evidence, the last glaciations in the Romanian Carpathians were characterized by cirque and valley glaciers, and where relief was favourable, occasional plateau ice masses formed. Through a combination of high altitudes, moisture from the Atlantic ocean to the west and a cold continental influence from the east, the northern part of the Romanian Carpathians (Rodna Mountains) had the longest valley glaciers, with lobes extending to as low as 700 m altitude (this study).

Absolute dating methods (e.g. surface exposure dating, OSL, IRSL) have been introduced in the last decades to help constrain the timing of glacial events in various parts of the country. Recent studies in the south-western part of the Carpathians (Retezat Mountains; Figure 2.2) have reconstructed three glacial advances, partially asynchronous with global climate records. Morphological and pedological investigations of the lowest moraines in Retezat Mountains indicate that an extensive maximum glaciation occurred well before the global LGM, presumably during the Early Devensian. Reuther et al. (2007) attempted to determine the glacial chronology using surface exposure dating but were hampered by the high degree of boulder weathering. It was argued that the maximum glacier advance occurred during MIS 4 (Early Devensian) rather than during MIS 2 (Late Devensian) as indicated by pollen analysis and deposition of loess (Cârciumaru, 1980). Significant climate cooling is also recorded by U/Th TIMS (thermo-ionisation mass spectrometry) of cave speleothems in north-west Romania with a discontinuity in carbonate growth during MIS 4 (Onac & Lauritzen, 1996; Tămaş & Causse, 2000/2001; Tămaş et al., 2005). The

lower temperatures during MIS 4 are in good agreement with other constraints using micromamals in cave deposits in south-eastern Romania (Rădulescu & Samson, 1992; Petculescu & Samson, 2001), and according to Constantin et al. (2007), a severe cold period is shown in a decrease in speleothem growth in the SW part of the Carpathians (Poleva Cave) between 40-35 ka, compared to the low temperatures of the global LGM (26-21 ka).

During the global LGM, the Romanian glaciers were less extensive and this was explained by the increased aridity in the Carpathians due to sea level being approximately 120-150 m lower than at present with a concomitant reduction in moisture sources for these mountains from the Mediterranean-, Marmara- and Black Seas (Major et al., 2006; Lambeck & Purcell, 2005; Kaplin & Selivanov, 2004). Conversely, the increased moisture released through the decay of the European ice sheet caused the glaciers in the Retezat Mountains to readvance during the Lateglacial, depositing moraines around 17-16 ka (Reuther et al., 2007).

2.2.3 Younger Dryas (YD)

The transition from glacial conditions of the Devensian to the warm Holocene interglacial was not uniform, both spatially and temporally. At the end of the Devensian glaciation an abrupt and severe cooling event, the Younger Dryas (YD), occurred in the high latitudes of the Northern Hemisphere, between 12.9 – 11.7 ka BP (Rasmussen et al., 2006; Lowe et al., 2008). It followed a warming period when large quantities of fresh water (ice-dammed meltwater, great amounts of icebergs from the Laurentide ice sheet and/or an increased amount of precipitation) reached the North Atlantic (Broecker, 2006). Generally, the Oceanic Polar Front lies to the north of the British Isles (Benn, 1997) but the input of fresh water caused abrupt shifts in sea surface and air temperatures resulting in a temporary slow down of the oceanic thermohaline circulation (Bond & Lotti, 1995; Bond et al., 1997). As less warmth was brought to the high latitudes of northwest Europe, the North Atlantic Polar Front migrated southwards to the latitude of northern Portugal. In addition recent studies have demonstrated that westerly winds also shifted abruptly during the YD winter season, likely due to the changes in sea ice conditions, and may be linked to the slowdown in the North Atlantic Ocean circulation and the cooling of the European climate (Li et al., 2005; Wunsch, 2006; Braconnot, 2007).

The YD is recorded in Greenland ice core records, thereby providing good age and duration control on this event and allowing European synchronicity to be established. It was one of the largest abrupt climate changes to have taken place within the last 100 ka (Alley, 2000). According to varved lake sediments in Western Germany, the YD was extremely abrupt (20-50 years), both at the beginning and at the end (Brauer et al., 1999). In spite of the short period of the YD, air and sea temperatures decreased to the level of the global LGM (Golledge, 2008), yet the ice extent across Europe was more limited and sporadically distributed across the continent. The landforms created during the YD glacial advance remain remarkably fresh as they have not been subsequently covered by ice advances and have been only superficially modified by postglacial processes.

During the YD, an extensive ice cap grew across the Scottish Western Highlands and several smaller ice caps were formed in other areas of Britain (Figure 2.6). The southern limits of the Scandinavian ice sheet lay across southern Norway, central Sweden and southern Finland (Humlum, 1997). The prominent moraines along the coast of Norway stand as evidence for renewed glacial advance from the higher elevation cirques (Larsen & Mangerud, 1981). Surface exposure ages from SW Finland confirm the deposition of moraines during the retreat of the YD Scandinavian ice sheet, with a mean age of 12.4 ± 1.5 ka (Beaulieu et al., 1994). YD glaciation in southern Sweden was restricted to cirque glaciers situated at very low altitudes in the Skärälid rock canyon, their survival having been dependent on topography and snow drift by easterly winds (Humlum, 1997). The Kleiner Arbersee area in the Bavarian Forest of Germany was completely ice free before the YD event as indicated by radiocarbon ages of basal lake sediments (Raab & Völkel, 2003). At this cold glacial episode, the Alps glaciers readvanced from smaller ice covered areas as indicated by samples (^{10}Be , ^{26}Al , pollen, varves) taken from moraines which yielded ages ranging within the YD stadial (Hormes et al., 2007). The Eastern Alps are thought to have been almost ice free throughout the Windermere interstadial and the YD is represented only by cirque glaciers at higher elevations (van Husen, 1997). The last major cooling phase before the warm Holocene was also recorded in the sediments of the Przedni Staw Lake in the Northern Carpathians (Lindner et al., 2003). Exposure dating of a moraine in the Ukrainian Carpathians indicates a YD deposition with a mean age of 12.1 ± 0.3 ka (Rinterknecht et al., 2011). YD glaciers have been reconstructed in the Romanian Carpathians based on ^{10}Be ages, pollen analysis and speleothems (e.g. Constantin et al., 2007; Feurdean et al., 2007; Reuther et al., 2007).

2.2.3.1 Younger Dryas in Scotland

The YD period of abrupt climate cooling led to a short-lived ice readvance in Scotland known locally as the Loch Lomond Stadial (LLS) (12.9 ka - 11.7 ka cal. yr BP; Lowe et al., 2008). Substantial research has been undertaken to reconstruct the ice extent and pattern of deglaciation during this time (e.g. Sissons, 1974; Golledge, 2008; Ballantyne, 2010). Recent applications of surface exposure dating to landform assemblages from the YD period have constrained the temporal limits of this last glacial advance and allowed for a better understanding of the spatial variability of ice across Scotland at that time.

Generally, landform assemblages in the Highlands relate to a distinct phase of valley glaciation with clear end moraines, boulder spreads or drift limits marking the maximum distribution of YD glaciers (Sutherland, 1984). Only limited topographic change has occurred since the YD, so that glacial landforms are better preserved with little of the glaciifluvial masking of deposits that occurred during the wasting of the larger Devensian ice sheet (Sissons, 1978, 1979a; Ballantyne, 1989; Benn & Ballantyne, 2005; Finlayson, 2006; Lukas & Benn, 2006). Periglacial trimlines can be observed on slopes, marking the transition from glaciated areas to upper ground that escaped glaciation but were intensively weathered in an extremely harsh periglacial environment (Ballantyne & Kirkbride, 1987).

Similar to the LGM, the high mountain area around Rannoch Moor acted as the major accumulation centre for the growth of the main YD Highland ice cap (Figure 2.6; Golledge & Hubbard, 2005; Golledge, 2008). Other smaller independent ice masses occupied corries, glens and several plateaux in the west and northwest Highlands, Grampians, and Cairngorms (Sissons, 1973; Gordon & Sutherland, 1993; Benn, 1997).

Precipitation and snow accumulation declined strongly eastward due to the distance of plateau accumulation areas from the western maritime air masses (Everest & Golledge, 2004), starving these areas and this is reflected in smaller and higher ice fields to the east (Sissons, 1979a; Hubbard, 1999). An eastward rise in the equilibrium line altitude was recorded between the Western Highlands ice cap and the Cairngorms, indicating a strong precipitation gradient across Scotland, likely much stronger than today (Sissons, 1980; Benn, 1997). At present, winds from the SW bring moderate or strong precipitation to the west of Scotland, and often very slight or no precipitation in the east. This gradient is likely to have occurred during the YD, although stronger SW winds added considerable snow, especially in areas sheltered from insolation. Sissons (1980) also argued that snow-bearing

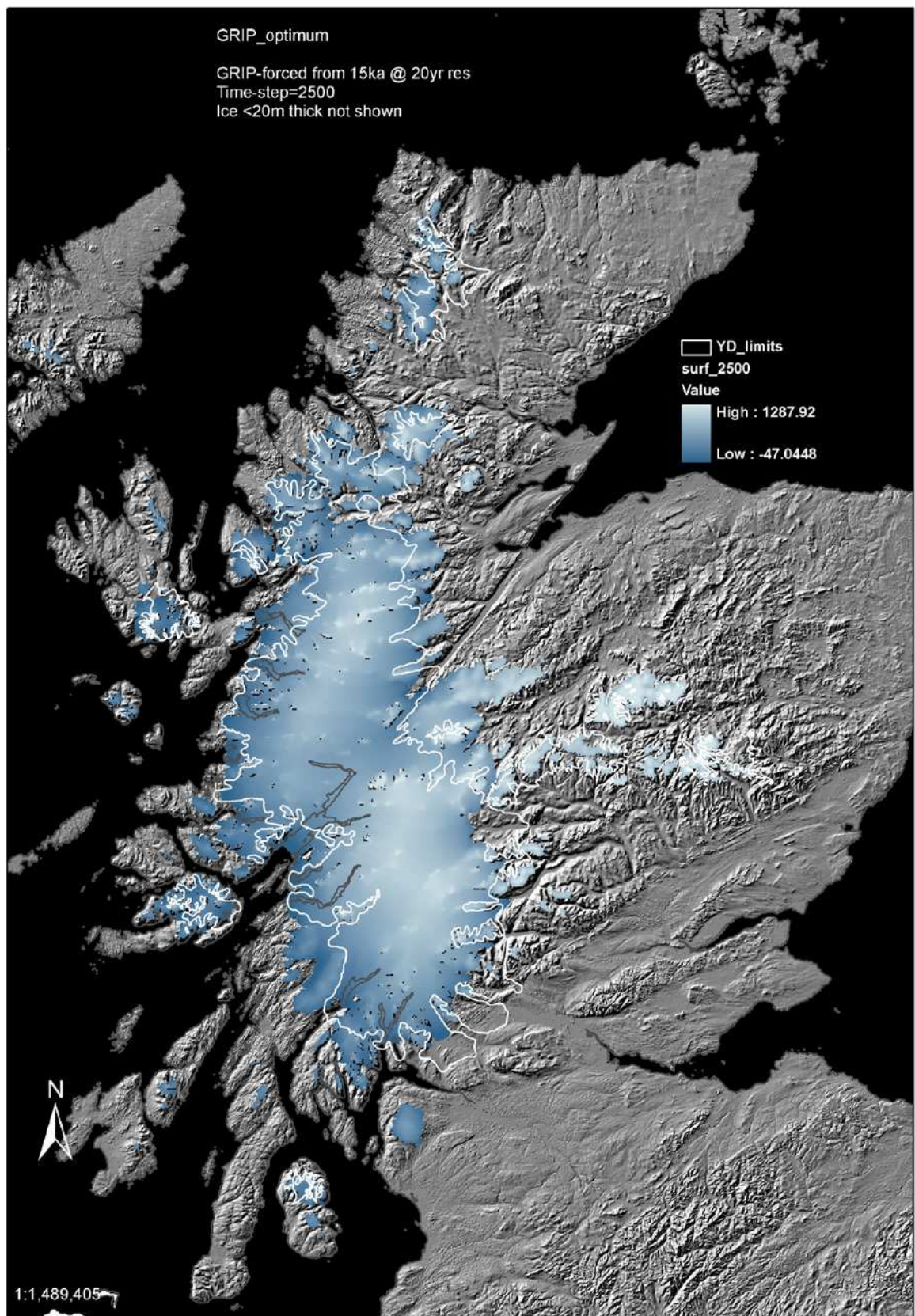


Figure 2.6. Model of maximum ice extent in Scotland during the Younger Dryas episode (Golledge et al., 2008).

winds were south-easterly whilst transfer of snow was by westerly and south-westerly winds. Despite its shortness (~1.2 ka), the mean July sea level temperature in Western Scotland was ~6-7°C, roughly 6°C below the modern values, and the mean annual

temperatures over Scotland during the YD registered a decrease of ~8-10°C (Sissons & Sutherland, 1976; Atkinson et al., 1987; Benn, 1997; Hubbard, 1999).

A rapid northwards migration of the North Atlantic Polar Front ended the YD stadial. However, the ice decay occurred as two phases: an initial phase of active deglaciation due to a fall in precipitation with interrupted retreat of ice, followed by an abrupt rise in air temperature (Atkinson et al., 1987) resulting in uninterrupted retreat and *in situ* ice stagnation at the end of the stadial (Benn et al., 1992; Bennett & Boulton, 1993; Benn, 1997; Brooks & Birks, 2000). Temperatures thereafter increased at a relatively rapid pace, around 1.7-2.8°C per century (Atkinson et al., 1987).

2.2.3.2 Younger Dryas in Romania

Pollen analyses in different areas of the Romanian Carpathians indicate climate change through vegetation migration patterns at the end of the last glacial cycle. Recent studies of lake sediments at intermediate elevations (ca.750 m) in north-western Romania (Gutâi Mountains) show a broad synchronicity with the present climate, with three periods of cold and dry climate, separated by warm and humid periods during the Lateglacial between 14.7-11.5 ka (Feurdean & Bennike, 2004; Feurdean et al., 2011).

The exposure ages of the Younger Dryas readvance in Retezat Mountains (13 – 11 ka), generated from boulders on moraines, correlate well with results from other mountains in Romania. According to Fărcaș et al. (1999), Reuther et al. (2007) and Björkman et al. (2002) forest vegetation gave way to open vegetation communities between 12.9-11.5 ka in the lower Reteza as well as west of Rodna, in Gutâi Mountains (Figure 2.2). This occurred coevally with the Younger Dryas glacier readvances at higher altitudes. The deposition of a speleothem in south-western Romania resumed at ~ 11.4 ka when rapid growth began at the beginning of the Holocene period (Constantin et al., 2007).

The abrupt increase of mean temperatures by at least 5-6 °C at 11.5 ka marks the beginning of the Holocene. This significant warming, within less than 15 years (Berner & Streif, 2000, cited by Terhürne-Berson, 2005), and increase of moisture availability is marked by the response of the terrestrial vegetation at Preluca Țiganului, north-western Romania (Feurdean & Bennike, 2004).

2.3 Outline of missing information

This thesis sets out to establish the environmental conditions in Europe during the last glaciation and to test the climate synchronicity from Scotland to Romania.

There is currently limited information regarding the pattern and timing of deglaciation of the Late Devensian ice sheet. Moreover, the spatial extent of the ice masses that reoccupied the Monadhliath Mountains during the Lateglacial has not been well established. A plateau ice cap and cirque glaciers have been predicted through numerical modeling to have covered the study area during the Younger Dryas (Golledge, 2008). However, there are no constraints on the timing of this short cooling episode.

At present, the main difficulty lies in a lack of sufficient glacial records in the Romanian Carpathians. Establishing the long-term glacial chronology in this region could provide important information in identifying the strongest influencing factors and their role in the regional distribution of temperature and precipitation. Moreover, the complex transmission of the climatic signals from high latitude maritime climates to lower latitude continental climates across Europe is currently not well understood.

Chapter 3

Methods

3.1 Introduction

In order to increase our understanding of the climatic changes during the Devensian glaciation in the Monadhliath and Rodna Mountains, it is necessary to identify the geomorphological signature and the chronological sequence of glacial events in these two areas. The glacial landforms in both areas have been partially mapped before by various authors and the aim of this project is to improve and provide new interpretations of the geomorphological evidence and set these within a chronological framework. As the temporal limits of the glaciations have never been securely established, I used surface exposure dating to constrain the deglaciation history of the Monadhliath and Rodna Mountains. This chapter begins with a description of the geomorphological mapping based on remote sensing and field mapping. Most of the chapter will detail the application of surface exposure dating, a useful technique to accurately constrain the timing of various processes. The three methods used for estimating the Equilibrium Line Altitude (ELA) employed in the glacial reconstructions will be discussed at the end of the chapter.

3.2 Remote sensing

Remote sensing was initially used to map the geomorphology of the study areas. It supplied the spatial data necessary to understand the glacial landform distribution and pattern before ground-truthing. Once the distribution of moraines and glacially modified bedrock surfaces were identified, sites were selected for surface exposure dating using the *in situ* produced cosmogenic nuclide ^{10}Be .

I used Ordnance Survey of Britain topographical maps (1:25 000), air photographs (1:24,000; RCAHMS), and high resolution digital elevation models (DEM) from the NEXTMap database for Scotland (5m horizontal resolution). The hillshaded DEMs were created with artificial illumination from various angles using ESRI's ArcGIS v. 9.3. Given that good satellite imagery was not available for Romania, I used topographical maps (1:50 000; DTM, DIMAP), orthophotomaps (1:5000; ANCPI), Aster data (NASA) (30m horizontal resolution) and SRTM imagery (90m horizontal resolution; NASA). A digital elevation model (DEM) for Rodna Mountains was interpolated from the contour line elevations of ASTER imagery (30 m horizontal resolution; NASA) and used as the base for the geomorphological maps.

3.3 Field mapping

Geomorphological maps were essential to establish the relative positions, altitudes and composition of the various glacial landforms within each study area and to identify suitable places to sample for surface exposure dating. Mapping in Scotland was carried out between October 2007 and May 2010, whilst mapping in Romania was carried during the 2008 and 2009 summers. The field mapping verified and refined the maps created from remotely sensed data, and identified new ice limits and geomorphological associations; rock samples were collected from glacial landforms. Contour lines were created from the NEXTMap dataset for Britain and the ASTER DEMs for Romania and compiled with the geomorphological mapping in the ESRI's ArcGIS 9.3. The maps were then improved in Adobe Illustrator CS and are presented and discussed further in Chapter 4, Figure 4.5 for the Monadhliath Mountains, and Chapter 5, Figure 5.5 for the Rodna Mountains. The geomorphological maps are also presented in Appendix C for both study areas.

3.4 Surface exposure dating

Surface exposure dating (SED) is a technique that utilises the concentration of cosmogenic nuclides produced in minerals at the surface of the Earth to directly date landforms (Cerling & Craig, 1994). Several stable and radioactive terrestrial cosmogenic nuclides (^{21}Ne , ^3He , ^{10}Be , ^{26}Al , ^{14}C , ^{36}Cl) are formed *in situ* in the lithosphere by secondary cosmic radiation (Lal, 1991). The concentration, rate of production, and rate of decay of terrestrial cosmogenic nuclides (TCN) are used to determine exposure ages, burial ages, or erosion rates of rocks and sediment for a variety of landforms and geomorphological processes such as deglaciation, landslides, formation of fluvial terraces, sediment transport and deposition rates, volcanic eruptions, uplift and incision rates, on timescales of 10^3 – 10^7 years (Masarik & Reedy, 1995).

The occurrence of TCN in the Earth's surface minerals and their potential as a dating tool was first suggested by Paneth et al. (1952) and Davis & Schaffer (1955), while Lal and Peters (1967) demonstrated that the concentration of some of these nuclides could be determined. However, the 'routine' measurement of extremely low concentration of naturally occurring radioactive cosmogenic nuclides (a few thousand atoms per gram) has only been possible through advances in accelerator mass spectrometry (AMS) in the early 1980s (Elmore and Phillips, 1987; Gosse & Phillips, 2001; Freeman et al., 2004, 2007).

In this study, we used the *in situ* produced cosmogenic nuclide ^{10}Be , which is formed in quartz, for constraining the deglaciation histories of the two field areas. This section will discuss the basic theory of the TCN method, and the advantages and uncertainties of its application.

3.4.1 Cosmic radiation

The Earth is exposed to a constant stream of cosmic radiation (CR) from all directions. The chemical and isotopic composition of matter exposed to cosmic radiation is subject to various changes. Cosmic radiation refers to particles that have been accelerated to almost light speed by the expanding shock waves produced from short lived supernovae explosions within our galaxy (Gosse & Phillips, 2001). There are approximately three supernovae per century occurring in the Milky Way galaxy providing the Earth with a

constant cosmic ray flux (Lal, 2007). Solar cosmic rays, produced in our solar system, have energies of 1-50 MeV depending on the solar activity. Stronger than the solar rays as they originate from outside our solar system, the galactic cosmic rays have energies of up to 100 GeV and can penetrate deeper into the Earth's atmosphere, producing more terrestrial cosmogenic nuclides at the Earth's surface (Cerling & Craig, 1994). CR undergoes various interactions and transformations on the way to Earth as it passes through the heliosphere, the magnetic field of the Earth and the Earth's atmosphere. The geomagnetic field of the Earth has the strongest influence over the cosmic ray flux.

3.4.1.1 Primary cosmic rays

Primary Cosmic Rays (PCR) are stable charged particles and consist mainly of highly energetic protons (~87%) and α particles (~12%) (Cerling & Craig, 1994; Dunai, 2010). The energy spectrum and composition of high-energy galactic cosmic rays is modulated by Earth's magnetic field and to a lesser degree by the Sun's magnetic field (= heliosphere) that is carried by solar winds amongst the planets of the Solar System and is governed by the Sun's 11 year solar cycle (Lal & Peters, 1967; Lal, 1991; Pigati & Lifton, 2004).

3.4.1.2 Secondary cosmic rays

The PCR are able to travel to Earth from their far-off sources because the space matter has low density. As they approach the Earth, the PCR interact with atmospheric matter and produce nuclear disintegrations in the upper atmosphere, depending primarily on the total nucleon flux (Lal, 2000). The high-energy collisions between PCR and other particles (e.g. gas molecules present in the atmosphere) result in the production of secondary cosmic rays (SCR). They include very high energy particles, mainly nucleons (e.g. protons, neutrons) and mesons (kaons, pions and muons) (Cerling & Craig, 1994; Gosse & Phillips, 2001). A cascade of collisions (Figure 3.1) occurs when the newly created particles move through atmospheric matter, producing more secondary cosmic rays. As a result of these collisions SCR have typically less energy than PCR, and slow down towards the surface of the Earth. Typical attenuation lengths of cosmic ray neutrons are 160 g cm^{-2} .

When hitting the Earth, these particles produce stable and radioactive nuclides in minerals exposed in the top few metres of surface. Most of the *in situ* cosmogenic nuclides are produced through the interaction of secondary galactic cosmic rays with terrestrial rocks because they have higher energies than solar cosmic rays and can therefore penetrate deeper into the Earth's atmosphere and crust, with sufficient energy to create nuclear interactions.

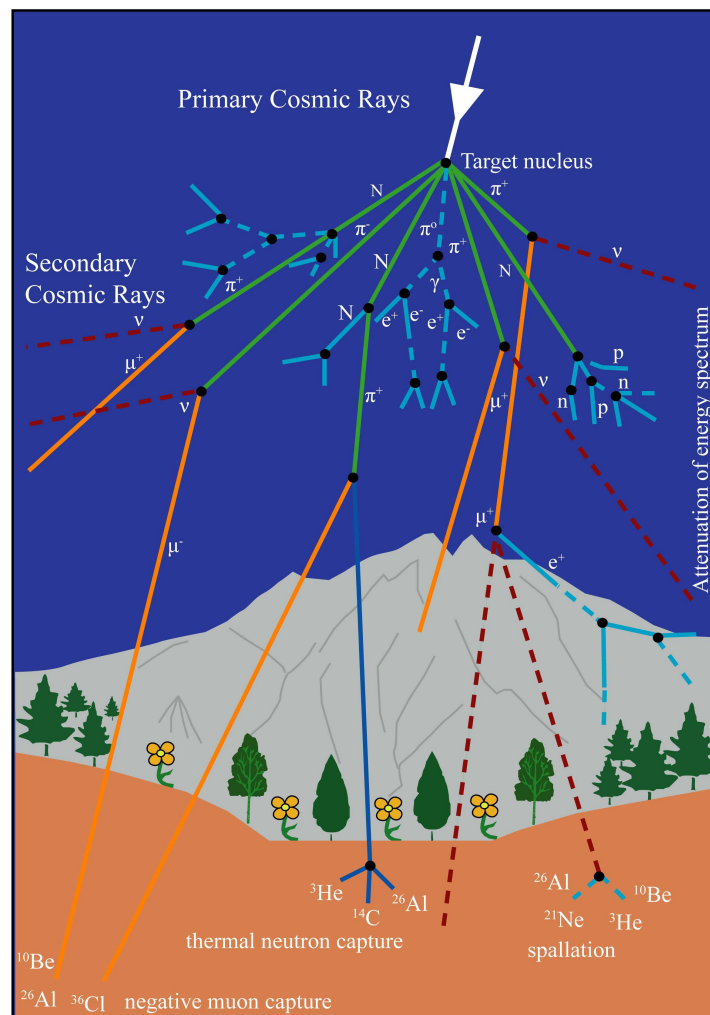


Figure 3.1. Cosmic ray cascade in the atmosphere and lithosphere (γ = gamma ray, μ = muon, π = pion, e = electron, n = neutron, p = proton, ν = neutrino, N = nucleon). Modified from Gosse & Phillips (2001) & CERN (2003).

The flux of cosmic rays to Earth's surface largely depends on the temporal changes in the Earth's geomagnetic field (Dunai, 2001). A weaker magnetic field allows greater penetration of cosmic rays into the atmosphere which consequently increases the production of cosmogenic nuclides (Cerling & Craig, 1994). Due to the present geomagnetic field configuration (axial dipole), stronger deflection of the cosmic particles occurs at the equator than at higher latitudes (Masarik, 2001) where the field lines are

nearly perpendicular to the Earth's surface so that charged particles of all energies reach the atmosphere almost undisturbed at geomagnetic latitudes above ca. 58° latitude (Lal, 1991; Lal and Peters, 1967; Gosse & Phillips, 2001). Therefore, the production of TCN at sea level is almost double at the poles than at the equator.

Deflection of the incoming cosmic radiation is also determined by the particles' magnetic rigidity (momentum per unit charge) (Lal & Peters, 1967; Masarik, 2001). The cosmic ray cutoff rigidity refers to the minimum energy needed for a particle in the upper atmosphere to penetrate the Earth's magnetic field at certain latitudes (Lal, 1988). Particles are accepted, deflected or attenuated based on their energy to penetrate the Earth's magnetosphere (Pigati & Lifton, 2004; Masarik, 2001). The cutoff rigidity of cosmic particles is also a function of the angle of incidence of cosmic rays on a surface.

When interacting with the atmospheric particles, the cosmic ray flux is attenuated and decreases exponentially (Lal, 1991). The attenuation length refers to the thickness of the mass through which the particles are travelling and it depends on the geomagnetic coordinates and the atmospheric depth. As the attenuation length of cosmic particles is higher at low latitude, higher rigidities are needed in order for particles to reach lower latitudes than at higher latitudes. The cosmic rays are exponentially attenuated between an atmospheric depth of 150 g cm⁻² at geomagnetic latitudes 60-90° and up to 220 g cm⁻² at the equator (0-10 km altitude; Lal, 1991).

Secondary cosmic ray flux at the Earth's solid surface also depends on atmospheric shielding as air pressure is not uniformly distributed and the cosmic ray intensity decreases exponentially with atmospheric depth. Thus the cosmic ray flux increases with increasing altitude due to a decrease in air pressure, and as a consequence the nuclide production rates increases with altitude (at a rate of about ~1%/10m at low altitude) (Lal and Peters, 1967; Lal, 1991; Stone, 2000).

3.4.2 Scaling factors and production rates

The accumulation of cosmogenic nuclides cannot be used to date any event unless we know the rates at which they are produced, both now and in the past. To convert the concentration of TCN in a rock sample to an exposure age requires an accurate knowledge of the nuclide production rate (Schaefer & Lifton, 2007). The production rate of TCN depends mainly on the cosmic ray flux, which is influenced by geographical location (latitude, longitude and altitude) and temporal variations in solar activity, the geomagnetic field strength, and atmospheric pressure. As a result of the latter three, the production rate of the nuclides is not uniform across time. Local shielding from the cosmic ray flux by topography and sample thickness must also be taken into account. The following section will consider various altitude and latitude scaling methods, sample shielding, and the global reference production rate.

3.4.2.1 Scaling factors

In order to estimate the exposure time of a surface to cosmic radiation accurate rates of local nuclide production need to be known (Lal, 2000; Stone, 2000; Gosse & Phillips, 2001). To compare data from different geographical locations requires corrections for the site-specific latitude, longitude and altitude according to production rates at sea-level and high latitude (SLHL) (Lal, 1991; Gosse & Phillips, 2001). There are currently several scaling methods in use. They are based on experimental measurements of neutron flux in the atmosphere, photographic emulsions, water targets and cloud chambers (Gosse & Phillips, 2001; Dunai, 2010).

The model of Lal (1991), based on the nuclear disintegrations of Lal & Peters (1967), provided the first latitude and altitude scaling factors to describe cosmic ray flux variations at the Earth's surface. The model implies that the Earth's magnetic field has an axially-symmetric purely dipole shape and does not include temporal changes of the Earth's magnetic field and its ability to deflect primary cosmic rays (Desilets, 2005). The intensity of the magnetic field is different from one area to another on Earth; however, the periods of time over which contemporary studies were applied (e.g. Nishiizumi et al., 1989) did not present significant variations. Lal's (1991) model presents a uniform relationship between latitude and altitude without considering the spatial variations in atmospheric pressure.

Stone (2000) based his work on Lal's model (1991) and includes revisions of the contribution by muons to TCN production, and the spatial differences in global surface air pressure, which affects the regional variation in TCN production rates by increasing/decreasing the flux of cosmic rays at the Earth's surface. This model does not include temporal magnetic field strength variations but allows for regional deviations in atmospheric pressure to be included in the production rate calculations. For example, Antarctic air pressure for the last 40 years is on average 25 hPa lower than over other continents, a depression which is likely to have been present during the past glaciations.

Another scaling method was developed by Dunai (2000) who takes into account the variations in the magnetic field intensity and in the atmosphere (i.e. climatic variation, anomalous pressure system) but assumes that the energy spectrum of cosmic rays is independent of altitude (Desilets, 2005). The model integrates the effect of non-dipole field components on the original neutron monitor data used by Lal (1991) and Stone (2000) at sea level. As a consequence, the results obtained by Dunai are up to 30% lower than those of Lal's whose scaling scheme took into account a high muon contribution.

Scaling factors for the production rates of TCN were also derived by Zreda et al. (1991), Masarik & Reedy (1995), Desilets & Zreda (2003), Lifton et al. (2005, 2008) and Desilets et al. (2006) but have not been widely used. They all use the same data set but with different description of the geomagnetic field, atmospheric pressure, and with/without secular variations (Dunai, 2010).

3.4.2.2 Shielding factors

Topography and other local obstructions

Cosmic radiation is equally distributed on a wide, flat and horizontal surface on Earth. However, when any obstruction occurs, the cosmic radiation is reduced and the surface receives only a reduced amount of the total incident radiation. Therefore, it is necessary to correct the production rate of TCN for shielding of the sampled surface. If the shielding is not taken into account, the diminished cosmic ray flux will lead to unrealistic production rates, and the smaller nuclide concentrations will implicitly produce erroneously young exposure ages.

Shielding could be due to the surrounding topography (e.g. high mountains, large rocks, steep valley sides), dipping sample surface, vegetation, sediment, snow or water (Dunne et al., 1999). Sampling for surface exposure dating would be ideal in a non-shielded environment, where surfaces are smooth and horizontal and the inclination angle to the horizon is 0° for the full 360° rotation (Figure 3.2). Slope angles of 25° or less are not very significant (Dunne et al., 1999), for example, a flat surface on the bottom of a cone with 45° slopes still receiving 80 % of the cosmic ray flux (Gosse & Phillips, 2001).

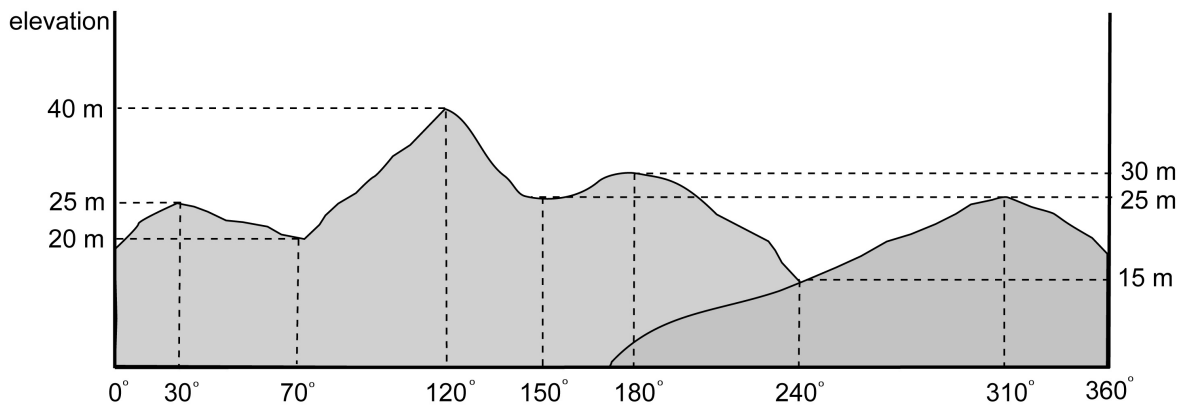


Figure 3.2. Diagram showing how to determine topographic shielding for a sampled surface using the measured azimuth and inclination angle at major breaks in slope of the surrounding topography.

The measurement of the topographic shielding effect on sampled surfaces is defined by compass bearing and clinometer measurements to the horizon. The topographic obstruction of the cosmic radiation on horizontal surfaces is derived by calculating the ratio of the present radiation flux in the sampled area to the maximum radiation flux that would be possible if the sky was not blocked by the surrounding topography (Dunne et al., 1999; Gosse & Phillips, 2001). The following formula is used for calculating the shielding factor:

$$S = 1 - \frac{1}{360^\circ} \sum_{i=1}^n \Delta\Phi_i \sin^{m+1} \theta_i \quad (1)$$

where S is the shielding factor for a series of n obstacles, each with a corresponding inclination angle θ_i , with an extent through an azimuth, $\Delta\Phi_i$, and m is 2.3, an experimentally determined constant (Dunne et al., 1999).

Sample thickness

The production rate of the TCN generally refers to the amount of nuclides formed at the top surface of the sample. The samples taken for this study were generally <3 cm thick which results in a < 3% reduction in nuclide production over the integrated sample depth (Figure 3.3).

Other factors

Production of cosmogenic nuclides depends on the shape, size and position of the target surface. Rounded boulder surfaces may receive a limited cosmic flux and consequently the production rate of nuclides will be 10-12% lower than wider flat surfaces (Masarik & Wieler, 2003). The samples in this study were collected from large and horizontal boulder surfaces and no corrections were needed for the exposure ages we produced.

The samples in the present study were taken from the top surface of boulders or from flat bedrock surfaces where vegetation did not obstruct. Corrections for potential snow cover were not applied as winter snow-cover history is difficult to constrain, however, samples were collected from the top surface of prominent upstanding boulders to minimise this effect. They are unlikely to have accumulated peat, or retained soil, since deglaciation.

3.4.2.3 Production rates

TCN are produced through three reactions between the high energy nucleons and the target nuclei in rocks exposed to cosmic radiation: spallation, thermal neutron capture and muon induced nuclear disintegrations, mainly by negative muon capture (Lal, 1991).

The nuclear spallation of cosmic ray particles occurs both in the atmosphere and in surface rocks (> 40 MeV; Lal, 1991) and refers to the collision of high-energy nucleons and the target nuclei. This nuclear reaction breaks apart the target atoms causing the formation of new lighter particles, such as protons and neutrons, which are expelled leaving behind a lighter nucleus with a smaller atomic number.

Negative muon capture reaction occurs when a negative muon enters into the target, slows down proportionally to the material density and is captured by a proton, generally resulting in production of a neutron and a neutrino, and sometimes a gamma photon. Due to the greater penetrating ability of muons compared to neutrons, negative muon capture occurs deeper in the Earth where it becomes dominant over spallation (Niedermann, 2002; Gosse & Phillips, 2001). Although at the surface muons produce only up to 3% of the total nuclides in a sample at high latitude and sea level, and even less at high altitudes (Bierman et al, 2002), the production rate due to muons is nonetheless taken into consideration in exposure ages studies.

Lal et al. (1960) marked the start of quantifying cosmogenic nuclide production rates by direct measurements of nuclide production in artificial targets exposed to cosmic radiation at mountain altitudes. The first measurements of cosmogenic nuclides in geological material were made to establish the exposure/burial history of Libyan desert glass by Klein et al. (1986). Cosmogenic nuclides were also directly measured in independently dated, high altitude, glacially polished bedrock surfaces in the Sierra Nevada (Nishiizumi et al., 1989). This seminal study set the scene for all calibration studies that followed. Geological calibration was continued by using surfaces with independently well-constrained ages (i.e. radiocarbon and thermo-luminescence dating), such as landslide exposures and lava flows (Kubik et al., 1998; Stone et al., 1998; Schaefer & Lifton, 2007; Putnam et al., 2010). Other methods of determining TCN production rates include prediction from a numerical simulation based on probabilities of the nuclear interactions involved in the production of TCNs (Masarik & Reedy, 1995). Nishiizumi et al. (1996, 2007) refined production rates of ^{10}Be and ^{26}Al in quartz through experimental laboratory measurements in targets of known nuclide concentration and by exposing target materials to cosmic rays at high elevations.

The calibration process has evolved over the last two decades and a global calibration data set has been established (Balco et al., 2008). The production rates of ^{10}Be derived for different scaling models, as used in the CRONUS-Earth online calculator version 2.2, are presented in Table 3.1. Production rates of different cosmogenic nuclides are generally known at present but are continuously being refined through the development of accurate and reliable local calibration sites. Recent studies have highlighted that the reference production rates derived from the global calibration data set are not necessarily appropriate in different local settings. Therefore, there is a general need to improve the quality and coverage of TCN production rates from local calibration sites (e.g. Balco et al., 2009; Putnam et al., 2010).

Table 3.1. Spallogenic production rates of ^{10}Be at sea level and high latitude (Balco et al., 2008).

Scaling models	$^{10}\text{Be}^b$ (at $\text{g}^{-1} \text{a}^{-1}$)
St	4.49 ± 0.39
De	4.41 ± 0.52
Du	4.43 ± 0.52
Li	4.87 ± 0.48

^a Scaling models: St = Lal (1991) / Stone (2000); De = Desilets et al. (2006); Du = Dunai (2000); Li = Lifton et al. (2005);

^b Using ^{10}Be half-life of 1.38 Ma (Korschinek et al., 2009; Chmeleff et al., 2009)

The production rate of nuclides changes depending on the geographical coordinates, altitude, shielding, the density of the rock, the depth of the sample and the length of time a sample has spent at or near the surface (Lal, 1991; Cerling & Craig, 1994).

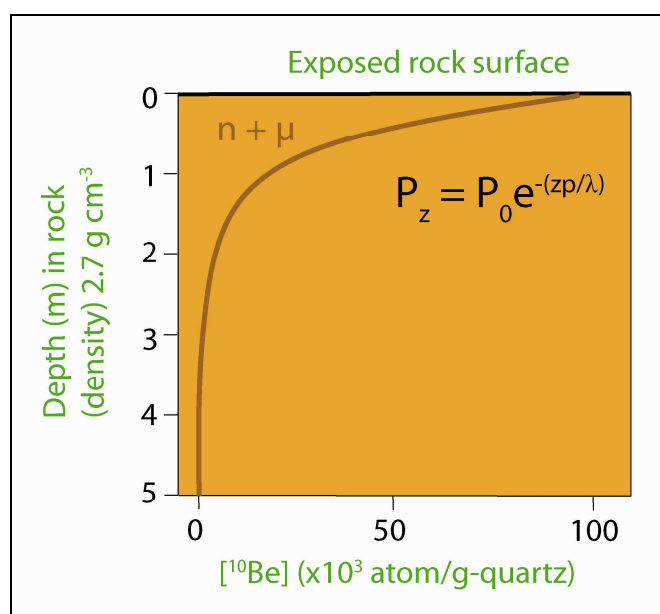


Figure 3.3. Exponential decrease of the ^{10}Be production rate. P = production rate, z = depth (cm), 0 = Earth's surface, ρ = rock density (g/cm^3), λ = attenuation length of cosmic rays in rocks (g/cm^2) (Lal, 1991).

The concentration of fast neutrons in the Earth's surface decreases exponentially with depth (Figure 3.3; Gosse & Phillips, 2001). The distance of penetration is determined by the density of the material. In rock of density $2.7\text{g}/\text{cm}^3$, over half of the radiation flux is attenuated within ~ 60 cm (assuming a cosmic ray attenuation length of $160\text{g}/\text{cm}^2$) and at 300 cm depth less than 1% of the surface neutron flux remains (Lal, 1991).

The attenuation length is also latitude/altitude dependent as geomagnetic field and the atmosphere change the energy of the cosmic radiation (Lal, 1991; Gosse & Phillips, 2001).

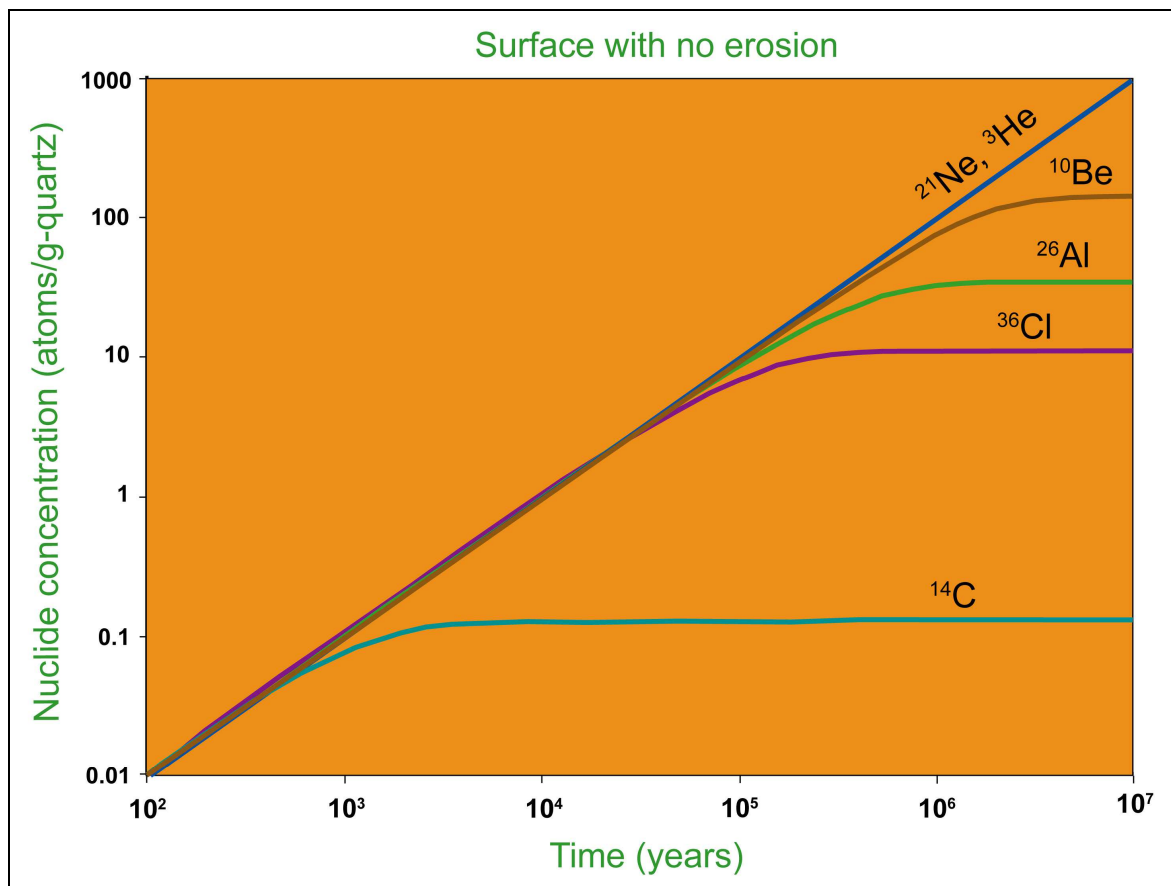


Figure 3.4. Concentration of *in situ* cosmogenic nuclides against time in the case of constant production rates (Lal, 1991; Granger & Muzikar, 2001).

The concentration of the radioactive nuclides in a continuously exposed surface will eventually reach saturation when the activity of the nuclide equals the rate of the radioactive decay of the nuclide in the sample (Figure 3.4). This secular equilibrium is reached after about four or five half-lives of each nuclide (Table 3.2) and effectively sets the upper limit of the surface exposure dating technique for different radionuclides.

Table 3.2. Target element and half-life of the commonly used cosmogenic nuclides in the geosciences (Cerling & Craig, 1994; Niedermann, 2002).

Nuclide	Main target elements in the lithosphere	Half -life
^3He	O, Si, Al, Mg	stable
^{21}Ne	Mg, Na, Si, Al	stable
^{10}Be	O, Si, Al	1.38×10^6 yrs
^{26}Al	Si, Al	0.71×10^6 yrs
^{36}Cl	Cl, K, Ca	0.30×10^6 yrs
^{14}C	C, O	5730 yrs

3.4.3 *In situ* cosmogenic ^{10}Be production

Radioactive ^{10}Be is a naturally occurring isotope and is the longest-lived of the seven known unstable isotopes of Be (Bierman et al., 2002). It is predominantly produced by cosmic ray spallation reactions of fast nucleons with oxygen in the atmosphere and in surface terrestrial rocks. Atmospheric ^{10}Be can be transported through precipitation and can contaminate terrestrial samples by adhering to quartz surfaces. Since a greater amount of ^{10}Be is produced in the atmosphere (ca. 1 million atoms $\text{cm}^{-2} \text{yr}^{-1}$) than *in situ* in terrestrial materials (ca. 2–20 atoms $\text{g-quartz}^{-1} \text{yr}^{-1}$) (Willenbring & Blanckenburg, 2010), for surface exposure dating using *in situ* produced ^{10}Be , the removal of the meteoric ^{10}Be through repeated acid etching is very important (Kohl & Nishiizumi, 1992).

In situ produced ^{10}Be can be formed in most minerals but for surface exposure dating it is most widely analysed in quartz and to a much lesser extent in olivine. Quartz can be found almost everywhere on the planet and has a simple composition (SiO_2) with a uniform oxygen content. It can be relatively easily separated from other minerals and cleaned from atmospheric ^{10}Be (Bierman et al., 2002). The main spallation target in quartz is oxygen by the reaction $^{16}\text{O} (n, 4p3n)$ to ^{10}Be (i.e. the removal of four protons and 3 neutrons from the oxygen-16 target nucleus). The global reference *in situ* production rate of ^{10}Be is 4.49 ± 0.39 atoms/ g-qtz/yr . The relatively long ^{10}Be half-life of 1.387 ± 0.012 Ma (Chmeleff et al., 2009; Korschinek et al., 2009) makes it suitable for cosmogenic dating of samples up to 4–5 Ma in age (Schaefer & Lifton, 2007). ^{10}Be decays via β electron emissions (Bierman et al., 2002) to stable Boron-10.

3.4.4 Sampling considerations and limitations

Accuracy of surface exposure dating depends on all the factors which influence the production rate of TCN, sampling strategies and the environmental conditions (Gosse & Phillips, 2001). There is often a limited availability of sampling sites and sufficient target minerals in samples. Adequate sampling places include surfaces with no significant sign of chemical/physical weathering (<3 cm). In order to reduce the uncertainties related to sample selection for constraining deglaciation histories, samples were collected from large stable boulders on the top crest of moraines (the least likely to have moved since deposition) or from bedrock surfaces that have been glacially eroded (abraded or plucked)

and no postglacial erosion. Several samples were collected from the same landforms where possible, so that exposure ages can be tested for consistency. There is also uncertainty regarding the exposure history of the sampled rocks in terms of inheritance of the nuclides from previous exposure periods and possible burial (shielding). Due to the deeply penetrating muons, pre-exposure erosion of the surfaces should be rapid with $> 2.5\text{m}$ removed in order to reset the cosmogenic clock to zero and avoid an inherited component in the measured cosmogenic nuclide concentration. Unrecognised inheritance leads to higher nuclide concentrations and therefore overestimates the exposure duration, whilst post exposure erosion removes material, including cosmogenic nuclides, thus reducing the nuclide concentration and underestimating apparent exposure ages (Bierman et al., 2002). Spatial or temporal shielding of cosmic radiation results in lower neutron flux and production rate, again leading to underestimated exposure duration.

In this study we sampled surfaces that appeared to be minimally affected by erosion, snow and vegetation cover over the entire exposure duration. Some of the glacially polished surfaces that we sampled indicate negligible surface erosion, but may indicate protection under till.

Rock samples (2-3 cm thick) were collected by hammer and chisel from boulders at or near the crest of moraine ridges and from glacially abraded bedrock surfaces. Location and elevation of the samples were determined in the field using a hand-held global positioning system (Garmin GPSMap60CX).

3.4.5 Exposure ages

Samples were processed by the author for ^{10}Be measurement at the Glasgow University – Scottish Universities Environmental Research Center (GU – SUERC) Cosmogenic Isotope Laboratory, following procedures adapted from Kohl & Nishiizumi (1992) as outlined in Appendix A. Pressed AMS targets were measured at the SUERC AMS Laboratory on the NEC 5MV Pelletron (Freeman et al., 2007). The nuclide concentration is provided as the ratio between ^9Be (stable) and ^{10}Be (radioactive) (Appendix B). Measured Be ratios were converted to nuclide concentration in quartz (N_{10}) using the equation:

$$N_{10} = \frac{[(R_{10s} \cdot C_{10s}) - (R_{10p} \cdot C_{10p})] NA}{qtz \cdot MBe} \quad (2)$$

$$\sigma N_{10} = N_{10} \cdot \sqrt{\left(\frac{\sigma R_{10s}}{R_{10s}}\right)^2 + \left(\frac{\sigma C_{10s}}{C_{10s}}\right)^2 + \left(\frac{\sigma R_{10p}}{R_{10p}}\right)^2 + \left(\frac{\sigma C_{10p}}{C_{10p}}\right)^2}$$

where R_{10s} and R_{10p} are the measured $^{10}\text{Be}/^9\text{Be}$ ratio in the sample and the process blank respectively, C_{10s} and C_{10p} refers to the amount of ^9Be spike added to the sample and to the procedural blank to generate the Be beam necessary to measure the AMS ratio, NA is Avogadro's number (6.022×10^{23}), qtz refers to the total amount of quartz dissolved to make the AMS target, and MBe is the atomic mass of Be. σ is the uncertainty in the measured quantities, and σN_{10} is the analytical uncertainty on the calculated nuclide concentration.

To calculate exposure ages I used the Cronus Earth online calculator which was developed by Balco et al. (2008) as part of the Cronus Earth and Cronus EU projects. This calculator marks an important step towards unifying data manipulation of exposure ages by providing an easily accessible and consistent means for calculating surface exposure ages or erosion rates from ^{10}Be and ^{26}Al measurements. The calculator requires entry of geographical data, sample thickness (attenuation length of 160 g cm^{-2} and rock density of 2.7 g cm^{-3}), the nuclide concentration (N), and the standard reference material used to normalise the AMS measurements. The calculator uses all the previously published scaling procedures so the exposure ages or erosion rates can be compared between various scaling schemes. Since it has been live, the calculator has been updated to reflect variations in results due to different AMS standards used by AMS laboratories, and the revision of the ^{10}Be half-life. The full documentation for version 2.1 can be found in Balco et al. (2008) with further updates for version 2.2 online at <http://hess.ess.washington.edu/>.

The calculated ages assume constant exposure, no cosmogenic nuclide inheritance from a previous exposure history, and no erosion of boulders or bedrock since exposure and thus the ages should be regarded as minimum ages.

In spite of the wide use of surface exposure dating, there are still various complications and uncertainties that can limit its utility. The calculated age uncertainties are expressed as $\pm 1\sigma$. Based on the uncertainty sources, exposure ages are usually reported with systematic and analytical uncertainties.

The analytical uncertainties refer to the uncertainties we can quantify during the sample processing and measuring. According to Balco & Schaefer (2006), the analytical uncertainties include three sources of uncertainty: the AMS isotopic ratio, the number of atoms in the procedural blanks and the number of atoms in the Be carrier spike mass.

Systematic uncertainties refer to the reliability of the method used. It includes the analytical uncertainty and the uncertainty associated with the ^{10}Be production rate, which in this study amount to 8.7% ($4.49 \pm 0.39 \text{ at g}^{-1} \text{ a}^{-1}$) and dominates the systematic uncertainty in the surface exposure ages. Uncertainties associated with environmental conditions of the surface sampled such as post-depositional movement of boulders, post glacial erosion, burial history, inheritance of nuclides from previous exposures or snow and vegetation cover are difficult to quantify. However, they can be minimised by only selecting samples that qualify based on rigorous geomorphological assessment.

For comparing the local surface exposure ages in the study areas I used only the analytical uncertainty. However, when comparing the ages from Scotland and Romania or when comparing the ages to calendar ages or other absolute ages the systematic error should be used as it takes into account all known uncertainties (Balco et al., 2008).

3.5 ELA reconstruction for the palaeoglaciers

The equilibrium line altitude (ELA) represents the line that separates the accumulation and ablation areas on a glacier and is an essential parameter for glacier reconstructions. Above the ELA snow accumulates faster than it ablates, whereas below it, the reverse occurs and ice is lost as well as snow. The resulting positive or negative mass balance determines whether the glacier builds (the terminus advances) or downwastes (the terminus retreats). The physical behaviour of glaciers is directly related to climate changes as they cause an altitude shift in the ELA based on the precipitation input and regional temperature. Any changes in the amount of snowfall lead to changes in the amount of accumulation, whilst rising or lowering temperatures lead to increased or reduced melting. This ELA shift prompts a retreat or advance of the terminus toward a new steady-state position.

ELAs were derived here based on the reconstruction of the palaeoglacier distribution and extent during the last glaciation in the Monadhliath and Rodna Mountains and was used to compare them with ELA data from elsewhere in Europe to get an insight into the patterns of glaciations and climate across the continent during late glacial cooling periods. A range of ELA reconstruction methods are available and three of the most commonly used methods were chosen here for comparative purposes: the area weighted mean altitude method (AWMA), the accumulation area ratio method (AAR), and the area altitude balance ratio method (AABR).

1. The area weighted mean altitude (AWMA)

The area weighted mean altitude method assumes that the accumulation and ablation gradients are equal when the glacier is at its maximum extent and in steady state (Sissons, 1974). However, an overestimation of the ELA tends to occur as ablation gradients are often steeper than were interpreted by Sissons (Benn & Ballantyne, 2005; Benn & Evans, 1998).

2. The accumulation area ratio (AAR)

Without considering the variations in glaciers hypsometry, the AAR method assumes that the accumulation area occupies a fixed proportion of the glacier area above the ELA (Porter, 1975; 2001). This yields typical steady state AAR values of 0.5-0.8 (for debris-covered glaciers the AAR may be as low as 0.10). This method can lead to erroneous ELA

estimates because glaciers vary greatly in size and shape. For example, glaciers with a wider accumulation area and a narrow ablation area may have a different AAR than glaciers with a narrow accumulation area and a wider ablation area (Benn & Gemmell, 1997).

3. The area altitude balance ratio (AABR)

The area altitude balance ratio method is the most reliable method as it includes both the glacier hypsometry and the variations in mass balance and can be used to estimate ELA for different mass balance ratios (Benn & Gemmell, 1997; Osmaston, 2005). This method assumes a certain value for the balance ratio, which are referred to as ablation gradient divided by the accumulation gradient. For example, $BR = 1.67$ implies that the vertical change in mass balance is 1.67 times greater than in the accumulation area. Balance ratios (BR) between 1.67 and 2.0 are frequently employed in studies in Scotland (Benn & Ballantyne, 2005; Finlayson, 2006; Ballantyne, 2007).

The surface of the past glaciers was reconstructed based on the geomorphological mapping of the glacial erosional and depositional landforms. Based on these empirical limits, the ELAs in this study were calculated and are presented in Chapter 4, Table 4.2 for the Monadhliath Mountains and Chapter 5, Table 5.2 for the Rodna Mountains. The AABR method was used as the best estimate for the glacial reconstructions and interpretations in this study.

Chapter 4

Scotland

4.1 Introduction

This chapter brings new evidence on the glacial history of the Monadhliath Mountains during the Late Devensian glaciation. The Monadhliath Mountains are part of the Scottish Highlands (Figure 4.1). There are currently no glaciers in this area and the lack of forest cover assists in mapping and interpreting the glacial landscape.

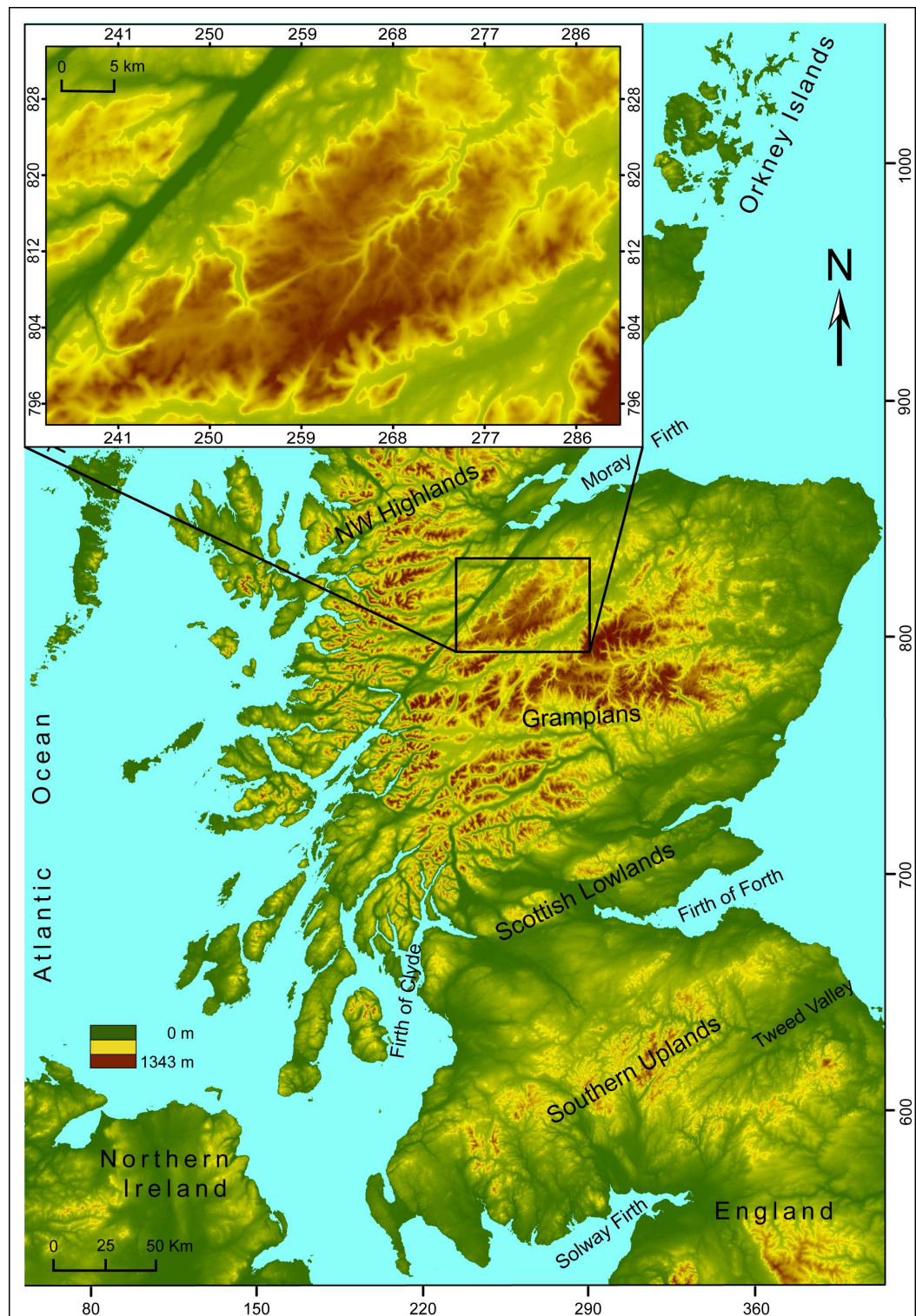


Figure 4.1. Position of the Monadhliath Mountains in the Scottish Highlands. Digital elevation models from SRTM data (NASA, 2004).

4.2 The Monadhliath Mountains

4.2.1 Geographical position

The Monadhliath Mountains, the largest range within the Grampian Mountains, lie to the west of the Cairngorms and Strathspey and to the east of Lochaber and The Great Glen Fault (Figure 4.2). They are aligned on a northeast to southwest direction. The highest elevation is Carn Dearg (945 m) but there are few distinctive peaks above 800 m altitude.

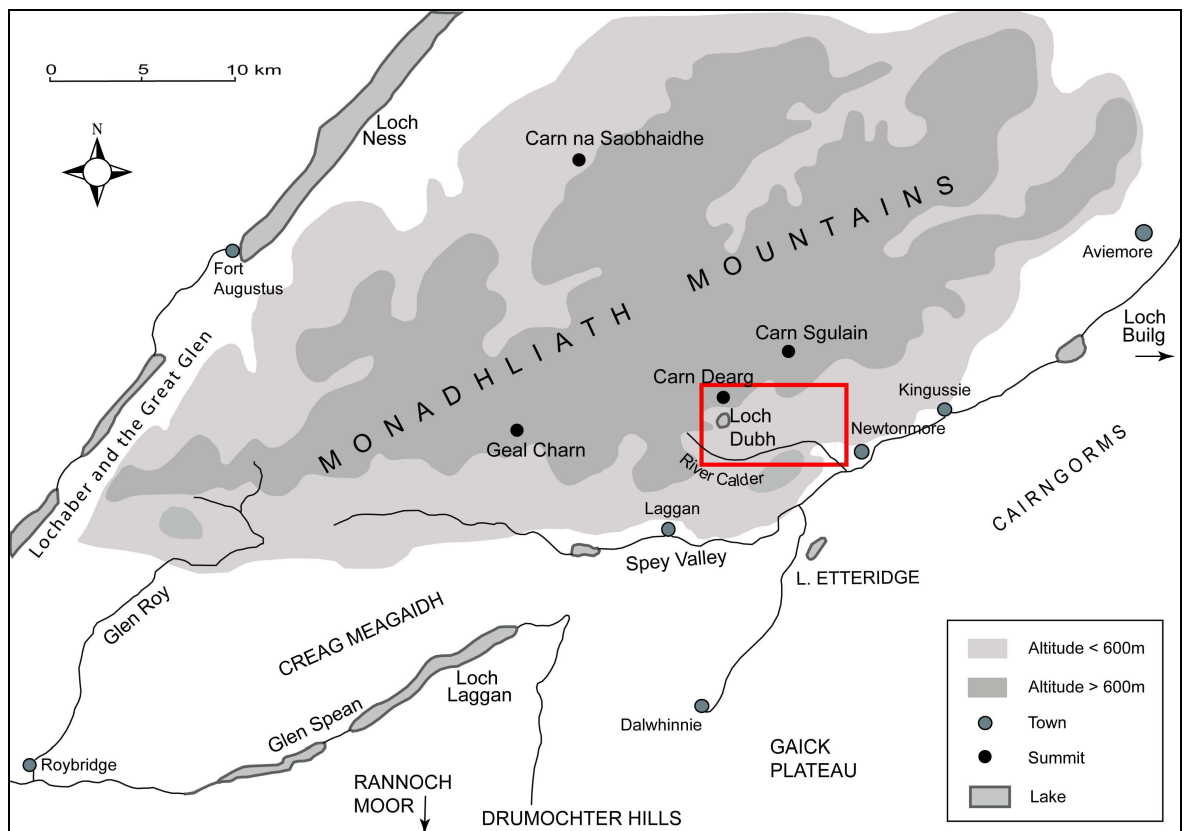


Figure 4.2. Monadhliath Mountains. Study area is marked with a box.

4.2.2 Climate

The moderate temperate climate of Scotland is the result of proximity to the relatively warm Atlantic Ocean in the west. The transition of moist oceanic air from the west towards the more continental climate in the east results in a strong precipitation gradient across Scotland. Located in the central part of Scotland, the Monadhliath Mountains receive an average of 1691 mm of rainfall a year and snow is maintained for up to 106 days a year. The average annual temperatures for lowland areas in the Monadhliath Mountains are around 8°C (Met Office, 2009).

4.2.3 Geology

The crystalline core of the Grampian Mountains stretches north-east and south-west and is occasionally pierced by plutonic igneous bodies (Peach & Horne, 1930). It is surrounded by belts of sedimentary rocks, less resistant to erosion. The Monadhliath Mountains are mainly composed of metamorphic rocks; the Monadhliath Schist comprises Precambrian (Moinian series) psammities and semi-pelites with mica-schists, quartz and feldspar (Figure 4.3). Other geological units include intrusions of igneous rocks such as granite, granodiorite, felsite and lamprophyres (Haselock et al., 1982; Lambert et al., 1982; Dayton, 2006).

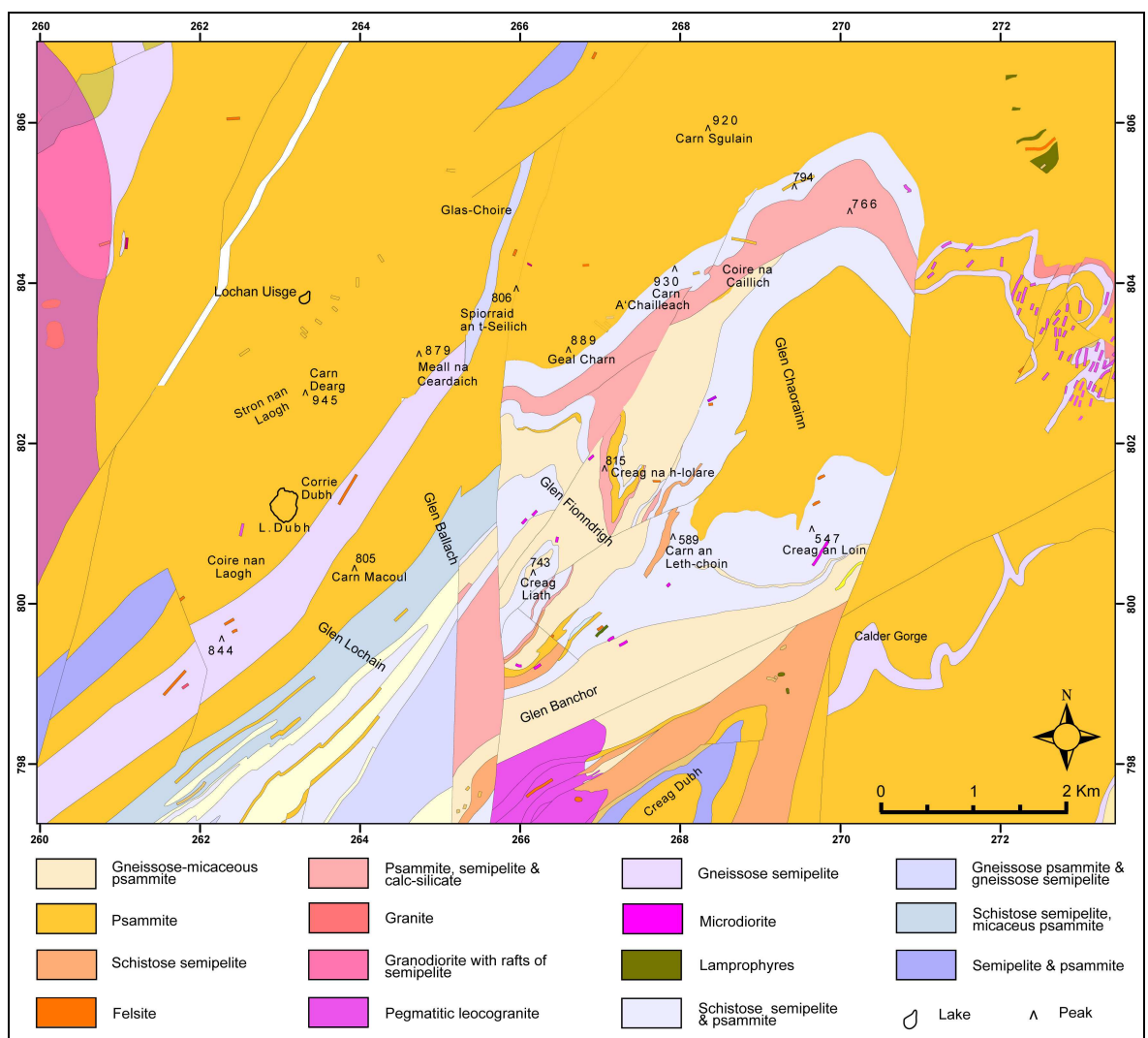


Figure 4.3. Geological map of the study area in the Monadhliath Mountains (Edina Digimap).

4.2.4 Earlier investigations in the Monadhliath Mountains

In comparison to other areas in Scotland, there has been limited research carried out in the Monadhliath Mountains (Barrow et al., 1913; Auton, 1998; Merritt, 1998). Young (1978) focused on the glacial and glacialfluvial landforms of the decaying British and Irish ice-sheet (BIIS) in the upper Spey Valley and mapped several features in the Monadhliath Mountains (moraine limits, kames, eskers, meltwater channels). The south-eastern part of the Monadhliath Mountains has also been the subject of three mapping projects (Gyte, 2004; Trelea, 2008; Boston, 2011) yet dates to constrain the glacial history have yet been published for this area. Recent numerical modelling proposed that during the YD stadial, the plateau of the Monadhliath Mountains was occupied by an independent ice field, from which outlet glaciers fed some of the south eastern corries (Figure 2.6; Golledge et al., 2008). In spite of accurately simulating many of the mapped glacier limits in Scotland (Sissons, 1974; Sutherland, 1984; Thorp, 1986; Ballantyne, 1989; Bennett & Glasser, 1991), the limited availability of empirical data in the Monadhliath Mountains does not allow a comparison with the high resolution model of the YD ice cap (Hubbard, 1999; Golledge et al., 2008) does not match mapped glacial limits. The work presented here provides the first direct chronological data on these glacial limits.

4.2.5 Study area

The study area is situated in the south-east of the Monadhliath Mountains (Figure 4.2), between ~900 m OD (the Monadhliath Plateau) and ~300 m OD (Glen Banchor) and covers an area of approx. 55 km². This study reports on four south facing glens (Glens Lochain, Ballach, Fionndrigh and Chaorainn) that are incised northward into the Monadhliath Plateau (Figure 4.4).

The field area includes eight summits with altitudes over 800 m: Carn Dearg (945 m OD), Carn A'Chailleach (930 m OD), Carn Sgulain (920 m OD), Geal Charn (889 m OD), Meall na Ceardaich (879 m OD), Creag na h-Iolair (815 m OD), Spiorraid an t-Seillich (806 m OD) and Carn Macoul (805 m OD) (Figure 4.5). They are located at the edge of the Monadhliath Plateau and on the interfluves that separate the glens.

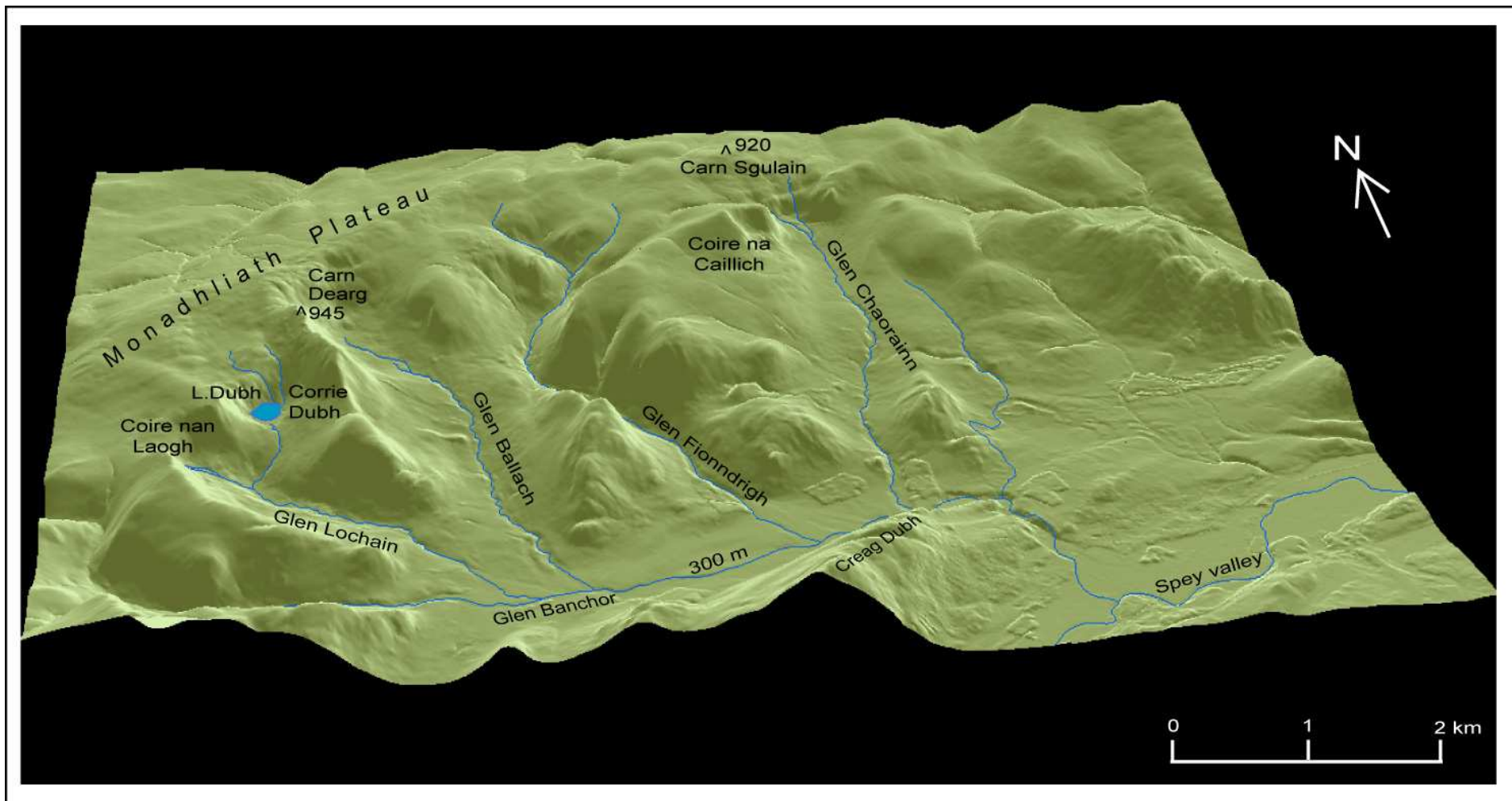


Figure 4.4. Digital elevation model of the study area in the south-eastern part of the Monadhliath Mountains.
Hill-shaded digital surface model from Intermap Technologies NEXTMap Britain topographic data.

4.3 Geomorphology

The results of the geomorphological mapping in the south-eastern Monadhliath Mountains are shown in Figure 4.5. The study area exhibits a range of glacial landforms. Several meltwater channels cut the high interfluves deep into the bedrock and glacially moulded surfaces indicate that ice flowed from the plateau into the lower cirques. Glacifluvial sediments were deposited along and at the bottom of the valleys and moraines were formed during ice retreat towards the higher ground. Extensive periglacial weathering is evident in the upper parts of the valley sides.

On the basis of altitude and groupings of landforms and sediments, the deglaciation history of the study area can be divided into two periods: the regional decay of the BIIS and the subsequent YD readvance and retreat of valley glaciers within each individual glen. These two periods will be discussed below in relation to the geomorphological findings.

4.4 Regional Glaciation

The highest elevation evidence for regional glaciation associated with the Late Devensian BIIS is the scouring and grooving of bedrock at altitudes and trends that are consistent with an inferred ice thickness of over 700 m and a SW-NE flow direction (Barrow et al., 1913; Sissons, 1980; Young, 1978). This north-easterly trend is matched by the orientation of high altitude meltwater channels (Sissons, 1967; Peacock, 1970; Sutherland, 1984; Thorp, 1984). The meltwater channels ignore pre-existing topography (Figure 4.5) by cutting across present interfluves (Young, 1978). Several channels (10-20 m deep and 120-500 m long) cut the western interfluve of Glen Lochain and across the col between Glen Lochain and Glen Ballach north of Carn Dearg and north and south of Carn Macoul (Figure 4.5). Meltwater was also channelled east across the interfluves on either side of Glen Fionndrigh. North of Carn A'Chailleach at 800 m OD, a 2 km long, 100 m wide and 50 m deep meltwater channel appears to terminate on the north-western edge of Glen Chaorainn valley, but its continuation is traced further east (Young, 1974, 1978; Trelea, 2008) and is interpreted as part of a more extensive subglacial drainage system. The trend of the meltwater channels is often continued at their eastern, lower elevation extremities by depositional glacifluvial landforms such as eskers, for example south of Creag an Loin.

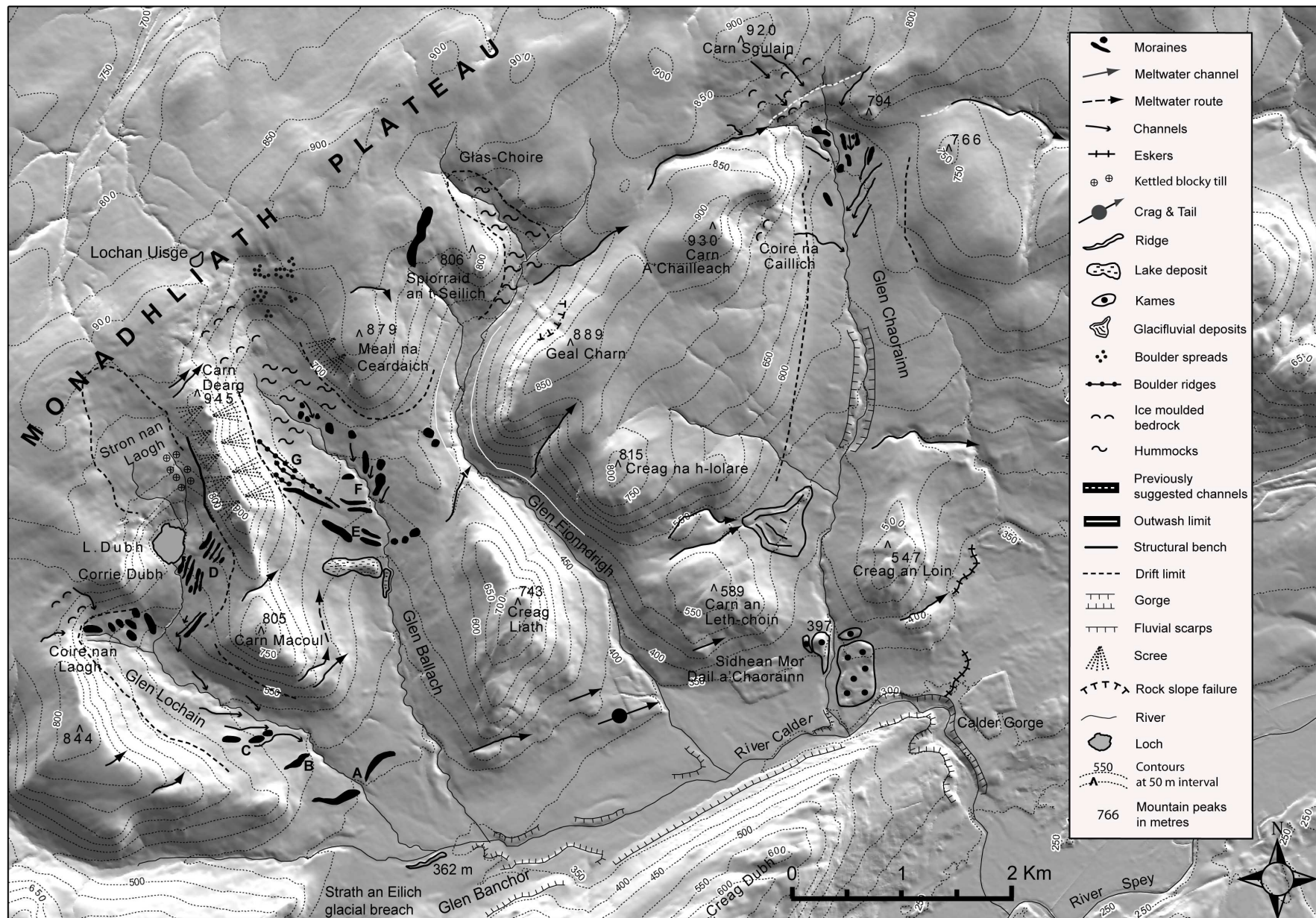


Figure 4.5. Geomorphological map of the study area. Hill shaded DEM from Intermap Technologies NEXTMap Britain topographic data. The map can also be found in the Appendix C.

The meltwater channels south of Creag Liath and Carn an Leth Choin (Figure 4.5) are considered to be ice-marginal, having formed along the lobe of Devensian ice that last occupied Glen Banchor.



Figure 4.6. Glacifluvial assemblages at the south end of Glen Chaorainn (see Figure 4.5).



Figure 4.7. Esker in the eastern part of Glen Banchor (see Figure 4.5).

Further to the east, several mounds and parallel ridges composed of glacial sediments at the south end of Glen Chaorainn indicate meltwater deposition (Figure 4.5 & Figure 4.6). The highest is Sidhean Mor Dail a'Chaorainn at 397 m OD, which is composed of subhorizontal laminated clays, silts, fine sand and gravel. A 600 m long, sinuous esker (Young, 1978) is located at the eastern end of Glen Banchor where it widens and joins the Spey valley (Figure 4.7). Its north-east orientation indicates deposition by the Spey ice lobe towards the NE (Figure 4.20), predating the formation of the Calder Gorge which has truncated the esker at the SW end.

South-east of Creag Liath an isolated bedrock surface protrudes from the surrounding low lying terrain. In the lee of this rocky crag, post-glacial incision by the river Fionndrigh has exposed sections in tills and the feature is therefore mapped as a crag-and-tail (Figure 4.5).

A low-elevation but prominent ridge (Figure 4.5, moraine A) stretches west-east in an arcuate shape just outside the entrances to Glens Lochain and Ballach at approximately 400 m OD. Another single-crested ridge is located in the south-west of Glen Banchor at the confluence of the rivers Lochain and Calder, aligned E-NE along the former direction of glacial drainage in the area (Figure 4.8). It contains discontinuous and undulating beds of sorted silts, sands, gravels and boulders, reflecting deposition in variable flow conditions.



Figure 4.8. South-western view of Glen Banchor showing the Strath an Eilich glacial breach and the ridge of outwash sediments (see Figure 4.5).

4.5 Valley glaciation

This section includes the morphological description of the four glens and the associated cirques. The geomorphology in the SE part of the Monadhliath Mountains was not entirely caused by the presence of ice masses. It is often the result of the interplay between the underlying geology and the ice erosion.

4.5.1 Glen Lochain

Glen Lochain is the westernmost valley in the study area and has a NW-SE orientation. It is drained by River Lochain which flows ca. 2.5 km until it reaches Glen Banchor. Glen Lochain contains two cirques - Corrie Dubh and Corrie nan Laogh. The highest point of the study area is Carn Dearg (945 m OD), located on the interfluvium that separates Corrie Dubh from Glen Ballach. Steep walls delimit Glen Lochain on the eastern side, whilst the western slopes become gentler in the lower half of the glen (Figure 4.9).



Figure 4.9. Glen Lochain, south view towards Glen Banchor. Moraines B and C are marked (see Figure 4.5).

The southern limit of the glen is marked by well-defined recessional moraines (Figure 4.5 & Figure 4.9). Moraine ridge (B) is located at the entrance of the glen. The up valley

moraine (C) is divided by channels into three parts. Much of the low ground in Glen Lochain is occupied by till mounds varying in height between 1-4 m and separated by postglacial fluvial channels. Sections show subangular locally sourced boulders mixed with very rounded Rannoch granite clasts, carried by ice into the Spey Valley (Thorp, 1987). The till is thicker on the gentler western slopes (Figure 4.9).

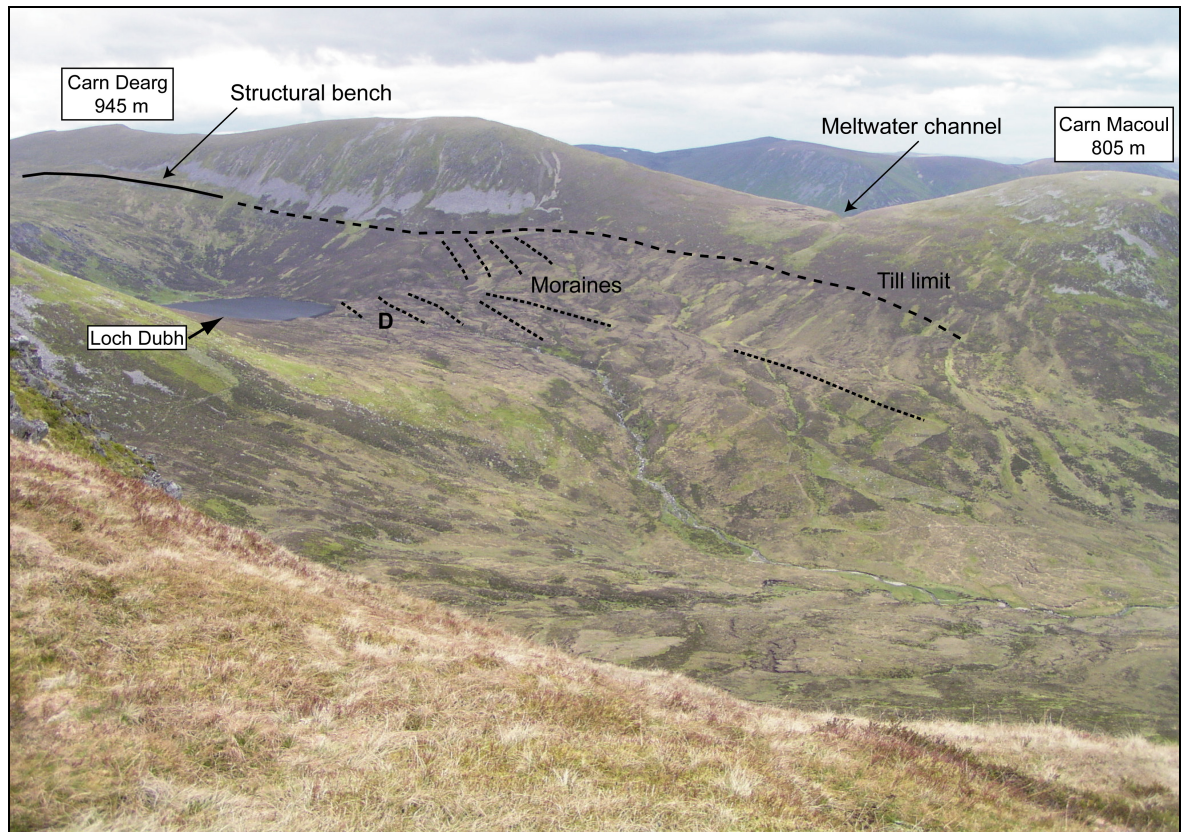


Figure 4.10. Glen Lochain and landform assemblages at Loch Dubh (see Figure 4.5).

altitude. Two sets of distinct sharp-crested parallel moraine ridges (D), composed of locally derived subangular clasts, and meltwater channels, descend obliquely down the southern valley side from ca. 730 m OD to ca. 630 m OD, marking successive ice-front positions during glacier retreat. The upper moraines extend towards the drift limit (Figure 4.10) which merges with the scree slopes above. A scree covered structural bench extends from 750 m OD to 800 m OD elevation along the eastern side of Corrie Dubh to the plateau. Between the upper limit of the headwall and the Monadhliath plateau there is a 2 km² area, Stron nan Laogh, where the locally derived blocky tills are hummocky and kettled (Figure 4.11).



Figure 4.11. Kettled blocky till on the plateau above Loch Dubh (see Figure 4.5).

4.5.2 *Glen Ballach*

Glen Ballach stretches for ca. 5 km in a NNW – SSE direction and is drained by Allt Ballach, a tributary of the River Calder. The western side of the valley comprises a high ridge culminating in Carn Dearg (945 m OD) at its northern end. This western ridge separates Glen Ballach from Corrie Dubh and Glen Lochain and is mantled by scree. The eastern valley side is also very steep, towards Meall na Ceardaich (879), but decreases in elevation to 550 m OD midway along the valley before rising again at Creag Liath (743 m OD) in the lower part of the glen.

Glen Ballach has an up to 2 km wide valley floor and preserves the richest glacial record in the study area. The most prominent feature in Glen Ballach (Figure 4.12) is a flat asymmetric ridge up to 60 m in height that extends 600 m from the western valley wall to the valley centre. Fluvial incision in the eastern part has exposed a 6 m high and 20 m wide section. The section exhibits lacustrine sediments dominated by well-sorted sands, with lenses of till, laminated clays, dropstones, and occasional current ripples indicating the presence of a proglacial lake. Auger samples to the west of the exposure confirmed that similar lacustrine sediments underlie the main part of the ridge. The western higher end of

this ridge is flat topped. A horizontal notch cut into bedrock, ~ 750 m in length, extends from the two meltwater channels (~ 750 m OD) north of Glen Banchor along the western valley side at ~ 560 m OD and merges with the highest part of the flat topped deposit (560 m OD). The combination of lacustrine sediments and bedrock notch at matching altitudes suggests an ice-marginal meltwater route from the meltwater channels into a proglacial lake.

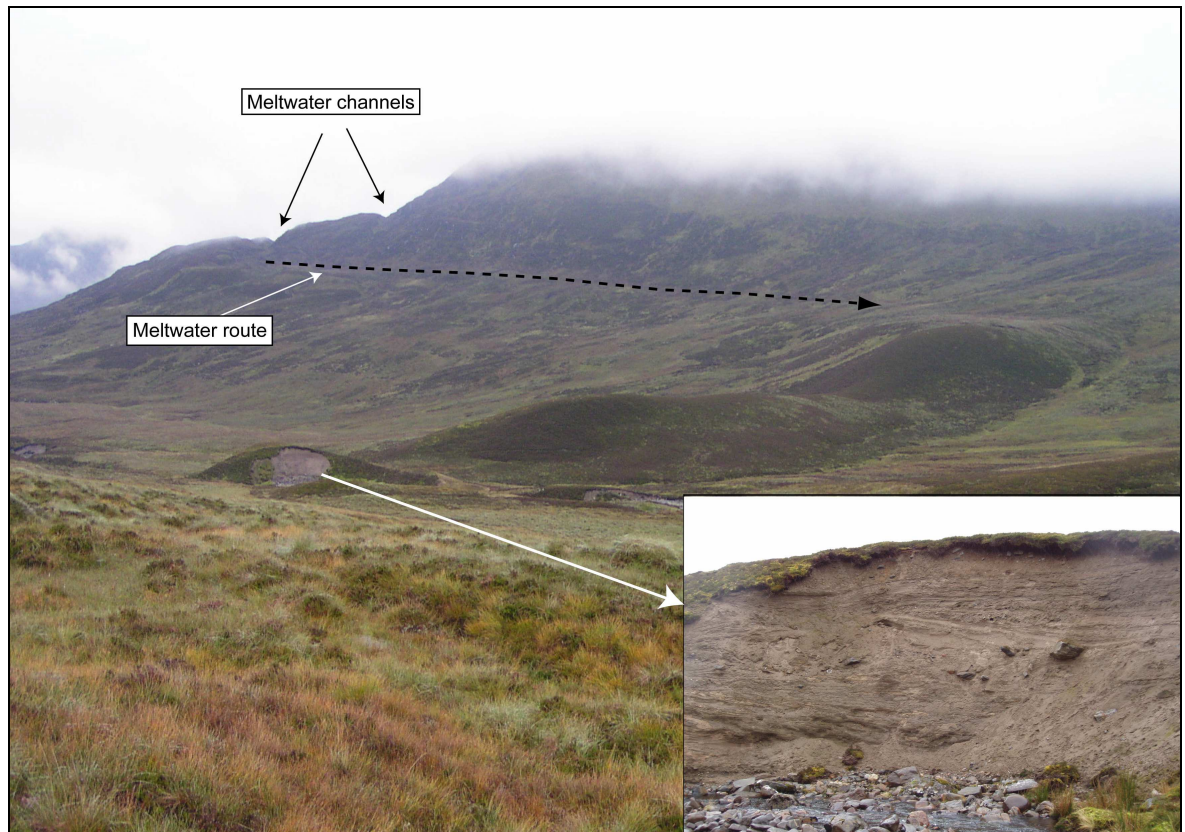


Figure 4.12. Glacialacustrine deposit in Glen Ballach. Inset shows the 6 m high section with interbedded layers of silts/clays and dropstones (see Figure 4.5).

Moraine ridges occur up-valley of the glacialacustrine deposit. Moraine E (Figure 4.5) extends in a wide arc across the valley as a subdued ridge that terminates in several mounds (2-4 m high) on the east side of the valley. A second arcuate moraine belt (F) occurs on higher ground between 580 and 680 m OD converging down valley and composed of local psammites (Figure 4.5 & Figure 4.13). The highest forms a distinct broad ridge scattered with boulders along the western slope of the valley. Towards the east, subdued discontinuous ridges extend uphill towards Meall na Ceardaich. On the western flank of the valley, a suite of continuous undulating ridges (G), composed of 1-2 m diameter locally derived subangular boulders, extends upslope (Figure 4.13). Ice moulded bedrock occurs higher up and subangular boulders distributed either individually or as boulder spreads are present on the eastern side of the valley head. Scoured bedrock steps

occur at the plateau edge with the plateau beyond being scattered with extensive boulder spreads and boulder ridges (Figure 4.5).

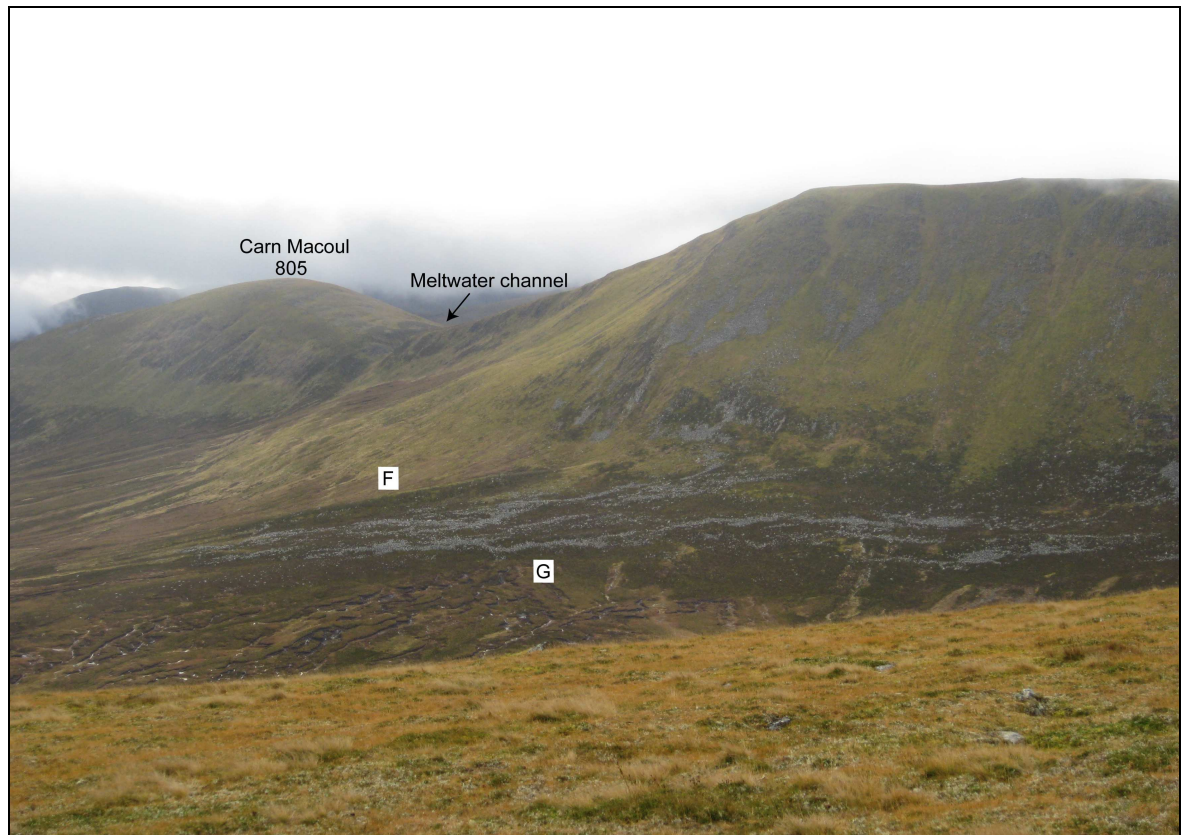


Figure 4.13. Moraine ridges in Glen Ballach (see Figure 4.5).

4.5.3 Glen Fionndrigh

The topography of Glen Fionndrigh differs significantly from the adjacent valleys; it is narrower and deeper with steeper sides. There is a low col in the west towards Glen Ballach and a higher col breaches the eastern interfluvium towards Glen Chaorainn. Rock slope failure has affected the western slope below Geal Charn (Figure 4.5). The glen is drained by Allt Fionndrigh which flows sinuously for about 6 km towards Glen Banchor.

Most of the valley floor is covered with thick fluvially-incised outwash deposits (Figure 4.14). Between 600 and 770 m OD the valley floor is covered with thick elongated hummocky deposits (2-4 m high), dissected by oblique shallow channels. Towards Glaschoire, the valley head terminates with a gently sloping basin that connects the glen and the plateau (Figure 4.15). A glacially moulded bedrock ridge is located at the head of the col towards Glen Ballach. It has an SW-NE orientation similar to the Late Devensian ice flow direction and continues with a 350 m long glacial moraine at its NW end (Figure 4.5).

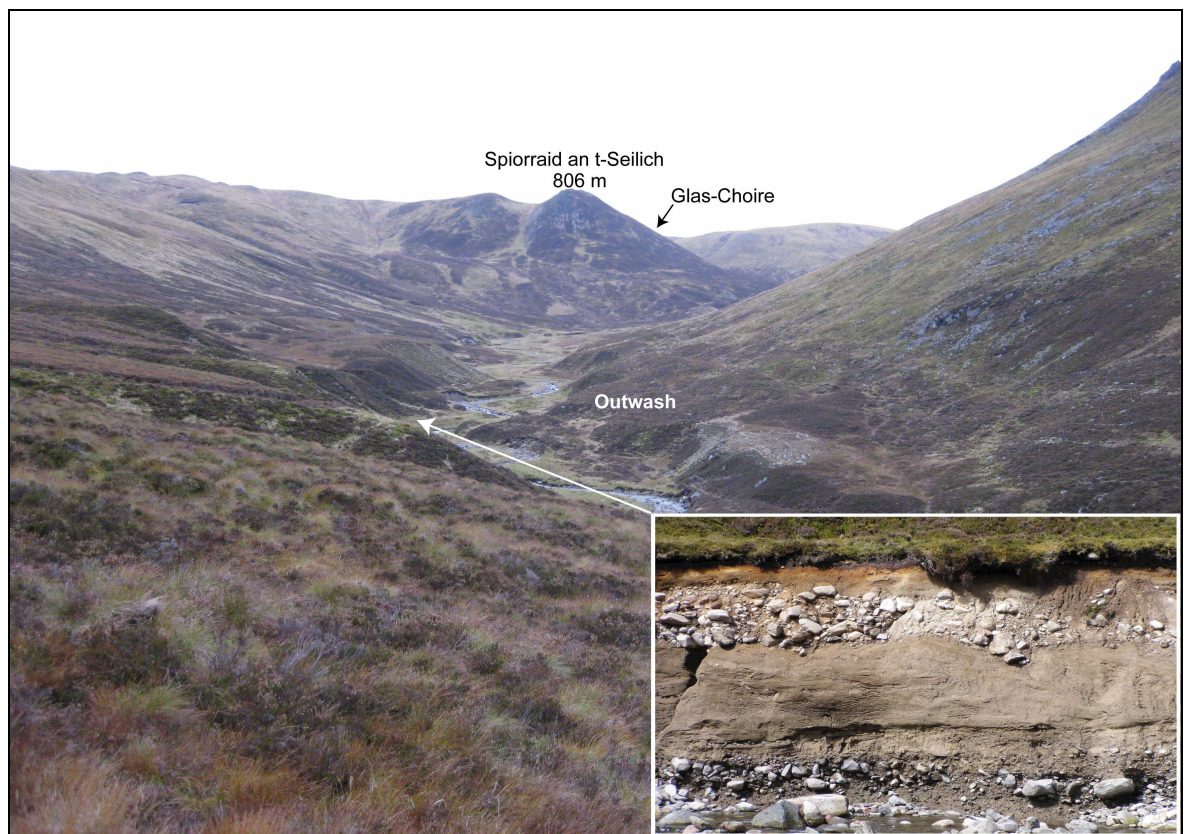


Figure 4.14. Outwash in Glen Fionndrigh. Inset shows detail (see Figure 4.5).

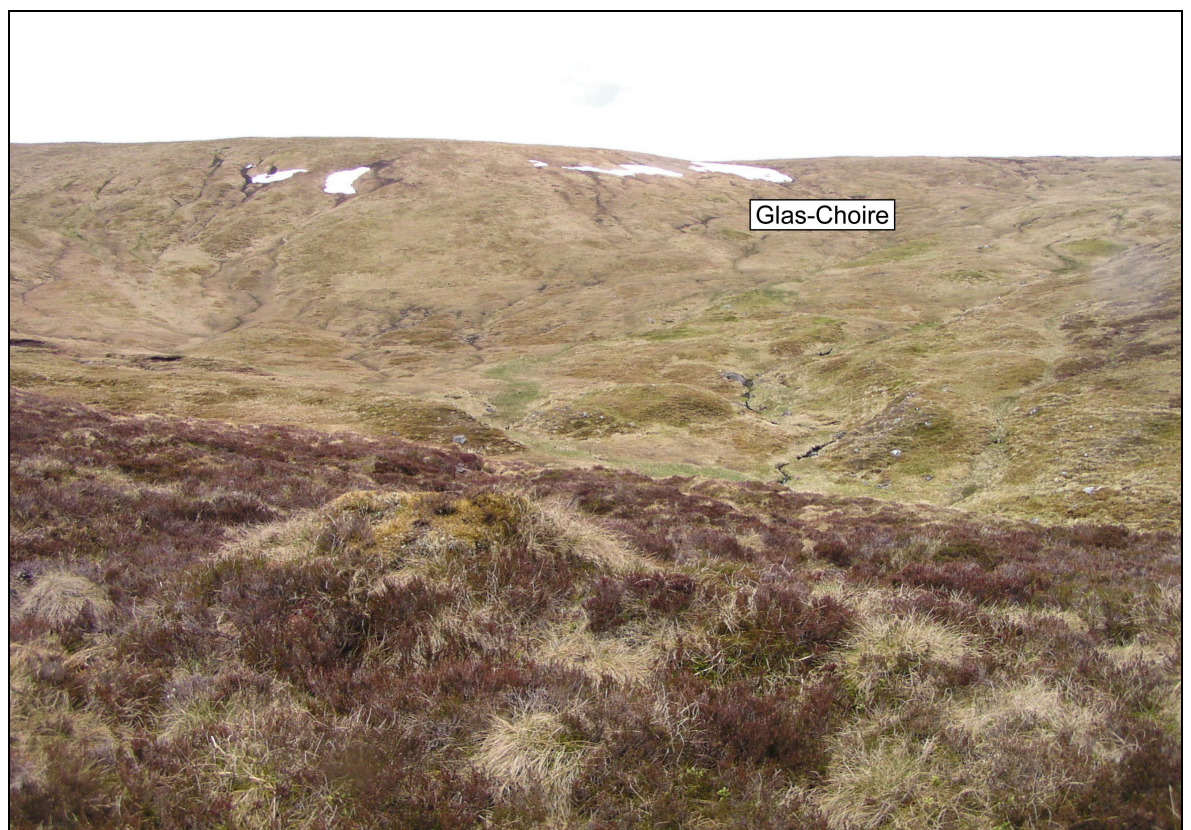


Figure 4.15. Hummocky deposits in upper Glen Fionndrigh (see Figure 4.5).

4.5.4 Glen Chaorainn

Glen Chaorainn is the widest and westernmost valley included in this study. It is drained by Allt Chaorainn flowing north to south. Towards the head of the glen slopes are steep, but down valley they gently decrease in elevation, whilst a very low interfluvium provides the eastern limit of the glen.

Glen Chaorainn has a shallow valley floor covered in glacial till (Figure 4.16), which are deeply incised by the river above 400 m OD. In the western, lower part of the glen glacial sediments overlie till. These deposits are incised by streams occupying the two meltwater channels on the western col (Figure 4.16).

The small, south-east orientated Coire na Caillich is located at 750 m OD on the western valley wall below A'Chailleach (930 m OD; Figure 4.5). Evidence of glacial erosion in Coire na Caillich is indicated by the concave shape, reverse slope and ice moulded bedrock on its floor.

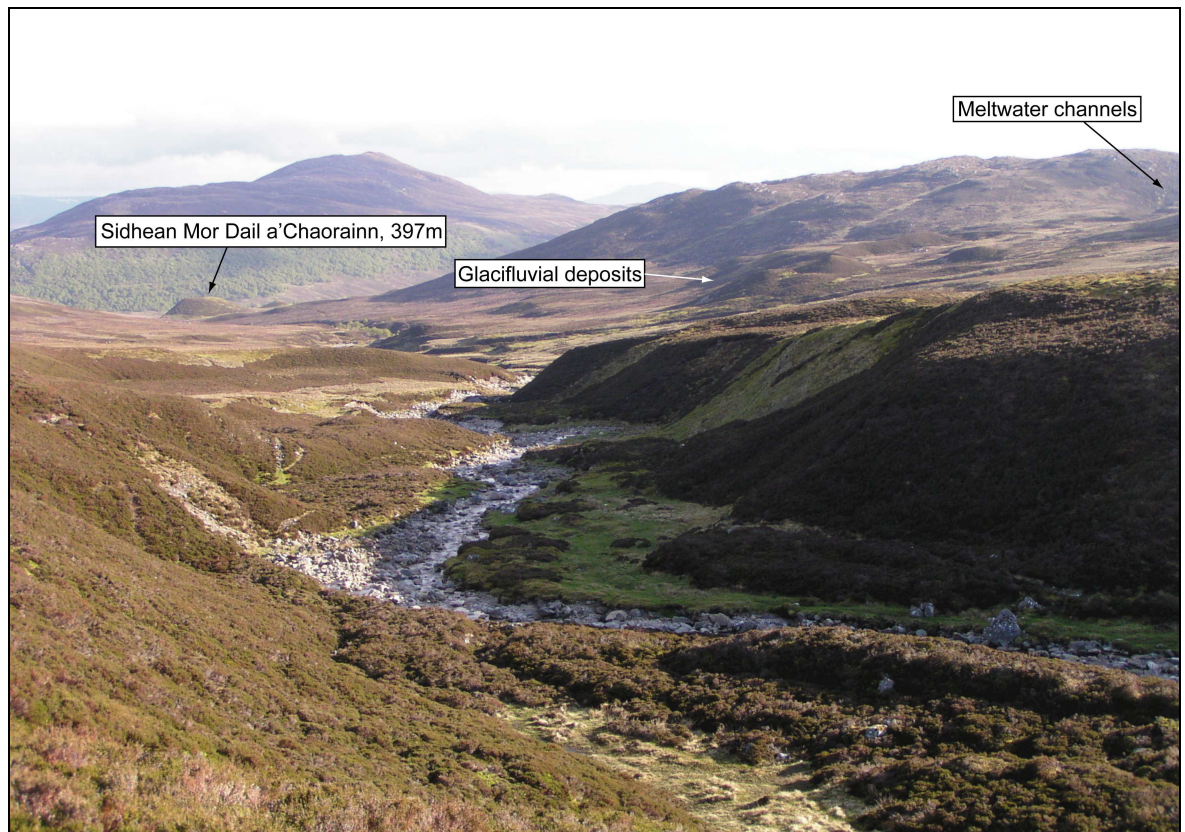


Figure 4.16. South view of Glen Chaorainn. The glacifluvial sediments were deposited by meltwater flowing across the interfluvium that separates Glen Chaorainn from Glen Fionndrigh (Figure 4.5).

On the opposite side of the valley from Coire na Caillich, glacial till has been fluvially

incised into long and wide ridges. The sediment cover thins towards the headwall of Glen Chaorainn and is dominated by elongated mounds separated by channels. Several glacially moulded bedrock knobs occur on the upper slope towards Carn Sgulain.

Above the headwall, the plateau has a similar stepped rim as above the Glen Ballach headwall, with a flat peaty area separated by steeper slopes (Figure 4.17). Here, this step is caused by the contact between the underlying micaceous psammite and the schistose semipelites and psammites (Figure 4.3).



Figure 4.17. The plateau edge above Glen Chaorainn (see Figure 4.5).

4.6 Surface exposure ages

In this study, the history of exposure to cosmic rays was determined by measuring the concentrations of *in situ* produced cosmogenic ^{10}Be in quartz from 14 boulders and 2 bedrock surfaces. Sampling methodology and sample processing procedures are detailed in Chapter 3, Subheading 3.4. The calculated age uncertainties are expressed as $\pm 1\sigma$ (Table 4.1). Although upstanding quartz veins indicate up to 3 cm of differential erosion at some sample sites since first exposure, the mean exposure ages in Table 4.1 assume a constant

exposure history, no cosmogenic nuclide inheritance and no erosion of boulders since deposition. The surface exposure ages should therefore be regarded as minimum ages. If erosion was taken into account, it would increase the ages of the samples by ~ 2.5 %. Corrections for potential snow cover were not applied as winter snow-cover history is difficult to constrain. However, to minimise this effect samples were collected from the top surfaces of prominent upstanding boulders that are also unlikely to have accumulated peat or soil since deglaciation.

Table 4.1 presents sample locations and the ^{10}Be exposure ages. Figure 4.19 shows the location of the samples.

Glen Banchor. Two boulders exposed on top of the long ridge in Glen Banchor, at 362 m OD, yielded exposure ages of 13.3 ± 1.4 ka and 13.0 ± 1.2 ka (mean = 13.1 ± 1.3 ka; Figure 4.5), coinciding with the end of the Windermere Interstade.

Glen Lochain. One sample was collected from the top of a large boulder on moraine B, which yielded an age of 11.8 ± 1.1 ka. Two samples were collected from boulders on top of the moraines near Loch Dubh (D), at 655 m OD, and gave minimum exposure ages of 10.2 ± 1.1 ka and 11.0 ± 1.0 ka, with a mean age of 10.6 ± 1.0 ka BP.

Glen Ballach. Boulders on top of the lake deposit at 550 m OD and 528 m OD gave two exposure ages of 11.6 ± 1.1 ka and 10.9 ± 1.0 ka, with a mean age of 11.2 ± 1.1 ka. Two exposure ages from boulders on the surface of moraine E at 520 m OD yielded 11.3 ± 1.0 ka and 10.8 ± 1.0 ka with a mean deposition age of 11.0 ± 1.0 ka. The exposure ages of two boulders on top of the upper ridges (F) gave exposure ages of 9.7 ± 0.9 ka and 9.9 ± 0.9 ka, with a mean age of 9.8 ± 0.9 ka.

Glen Chaorainn. Three boulders sampled on the till ridges in Glen Chaorainn, at ~640 m OD, give ages of 16.2 ± 1.5 ka, 14.1 ± 1.3 ka and 11.6 ± 1.0 ka. Bedrock outcrops at 755 m OD on the plateau edge above the headwall yielded ^{10}Be ages of 12.5 ± 1.2 ka and 11.1 ± 1.0 ka suggesting ice free conditions at 11.8 ± 1.1 ka (mean value).

Table 4.1. Sample information and surface exposure ages.

Lab ID	Lithology	Lat (°N)	Long (°W)	Elev. (m OD)	Shielding ^a (factor)	Thickness ^b (cm)	Quartz mass (g)	[¹⁰ Be] ^c (x10 ⁴ atom g ⁻¹)	Exposure age ^d (ka)	Ages including erosion ^e	Mean ages ^f (ka)
Drift ridges											
01	Psammite	57.11	4.15	646	0.9898	2 (0.9833)	21.78	15.26 ± 4.87	16.2 ± 1.5 (0.5)	16.9 ± 1.6 (0.5)	15.1 ± 1.4 (0.4) (excluded)
02	Psammite	57.11	4.15	641	0.9959	2 (0.9833)	25.32	13.38 ± 4.27	14.1 ± 1.3 (0.4)	14.7 ± 1.4 (0.5)	
03	Psammite	57.11	4.15	634	0.9959	3 (0.9751)	26.46	10.84 ± 0.35	11.6 ± 1.0 (0.4)	12.0 ± 1.1 (0.4)	
Glen Banchor Ridge											
04	Psammite	57.05	4.05	362	0.9990	3 (0.9751)	26.17	9.72 ± 0.60	13.3 ± 1.4 (0.8)	13.8 ± 1.5 (0.9)	13.1 ± 1.3 (0.6)
05	Psammite	57.05	4.22	362	0.9990	3 (0.9751)	25.89	9.46 ± 0.35	13.0 ± 1.2 (0.5)	13.4 ± 1.3 (0.5)	
Moraine B											
06	Granite	57.06	4.23	470	0.9974	4 (0.9670)	24.21	9.24 ± 0.31	11.8 ± 1.1 (0.4)	11.9 ± 1.1 (0.4)	
Moraine D											
07	Psammite	57.07	4.25	655	0.9938	3 (0.9751)	26.12	9.73 ± 0.60	10.2 ± 1.1 (0.6)	10.5 ± 1.1 (0.6)	10.6 ± 1.0 (0.4)
08	Psammite	57.07	4.25	655	0.9938	3 (0.9751)	26.36	10.47 ± 0.33	11.0 ± 1.0 (0.3)	11.3 ± 1.0 (0.3)	
Lacustrine deposit											
09	Quartz vein	57.08	4.23	550	0.9980	3 (0.9751)	31.09	9.91 ± 0.34	11.6 ± 1.1 (0.4)	e = 0	11.2 ± 1.1 (0.4)
10	Quartz vein	57.08	4.23	528	0.9949	3 (0.9751)	26.60	9.21 ± 0.38	10.9 ± 1.0 (0.4)		
Moraine E											
11	Psammite	57.08	4.23	520	0.9963	3 (0.9751)	23.76	9.52 ± 0.30	11.3 ± 1.0 (0.3)	11.6 ± 1.1 (0.4)	11.0 ± 1.0 (0.3)
12	Psammite	57.08	4.22	520	0.9963	3 (0.9751)	23.98	9.07 ± 0.30	10.8 ± 1.0 (0.3)	11.1 ± 1.0 (0.3)	
Moraine F											
13	Quartzite	57.08	4.23	600	0.9945	6 (0.9510)	24.77	8.53 ± 0.32	9.7 ± 0.9 (0.4)	e = 0	9.8 ± 0.9 (0.3)
14	Quartz vein	57.08	4.23	579	0.9945	2 (0.9833)	27.00	8.83 ± 0.31	9.9 ± 0.9 (0.3)		
Bedrock knobs											
Glen Chaorainn											
15	Psammite	57.11	4.16	755	0.9852	4 (0.9751)	21.43	12.83 ± 0.52	12.5 ± 1.2 (0.5)	13.0 ± 1.3 (0.5)	11.8 ± 1.1 (0.4)
16	Psammite	57.11	4.16	755	0.9872	3 (0.9833)	20.73	11.46 ± 0.38	11.1 ± 1.0 (0.4)	11.5 ± 1.1 (0.4)	

^a Shielding by distant objects computed after Dunne et al. (1999);

^b Sample thickness correction using a rock density of 2.7g cm⁻³ and an attenuation length of 160g cm⁻²; thickness correction factor is given in the parentheses.

^c ¹⁰Be concentrations in quartz;

^d Exposure ages calculated using Cronus-Earth ¹⁰Be – ²⁶Al exposure age calculator v. 2.2 (<http://hess.ess.washington.edu/>). They assume zero erosion, scaling factors from Stone (2000) and a production rate of 4.49 ± 0.39 atom (g SiO₂)⁻¹ a⁻¹ (Balco et al., 2008);

^e Erosion corrected ages using 3 mm/kyr;

^f Mean ages with no erosion. All exposure ages are given with the systematical uncertainty and the analytical uncertainty in the parentheses.

4.7 Discussion

4.7.1 The pattern of Late Devensian deglaciation in the SE Monadhliath Mountains

The reconstructions indicate that the strongest glacial influence on the topography was caused by the last ice sheet that occupied the study area. The downwasting of the Late Devensian ice sheet is successively marked by bedrock-floored meltwater channels at 700-800 m OD, representing the highest elevation evidence of ice sheet glaciation in the field area (Figure 4.5). The absence of sediments in these high channels indicates they were not covered during subsequent ice readvances in the area (Sissons, 1974; Benn & Ballantyne, 2005).

Continued downwasting led to topographic confinement of the ice and the formation of meltwater channels at 550-600 m OD and the exposure of till deposits on the col between Glens Ballach and Fionndrigh at an elevation of 570-600 m OD (Figure 4.18). The conical morphology of these till deposits is likely due to erosion and subsequent slope adjustment after ice retreat.

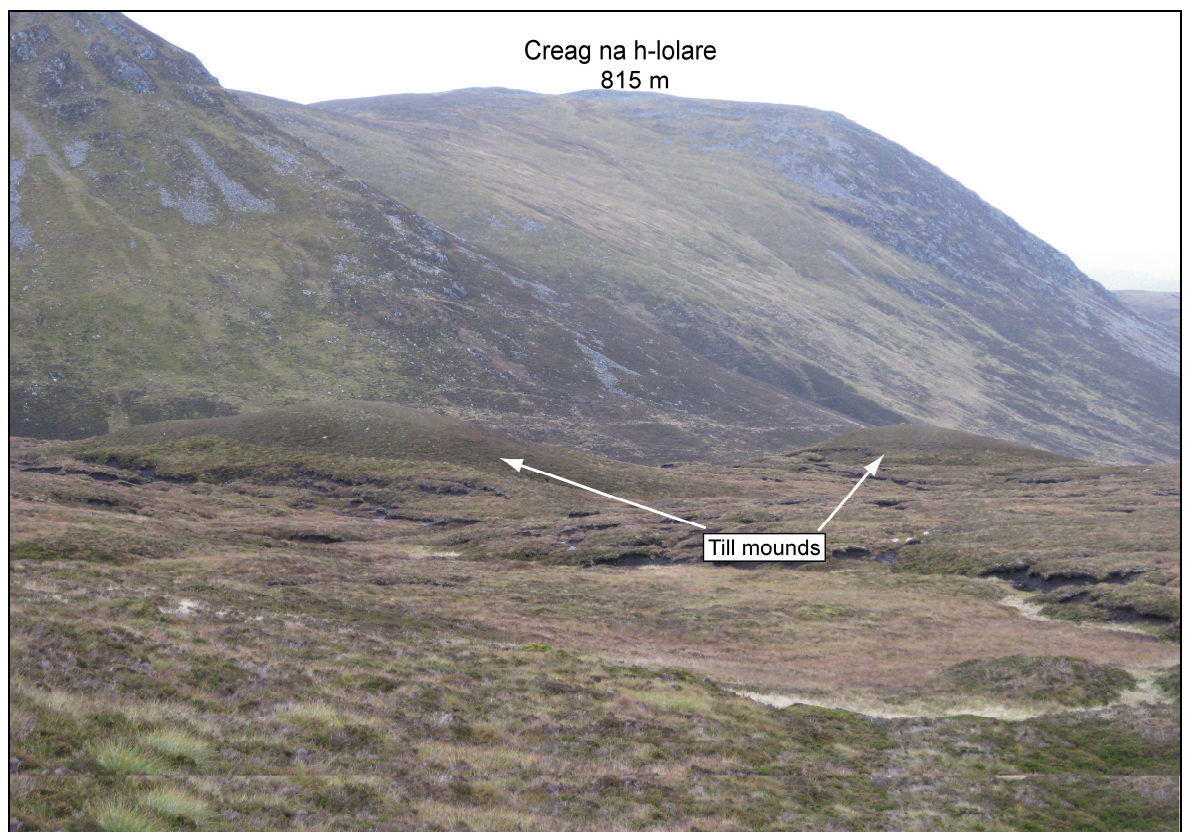


Figure 4.18. Till mounds on the interfluvium between Glen Ballach and Glen Fionndrigh (see Figure 4.5).

On the basis of the position and altitude of meltwater channels and glacial deposits, it is possible to reconstruct the temporal sequence of deglaciation in the study area (Figure 4.20). The increasing topographic control on ice configuration is noticeable in the change of the meltwater channel direction from NE to E (Young, 1978) along the northern part of the Banchor glacier (Figure 4.20).

Evidence of an early separation between ice in the main Banchor valley and ice in the smaller tributary valleys to the north can be found in both Glen Chaorainn and Glen Ballach. The glacialfluvial deposits on the western valley wall in Glen Chaorainn have been deposited by meltwater streams flowing through the two channels that cut the interfluvium from Glen Fionndrigh. This implies Glen Banchor ice protruding into Glen Fionndrigh was thick enough to supply meltwater to scour these channels. At the same time, the ice surface of the Glen Chaorainn glacier must have been low enough to allow deposition of the glacialfluvial sediments (Figure 4.5 & Figure 4.20). If any water was impounded within a lake at this time, no evidence remains of the lake itself. Postglacial channel and river incision has subsequently modified this deposit into ridges that have previously been interpreted as eskers (Young, 1978; Trelea, 2008).

The separation between ice in Glen Banchor and Glen Ballach is marked by the ~60 m thick lacustrine deposit. Towards the end of the Late Devensian, as the Ballach glacier and the Banchor ice lobes retreated, there existed no escape route for meltwater and so it ponded in the area between the termini to form a proglacial lake. The flat top nature of the deposit and the presence of dropstones in the lacustrine deposits is consistent with this interpretation. The two ice-marginal meltwater channels that extend northwards along the western valley wall are likely to have been part of the inflow to the lake (Figure 4.12). This deposit was considered by Young (1978) to be an esker associated with the meltwater channels at 730 m OD on the west col and 550 m OD on the east col (Figure 4.5), implying formation when ice was flowing west to east and was at least 400 m thick. However, the presence of dropstones in the fine sands of the lacustrine deposit indicates a low energy environment that is not compatible with the high gradient (~30%) of the proposed subglacial channel. Alternatively, Merritt (1998) and Trelea (2008) argued for its deposition as a moraine of Glen Banchor ice, which, on retreat, resulted in the impoundment of a lake. Another interpretation was given by Gyte (2004) who argued for deposition as a moraine by south flowing Glen Ballach ice. However, the morainic interpretations are difficult to reconcile with the entirely lacustrine stratigraphy of the deposit and I found no evidence of lacustrine sediments in stream sections south of the

main deposit and no evidence of a morainic plug downvalley against which any lake would have impounded.

At this stage, ice to the south in Glen Ballach must have been sufficiently thick to obstruct water from the retreating higher glaciers from infiltrating within/beneath it or spilling over the terminus (Clapperton et al., 1975). The reconstructed ice limits (Figure 4.20) show Glen Ballach to accommodate a lake, which was fed from the two meltwater channels on the western valley wall and drained towards Glen Fionndrigh over the eastern col, incising it in the process. Similar situations have been documented during the deglaciation of the Spey Valley with ice-dammed lakes forming between the regional ice and the local glaciers (Brazier et al., 1998; Golledge, 2002).

Within Glen Banchor, lowering of the ice dam allowed lake water to be redirected along the Glen Banchor ice margin, cutting meltwater channels at 400-450 m OD south of Creag Liath and Carn an Leth-choin. The lake survived until the Glen Banchor ice thinned and retreated sufficiently to remove the ice dam and allow water to exit to the east along the ice margin.

Meltwater produced during the detachment of Spey, Banchor and Chaorainn ice deposited glacifluvial landforms at the southern end of Glen Chaorainn implying that ice surface was at least 400 m OD (Sidhean Mor Dail a'Chaorainn, 397 m, Figure 4.5 & Figure 4.6). The pattern of deglaciation indicates that thinning of ice was associated with the formation of the north-east trending eskers by the Spey ice lobe which occupied the wider area of eastern Glen Banchor (Figure 4.7). The southernmost esker ends abruptly at the Calder Gorge indicating that the gorge was formed after the esker. Deposition of glacifluvial landforms at the southern end of Glen Chaorainn between the three differently sourced ice masses of Spey, Banchor and Chaorainn, suggests downwasting of Glen Banchor ice and retreat of ice in the valleys (Figure 4.20). Downwasting to an elevation of 400 m would also suggest that the moraine deposition at A in lower Glen Lochain (Figure 4.5) was constructed by Glen Banchor ice as a lateral moraine, an interpretation at least partly supported by its arcuate shape into Glen Lochain.

In the upper part of Glen Chaorainn, the sediment drift thins considerably and a wide basin stretches towards the headwall. Trelea (2008) argued that the flat basin may be due to ice scouring and removal of the Late Devensian sediments during the YD readvance. However, the hummocks on the basin floor are not the result of *in situ* melting of ice at the

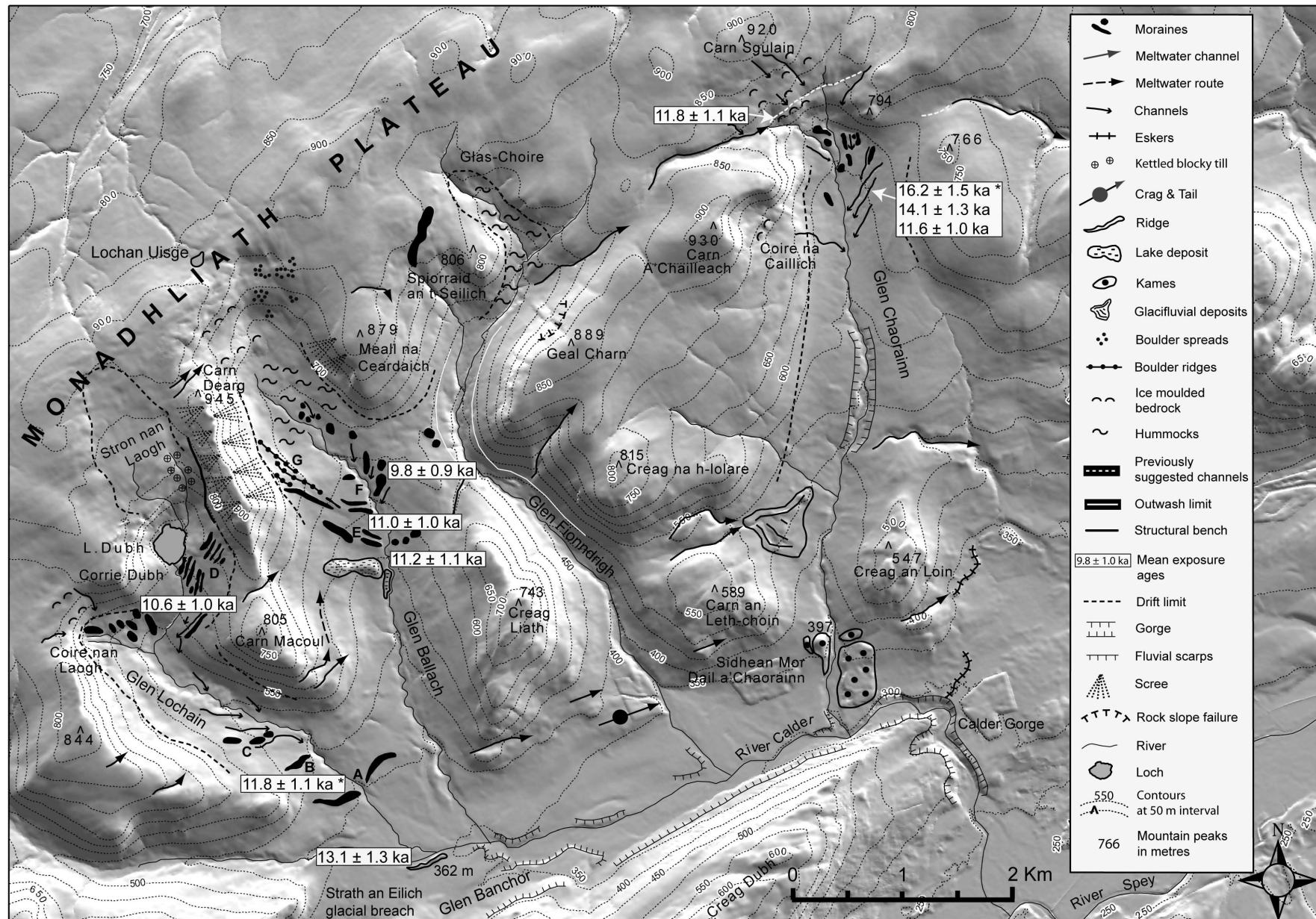


Figure 4.19. Surface exposure ages plotted on the geomorphological map. * indicates individual exposure ages.

beginning of the Holocene, but were likely created by meltwater emanating from ice on the plateau above the western side of the corrie, depositing sediment and subsequently eroding it to produce these elongated mounds. The final deglaciation phase of Late Devensian ice in Glen Chaorainn is represented by boulders on the ridges on the upper east side. One of these ages (11.6 ± 1.0 ka) is younger than the other two ages. This is a low relief boulder and is suspected to have been uncovered or overturned by post depositional processes. Moreover, there is no evidence to suggest deposition during the Younger Dryas ice advance and only outwash and till deposits related to the LGM ice sheet deglaciation are present at this site. We interpret the 16.2 ka age as the initial stabilization of the till cover and the 14.1 ka age as an indicator of periglacial activity on the deposit. Given the uncertainty associated with these exposure dates, the two ages are statistically the same and the deposition of the boulders during the LGM deglaciation is supported by the geomorphological evidence. If the younger age (11.6 ± 1.0 ka) is excluded, the mean value of the other two ages is 15.1 ± 1.4 ka, older than most of the dates from elevated position in the other valleys. The exposure ages provide a minimum date for the disappearance of ice from this site and suggest that this site in Glen Chaorainn escaped glaciation during the YD (Figure 4.20), in agreement with basal radiocarbon ages from nearby Loch Etteridge at ca. 300 m OD (15.3 ka BP) (Figure 4.21). This predates the rapid warming related to the Windermere Interstadial of ca. 14.7 – 12.9 ka BP and is consistent with ice sheet retreat before the rapid warming at 14.7 ka BP (Brooks and Birks, 2000) and coleopteran evidence (Atkinson et al., 1987).

One landform in Glen Banchor that remains to be discussed is the ridge of stratified gravel and sand lying at 362 m OD that has been previously interpreted as a Late Devensian esker thought to have formed during the continuous westward retreat of the Banchor ice (Young, 1978; Gyte, 2004; Trelea, 2008). Morphologically, the ridge appears long and sharp-crested with sediments exposed in a section eroded by the River Calder, suggesting glacifluvial deposition with associated deformation related either to ice overriding or the subglacial infilling of small channels. A mean age of 13.1 ± 1.3 ka produced from two boulders on top of the ridge indicates the boulders have been exposed since the Windermere interstadial (14.7 - 12.9 ka BP; Lowe et al., 2008) (Figure 4.21). As the ridge lies very close to the elevation of several near-by fluvial terraces (365 m OD), the interpretation favoured here is that the feature is indeed a glacifluvial deposit but that it is an eroded remnant of a more extended glacifluvial outwash plain that covered the low lying area of Glen Banchor following deglaciation. Lateral incision of the outwash plain by the River Calder throughout the Lateglacial and Holocene has imparted the illusion of a

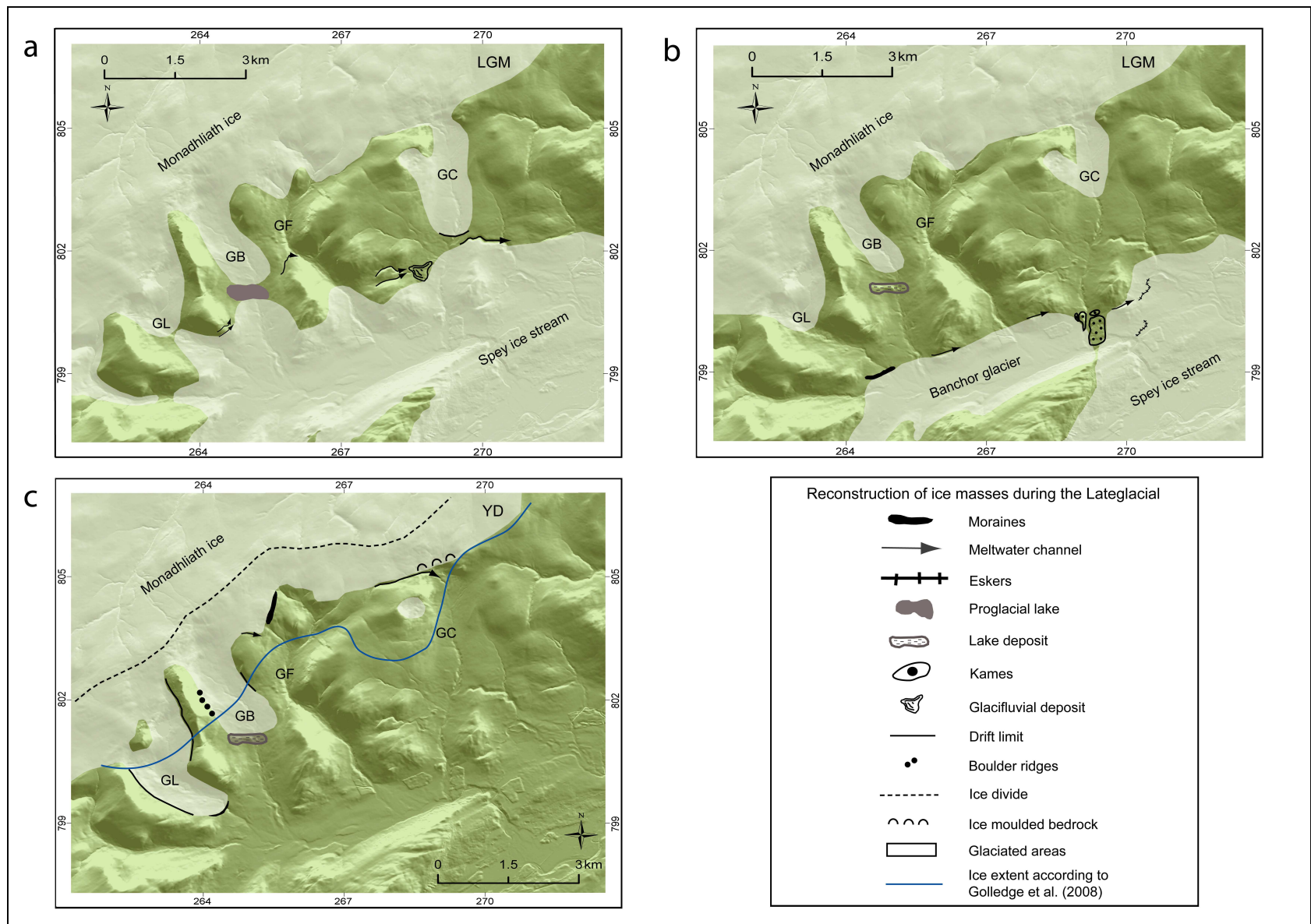


Figure 4.20. Schematic representation of the glaciation pattern in the Monadhliath Mountains: a. 1st stage of the Late Devensian ice sheet deglaciation; b. 2nd stage of the Late Devensian ice sheet deglaciation; 3. Younger Dryas ice readvance. The glens considered in this study are also marked (GL = Glen Lochain; GB = Glen Ballach; GF = Glen Fionndrigh; GC = Glen Chaorainn).

sharp-crested ridge. The exposure ages indicate the time since exhumation of the two boulders from sediment. The extent, thickness and nature of the sediments suggest that the wastage of ice produced an extensive outwash plain at the end of the Late Devensian glaciation (Young, 1974; Gray, 1995).

4.7.2 Younger Dryas

The only subsequent period of severe cooling in the Monadhliath Mountains is the Younger Dryas (YD), a period that saw the formation of corrie glaciers and, possibly, a thin plateau ice field. The YD limit of the glacier in Glen Lochain is indicated by the deposition of moraine B at 11.8 ± 1.1 ka BP (Figure 4.5). Thereafter an intermittent retreat of the glacier towards higher ground is marked by moraine C. Towards the close of the YD, a series of recessional moraines and meltwater channels were formed in Corrie Dubh where the mean ages of boulders indicate that it was ice free by 10.6 ± 1.0 ka BP. This exposure age is in good agreement with dates derived from a kettle hole in the Pass of Drumochter, where deglaciation had occurred before 9405 ± 260 ^{14}C yr BP (ca. 10.5 ka BP; Figure 4.21) (Walker, 1975; Benn & Ballantyne, 2005); the calibrated age is ca. 10.6 ± 745 kcal BP using the OxCal v4.1.7 (Bronk Ramsey, 2010). The ridge above Loch Dubh coincides with the upper YD drift limit and it is possible that the glacier margin coincided with a structural bench, so that the boulder ridge formed as a lateral moraine. Golledge (2007) argued that moraines can be bedrock cored and may show alignments similar to the structural trend of the underlying strata. The kettled blocky till in the plateau above Loch Dubh indicates local ice stagnation at the end of the YD. The existence of two phases of ice decay at the end of the YD was noted by Benn et al. (1992), Bennett & Boulton (1993) and Benn (1997) and interpreted as an initial phase of active deglaciation due to a fall in precipitation with interrupted retreat of ice, followed by an abrupt rise in air temperature (Atkinson et al., 1987) resulting in uninterrupted retreat and local ice stagnation.

During the Younger Dryas stadial, the glacier in Glen Ballach reoccupied the area north of the Late Devensian lacustrine deposit. The height of this deposit and the lack of geomorphological evidence downvalley suggest that ice did not advance further southwards beyond the lake deposit. The mean age obtained from two boulders on top of the lacustrine deposit indicates the time of their deposition at ca. 11.2 ± 1.1 ka ($n = 2$). The flatness of the lake feature does not support exhumation of the boulders that lie on its top surface and the exposure age of the boulders suggests subsequent deposition. The most

likely explanation is for YD ice to have abutted the north side of the pre-existing lake deposit and the boulders to be subsequently deposited by meltwater transport from the near-by ice margin. A series of recessional moraines were formed during glacial retreat, with a boulder from the southernmost (E) producing a mean age of 11.0 ± 1.0 ka ($n = 2$). Further up valley, boulders from a series of bouldery recessional moraines yielded a mean age of 9.8 ± 0.9 ka ($n = 2$), constraining the timing of moraine stabilization. The wide flat basin towards the corrie delimited in the south by successive moraines may imply that the YD glaciers excavated any previous deposited debris in this area and incorporated it into the moraine sequences at lower altitudes (e.g. Benn et al., 2005).

The uniform pattern of moraines in Glen Lochain and Glen Ballach, strongly suggests active glacier retreat at the end of the YD. The valley glaciers deposited moraines that are now somewhat discontinuous across the valleys due to later fluvial erosion. The moraines in Glen Lochain and Glen Ballach have typical YD stadial forms being arcuate down-valley, narrow, often sub-parallel nested ridges, covered in large, locally derived boulders (Sissons, 1979b; Benn et al., 1992) separated by meltwater channels. The consistency of the moraine ages in both valleys suggests synchronous formation and rapid ice decay, likely due to a rapid rise in summer temperature that has been demonstrated elsewhere by subfossil assemblages of coleoptera (Atkinson et al., 1987; Coope, 1998) and chironomid evidence (Brooks & Birks, 2000). However, the altitude difference of ca. 50 m between the glaciers termini in the two adjacent valleys (moraine B at 470 m OD and the lacustrine deposit at 520 m OD) suggests two coeval glaciers of different size. Benn & Ballantyne (2005) and Gordon et al. (1995) suggested that adjacent valley glaciers can behave differently in similar climatic conditions and thus may vary significantly in size, shape, and altitude. In this part of the Monadhliath Mountains there are at least two environmental factors that may have influenced the YD glaciers. First, there is a significantly greater plateau area to the north and west above Glen Lochain than above Glen Ballach and so the mass balance of the Glen Lochain glacier will have been favoured by snow blowing from the greater plateau source area to the west, augmented by snow from its own relatively flat western interfluvium, similar to the effects mentioned by Sissons (1980) and Mitchell (1996). The Glen Ballach glacier was down-wind of this and augmented by lower snow contributions from its narrow western ridge. Second, the Glen Lochain glacier was fed by ice flowing from two corrie accumulation areas that coalesced down valley to form a long valley glacier. Both of these factors contributed to the Glen Lochain glacier extending to lower altitudes than the Glen Ballach glacier during the YD.

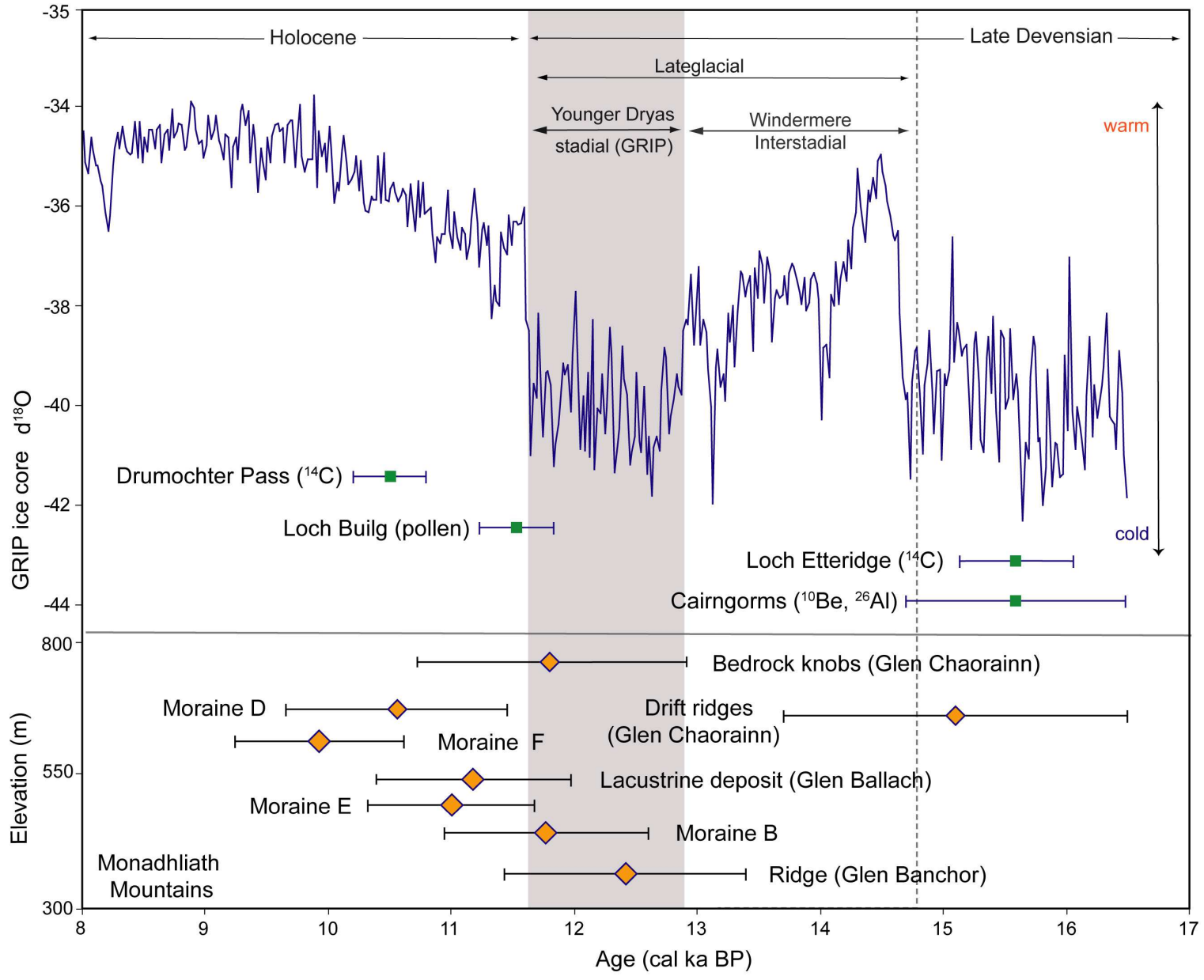


Figure 4.21. Monadhliath Mountains. ^{10}Be exposure ages plotted against the GRIP ice core (Rasmussen et al, 2006) and other Scottish dates (Clapperton et al., 1975; Walker, 1975; Phillips et al., 2006).

Comparing the four glens, the western glens are mostly covered in till, while the eastern glens have thicker outwash deposits. The general lack of YD evidence in the eastern corries and glens strongly suggests that they escaped YD glaciation. For example, Glen Fionndrigh has no evidence of YD glaciation as the valley floor is covered in thick Late Devensian outwash, deeply dissected by stream erosion. Hummocky deposits suggest rapid retreat of Devensian ice towards the plateau, possibly during the Windermere interstadial.

The glacially moulded bedrock knobs on the plateau edge provide a YD mean age of 11.8 ± 1.1 ka ($n = 2$) which may be interpreted as ice situated along the plateau edge. The smoothed and rounded tops and asymmetric north-south profile of the bedrock outcrops at the plateau edges suggest ice flow over the corrie edges from the plateau above. Additionally, the nearby Coire na Caillich on the western side of Glen Chaorainn, at ca. 750 m OD elevation, contains no frost-shattered material but glacially moulded surfaces and a reverse slope which indicates ice cover during the YD.

4.8 Younger Dryas ELA reconstruction and palaeoclimatic implications

In order to reconstruct the palaeoclimate of the Monadhliath Mountains during the YD glaciation, the equilibrium line altitudes (ELAs) are derived for comparison with data from other places in Scotland. A range of ELA reconstruction methods are available and three of these are used here for comparative purposes: the area weighted mean altitude (AWMA), the accumulation area ratio (AAR) and area altitude balance ratio (AABR) methods (see 3.5).

For ELA calculation in the Monadhliath Mountains the valley glaciers were treated separately from any ice on the plateau, so the ELA values must be seen as minima. Ice surface limits were constructed on the NEXTMap DEM, allowing the estimation of the hypsometric curves of the glaciers, the measurement of the glacier areas and the calculation of the palaeo-ELAs using the three methods (Table 4.2). The AABR method yielded consistent ELAs which rose from 643 m and 689 m in the western valleys to 809 m in the east, lower than previous estimates (Sissons, 1980; Trelea, 2008), and indicating a strong decline in the snow input eastwards. The larger Glen Lochain glacier appears to have benefited from a lower ELA, attributed to snow accumulation in both feeder corries

(Coire nan Laogh and Corrie Dubh; Figure 4.5) and a more extensive snow-blow source area on the plateau. The reconstructed Glen Ballach glacier had a higher ELA than the glacier in Glen Lochain and the east-facing Coire na Caillich glacier higher still, but with no ice in the main valley (Table 4.2). This pattern conforms to a more general eastward rise in ELA from west to east found in other reconstructed icefields in Scotland (Benn, 1997; Benn & Ballantyne, 2005), consistent with a steep precipitation gradient decreasing from west to east that was more pronounced during the stadial than at present (Sissons, 1980; Hubbard, 1999).

A steep precipitation gradient decreasing from west to east occurred in Scotland during the Younger Dryas stadial (Sissons, 1980; Hubbard, 1999). At present, western Scotland receives the maximum rainfall (4577 mm) whilst the eastern part is more continental, cooler and with less precipitation (550 mm) (Met Office, 2011). ELAs in West Drumochter Hills to the southwest of the Monadhliath are estimated at 622-656 m (AABR) (Benn & Ballantyne, 2005) whilst the ELAs of the two main glaciers in the Monadhliath Mountains lie between 643-689 m (AABR). The ice masses in the Cairngorms, 30 km east of the Monadhliath lie higher than 750 m during the Younger Dryas, thus the ELA was much higher (Purves et al., 1999).

Table 4.2. Reconstructed equilibrium line altitudes (ELA) for the YD glaciers in Monadhliath Mountains. AWMA = area-weighted mean altitude (Sissons, 1974); AAR = accumulation area ratio (Porter, 2001); AABR = area altitude balance ratio (Osmaston, 2005).

Glaciers	Area (km ²)	AWMA	ELA (m)				
			AAR		AABR		
			0.5	0.6	0.67	1.8	2.0
Lochain	3.10	670	620	600	647	643	639
Ballach	2.68	714	650	630	693	689	684
Caillich	0.20	819	770	760	811	809	807

4.9 A plateau ice field in the Monadhliath Mountains during the YD?

The Late Devensian ice sheet that covered the Monadhliath Mountains left a geomorphic signature that has overprinted much of the study area (Golledge, 2007). However, there is also evidence that during the YD the Monadhliath may have supported an independent plateau ice mass with ice flowing down into the tributary valleys to augment valley glaciers. The SW-NE trending 20 km² plateau above the tributary valleys lies mainly above 800 m OD and certainly acted as a feeder area for snow-blow but, due to an extensive peat cover, there is limited evidence visible on the plateau to confirm ice presence during the YD.

According to Manley (1959) and Sissons (1980), an alpine style glaciation in Scotland would imply ice accumulating and flowing from the valley heads. However, smaller YD plateau ice fields have been reconstructed separately from the larger Highland ice cap in the Cairngorms (Sugden, 1970; Brazier et al., 1998), the Gaick area (Sissons, 1973), West Drumochter Hills (Benn & Ballantyne, 2005), north of Glen Roy (Benn & Evans, 1998) and Creag Meagaidh massif (Finlayson, 2006, 2008). These ice caps on the high plateau feed ice via steep valley-heads to outlet glaciers in the main troughs (Evans et al., 2002). Depending on the basal regime of the plateau ice, the geomorphological evidence may be limited because there may be limited movement across the ice-bedrock interface where cold based ice occurs (Hall & Glasser, 2003). On the other hand, warm-based ice streaming over the plateau lip is likely to produce significant erosional evidence, as indicated by the exposure ages from plateau edge samples in this study.

Ice supply depends on a variety of factors. Gellatly et al. (1989) argue that altitude enhances nourishment of valley and corrie glaciers through snow blow from the adjacent slopes and ice avalanches fed from the plateau ice margin. According to Payne & Sugden (1990), topography is a major control in distribution of glaciers through shape and altitude because it can influence snow and ice build-up in particular locations. Nevertheless, any YD icefield in the Monadhliath Mountains appears to have been small and dependent upon favourable site attributes. The possibility that the western corries accumulated more snow and glaciers advanced further down valley than the eastern ones during the YD could be attributed to the larger plateau area towards the west (Figure 4.5). Such a topographical control is supported by Whalley et al. (1995) who imply that a plateau ice cap is very sensitive to climate. Minor changes in the ice supply from the adjacent plateau icefield will

be transmitted to the downvalley glaciers which will change the climatic sensitivity of the whole system according to their size (Whalley et al., 1995).

The reconstructed ice field in the south-east of the Monadhliath Mountains (Figure 4.20) broadly accords with the ice limits depicted by the ice field and outlet glacier simulation of Gollledge et al. (2008). However, our geomorphological evidence and exposure ages suggest a more extensive YD glaciation. The Glen Banchor glacier tributaries were likely fed by outlet glaciers from an ice field occupying the plateau. However, the lack of geomorphological evidence on the plateau does not allow us to establish the overall configuration of the ice mass, although convincing evidence exists for ice flowing into the corries (e.g. the scoured plateau edge of Coire nan Laogh, Corrie Dubh, Glen Ballach and the YD ages in Glen Chaorainn).

The wastage of plateau icefields is characterised by up-valley retreat of outlet glaciers towards the plateau. However, the recession of the valley glacier outlets is non-linear and characterised by de-coupling events as the feeder icefalls thin and separate from the plateau summit ice so that the plateau ice has an ELA of its own, unrelated to the ELA of the outlet below (Gellatly et al., 1989; Whalley et al., 1995). Gellatly et al. (1989) show that the decline in the supply from the summit feeder areas leads to a rapid response in the glaciers at lower altitudes until they begin to adjust to a new ELA condition. Studies in north-west Scotland indicate that during the YD glaciation, ice decay occurred on the highest ground first, with decoupled ice in the valleys and corries surviving for longer (Bennett & Glasser, 1991; Bennett & Boulton, 1993).

The rapid retreat of small outlet glaciers reflects their sensitivity to climate change and variations in the ice fed from the plateau, but their response is reflected by an elevation change in the position of their ELA. Plateau ice fields are more vulnerable to climate fluctuations than downvalley glaciers because even small elevation increases of the ELA may exceed the maximum altitude of the ice field (Whalley et al., 1995). We suggest that ice in the Monadhliath valleys survived as remnant glaciers well after the feeder ice on the plateau had decoupled and wasted away, hence the young exposure ages in the valleys (e.g. moraine F; Figure 4.13). No recessional moraines occur on the plateau such as those found in Lake District (McDougall, 2001), but the moulded plateau edge of Glen Chaorainn, the presence of ice moulded bedrock knobs separated by subglacial meltwater channels on the plateau edge, the moulded edge of Coire na Caillich, and absence of sediments all suggest warm-based ice flow over the plateau edge at ca. 11 ka (Table 4.1). Ice from the plateau above Glen Chaorainn seems to have reached the headwall without flowing over and hence

no YD modification can be traced in the Glen itself. The stagnation of the Monadhliath plateau ice field at or close to the plateau edge is given some support from individual boulder ridges and spreads that lie on or close to the plateau edge (Figure 4.5). This may indicate debris release on ice melt as the ice field margin stagnated at the plateau edge at the end of the YD. An alternative explanation is that the boulder accumulations have survived from the LGM glaciation under cold-based ice. Unfortunately, no exposure dates of these boulders exist to allow refinement of these ideas.

4.10 Conclusions

1. The glacial geomorphology of the Monadhliath Mountains clarifies the final downwasting and readvance pattern at the end of the Devensian glaciation. A proglacial lake developed between two glacier termini in Glen Ballach, similar to other ice impounded lakes during the Lateglacial (14.7 – 11.5 ka BP). The glacialfluvial landforms show that the stillstand was followed by ice thinning and retreat. Field evidence indicates a subsequent Younger Dryas plateau ice field with glaciers spilling southward into the glens. The active retreat of these valley glaciers is marked by successive recessional moraines in the western glens.
3. Our surface exposure ages are consistent with other dates from neighbouring areas. The deglaciation of the Late Devensian ice sheet in the Monadhliath Mountains occurred at 15.1 ka, roughly at the same time as the near-by Loch Etteridge (15.3 ka BP). We place the retreat of the Younger Dryas glaciers in the Monadhliath Mountains between 11.8 ka and 9.8 ka at the end of the Younger Dryas period (12.9 ka - 11.7 ka BP).
4. Equilibrium Line Altitudes (ELAs) for the main YD glaciers in the valleys, calculated using area-altitude balance ratios, ranged from 643 to 689 m OD in the west and 809 m OD in the east. This west-east increase is consistent with a linear rise of the ELA during the YD in Scotland from west to east which is attributed to topographically controlled variations in snow supply. This additional snow supply may explain the discrepancy between mapped and modelled YD ice extent in the Monadhliath Mountains, similar to that found for the Beinn Dearg massif further north (Finlayson et al., 2011).

5. The limited extent of glaciers and the formation of a plateau ice field during the YD agree well with the independent Monadhliath ice cap interpretation of Gollledge et al. (2008); however, the exact extent of the plateau ice cannot yet be established or dated.
6. The distribution of surface exposure ages and the relative chronology of the mapped glacial features yield a coherent deglaciation pattern across the south-east part of the Monadhliath Mountains, and fit well with the wider climatic gradients across Scotland at that time.

Chapter 5

Romania

5.1 Introduction

This chapter focuses on the reconstruction of glacier extent and dynamics, and the deglaciation pattern in the Rodna Mountains. There are no glaciers in these mountains at present; however, perennial snow patches persist in sheltered areas. The Rodna Mountains are part of the central Mesozoic-crystalline belt of northern Romania (Figure 5.1), the nature of these rocks helped to preserve an extensive glacial landscape.

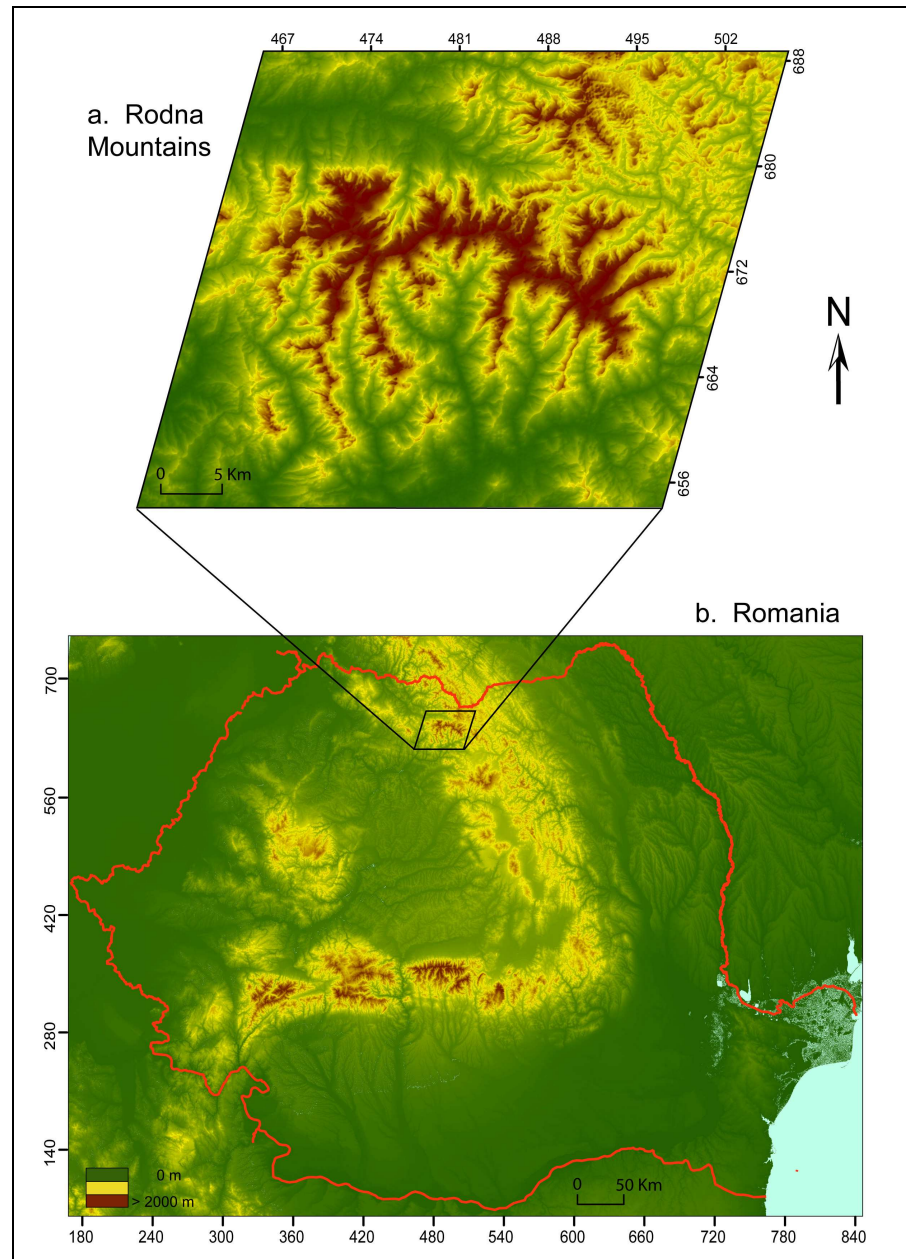


Figure 5.1. Position of the Rodna Mountains in the Romanian Carpathians. Digital elevation models from the ASTER (a) and SRTM (b) imagery data (NASA, 2004).

5.2 Rodna Mountains

5.2.1 Geographical position

The Rodna Mountains, located in northern Romania (Figure 5.1), are dominated by a central west to east oriented ridge with elevations of up to 2303 m. They are bordered to the north by the Maramureş Mountains, and decrease in altitude towards the Someşul Mare valley, which separates them from the Bârgău Mountains in the south. They are bordered by the Țibleş Mountains in the west and the Suhard Mountains in the east (Figure 5.2).

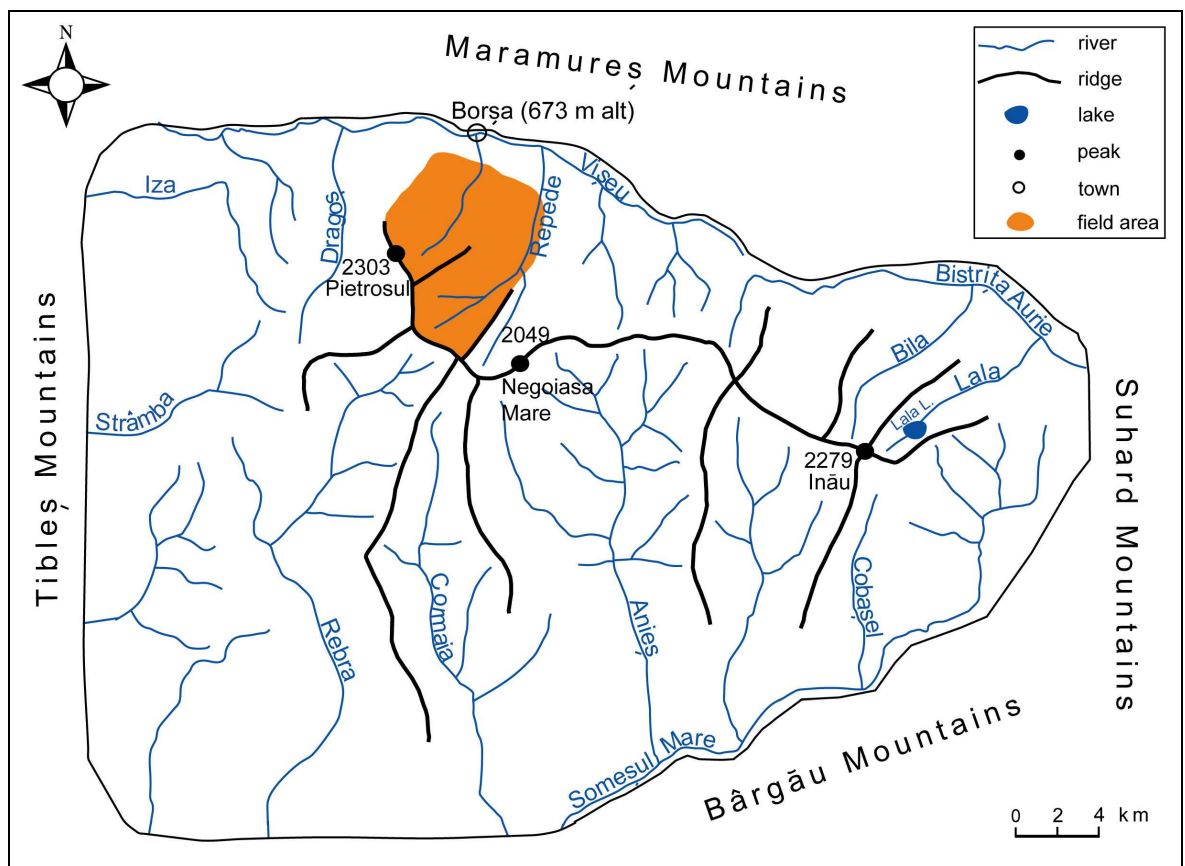


Figure 5.2. Position of field area in the NW part of Rodna Mountains. Modified from various sources.

5.2.2 Climate

The position in the Eastern Carpathians and the relatively high elevation of the Rodna Mountains helps create a distinctive local climate. The Rodna Mountains are located in the transition area between western oceanic air masses and the drier continental influences from the east. The east-west orientation of the main ridge creates a topographic barrier to

the southward movement of cold air masses originating in the Baltic. Mean annual temperatures in the Rodna Mountains range between -1.5 °C above 2200 m, 0 °C at 2000 m alt, ca. 2 - 2.5°C at 1650 m at the upper limit of forest on the northern slopes, and 6-7 °C in the valley bottoms at <1000 m altitude and are 1°C lower on the north side of the mountains than on the south side (Coldea, 1990; Donița, 2005).

Dominant moisture bearing winds originate in the northwest (Mîndrescu et al., 2010). Precipitation shows a significant altitudinal gradient and ranges from ca. 750-800 mm/yr at the foot of the mountains (mostly rain) to ca. 1200-1400 mm/yr at mid altitudes, and over 1400 mm/yr in the highest areas of the mountains. Precipitation is strongly seasonal, falling predominantly during the summer with a minimum in January (66 mm). Snow fall occurs on the highest summits from September and snow cover is maintained at altitudes over 1800 m from November to June, with snow being maintained in many sheltered areas until July and perennially in favoured spots (PNMR, 2006).

5.2.3 Geological structure

The Rodna Mountains are composed in the centre of crystalline rocks dominated by schists, crystalline limestone, ortho- and paragneisses, serpentines, amphibolites and quartzite surrounded by a discontinuous belt of sedimentary rocks comprising limestone, conglomerate, sandstone, marl, phillites and argillaceous-sandstone (Figure 5.3). The crystalline-sedimentary contact is rectilinear north and south of the mountains, due to two major faults. Neogene dykes, sills and necks (rhyolite, dacite, andesite, breccia, granite and to a lesser extent basalt) appear mainly in the southern and south-eastern part of the Rodna Mountains along the Someșul Mare river. The crystalline core of the Rodna Mountains has a general monoclinical position, with a NW-SE orientation, dipping SW. This results in a strong cuesta form, especially in the eastern part of the mountains. Intensive folding occurred during the Stiric orogenesis resulting in the sedimentary rocks being folded into synclines and anticlines (Sîrcu, 1978).

The Rodna Mountains are an asymmetric horst bounded by the Rodna (Dragoș-Vodă) fault in the north and the Someș fault in the south. The north-south asymmetry of the Rodna Mountains is due to the fact that the Rodna fault occurs much closer to the main W-E ridge, compared to the Someș fault. Thus the northern slopes are shorter and more abrupt

than the southern ones (Sîrcu, 1978) and the north and south draining valleys are deeply incised.

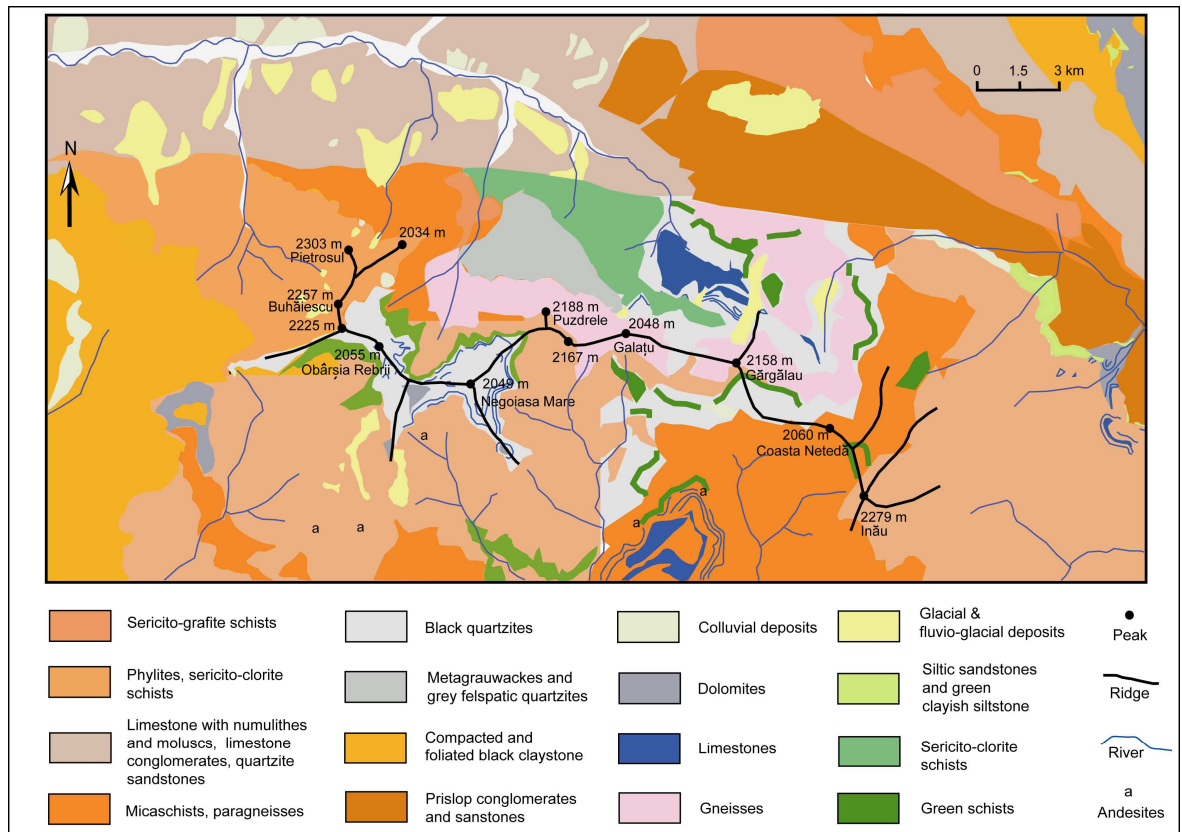


Figure 5.3. The geological map of the Rodna Mountains, sheets 20a Pietrosul Rodnei and 20b Ineu (Geological and Geophysics Institute of Romania).

5.2.4 Earlier investigations in the Rodna Mountains

The Quaternary glaciations in the Rodna Mountains have been studied by many researchers as summarised by Sîrcu (1978). In 1891, Lehmann identified the Lala cirque and glacial valley, and the moraine blocking a lake at 1820 m altitude (Figure 5.2). Based on the pattern of moraines on the northern slopes Sawicki (1912) concluded that a single glaciation occurred with three stages of retreat. For long it was thought that the Quaternary glaciations affected only the northern side of the Rodna massif, though Sawicki (1912) and Morariu (1940) noted several small cirques on the southern flanks. Sawicki tried to explain the uneven cirque distribution as the result of climatic differences, with glaciers forming extensively on the northern slopes due to the higher amount of precipitation. Sîrcu (1978) argued that the southern cirques are caused by seasonal snow accumulation and not by ice because of the absence of hollows for snow to accumulate to sufficient depth. He considered that winds played a more important role in snow accumulation than the

orientation of the slopes. A similar scenario was proposed for the Southern Carpathians by de Martonne (1924) who noted more glaciated valleys on the southern slopes than on the northern ones and attributed this to western moisture bearing winds from the Atlantic, on the assumption that the direction of the dominant winds are likely to have been the same as at present. Today the dominant source of humidity for Romania is the Atlantic Ocean, hence west and northwesterly winds were thought to have brought greater amounts of precipitation to the northern slopes of the higher mountains, rather than the south (Romer, 1906 in Sîrcu, 1978). Lack of precipitation on the southern sides was caused by the föhn effect of these winds explaining the relatively more abundant glaciated features on the northern slopes (Sawicki, 1912).

Sawicki (1912) identified a series of moraines at 800 m altitude in the Repede valley (on the northern flank) (Figure 5.2) as indicators of the glaciers maximum extent. His work was continued by Lajos (1927) and Krätner (1930), who found a latero-frontal moraine in the Bila valley (Figure 5.2) which suggested that on the north-eastern side of the Rodna Mountains the glaciers descended to only 1350 m altitude. According to Pawlovski (1936), at the maximum advance, ice extended to lower altitudes than previously suggested. He identified a latero-frontal moraine at 762 m in the Pietroasa valley (Figure 5.4).

Sîrcu (1978) suggested three hypotheses regarding the last Quaternary glaciations in the Rodna Mountains: 1) three glacial cycles (Mindel, Riss, Würm), 2) two glacial cycles (Riss and Würm) and 3) a single glacial cycle with three stages, similar to Sawicki (1912). His assumptions were based on the fact that three successive moraine deposits were found at different elevations in several valleys and each moraine was related to different (undated) periods of deposition. The existence of latero-frontal moraines indicates an approximate glacial extent, though no evidence unequivocally delimits the maximum extent. It also allowed the calculation of the equilibrium line altitude (ELA) position corresponding to the time of deposition of these moraines. The calculations by Sîrcu (1978) indicate that the ELA was situated at 1550 m in the first phase, at 1800 m in the second and at 2000 m in the last phase. An alternative to progressively smaller ice extent was the possibility that the second advance of glaciers was more extensive and overran the earlier moraines, but the evidence for this is insufficient. Sîrcu (1978) insisted that the last glacial advance was restricted to cirque glaciers and attributed this to a short duration cooling event, the first indication of a possible Younger Dryas event in the Rodna Mountains.

5.3 Study area

The study area ($\sim 50 \text{ km}^2$) is situated in the northwestern part of the Rodna Mountains (Figure 5.2). It comprises the two cirques of Zănoaga and Iezer draining into the Pietroasa Valley, and the Buhăiescu glacial complex with four smaller cirques: Tăuri, Curmătura, Rebra and Buhăiescu Mare draining into the Repede Valley (Figure 5.4 & Figure 5.5). Compared to other areas explored in the Rodna Mountains, the study area has the greatest variety of erosional and depositional glacial landforms.

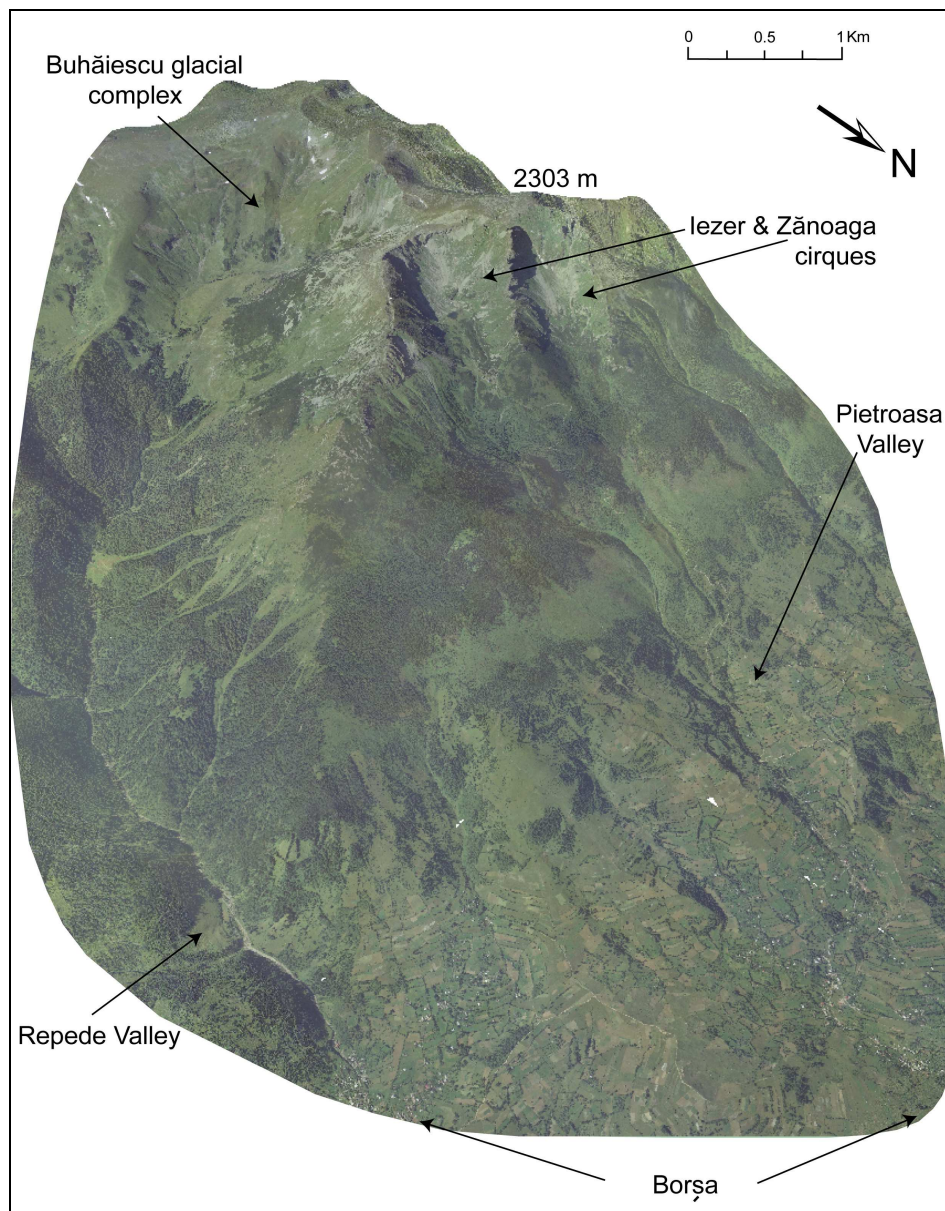


**Figure 5.4. Orthophotomap of the study area overlaid on a 3D surface.
The image terminates at 700 m altitude.**

Fieldwork was carried out between 2303 m and 700 m altitude, restricted in the lower half by the town of Borșa which spreads towards higher altitudes (~900 m) and the extensive forests (up to 1700 m altitude) which limited remote sensing and restricted access to certain areas, especially in the Repede valley (Figure 5.4). The field area includes five summits with altitudes over 2000 m, situated on the main ridge: Pietrosul (2303 m), Buhăiescu (2268 m), Curmătura Buhăiescu (2225 m), Rebra (2119 m) and Obarșia Rebrii (2055 m) (Figure 5.5). Ridges, extending from the main ridge, separate the cirques.

5.4 Geomorphology of the study area

Although this study is about past glacial activity and the climatic implications, the landscape of the Rodna Mountains is the result of various earth surface processes. Each produces a distinct morphology which is subsequently altered as the landscape evolves. Therefore, the following geomorphological descriptions include details of all findings in each cirque and valley.

Generally, the relief of the study area has been modified by glaciers as shown by characteristic overdeepened valleys and glacial cirques, many of them occupied by lakes. Most of the glacial valleys on the northern slopes of the Rodna Mountains are obsequent, with stepped longitudinal profiles (Figure 5.13). Cirque walls are dominated by talus slopes.

Various glacial erosional and depositional features are found at the bottom of the cirques and along the valleys together with periglacial landforms such as tors, talus, rock chutes, boulder fields, protalus ramparts and nivation niches (Figure 5.5).

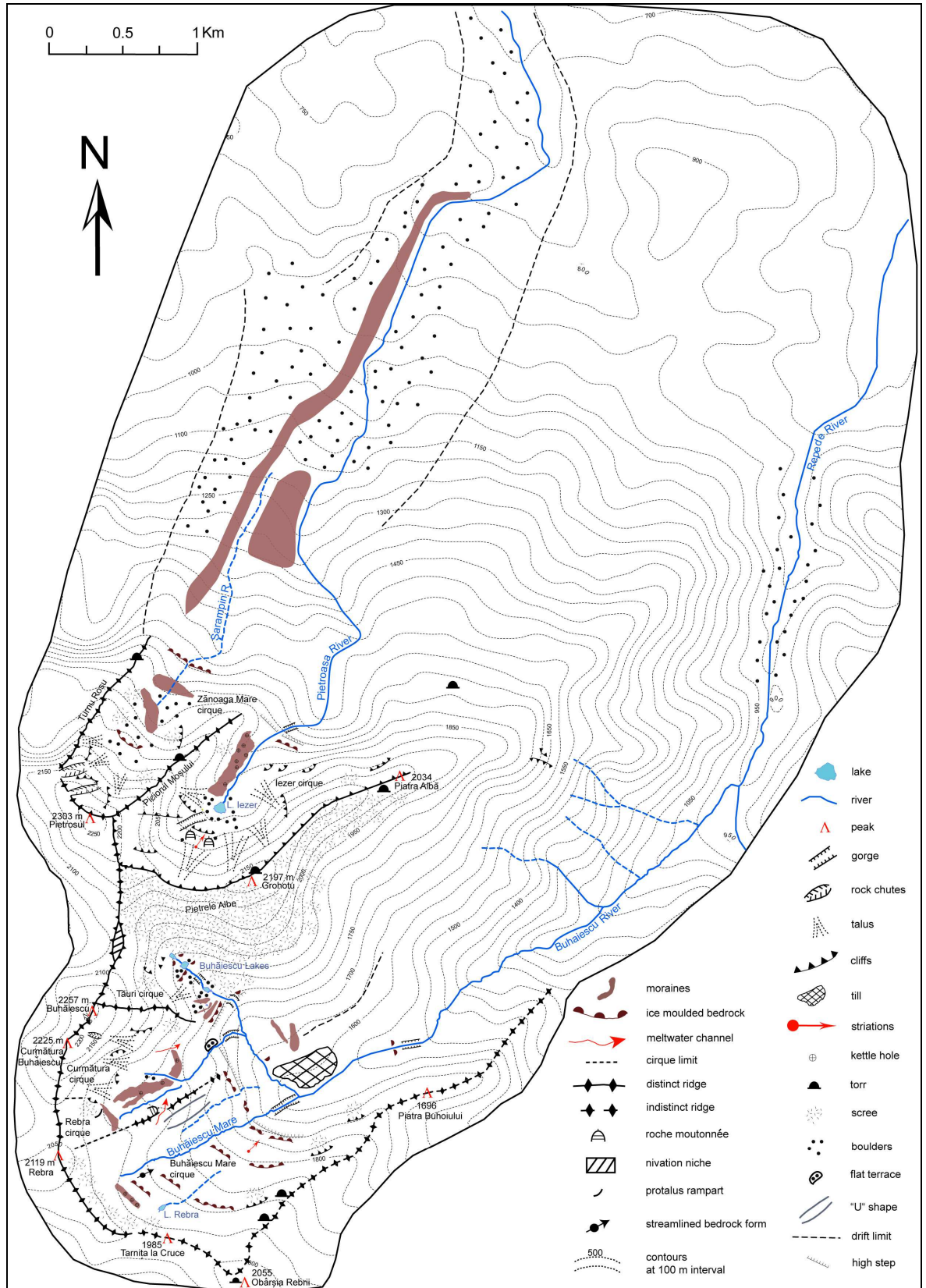


Figure 5.5. Geomorphological map of the study area. The map of the northern (Figure 5.10) and the southern cirques (Figure 5.16) with the draining valleys are presented separately in the next pages. The map can also be found in Appendix C.

5.4.1 Zănoaga Mare cirque

Zănoaga Mare is the westernmost cirque in the study area and has a north-eastern orientation. It is a long, relatively narrow cirque with a concave amphitheatre shape in the higher part and opens out at about 1650 m (Figure 5.6). The highest peak of the Rodna Mountains, Pietrosul rises to 2303 m at the top of the cirque back wall. The back wall is almost vertical for ca. 400 m, but is cut by several rock chutes which feed the lower talus cones, the largest of which lies in the south-east part of the back wall. A deep, almost vertical, rock chute on the western part of the same wall is 250 m long and feeds another talus cone (Figure 5.5).

The back wall of this cirque continues into two lower ridges: the Turnu Roşu in the north and Piciorul Moşului in the south. The Turnu Roşu northern ridge progressively decreases in elevation towards the north-west part of the cirque where it encounters the only red-coloured limestone found in the field area. This limestone has been intensively modified by frost-shattering into rock towers that are several tens of metres high. The upper part of the side walls are mostly rock, terminating in scree slopes.

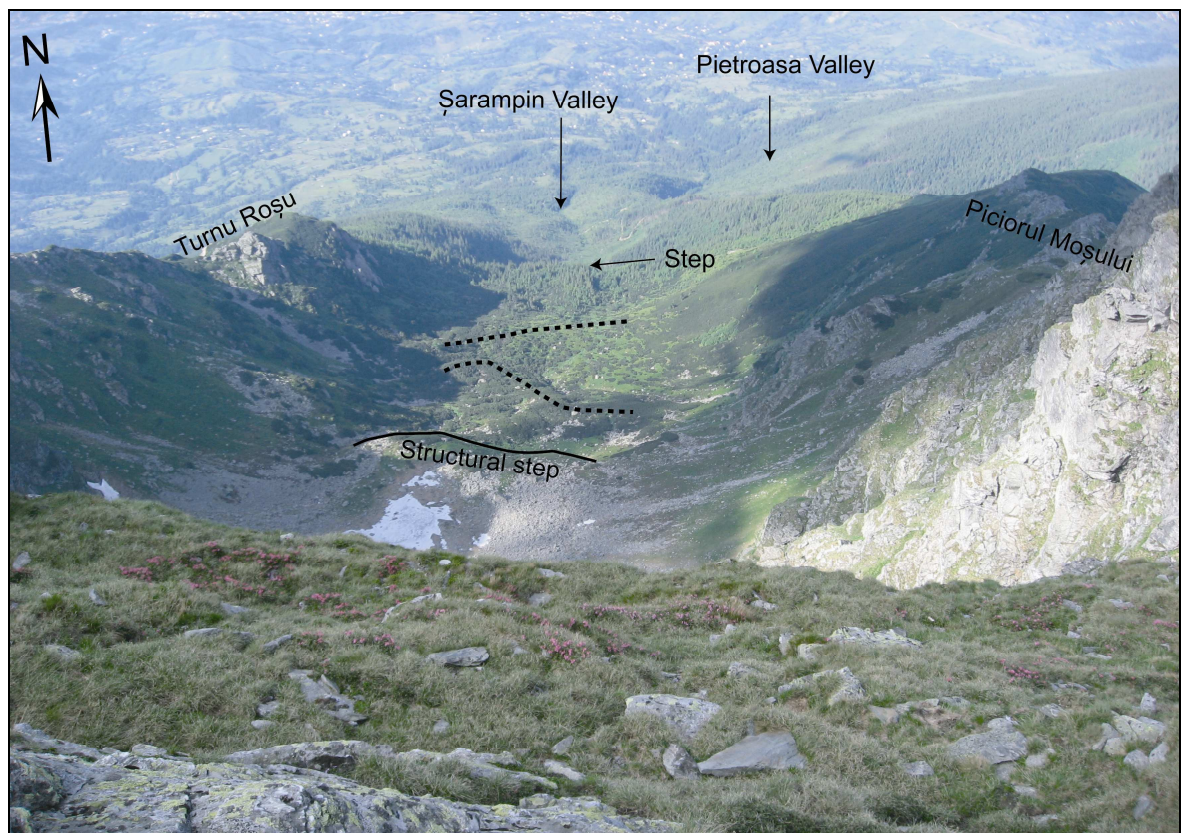


Figure 5.6. Zănoaga Mare cirque. Dashed lines indicate the two moraines (see Figure 5.10).

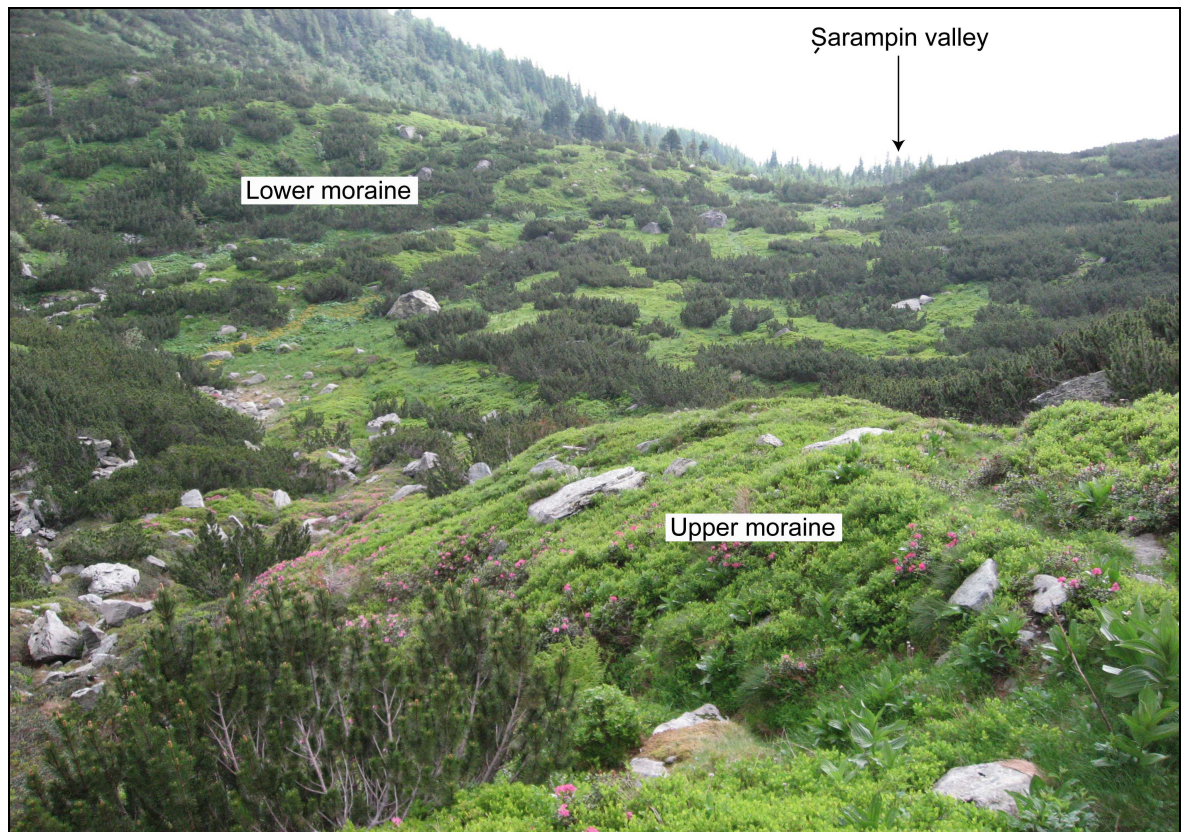


Figure 5.7. The lower moraine (1750 m) and part of the upper moraine (1800 m) in the Zănoaga Mare cirque (see Figure 5.10).

Piciorul Moșului is a rugged NW oriented ridge, separating the Zănoaga Mare and Iezer cirques. Towards the north-east, the side slope is abrupt and covered in rock debris at ca. 1950 m, whilst towards the mouth of the cirque the side slope and the top of the ridge is extensively vegetated with *Pinus Mugo*. Several tors occur on the ridge (Figure 5.10).

Figure 5.13 shows the long profile of the cirque. Protalus ramparts occur in the highest part with no evidence suggesting boulder transport by ice to these features. However, the bedrock step in the upper part at 1950 m altitude (Figure 5.6 & Figure 5.10) is ice moulded and covered in bouldery deposits left by the last ice mass that occupied this cirque. The lower two steps at 1800 and 1750m, although previously interpreted as structural steps (Șîrcu, 1978) are in fact two recessional moraines that have a rounded shape, a steeper ice proximal side and are composed of boulders. The 1800 m altitude moraine extends from the west wall in an arcuate up-valley shape (Figure 5.5). The lower moraine, at 1750 m elevation, stretches across from the Turnu Roșu ridge to the Piciorul Moșului ridge and is bisected by a stream (Figure 5.7). Some of the boulders (ranging in size from about 2.5 m to 4 m above ground) on the moraines suggest a supraglacial transport mechanism, as the side-walls are too distant for rockfall. Other small bouldery deposits were abandoned by ice as ground moraines when ice ablated in this cirque (Figure 5.10).

Unlike other cirques in the study area, Zănoaga Mare has a smooth transition to the lower valley, with only a small bedrock step marking the end of the cirque.

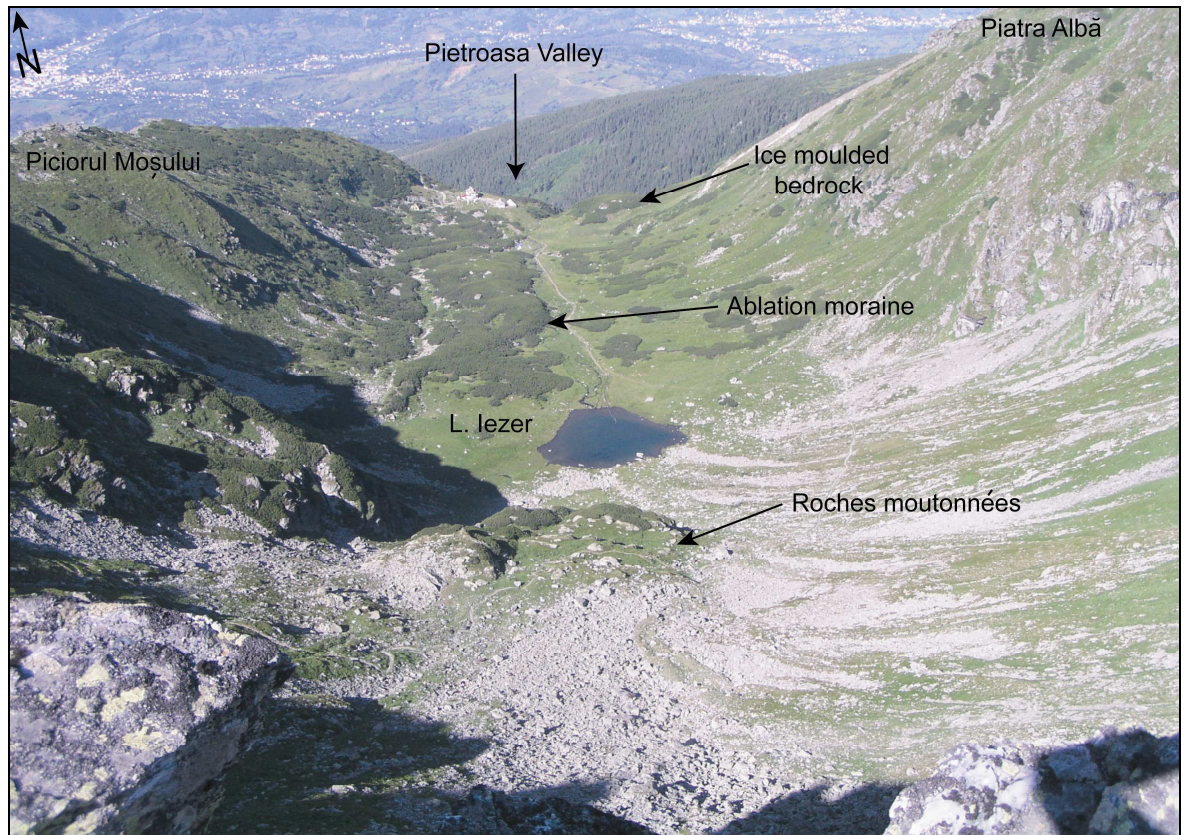


Figure 5.8. Iezer cirque (see Figure 5.10).

5.4.2 Iezer cirque

Similar to Zănoaga Mare, the Iezer cirque is a steep-walled semicircular trough-like basin, which gradually opens toward lower altitudes (Figure 5.8). Although with the same NNE orientation as Zănoaga Mare, the topographical details are very different. The Iezer cirque is delimited by the Picioarul Moşului ridge separating it from the Zănoaga Mare cirque in the NW and the long, rugged Pietrele Albe ridge in the SE (Figure 5.10). The back wall of the Iezer cirque is almost entirely covered with active talus cones composed of various sized boulders (up to 2 m in length). Frost shattered debris slopes cover the rest of the NW wall, but they are stabilised by vegetation except for a few active areas. The eastern side wall consists mostly of steep cliffs which generate limited debris, especially in the northern part due to the presence of limestone.

In transverse profile, the Iezer cirque has an overdeepened “U” shape with two steps evident in the longitudinal profile (Figure 5.13). The higher step is located above Lake Iezer at ca. 1900 m, covered mostly in frost-shattered debris, and a series of roches moutonnées (2-5 m in length; Figure 5.9) with striations and grooves preserved along the flanks (Figure 5.11). A steep cliff separates it from the cirque floor and Lake Iezer at 1825 m.



Figure 5.9. Roches moutonnées in the upper part of the Iezer cirque (Figure 5.10).

Evidence for glacial scouring, other than the roches moutonnées, is indicated by the lake basin (Figure 5.8) and large areas of glacially moulded bedrock on top of the second step at the northern end of the cirque (Figure 5.12). The rounded vegetated bedrock ridge on the edge of the step (Figure 5.8), curves up valley around the former glacier terminus. This step drops more than 200 m down to the lower valley (Figure 5.13). Most of the cirque floor is occupied by a 538 m long and 100 m wide ablation moraine. Several large kettle holes (up to 10 m diameter) occur on this moraine, suggesting in situ stagnation and melting of ice in this cirque at the end of the last glaciation. Elongated ridges curved by drainage occur as talus slopes remnants on the eastern side of this moraine (Figure 5.8).

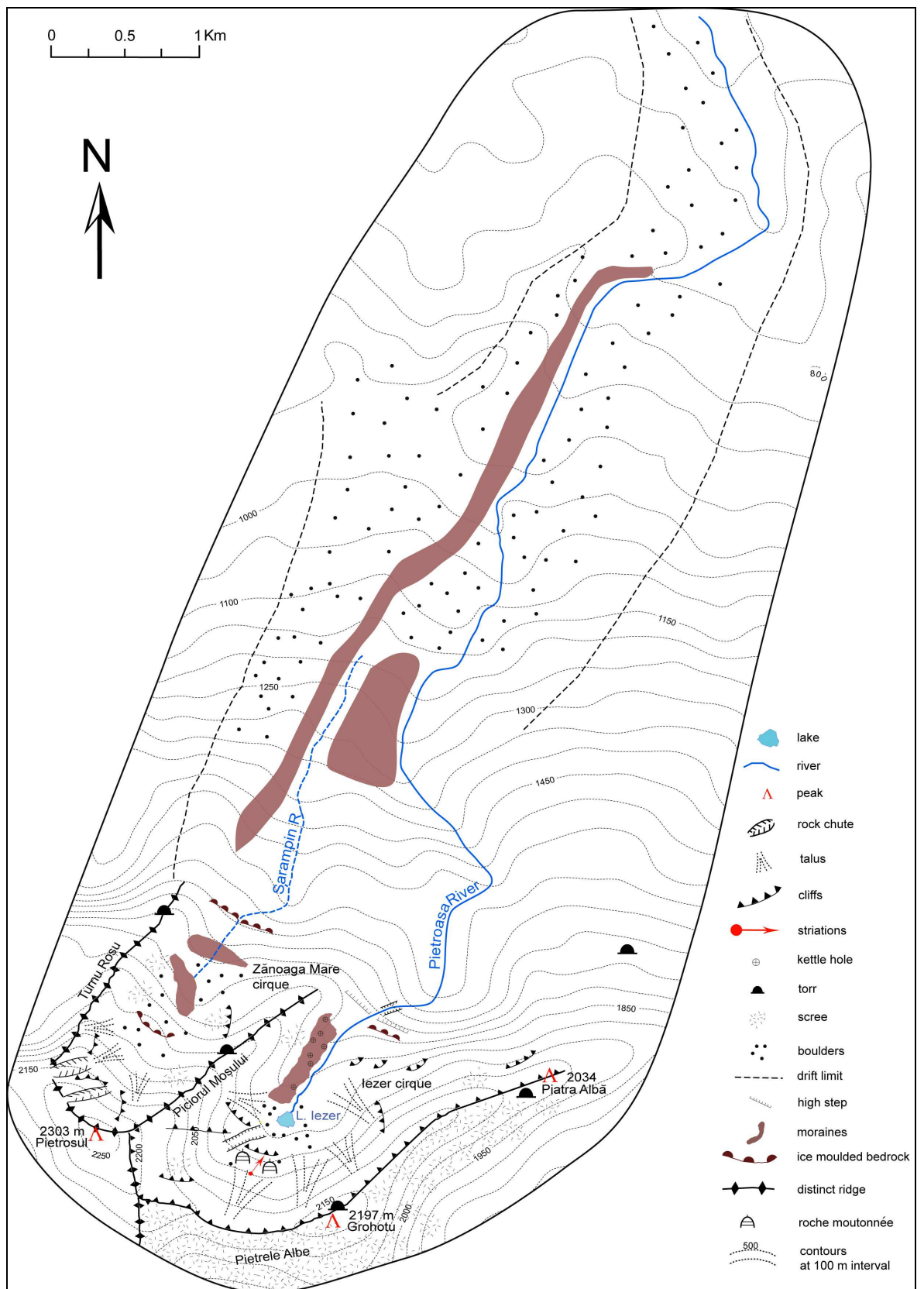


Figure 5.10. Geomorphological map of the NW part of the study area including the Iezer and Zănoaga Mare cirques and the Șarampin and Pietroasa Valley.

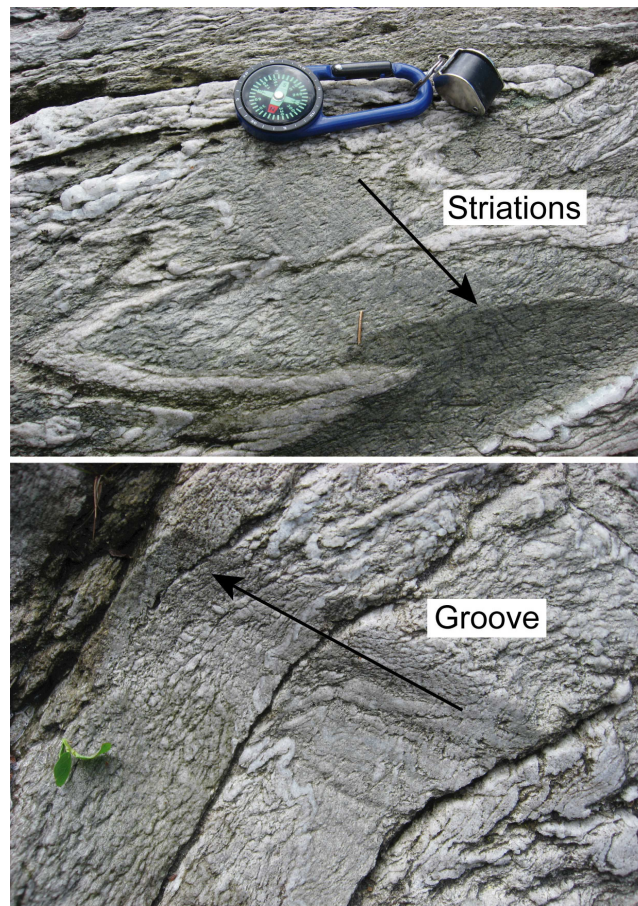


Figure 5.11. Glacially abraded surfaces (see Figure 5.10).

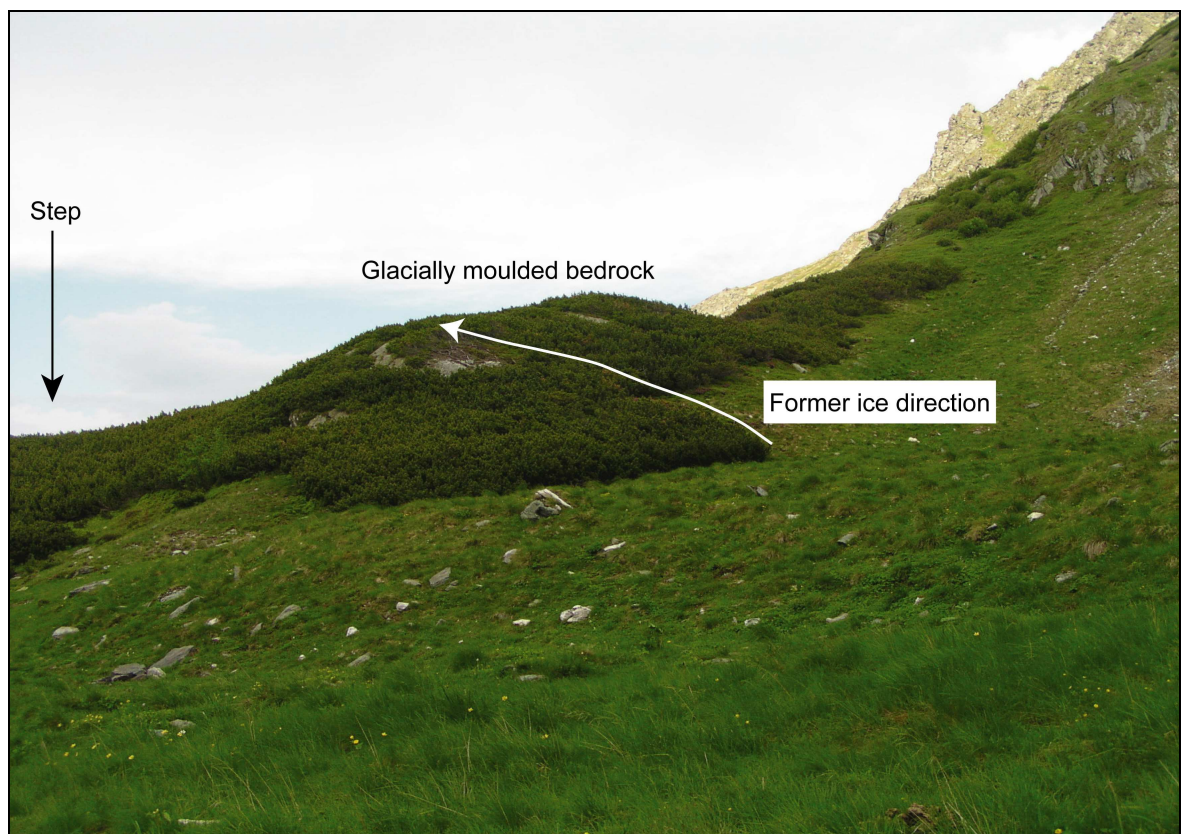


Figure 5.12. Glacially moulded bedrock above the lower step at Iezer cirque (see Figure 5.10).

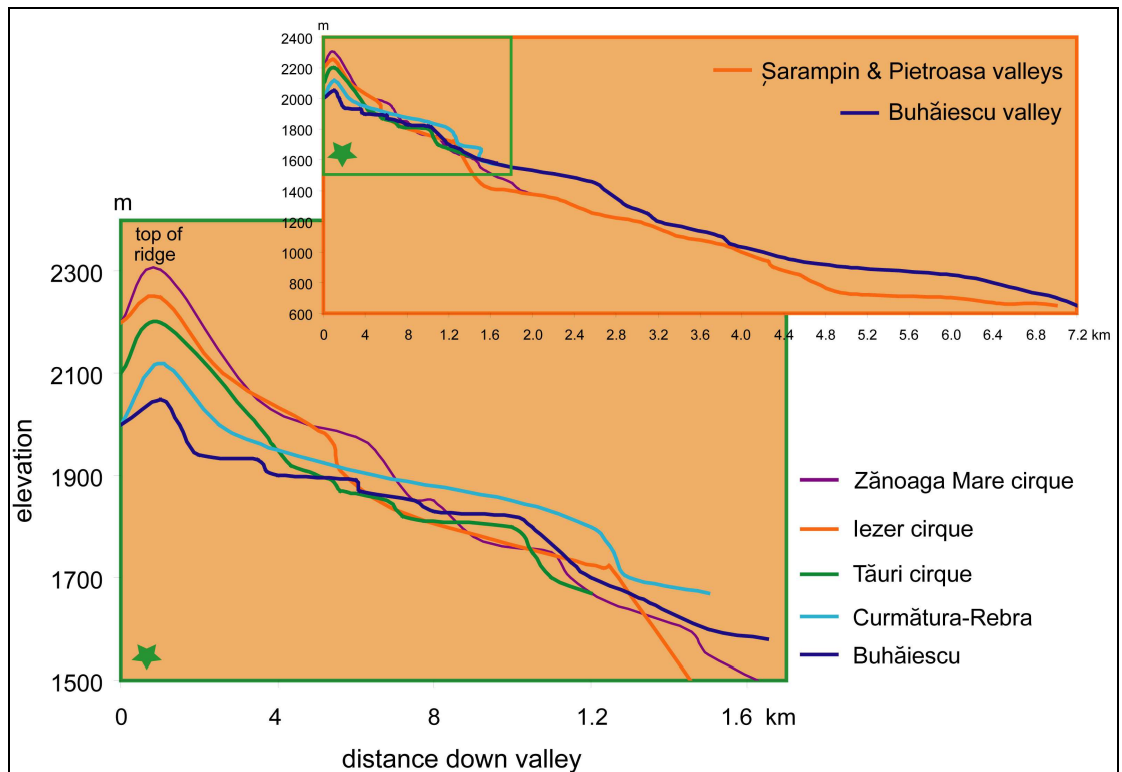


Figure 5.13. Longitudinal profile of the cirques in the study area generated from the DEM.

5.4.3 Pietroasa and Șarampin valleys

The Pietroasa valley extends to the northwestern part of the study area, and is the most important access route to the mountain on the northern side of Pietrosul (2303 m). The narrow and deep valley extends from below the lower step in the Iezer cirque at 1450 m to where it meets the Șarampin valley at 1100 m altitude. A large medial moraine separates the two valleys (Figure 5.10). The moraine stretches for 550 m between 1300 m and 1650 m altitude and it is composed of a matrix supported diamicton with various boulder sizes and shapes (Figure 5.14).

The Șarampin valley has a low angled gradient with bedrock steps in the upper part but it narrows and deepens between 1250 m and 1130 m. A long lateral moraine extends for almost 4 km along the western side of the Șarampin and Pietroasa valleys. It starts as a very shallow ridge from Turnu Roșu and becomes narrower (up to 100 m wide) and higher (4 – 20 m) lower down (Figure 5.15). Excavations for building roads and houses have revealed the composition of the moraine and confirm that it consists of a matrix supported diamicton with sub-angular boulders of various sizes. The occurrence of the red-coloured limestone from Turnu Roșu throughout the deposit, and the clast morphology suggest ice

transport. West of the lower end of the Şarampin valley, before curving towards the Pietroasa valley, the landscape contains more than 300 m wide boulder spreads (Figure 5.10).

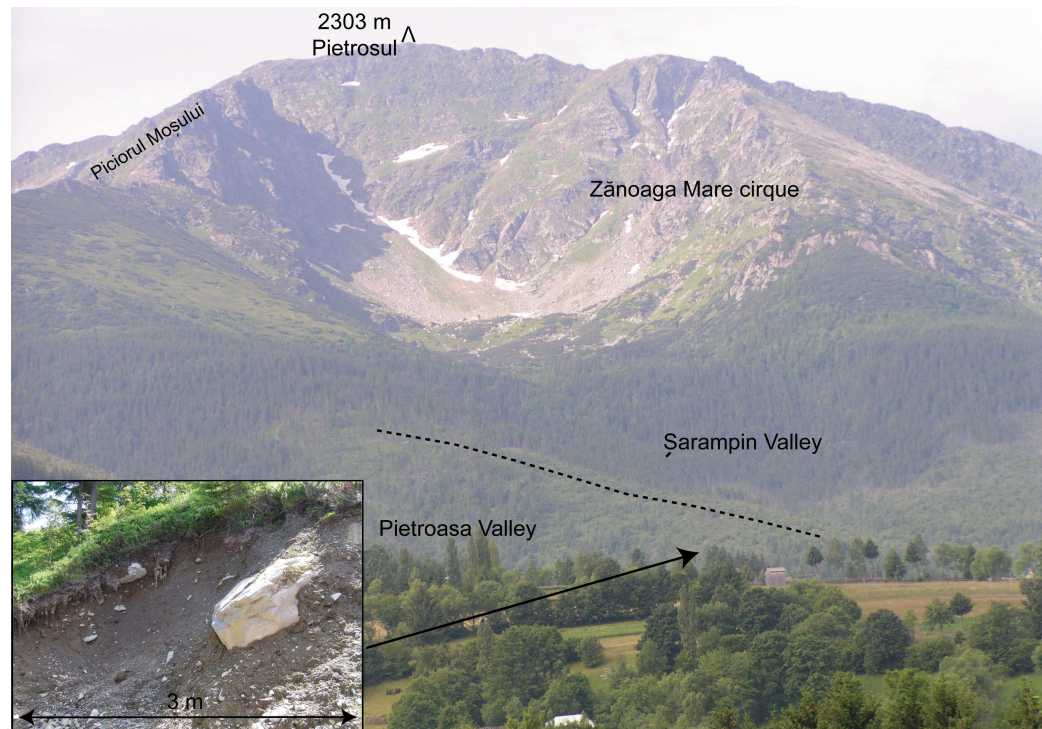


Figure 5.14. Medial moraine (dashed line) between Pietroasa and Şarampin valleys (see Figure 5.10).



Figure 5.15. Lateral moraine on the western side of the Pietroasa valley (see Figure 5.10).

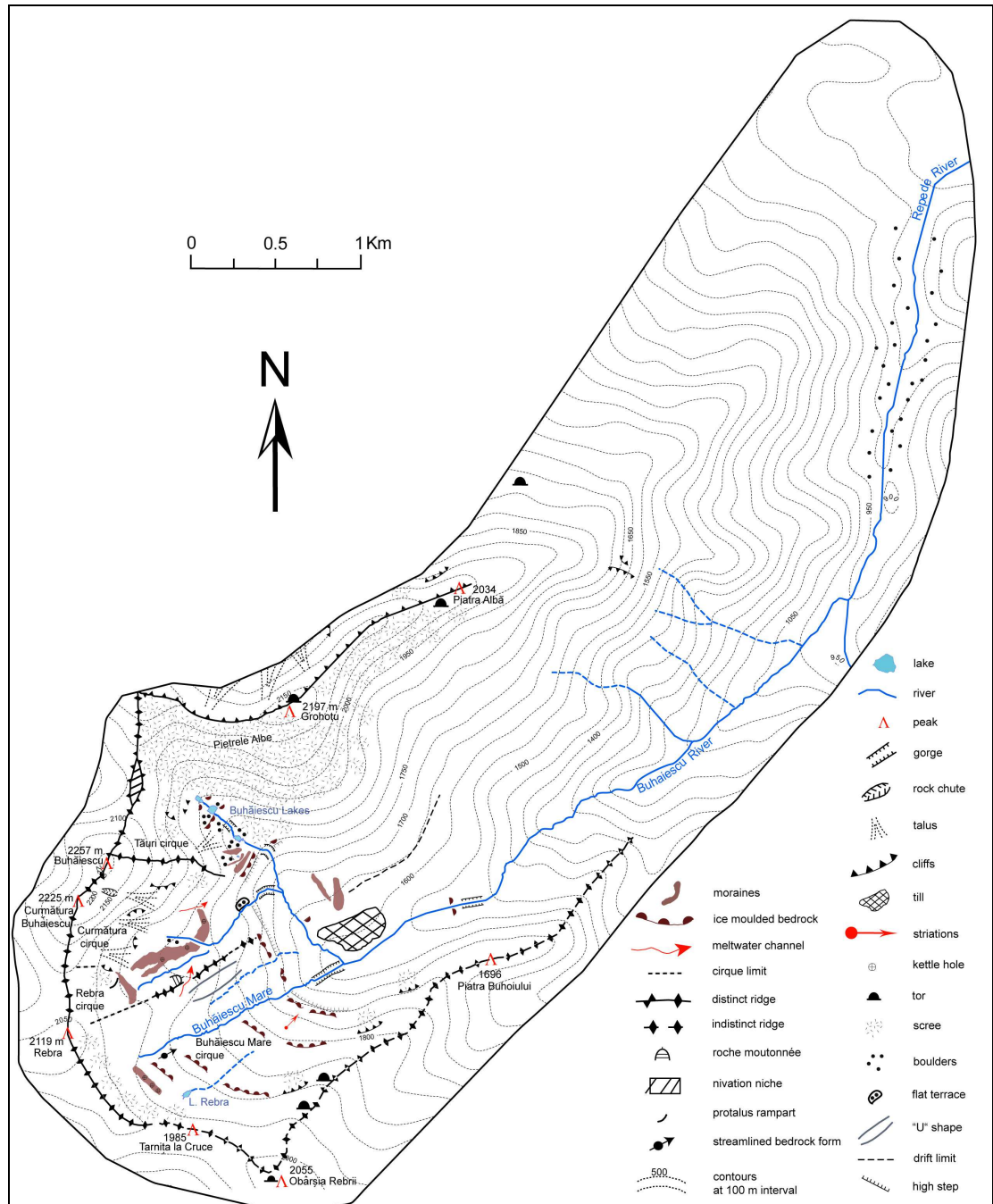


Figure 5.16. Geomorphological map of the SE part of the study area.

5.4.4 Buhăiescu cirque complex

Buhăiescu is a wide glacial complex in the Rodna Mountains, similar to the ones in the Southern Carpathians of Romania (Reuther et al., 2007). It comprises four independent cirques, Tăuri, Curmătura, Rebra and Buhăiescu Mare draining into the Buhăiescu valley and further down into the Repede valley.

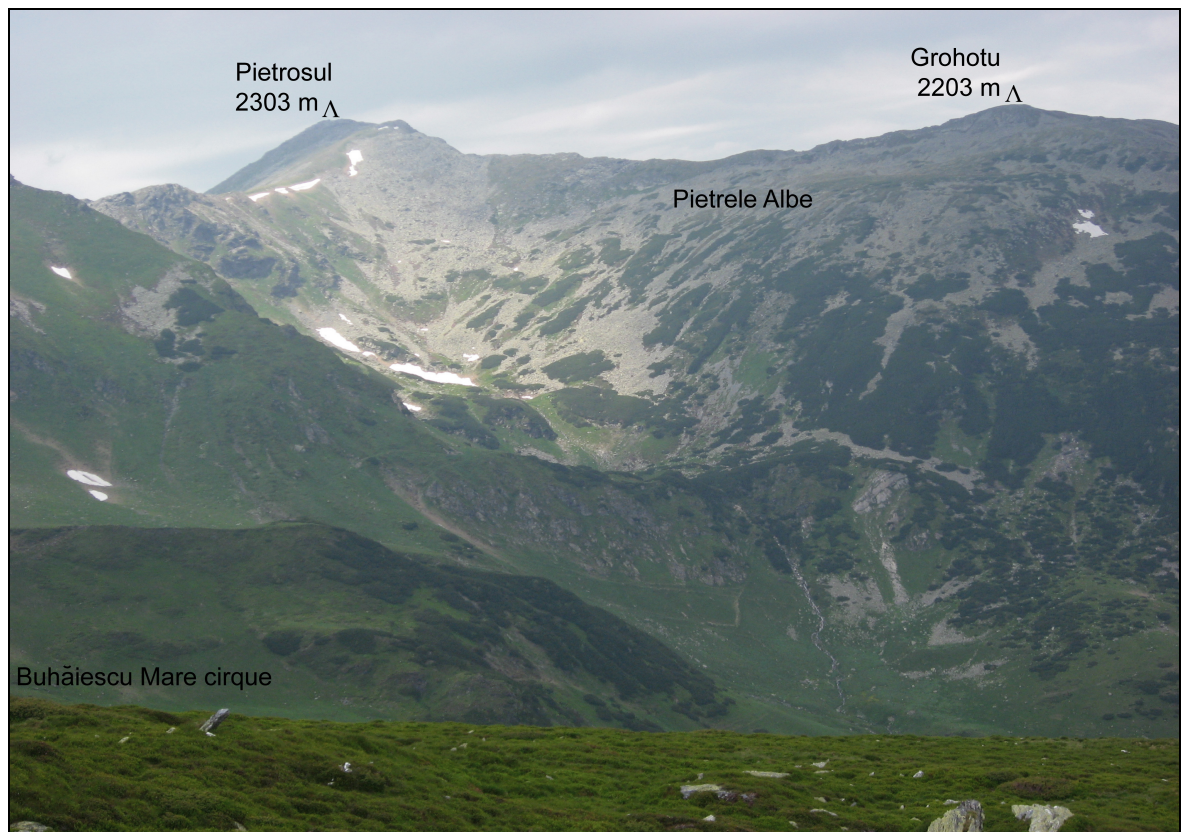


Figure 5.17. View of the Tăuri cirque from the east (see Figure 5.16).

5.4.4.1 Tăuri cirque

Tăuri cirque, located between the Pietrele Albe (= white stones) ridge and the steep north-eastern wall of Buhăiescu (2268 m), is a hanging cirque with a NW-SE orientation (Figure 5.17). The southern side slopes of Tăuri cirque are very abrupt in the upper part, while the northern slope is less steep and convex, making it difficult to delimit the northern cirque boundary. Almost the entire slope of Pietrele Albe is covered by active, very angular, frost-shattered material continuously being transported downhill by creep and avalanches. In the upper non-vegetated part, the in situ boulders are up to 3 m in size (a-axis). Lower down,

the boulders are partially stabilised by vegetation of *Pinus Mugo* and *Juniperus*. Some have been reactivated by fluvial erosion at the base of the slope.

Unlike other cirques in the Rodna Mountains, the Tăuri cirque has a very narrow short profile with distinct steps (Figure 5.13 & Figure 5.17). There are 3 glacial lakes, each situated on 3 different glacially moulded bedrock steps at 1896 m, 1868 m and 1819 m (Figure 5.18). The crystalline limestone is clearly visible in the lower part of Tăuri cirque where it forms the final 140 m high step between 1800 and 1660 m altitude (Figure 5.17).

Glacial deposits, with distinct ridges cover the top of the final steep step at the south-eastern end of the cirque (Figure 5.18). It is not clear if these ridges represent individual moraines, or are the result of post depositional stabilisation.



Figure 5.18. Tăuri cirque with the Lakes Buhăiescu and moraine ridges (see Figure 5.16).

5.4.4.2 Curmătura (- Buhăiescu) cirque

The Curmătura cirque is situated in the central western part of the Buhăiescu glacial complex, south of Buhăiescu peak (2268 m) (Figure 5.16). Steep walls stretching from the

peak delimit this cirque on the northern and western side, while the south-eastern limit is provided by the low altitude ridge separating it from the Buhăiescu Mare cirque. Here the glacier deposited the largest moraine in the Buhăiescu glacial complex. At its south-eastern end, the moraine is composed of two ridges which join as the moraine curves towards the north around the former shape of the glacier (Figure 5.19). The ice distal part of the moraine is steeper and higher than the proximal side, especially at the lower end where the moraine has been incised by a small stream which meanders on the flat inner part of the moraine (Figure 5.20). The cirque's floor is located above ~1850 m altitude. The moraine ridge contains several kettle holes (up to 3 m in diameter). A meltwater channel was incised into bedrock at the northern end of the moraine (Figure 5.16).

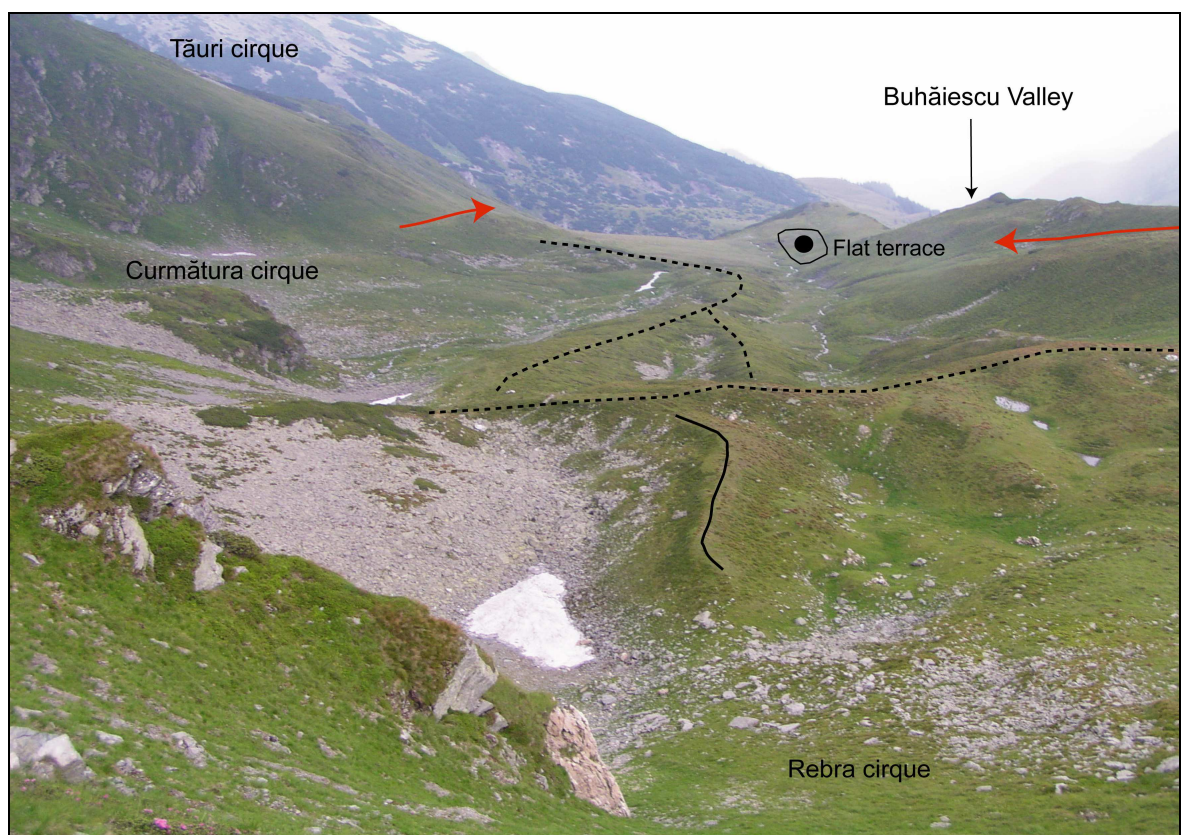


Figure 5.19. Curmătura & Rebra cirques of Buhăiescu glacial complex (dashed line = moraine ridges; solid line = protalus rampart; red arrows = meltwater channels) (see Figure 5.16).

5.4.4.3 Rebra cirque

The former limits of the glacier are clearly marked by a long arcuate moraine; however, there is a smaller ridge perpendicular to this moraine, created by frost-shattered material rolling down snow slopes in winter and spring (Figure 5.19). This is confirmed by field

observations as snow patches occur in these niches until late June – early July and this process can still be seen, although at smaller scale than in winter.

The moraines in both the Curmătura and Rebra cirques are very well preserved indicating that they were deposited by the last ice masses that occupied the area. The streams that drain these cirques join downhill and have incised the steep step between 1800 and 1680 m at the lower end of the Curmătura glacial valley. At the level of this step, on the southeast side of the river, there is a 30 m wide and 100 m long flat area (Figure 5.21). The bedrock dips southwest hence the flatness of this area may be related to a depositional process. Based on the evidence, we cannot confirm if the sediment was deposited as a kame terrace by meltwater of the retreating glacier or as a river terrace.



Figure 5.20. Distal slope of the moraine in the Curmătura (- Buhăiescu) cirque (see Figure 5.16).

5.4.4.4 Buhăiescu Mare cirque

The Buhăiescu Mare cirque is the largest cirque in the glacial complex and is situated in the south east part of the study area. It is delimited to the south by Tarnița La Cruce (1985 m), to the east by the rounded ridge of Piatra Buhoiului (1696 m), and to the west by a

small, subdued bedrock ridge which separates it from the western cirques (Curmătura & Rebra). Several intensively weathered tors are situated on the Piatra Buhoiului. The ridge towards the Rebra and Curmătura cirques shows clear evidence of ice moulding, especially in the upper part where a roche moutonnée occurs. A meltwater channel has deeply incised this ridge when ice flowed over its top (Figure 5.19). The Buhăiescu Mare cirque differs considerably from the other cirques as it is very wide and shallow and therefore exhibits a larger accumulation area. The cirque floor is characterised by large structural bedrock steps separated by shallow gradient areas (Figure 5.21). Rebra Lake is located in one of these areas (Figure 5.16). In the higher part of the cirque, an accumulation of mainly large angular boulders occurs behind an ice moulded bedrock ridge. This is interpreted as an ablation moraine (Figure 5.16). This hypothesis is supported by the presence of several kettle holes. The lack of fine material in the deposit suggests that the fine material has been remobilised, partially filling the basin occupied by Lake Rebra. Towards the west, a 28 m long streamlined bedrock form is aligned to the former ice flow direction (Figure 5.16). Further north, a shallow “U” shape valley was eroded through the bedrock steps also indicating ice flow on the same direction (Figure 5.16).

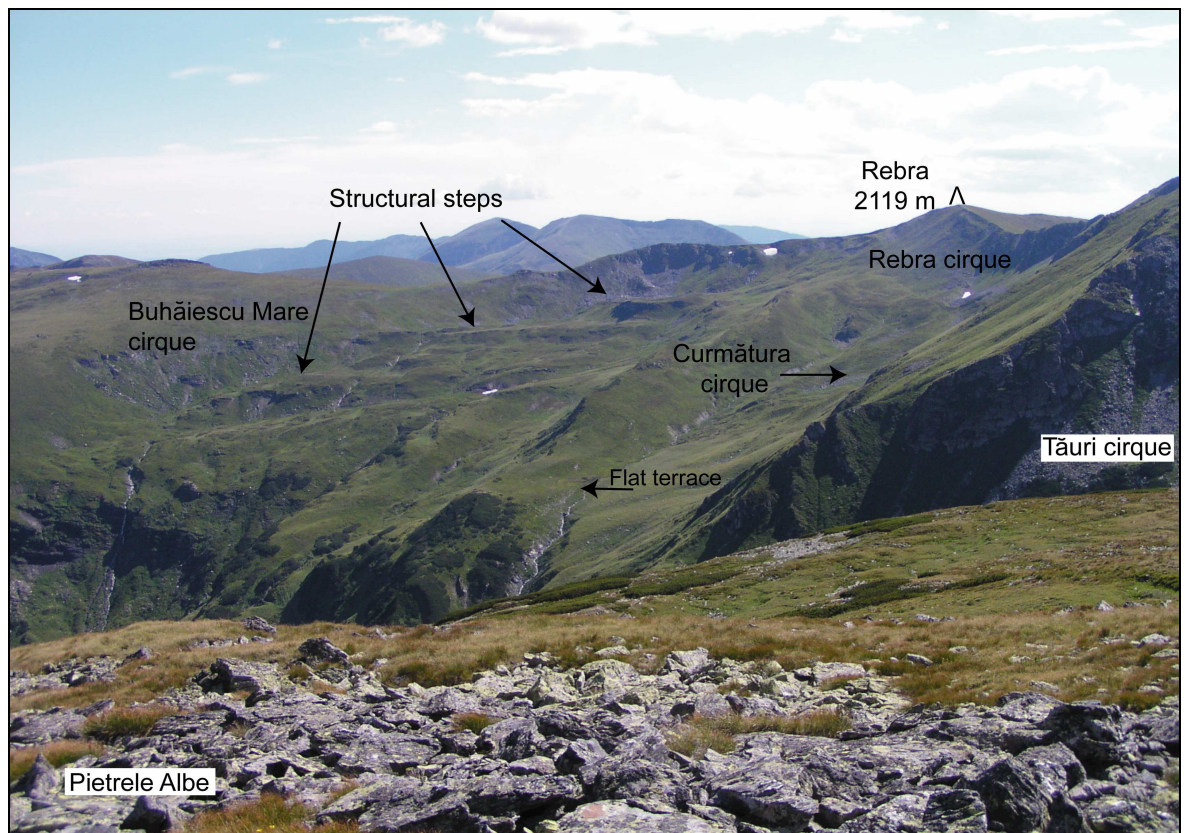


Figure 5.21. Buhăiescu glacial complex (see Figure 5.16).

In the lower north-west part of the cirque, striations have been very well preserved on a very smooth ice polished surface (Figure 5.22). The Buhăiescu Mare cirque is separated from the Buhăiescu Valley by a 200 m high step.

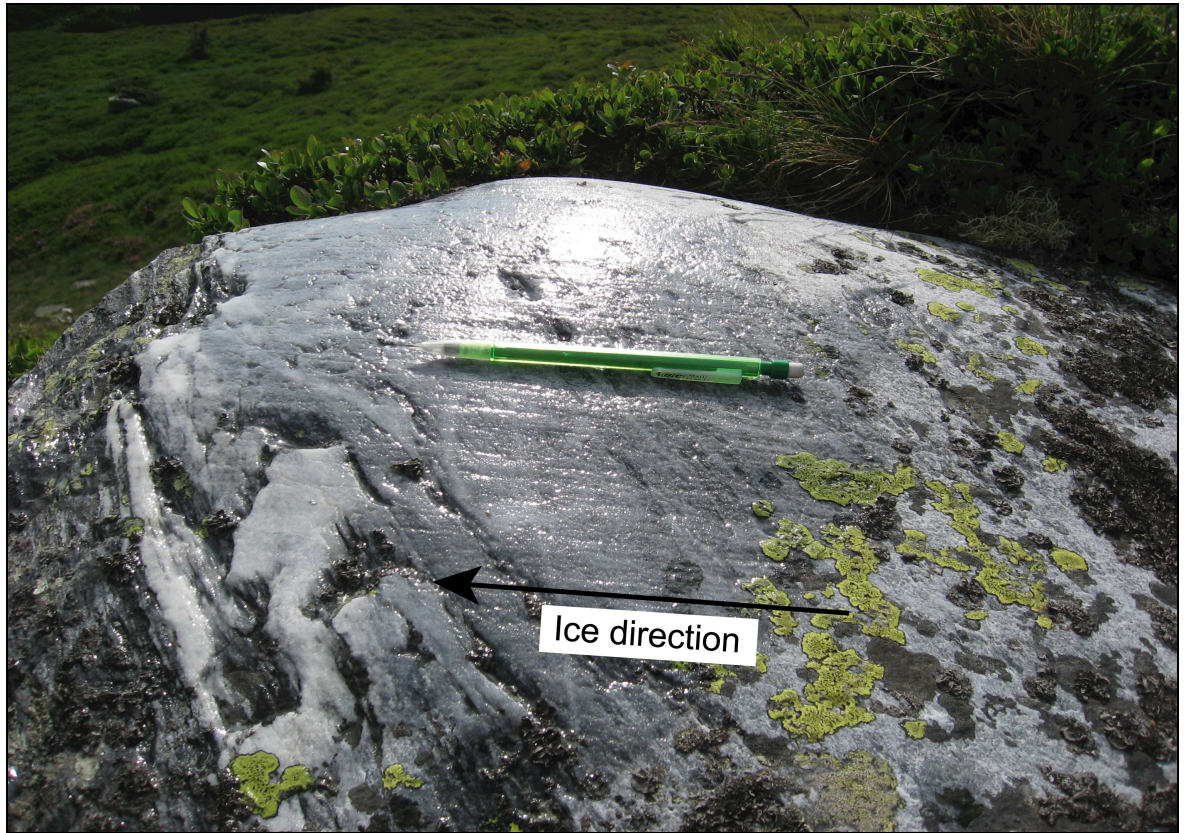


Figure 5.22. Glacially striated surface at the lower end of the Buhăiescu Mare cirque (see Figure 5.16).

5.4.5 Buhăiescu Valley

Below the high step separating the Buhăiescu glacial complex from Buhăiescu Valley a large, flat-topped till deposit extends for 500 m along the northern valley side (Figure 5.23). Post-depositional fluvial erosion has removed the south-eastern part of the deposit and incised 30 m below the flat upper surface of the deposit. It is not clear if all of the 30m of relief on the deposit is till, or if it is a draped deposit over the bedrock. Two moraine ridges descending from Pietrele Albe are located above the valley deposit (Figure 5.23).

The Buhăiescu valley is a deep glacial trough downstream of the four cirques that form the Buhăiescu glacial complex. The trough extends for ca. 1.5 km between 1600 and 1500 m elevation where it encounters a lithological boundary between micaschists/paragneisses and gneisses. Downstream of this boundary the fluvial channel is dominated by

knickpoints until another lithological transition from gneisses to greywacke is encountered at 1200 m elevation and the valley becomes more U-shaped again and joins the Repede valley (Figure 5.16).



Figure 5.23. Glacial landforms on the Buhăiescu Valley. The dashed lines follow the crest of two moraines (see Figure 5.16).

5.4.5.1 Repede Valley

The Repede valley drains a substantial part of the NW area of the Rodna Mountains (Figure 5.2). The valley is narrow, especially in the upper part where it is deeply incised into bedrock. The only glacial evidence still preserved in this valley are the boulders scattered in the middle reach (Figure 5.16), where the slope gradient becomes less steep and the valley starts to widen. The boulders have diameters of up to 3 m and are subrounded and rounded. In the lower part, the Repede valley becomes very wide, however, it is heavily inhabited and the land is cultivated. No glacial geomorphological evidence was found here.

5.5 Surface exposure ages

5.5.1 Sample sites and sample processing

Suitable sites for sampling were chosen both during the remote sensing process and then verified on the ground during fieldwork. The abundance of quartz in the crystalline rocks of the Rodna Mountains made sampling for surface exposure analysis relatively easy. A total of 43 samples were collected from glacial landforms in Pietroasa valley (11), the five cirques (26), the Buhăiescu glacial trough (5) and from a tor on the Piatra Buhoiului ridge (Figure 5.24). Samples were taken from glacial moraines, till deposits, striated bedrock surfaces and a roche moutonnée. Sampling and sample processing procedures are detailed in Chapter 3, Subheading 3.4. The calculated age uncertainties are expressed as $\pm 1\sigma$ (Table 5.1). The exposure ages assume constant exposure history, no inheritance and no erosion of boulders since deposition and thus the ages should be regarded as minimum ages. If erosion was taken into account, it would increase the ages of the samples. The only way to quantify bedrock erosion in the field area was to measure micro-relief on quartz veins where the maximum relief observed was 30 mm, averaged over the exposure duration this would increase the ages by $\sim 2.8\%$ for a 33 ka exposure and $\sim 2.6\%$ for a 10 ka exposure. However, the preservation of striations and glacial polish in the study area indicates insignificant bedrock erosional loss since deglaciation.

5.5.2 Surface exposure ages

Table 5.1 presents the details of each sample together with the ^{43}Be exposure ages collected in the Rodna Mountains and the map (Figure 5.24) shows their location.

The tor sample from the Piatra Buhoiului ridge yielded an exposure age of 93.2 ± 8.7 ka.

Pietroasa and Șarampin valleys. Three large boulders (2-6 m a-axis) were sampled from the lowest elevation boulder spread on the western side of the Pietroasa valley. The more distinct lateral moraine ridge could not be sampled due to anthropogenic modification. A boulder embedded within a till cover of a bedrock ridge yielded an age of 37.2 ± 3.4 ka. One kilometre to the south and 100 m higher, a 6 m long boulder composed partially of red

limestone and therefore transported from Turnu Roșu, gave an age of 36.6 ± 3.3 ka. A boulder in close proximity yielded an age of 33.3 ± 3.0 ka.

Eastwards and at lower elevation in the Pietroasa Valley slope a boulder was abandoned at 26.6 ± 2.4 ka. Another boulder on the western side of the lateral moraine in the Șarampin valley yielded an exposure age of 18.3 ± 1.6 ka. These two boulders indicate the retreat of ice towards higher ground. A massive boulder collected from the ice proximal side of the lateral moraine gave an exposure age of 12.4 ± 1.1 ka.

Four samples were collected from large boulders (>2 m above the surface) along a vertical transect on the medial moraine crest between the Șarampin and Pietroasa valleys. In ascending elevation boulder exposure ages are 17.5 ± 1.6 ka, 15.7 ± 1.4 ka, 16.4 ± 1.5 ka and 17.2 ± 1.5 ka (mean of 16.7 ± 1.5 ka). A fifth quartzite boulder, located at the highest elevation on the medial moraine crest, and only 20 cm above the ground surface, gave a younger exposure age of 10.5 ± 0.9 ka, not included in the mean age.

Zănoaga Mare cirque. Samples collected from the moraines in the Zănoaga Mare cirque gave exposure ages of 12.3 ± 1.1 ka, 12.7 ± 1.1 ka, 11.5 ± 1.0 ka (mean = 12.1 ± 1.1 ka) from the lower moraine. Two boulders from the upper moraine were dated to 11.1 ± 1.0 ka and 11.3 ± 1.0 ka (mean = 11.2 ± 1.0 ka).

Iezer cirque. On the step below the Iezer cirque glacially moulded bedrock gave an exposure age of 13.4 ± 1.2 ka. Boulders on the ablation moraine above the step yielded exposure ages of 11.5 ± 1.0 ka, 13.1 ± 1.2 ka and 13.1 ± 1.2 ka (mean = 13.1 ± 1.2 ka). The younger age of 11.5 ± 1.0 ka was produced from a single small clast on top of the moraine and is not included in the mean. It is likely that this low relief clast may have been covered for longer periods than the rest of the boulders. The plucked face of the rock step above Lake Iezer was sampled yielding 9.7 ± 0.9 ka and 9.3 ± 0.9 ka (9.5 ± 0.9 ka). The top of the step, composed of several roches moutonnées, some striated and grooved, yielded an exposure age of 12.5 ± 1.1 ka.

Buhăiescu valley. One boulder embedded in the surface of the large till deposit along the western side of Buhăiescu valley, just below the lowest bedrock step, yielded an age of 15.8 ± 1.4 ka. Further upstream, towards Tăuri cirque, a boulder was abandoned at 13.4 ± 1.2 ka. A further three boulders from a lateral moraine on the slope from Pietrele Albe gave ages of 13.6 ± 1.2 ka, 10.4 ± 0.9 ka and 12.5 ± 1.1 ka (mean = 13.0 ± 1.1 ka).

Tăuri cirque. In the lower part of the Tăuri cirque, boulders from the two moraine ridges above the final bedrock step have exposure ages of 12.0 ± 1.1 ka, 12.8 ± 1.1 ka, 12.5 ± 1.1 ka, 12.5 ± 1.1 ka (mean = 12.4 ± 1.1 ka), and 16.7 ± 1.5 ka.

Curmătura cirque. The forked-moraine in the Curmătura cirque (Figure 5.16) yielded exposure ages of 13.4 ± 1.2 ka, 14.1 ± 1.3 ka, 12.6 ± 1.1 ka, 12.1 ± 1.1 ka, 13.2 ± 1.2 ka and 13.5 ± 1.2 ka (mean = 14.3 ± 1.3 ka).

Buhăiescu Mare cirque. The striated surfaces in the Buhăiescu Mare cirque suggest that deglaciation of this area occurred at 14.1 ± 1.3 ka and further up-valley, the streamlined bedrock form yielded an exposure age of 14.3 ± 1.3 ka.

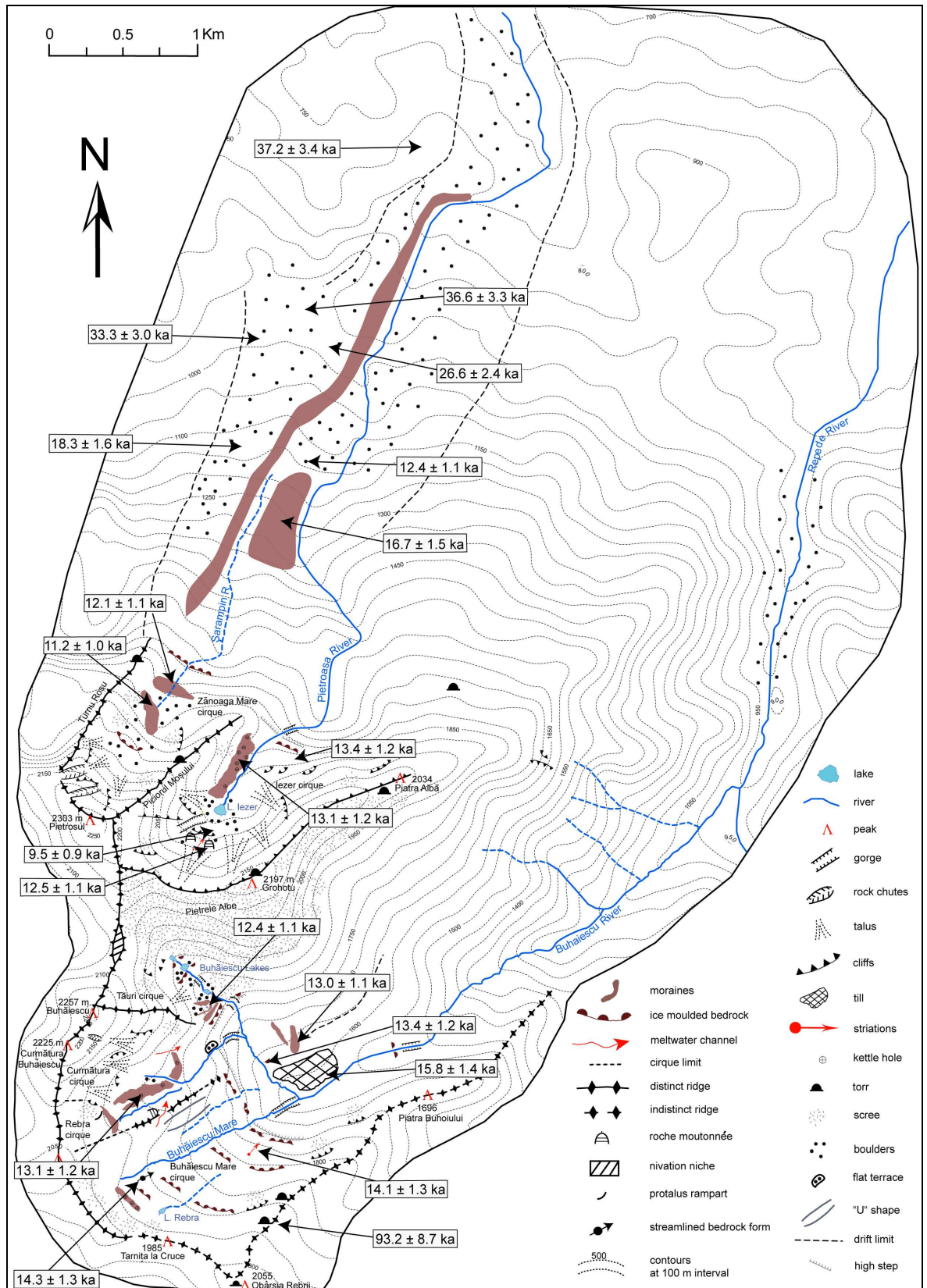


Figure 5.24. Surface exposure ages plotted on the geomorphological map.

Table 5.1. Sample characteristics, ¹⁰Be concentrations and calculated surface exposures ages.

Lab ID	Lithology	Sampled surface	Lat (°N)	Long (°E)	Elev. (m)	Shielding ^a (factor)	Thickness ^b (cm)	Quartz mass (g)	[¹⁰ Be] ^c (x10 ⁴ atom g ⁻¹)	Exposure age ^d (ka)	Mean ages ^e (ka)
Pietroasa Valley											
RD 27	Gneiss	Boulder	47.63	24.66	868	0.9984	4 (0.9670)	24.55	38.63 ± 1.10	37.2 ± 3.4 (1.0)	
RD 28	Gneiss	Boulder	47.62	24.65	970	0.9952	5 (0.9590)	22.03	40.89 ± 1.17	36.6 ± 3.3 (1.0)	
RD 29	Gneiss	Boulder	47.62	24.64	1116	0.9931	3 (0.9751)	26.25	23.42 ± 0.65	18.3 ± 1.6 (0.5)	
RD 49	Gneiss	Boulder	47.62	24.65	999	0.9951	2.5 (0.9792)	46.69	38.93 ± 0.78	33.3 ± 3.0 (0.6)	
RD 50	Schist	Boulder	47.62	24.65	969	0.9945	2.5 (0.9792)	32.27	30.38 ± 0.96	26.6 ± 2.4 (0.8)	
RD 01	Gneiss	Boulder	47.62	24.65	1108	0.9895	3 (0.9751)	25.28	15.77 ± 0.49	12.4 ± 1.1 (0.4)	
Medial moraine											
RD 30	Schist	Boulder	47.61	24.64	1379	0.9841	4 (0.9670)	25.11	16.32 ± 0.50	10.5 ± 0.9 (0.3)	(excluded)
RD 31	Schist	Boulder	47.61	24.64	1344	0.9864	2 (0.9833)	25.66	26.93 ± 0.75	17.5 ± 1.6 (0.5)	
RD 32	Schist	Boulder	47.61	24.65	1237	0.9882	2 (0.9833)	26.20	22.32 ± 0.63	15.7 ± 1.4 (0.4)	16.7 ± 1.5
RD 33	Schist	Boulder	47.61	24.65	1170	0.9897	4 (0.9670)	24.38	21.70 ± 0.66	16.4 ± 1.5 (0.5)	
RD 34	Schist	Boulder	47.61	24.64	1245	0.9881	1.5 (0.9874)	23.73	24.70 ± 0.64	17.2 ± 1.5 (0.4)	
Zănoaga Mare cirque											
RD 02	Schist	Boulder	47.60	24.64	1669	0.9454	5 (0.9590)	31.05	22.76 ± 0.66	12.3 ± 1.1 (0.3)	
RD 03	Schist	Boulder	47.60	24.64	1669	0.9454	2 (0.9833)	27.28	24.14 ± 0.68	12.7 ± 1.1 (0.3)	12.1 ± 1.1
RD 04	Schist	Boulder	47.60	24.64	1669	0.9454	3 (0.9751)	28.95	21.65 ± 0.63	11.5 ± 1.0 (0.3)	
RD 05	Schist	Boulder	47.60	24.63	1753	0.9058	5 (0.9590)	24.36	10.89 ± 0.40	5.7 ± 0.5 (0.2)	(excluded)
RD 06	Schist	Boulder	47.60	24.63	1767	0.9330	2 (0.9833)	25.85	22.50 ± 0.65	11.1 ± 1.0 (0.3)	
RD 07	Schist	Boulder	47.60	24.63	1767	0.9330	2 (0.9833)	24.24	22.83 ± 0.63	11.3 ± 1.0 (0.3)	11.2 ± 1.0
Iezer cirque											
RD 08	Schist	Bedrock	47.60	24.64	1801	0.9599	4 (0.9670)	24.65	24.14 ± 0.77	11.5 ± 1.0 (0.3)	
RD 09	Schist	Boulder	47.60	24.64	1801	0.9599	4 (0.9670)	27.02	27.42 ± 0.79	13.1 ± 1.2 (0.3)	13.1 ± 1.2
RD 10	Schist	Boulder	47.60	24.64	1801	0.9599	2 (0.9833)	25.11	27.92 ± 0.81	13.1 ± 1.2 (0.3)	
RD 11	Schist	Boulder	47.60	24.65	1794	0.9679	3 (0.9751)	27.34	28.51 ± 0.79	13.4 ± 1.2 (0.3)	
RD 12	Schist	Bedrock	47.60	24.65	1898	0.9178	2 (0.9833)	26.72	27.45 ± 0.72	12.5 ± 1.1 (0.3)	
RD 40	Schist	Bedrock	47.59	24.64	1908	0.7314	3 (0.9751)	25.19	16.96 ± 0.50	9.7 ± 0.9 (0.4)	
RD 41	Schist	Bedrock	47.59	24.64	1908	0.7116	3 (0.9751)	26.51	15.96 ± 0.46	9.3 ± 0.9 (0.3)	9.5 ± 0.9
Buhăiescu Valley											
RD 16	Schist	Boulder	47.58	24.64	1688	0.9683	2 (0.9822)	24.28	26.46 ± 0.75	13.4 ± 1.2 (0.4)	
RD 17	Schist	Boulder	47.58	24.65	1636	0.9872	3 (0.9751)	26.48	30.24 ± 0.78	15.8 ± 1.4 (0.4)	

Lab ID	Lithology	Sampled surface	Lat (°N)	Long (°E)	Elev. (m)	Shielding ^a (factor)	Thickness ^b (cm)	Quartz mass (g)	[¹⁰ Be] ^c (x10 ⁴ atom g ⁻¹)	Exposure age ^d (ka)	Mean ages ^e (ka)
RD 18	Schist	Boulder	47.58	24.65	1706	0.9834	3 (0.9751)	24.85	25.31 ± 0.73	12.5 ± 1.1 (0.3)	13.0 ± 1.1
RD 19	Schist	Boulder	47.58	24.65	1718	0.9834	1 (0.9916)	23.01	21.61 ± 0.63	10.4 ± 0.9 (0.3)	
RD 20	Schist	Boulder	47.58	24.65	1741	0.9834	2 (0.9833)	23.30	28.38 ± 0.80	13.6 ± 1.2 (0.4)	
La Tăuri											
RD 21	Schist	Boulder	47.58	24.64	1864	0.9685	5 (0.9590)	21.90	26.38 ± 0.76	12.0 ± 1.1 (0.3)	12.4 ± 1.1 (excluded)
RD 22	Schist	Boulder	47.58	24.64	1847	0.9685	3 (0.9751)	24.47	28.15 ± 0.81	12.8 ± 1.1 (0.3)	
RD 23	Schist	Boulder	47.58	24.64	1842	0.9685	4 (0.9670)	24.97	27.32 ± 0.77	12.5 ± 1.1 (0.3)	
RD 24	Schist	Boulder	47.58	24.64	1847	0.9580	2 (0.9833)	26.56	36.64 ± 0.97	16.7 ± 1.5 (0.4)	
RD 25	Schist	Boulder	47.58	24.64	1847	0.9580	4 (0.9670)	24.70	26.97 ± 0.79	12.5 ± 1.1 (0.3)	
Curmătura Buhăiescu											
RD 26	Schist	Boulder	47.58	24.64	1904	0.9984	3 (0.9751)	23.58	31.69 ± 0.88	13.4 ± 1.2 (0.3)	13.1 ± 1.2
RD 35	Schist	Boulder	47.58	24.63	1865	0.9818	3 (0.9751)	25.79	31.91 ± 0.94	14.1 ± 1.3 (0.4)	
RD 36	Schist	Boulder	47.57	24.63	1918	0.9818	2.5 (0.9792)	25.91	29.76 ± 0.86	12.6 ± 1.1 (0.3)	
RD 37	Quartzite	Boulder	47.57	24.63	1957	0.9655	2.5 (0.9722)	26.31	29.11 ± 0.80	12.2 ± 1.1 (0.3)	
RD 38	Schist	Boulder	47.57	24.63	1973	0.9737	2.5 (0.9722)	26.80	32.27 ± 0.92	13.2 ± 1.2 (0.4)	
RD 39	Quartzite	Boulder	47.57	24.63	1979	0.9857	2 (0.9833)	26.39	33.74 ± 0.98	13.5 ± 1.2 (0.4)	
Buhăiescu Mare											
RD 13	Schist	Bedrock	47.57	24.64	1819	0.9937	2 (0.9833)	25.22	31.58 ± 0.93	14.1 ± 1.3 (0.4)	14.3 ± 1.3 (0.4)
RD 14	Schist	Bedrock	47.57	24.63	1971	0.9932	4 (0.9670)	25.10	35.00 ± 1.00	14.3 ± 1.3 (0.4)	
Obârșia Rebrii torr											
RD 15	Schist	Bedrock	47.57	24.65	1943	0.9988	4 (0.9670)	23.13	220.55 ± 13	93.2 ± 8.7 (2.7)	

^aShielding by distant objects computed after Dunne et al. (1999);

^b Sample thickness correction using an exponential decrease in production with depth assuming a rock density of 2.7 g cm⁻³ and an attenuation length of 160g cm⁻²; thickness correction factor is given in the parentheses.

^c ¹⁰Be concentrations. ¹⁰Be/⁹Be ratios measured against NIST SRM 4325 with nominal value of 3.06 x 10¹¹;

^d Exposure ages calculated using Cronus-Earth ¹⁰Be – ²⁶Al exposure age calculator v. 2.2 (<http://hess.ess.washington.edu/>). They assume zero erosion, scaling factors according to Stone (2000) and a spallation production rate of 4.49 ± 0.39 atom (g SiO₂)⁻¹ a⁻¹ (Balco et al., 2008). All exposure ages are given with the systematical uncertainty and the analytical uncertainty in the parentheses.

5.5.3 Discussion

5.5.3.1 Pattern of deglaciation in the study area

Previous investigations in the Rodna Mountains have shown that several glacial advances and retreats occurred during the late Quaternary, the least extensive during the last glaciation. However, this section then sets out to discuss the field investigations and surface exposure ages obtained from the Rodna Mountains in the present study. This should allow the palaeoclimatic environment in this part of northern Romania to be reconstructed (Figure 5.24 & Figure 5.25).

The sample from the tor on the easternmost ridge of the field area was collected to test the preservation of the landscape throughout the glacial episodes. The minimum exposure age of 93.2 ± 8.7 ka and its high degree of weathering suggest that the site escaped glaciation during the Devensian maximum glacial advance (Figure 5.25). No glacial evidence can be found on the tors or on the ridge and the nuclide concentration is probably controlled by bedrock erosion rates (Phillips et al., 2006). This suggest that at the maximum advance of ice in the Rodna Mountains, ice height in the Buhăiescu cirque did not reach the crest of this ridge and must have been less than 200 m thick, this being the difference between the ridge and the cirque floor.

The glacial till deposits found in the Pietroasa and Repede valleys, suggest a former ice advance to low elevations of ca. 700 m altitude (Figure 5.24). It is likely that the ice reached lower elevations than this but any evidence has been obscured or removed by urbanisation and cultivation. The area on the western side of the Pietroasa valley is scattered with boulders of various dimensions at an elevation of ca. 800-1000 (Figure 5.10 & Figure 5.24). At the western interfluvium of this valley, the surface exposure ages from 3 boulders suggest deglaciation between ca 37.2 – 32.2 ka (Figure 5.24). As the glacier tongue was gradually thinning to below the western sidewall, boulders were abandoned at about 26.6 ka (Figure 5.24). Once the main body of ice was confined to the valley, the glacier deposited a lateral moraine that stretches for almost 4 km along the Șarampin and Pietroasa valleys (Figure 5.24). The size and shape of this moraine suggests that its deposition occurred over a long time (26-18 ka) and the retreat of ice was quite slow. At the lower end of the Șarampin valley, a boulder sampled on the outside area of the lateral moraine indicates a deglaciation age of 18.3 ka (Figure 5.24).

As the ice retreated and separated into individual ice masses in Șarampin and Pietroasa valleys, the scoured material from Piciorul Moșului ridge (Figure 5.10 & Figure 5.14) was deposited as a medial moraine between the two ice masses. The exposure ages from this moraine suggest this occurred at ca. 16.7 ka (mean age) (Figure 5.25). The outlier age of 10.5 ± 0.9 from a boulder at the upper end of the moraine is interpreted as exhumed or overturned post depositionally, possibly as a result of forestry operations nearby. The age of 12.4 ± 1.1 ka from a large boulder at the lower limit of this deposit appears anomalously young and is likely to reflect post depositional exhumation during the Younger Dryas (see below).

As the two ice masses separated and the western glacier retreated to the Zănoaga cirque, locally derived material was deposited in the form of recessional moraines, two of which gave very consistent exposure ages, with the outer and lower moraine being deposited at ca. 12.1 ka, and the inner and higher moraine being formed before 11.2 ka (Figure 5.25). The rest of the Zănoaga cirque consists of several small ground moraines which indicate in situ melting of the ice in this part of the Rodna Mountains. The young age of 5.7 ± 0.5 ka from the third boulder on the upper moraine suggests that the boulder was overturned after deposition.

The glacier on the Pietroasa valley retreated towards the Iezer cirque and a glacially moulded surface above the high step became exposed following deglaciation at ca. 13.4 ka. The slower retreat and deglaciation of the Pietroasa glacier likely relates to the larger accumulation area and the deeper Iezer cirque. The in situ downwasting of ice in the cirque is evidenced by the presence of large kettle holes on an ablation moraine that extends for more than half of the cirque floor length. Exposure ages from two boulders on top of the moraine suggest deglaciation at ca. 13.1 ka (Figure 5.25), whilst another small single clast within 2 m of the boulders indicates deglaciation at 11.5 ka (Figure 5.25). The sample was a small clast derived from the top of a severely weathered boulder suggesting post depositional weathering and erosion, and therefore a lower ^{10}Be concentration. The last ice in the southern part of the cirque retreated from the roches moutonnées above Lake Iezer at 12.5 ka (Figure 5.25). The cliff below the roches moutonnées (Figure 5.9) gave a mean value of about 9.5 ka, and the interpretation favoured here is that this cliff suffered intense frost weathering and collapsed after deglaciation. Rock slope failures are common after deglaciation and are caused by pressure release and severe periglacial activity (Ballantyne, 1986; Jarman, 2006).

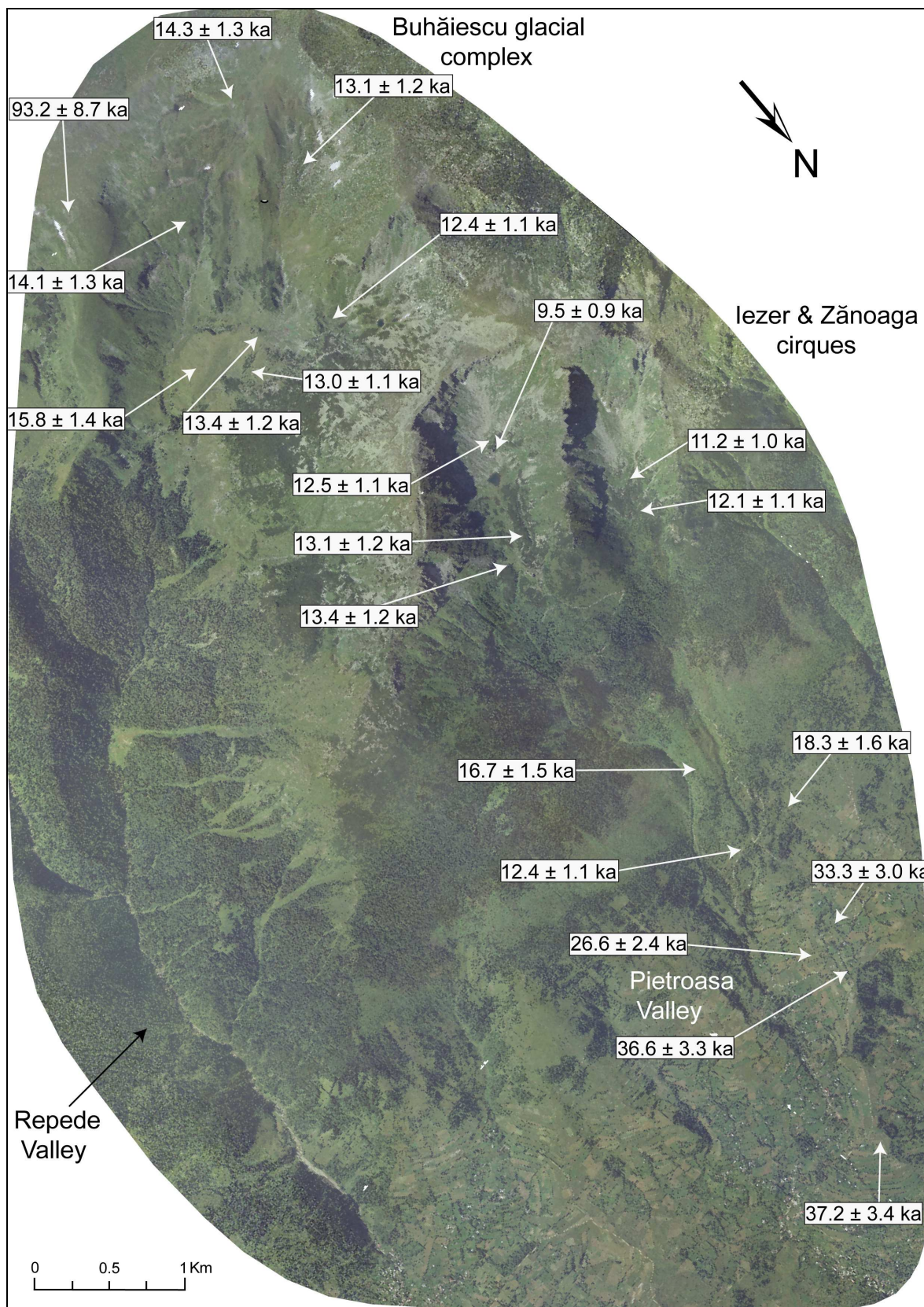


Figure 5.25. Surface exposure ages of the boulders and bedrock samples from the study area plotted on the 3D image of the orthophotomaps. The area covered is the same as in Figure 5.4 & Figure 5.5, here the 3D image has been tilted for a detailed view.

Several glaciers from the high accumulation areas of Buhăiescu and Negoiasa Mare (Figure 5.2) flowed down the Repede valley. Till deposits and rounded boulders scattered along the middle part of the Repede valley are evidence for the presence of ice in this area during the last glaciation (Figure 5.16).

The Buhăiescu valley acted as the outlet for the cirques of the higher glacial complex. During deglaciation the tributary glacier from Tăuri cirque became disconnected from the main valley glacier. The intervening space was filled with glacial sediments which are preserved mostly intact on the western side of the valley. Deposition occurred at about 15.8 ka as suggested by the age produced from a boulder embedded in the top of the deposit (Figure 5.24).

The glacier emanating from the Buhăiescu glacial complex had split into individual ice masses by 14-15 ka. Based on the sample from striated surfaces at the lower end of the Buhăiescu Mare cirque and the streamlined bedrock form higher up in the cirque were completely deglaciated by 14 ka (Figure 5.25) leaving behind glacially abraded structural steps and an ablation moraine with kettle holes that held the last ice in this cirque (Figure 5.24). Final deglaciation in the Curmătura and Rebra cirques of the Buhăiescu glacial complex occurred later at 13.1 ka (Figure 5.25).

In the valley immediately below the bedrock step leading up to Tăuri cirque a single boulder was abandoned by the retreating Tăuri cirque ice at ca. 13.4 ka. The retreating glacier deposited two moraines on the Buhăiescu valley on the northern slope from Pietrele Albe (Figure 5.18). The mean value of two exposure ages from boulders on one of the moraines suggests deposition at ca. 13.0 ka (Figure 5.24). A third boulder yields a younger age of 10.4 ka. It is likely to have been exhumed from the deposit at a later stage. The distribution of five ages from the two moraines in the Tăuri cirque clusters around 12.4 ka (Table 5.1). The older age of 16.7 ± 1.5 ka was produced from a low relief boulder which probably had nuclide inheritance, implying a previous exposure to cosmic rays before the last glacial advance, with last ice not eroding the rock surface sufficiently to remove the pre-acquired nuclides.

5.5.3.2 Glacial and climatic implications in the study area

The consistent distribution of the exposure ages and the geomorphological interpretations indicate a slow and continuous retreat of ice towards the cirques, where ice was maintained until the beginning of the Holocene (Figure 5.26). Ice stillstands or small re-advances were possible during the global LGM and the Younger Dryas episode. However, there is no field evidence to suggest a complete deglaciation after each glacier advance and any re-advances of ice during a favourable climate must have occurred on a very small scale.

As the snow bearing winds were coming from the west during the glacial maxima, the cirques in the study area would be favoured on north-eastern facing sites. The differences in the spatial distribution of ice in the study area and the various retreat rates as determined by the exposure ages depend on a variety of factors (Figure 5.26). Insolation would be the major cause of this effect as the northern cirques (Zănoaga Mare & Iezer) are narrower and deeper and therefore receive less solar radiation. Similarly, the aspect of the northern cirques facilitated less ablation than the southern cirques in the Buhăiescu glacial complex (Tăuri, Curmătura, Rebra, Buhăiescu Mare). Although the cirque floors in our study area are located at similar elevations (above 1800 m, Figure 5.13) and have the same NNE orientation (except the Tăuri cirque - SE), the faster retreat and intense melting of the ice in the Buhăiescu Mare cirque was probably caused by its shape, size and aspect (Figure 5.21). It is a wide and shallow cirque where solar radiation was stronger than in the other cirques which are deep, narrow and sheltered by high side walls (e.g. Figure 5.6, Figure 5.8 & Figure 5.17).

5.5.3.3 ELA reconstruction and palaeoclimatic implications

Two methods were used to calculate the ELAs to compare them with other mountains of Romania and other places in Europe: the accumulation area ratio (AAR) and the area-altitude balance ratios (AABR) (see 3.5). The vertical height of the ice surface and the extent of the glacial imprint was delimited using orthophotomaps overlaid on a 3D surface (Figure 5.26). The hypsometric contours of the ice surface and ice extent were measured for the locally observed maximum and YD glacial extent.

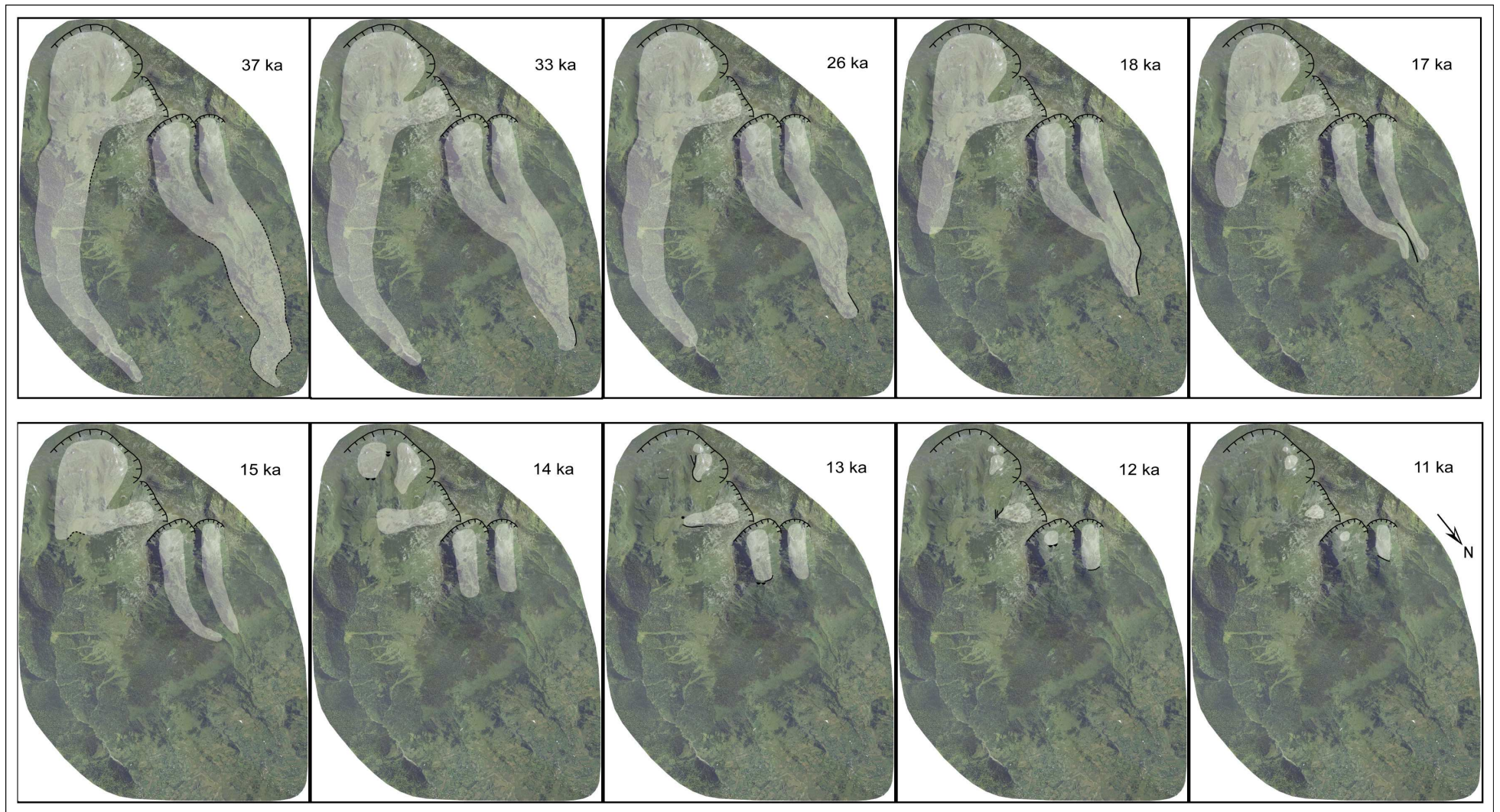


Figure 5.26. The pattern of deglaciation in the NW part of the Rodna Mountains between 37-11 ka. Dashed lines = drift limit, solid lines = moraine ridges, half moon = glacially moulded bedrock, circle = boulder.

For the last local maximum advance at about 37 ka an ELA of 1258 m and 1336 m was calculated for the Pietroasa and Buhăiescu glaciers respectively, using a balance ratio of 1.8 (Table 5.2), the same as for Scotland (Table 4.2). There is a general lowering in ELA estimates from south to north in the Romanian Carpathians, consistent with the spatial differences in temperature and precipitation which were probably more pronounced during the cold glacial periods. In the southern Carpathians, the moisture bearing winds from the Atlantic brought the highest amount of precipitation to the Retezat Mountains (Figure 2.2). Therefore, the glaciers in the western massifs extended for longer distances (ELA at 1725 m at the last maximum ice advance and 1770 m at the late glacial advance) than in the eastern massifs. Nevertheless, the northern position in the Romanian Carpathians together with the dominant western winds and cold air flows from the east caused the Rodna Mountains to receive higher amounts of solid precipitation. This allowed for more ice accumulation and glacier advance to lower elevations (< 700 m altitude) than in the Retezat Mountains (1050-1200 m altitude; Urdea & Reuther, 2009). The cirque floors in the Rodna Mountains are lower than in the Southern Carpathians, however, their NNE orientation favoured a lower ELA (Mîndrescu et al., 2010).

Table 5.2. The equilibrium line altitudes (ELA) for the Last Glacial Maximum and YD glaciers in the Rodna Mountains. AAR = accumulation area ratio (Porter, 2001); AABR = area altitude balance ratio (Osmaston, 2005).

Stage	Glaciers	Area (km ²)	ELA (m)				
			AAR		AABR		
			0.65	0.75	0.67	1.8	2.0
LLGM	Pietroasa	7.21	1280	1124	1383	1258	1237
	Buhăiescu	8.93	947	890	1494	1336	1319
YD	Zănoaga Mare	0.44	1804	1773	1850	1846	1841
	Iezer	0.39	1874	1878	1969	1965	1961
	Tăuri	0.29	1885	1849	1947	1944	1940
	Curmătura	0.18	1953	1957	1913	1911	1909
	Rebra	0.05	1892	1877	1937	1935	1933

The ELA values for the reconstructed YD lie between 1846 m and 1935 m, with the variations of the values between the cirques being related to the differences between the elevation of the cirques' floor, the size of the ice accumulation areas, the shape and aspect

of each cirque. The ELA in the Retezat Mountains was estimated to have been located at 2030 m during the YD glacier advance (Reuther et al., 2007) which supports the hypothesis of a steep north-south precipitation gradient across the Romanian Mountains.

5.5.3.4 Comparison with the palaeoclimate records in the Romanian mountains

The cirques with NNE orientation (Zănoaga Mare, Iezer, Curmătura, Rebra, Buhăiescu Mare) and the ice presence at lower elevations in the Rodna Mountains relates to the general WNW palaeowinds during the last glacial cycle. In spite of their high altitudes, the mountains east of Rodna did not support glaciers throughout the Late Devensian glaciation, in contrast with the lower altitude mountains in Western Carpathians, emphasizing the important role of these winds (Mîndrescu et al., 2010).

The last local maximum glaciation in the study area occurred between 37-26 ka. This is supported by a significant temperature decrease, indicated by pollen analysis and interpretations of loess deposits (Cârciumaru, 1980). This temperature decrease occurs earlier than the global LGM. Applications of U/Th TIMS in cave deposits located in the northwestern part of Romania show a decrease or discontinuity in speleothem growth at the same time (Lauritzen & Onac, 1995; Onac & Lauritzen, 1996). An early maximum ice advance in the Rodna Mountains is also supported by other evidence in speleothems in SW Romania, showing climatic conditions similar to the cold episode at 40-35 ka (Constantin et al., 2007). Although no boulders were suitable for surface exposure dating in the Southern Carpathians, morphological and pedological investigations on the lowest elevated moraines confirmed that a maximum ice advance in the Romanian Carpathians occurred earlier in the last glaciation, presumably during the Early Devensian (Reuther et al., 2007).

Glacial retreat in the Pietroasa and Buhăiescu valleys by 26 ka (Figure 5.26) may coincide with a moderate warming of the climate between 33-27 ka (Constantin et al., 2007). Retreat appears to have been slow as suggested by the age of lateral moraine abandonment at about 18 ka and medial moraine deposition at about 16 ka (Figure 5.24). Surface exposure ages

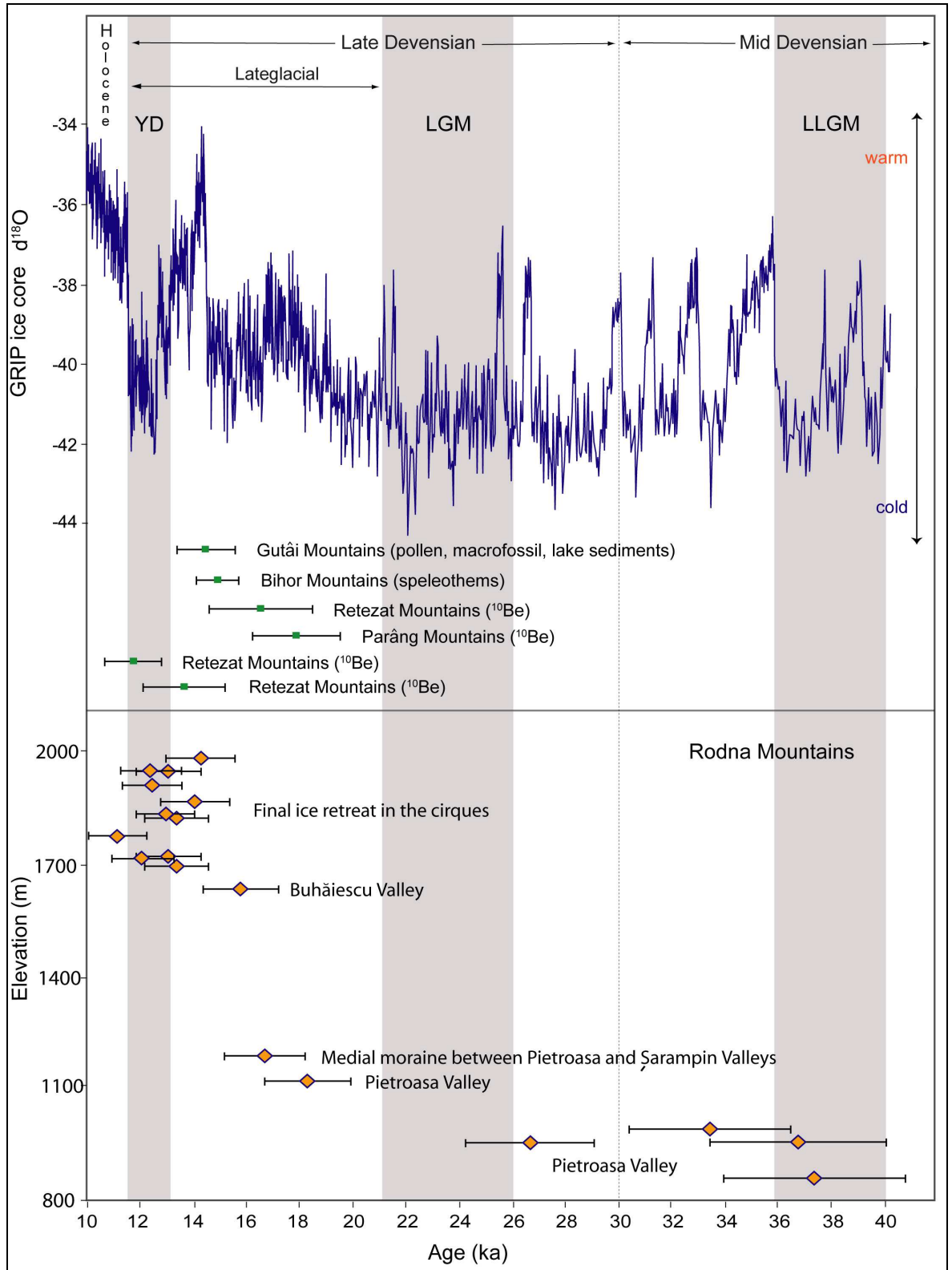


Figure 5.27. Rodna Mountains. ^{10}Be exposure ages plotted against the GRIP ice core (Rasmussen et al., 2006) and other Romanian dates (Reuther et al., 2007; Tămaș et al., 2005).

from the northern slopes of the Retezat and Parâng Mountains confirm that deglaciation during the Lateglacial occurred at ca. 16.8 ± 1.8 ka, and ca. 17.9 ± 1.6 ka respectively (Figure 5.27) (Reuther et al., 2007; Urdea & Reuther, 2009).

Continuing speleothem growth after 14.8 in western Romania is thought to be due to an increase in the temperature or moisture availability in the area at the end of the global LGM (Figure 5.27; Tămaş et al., 2005). The deglaciation chronology in the study area (Figure 5.26) also agrees well with dates from lake sediments in north-western Romania, which show a general warming of the climate at 14.5 ka respectively (Figure 5.27; Wohlfarth et al., 2001), corresponding to the deglaciation times recorded in the Greenland ice cores (GI-1e, 14.7 ka; Walker et al., 1995; Björk et al., 1998). At ca. 13 ka the Tăuri glacier retreated towards the cirque, at a time when climate is suggested to have been warm and dry after 13.8 ka at lower altitudes west of the Rodna Mountains (Wohlfarth et al., 2001).

Deglaciation in most of the corries on the northern slopes of Rodna Mountains occurred between 13-12 ka with ice persisting until ca. 11 ka in the Zănoaga Mare cirque (Figure 5.26). Our exposure ages for the presence of the Younger Dryas event in the Rodna Mountains correlate well with results from the Retezat Mountains (13-11 ka; Reuther et al., 2007; Figure 5.27). At lower elevations in the Gutâi Mountains (Figure 2.1), open vegetation communities recurred between 12.9 - 11.5 ka as a response to a cold period (Feurdean, 2005; Björkman et al., 2002). This was coeval with the Younger Dryas readvance at higher altitudes, in the Bihor Mountains (Figure 2.1) the cold stage being recorded between 12.6 - 11.4 ka (Tămaş et al., 2005). Our deglaciation ages also correlate well with the rapid growth of a speleothem at ~ 11.5 ka in the Poleva cave (300 km south-westwards) at the beginning of the Holocene warm period (Constantin et al., 2007). An abrupt increase of air temperatures was also recorded in the Gutâi Mountains after ca. 11.5 ka (Feurdean & Bennike, 2004). The ages of 9.5 ka on the steep cliff above the Lake Iezer (Figure 5.24) match reasonably well with a short cold period recorded in the speleothems in the Bihor Mountains between 9.4 - 9.1 ka (Tămaş et al., 2005) and could indicate increased frost weathering activity at this time.

5.5.4 Conclusions

1. Geomorphological mapping of ca. 50 km² in the north-western part of the Rodna Mountains suggest a maximum extent of ice to at least 700 m altitude. The reconstructed glacial history points to a slow retreat of ice towards higher ground. The large dimensions of certain glacial features suggest ice stillstands which may have occurred between the retreating episodes.
2. The surface exposure ages are consistent with the geomorphological interpretations. The last maximum advance of ice in the Rodna Mountains during the Devensian glaciation is asynchronous to global climate records. This difference in timing and spatial extent will be addressed in detail in Chapter 6. The local LGM occurred before 37 ka and ice retreated slowly towards the cirques. Ice stillstands or advances may have occurred during the global LGM or after, when the release of moisture in the atmosphere was greater, however, the geomorphology does not provide any evidence to support this. The deglaciation during the Late Glacial occurred synchronous with other places in Romania and Central and Western Europe. Final ice occupation of the higher cirques occurred during the YD as evidenced by the deglaciation ages of 13-11 ka from moraines and bedrock.
3. The calculated ELA, using the area-altitude balance ratios, during the local LGM is lower (1258 m) than in the Southern Carpathians (1725 m). There is an increase of the ELA values in the cirque glaciers in the study area from west to east (1846 - 1935 m) during the Younger Dryas. This is interpreted as indicating a moderate precipitation (W-E) and insolation gradient which favoured slow ice accumulation and longer maintenance in sheltered areas.

Chapter 6

Synthesis

6.1 Introduction

This chapter summarizes the main findings in this thesis and aims to synthesize both the resulting chronology and the palaeoclimatic implications. Prior to the results of this research study, the glacial extent in the Monadhliath Mountains was uncertain for the period spanning between the LGM and the early Holocene and no absolute dating technique had been applied to establish the chronology of glacial events in this area. Similarly, in the Romanian mountains there was an almost complete lack of age control regarding the maximum extent of the glaciers, and no palaeoenvironmental reconstruction had been made in the Rodna Mountains for the Late Devensian glaciation.

Given the abundance and the stability of the observed and mapped glacial landforms, and the occurrence of suitable dating material, surface exposure dating was applied to directly date glacial deposits and ice-eroded surfaces. The combination of geomorphological data and the exposure ages allowed the timing, rate and extent of the last glacial advances and the pattern of deglaciation to be clarified.

This research brings new empirical data to a developing chronological framework of European climate change, while the reconstructed environmental conditions in the Monadhliath and Rodna Mountains provide new insights into the temporal and spatial variability of Last Glacial climate fluctuations across Europe.

6.2 Ice sheets and climate in the North Atlantic

Both atmospheric and oceanic circulations are responsible for the balance of air and ocean temperatures around the globe. In the North Atlantic, warm surface waters are moved from the tropics north towards the Arctic via the North Atlantic Drift (an extension of the Gulf Stream). As this water moves north, evaporation and cooling increase the salinity and density of the water and eventually it sinks at the polar front returning south as North Atlantic Deep Water (Broecker et al., 1985; Nesje et al., 2000). This thermohaline circulation (THC) plays an important role in the distribution of heat and moisture transfer between the warm surface waters and the atmosphere. The resulting atmospheric warmth is transmitted eastwards by westerly winds, mostly during the winter time (Florineth & Schlüchter, 2000).

Being very sensitive to salinity and temperature, any changes in these variables affect the THC and may lead to the reduction in the supply of warm water to the higher latitudes and hence a reduction in the warm air released across NW Europe (Rahmstorf, 2003). Such a reduction could be caused by the input of large amounts of freshwater into the North Atlantic decreasing surface water salinity and slowing down the sinking process (Bigg et al., 2003). The strength of the THC has been reduced in the past, causing a decrease in atmospheric temperature and moisture in NW Europe and a southward displacement of the Polar Front (Ruddiman & McIntyre, 1981; Kuhlemann et al., 2008; Kwiecien et al., 2009).

Glaciers are sensitive terrestrial indicators of climate change, responding rapidly and markedly to changes in both temperature and precipitation (Oerlemans, 2005). Conversely, large ice sheets can themselves influence regional and global climate by amplifying and potentially driving the climate, depending on the ice sheet size and preservation through time (Clark et al., 1999). According to Rohling (2003), the transmission of the climatic signal takes place through the atmosphere rather than through oceanic circulation. For example, winds blowing over Arctic sea ice bring cold dry air over the northern European continent reducing the atmospheric moisture budget (Pinot et al., 1999). Moreover, the air above an ice sheet is cold and dense and moves downslope as katabatic winds affect primarily ice-proximal areas. Large anticyclones are usually formed at the ice surface with air draining to the south in the northern hemisphere. This moves the zone of cyclogenesis further to the south (Clark et al., 1999; Bigg et al., 2003).

Generally, ice sheets grow slowly and shrink relatively faster, especially when there is a rapid change in climatic conditions (Clark et al., 1999). The pattern and extent of past glaciations can provide information on the mechanism involved in the origin and transmission of climatic signals. Ice sheets are composed of layers of snow, which compact to ice over tens of thousands of years trapping gases, dust and water molecules. Hence they are archives of changes in atmospheric chemistry and temperature at the time of snow deposition. Large climatic oscillations in the North Atlantic region are recorded in Greenland ice cores and in deep-sea sedimentary units, providing valuable and detailed information on the Earth's environmental history (Peltier et al., 2006). The large climatic oscillations are unlikely to have influenced all of Europe to the same extent or at the same time, since local factors can lead to different climate change responses (Boulton et al., 2001).

6.3 Timing and extent of Devensian glaciation in Europe

6.3.1 North-western Europe

During the Devensian glaciation, the north-western part of Europe was repeatedly covered by ice masses. There is evidence that by ca. 50 ka the Scandinavian ice sheet had already retreated from the latitude of Denmark (Siegert et al., 2001; Svendsen et al., 2004; Wohlfarth et al., 2008). Smaller readvances were still possible between 54-46 ka, caused by increased temperature and, implicitly, higher amounts of precipitation in the Baltic area (Houmark-Nielsen, 2010).

During the most recent glaciation, the British Irish Ice Sheet (BIIS) developed and expanded from the mountains around the Rannoch Moor area of Scotland, and from other smaller high areas across Britain. The onset of glaciation in Britain occurred after 35 ka following an ice free period (Bradwell et al., 2008b). According to the simulations of Hubbard et al. (2009), ice streams formed between ca. 38-32 ka and flowed towards the Moray Firth, the Minch and the Central Lowlands (Figure 2.1) but remained terrestrial during this time. After slowly coalescing with the other ice masses in the British Isles, the BIIS margins reached below modern sea level towards the continental shelf edge.

A parallel evolution occurred in Scandinavia, where glaciers expanded from their valleys to the south and south-east towards central Europe and westwards across the continental shelf. During the Late Devensian several ice lobes spread across western Poland, Germany, Lithuania and Belarus (Svendsen et al., 2004; Marks, 2010). The ice sheet reached its maximum extent at ca. 21 ka, the western and eastern margins of the ice sheet having an asynchronous advance and retreat (Wohlfarth et al., 2008).

At the maximum expansion, the NE ice streams of the BIIS joined the Fennoscandian ice sheet (FIS) to form the NW European ice sheet. The large ice sheet also spread eastwards towards NW Russia to coalesce with ice sheets from the Barents Sea, Svalbard and Kara Sea, together known as the Eurasian ice sheet (Figure 2.3) (Svendsen et al., 2004, Wohlfarth et al., 2008). Large areas of the Atlantic continental shelf were exposed during the maximum extent of this ice sheet (and others as well) as sea level was ~120 m lower than today (Peltier & Fairbanks, 2006).

Deglaciation of the NW European ice sheet occurred after 17 ka (Svendsen et al., 2004). The BIIS reached the coast by 16 ka (Hubbard et al., 2009) and ^{10}Be exposure ages indicate deglaciation of the Last Devensian ice sheet in the Monadhliath Mountains at ca. 15 ka (this study). However, a complete deglaciation did not occur everywhere in Britain as ice was maintained in topographically favourable locations throughout the Lateglacial (Bradwell et al., 2008a).

The retreating Scandinavian glaciers readvanced during the Lateglacial in response to the severe climate cooling of the Younger Dryas period. This also caused other ice readvances in Europe. An ice cap grew over the Scottish Highlands while smaller ice caps and corrie glaciers covered other areas in the British Isles (e.g. Cairngorms, Isle of Skye, Brecon Beacons) (Sugden, 1970; Ballantyne, 1989; Carr, 2001). During this short cold episode, the Monadhliath Mountains sustained a separate plateau ice cap, located to the east of the Central Highlands ice cap, which coalesced with the valley glaciers below. Boulders from moraines in three cirques in the Monadhliath Mountains were last abandoned by ice at ca. 11-10 ka (this study).

6.3.2 South and east Europe

During the Devensian glaciation, unlike north-western Europe, south and south-eastern Europe was affected by more restricted ice fields such as small ice caps and mountain glaciers, specifically in south Germany, the Pyrenees, the Alps, the Vosges and Jura Mountains, the Massif Central, the Carpathians and the Ural Mountains (Ehlers & Gibbard, 2004). The maximum advance of ice in the Pyrenees occurred early in the Devensian glaciation between 70-50 ka and glaciers retreated slowly towards the end of the glaciation (Jalut et al., 1992; García-Ruiz et al., 2003; Calvet, 2004). Isotopic record from speleothems in the south-western part of the Romanian Carpathians support a cold climate between ~ 67-58 ka (Constantin et al., 2007) and speleothems in the Tatra Mountains also indicate two cold episodes at ca. 55 ka and 40-35 ka (Bogdan & Leszek, 1999). The Ural Mountains had more extensive glaciers at ca. 50-60 ka than during the global LGM (Mangerud et al., 2008). The last local glacial maximum (LLGM) in the Cantabrian Mountains has been constrained between ca. 48-32 ka (Sanchez & Arquer, 2002; Jalut et al., 2010). Other high altitude areas in east and south-east Europe experienced the LGM at an earlier time. The maximum position attained by mountain glaciers in the Romanian

Carpathians was before 37 ka (this study) and the relative chronology of moraine deposits in the Southern Carpathians (Retezat Mountains) supports this earlier maximum glaciation, which is asynchronous with global climate records (Reuther et al., 2007). This is also consistent with reconstructions in the Massif Central, Iberia and the Albanian Alps (Straus, 1992; Gillespie & Molnar, 1995; Marjanac & Marjanac, 2004; Milivojevič et al., 2008). Moreover, dating of glacial sediments in Greece indicates a wider maximum ice extent few thousand years prior to the global LGM (Woodward et al., 2004; Hughes et al., 2006). Similarly, the glaciers in the Bavarian Forest and the Tatra Mountains attained their maximum position at ca. 32 ka and 32-30 ka, respectively (Raab & Völkel, 2003; Lindner et al., 1990, 2003).

Southwards of the Scandinavian ice sheet, the ice cap in the Alps was the largest glaciated area of the Late Devensian Glaciation, attaining a simultaneously maximum extent with the NW Europe ice sheet (Florineth & Schlüchter, 1998, 2000). The eastern Alps sustained piedmont glaciers which reached their maximum extent between 24-21 ka (van Husen, 1997; Reitner, 2007). During the global LGM, the high altitude Caucasus Mountains had restricted glaciation, with cirque and valley glaciers of up to 50-70 km in length (Gobejishvili, 2004).

The retreat of mountain glaciers in Europe after the LGM occurred at different times in different places, and readvances of ice were common during this time of increased moisture budget. The Alps, the Carpathians and other regions had synchronous readvances during the overall deglaciation period when areas in Europe responded rapidly to the H1 cold event (16.6 ka; Ivy-Ochs et al., 2004; Reuther et al., 2007). The subsequent Bölling-Allerod warming substantially diminished glacier extents, allowing tree populations to spread. However, there were suitable topographical locations where ice masses were maintained during the Lateglacial (e.g. the Rodna Mountains). Just before the Holocene warming, the last major advance of ice during the Devensian glaciation occurred synchronously across the European mountains during the Younger Dryas cold event (12.9-11.7 ka).

6.4 Palaeoclimatic implications

6.4.1 *Glacial-climate relationships in the Scottish Highlands*

The weather systems in the North Atlantic are dominated by the North Atlantic Oscillation (NAO), a large scale process that is driven by the pressure gradients between the Icelandic Low and the Azores High pressure systems. The strong westerly winds created along this gradient serve to transport excess heat from the equatorial regions towards the higher latitudes and bring precipitation to the western side of Europe. During the course of a year, the position of the Northern Hemisphere jet stream changes latitudinally due to temperature variations and this has a direct impact on the climate of Western Europe. The position of the jet stream is located in a more southerly position in winter, at about 48°N and is responsible for mild and wet winters in Scotland (Penaud et al., 2009). In summer, the jet stream is weaker and moves northwards (~59°N) resulting in drier conditions in southern Europe (Harrison et al., 1992, 1996; Florineth & Schlüchter, 2000).

The location of Scotland on the western coast of Europe means that its climate is dominated by proximity to the North Atlantic Ocean ensuring that it recorded the cyclic climatic changes faster than European regions located further south or east (Sutherland, 1984). The palaeoclimatic reconstructions in Scotland largely agree with the high-amplitude air temperature oscillations and precipitation patterns identified in Greenland ice cores (Atkinson et al., 1987; Brooks & Birks, 2000). Towards the Late Devensian, in response to the changes in the North Atlantic Ocean circulation and therefore decline in the heat transport towards higher latitudes, Scottish glaciers expanded to form the northern part of the BIIS. This expansion occurred after 38-34 ka based on organic deposits at Tolsta in northern Lewis and at Sourlie, near Glasgow, and the dating of woolly rhinoceros remains at Bishopbriggs, also near Glasgow (Gordon & Sutherland, 1993; Bradwell et al., 2008b, Jacobi et al., 2009). The BIIS and the European ice sheet grew synchronously during the LGM (26-21 ka) and at their maximum extents they would have contributed to the cooling of the neighbouring areas (Bradwell et al., 2008b).

The considerable temperature and rainfall gradients between the west and east of Scotland were markedly stronger during the last glacial advance. A difference can be seen in the distribution of solid precipitation and ice formation during the Younger Dryas, when the NW Highlands of Scotland were covered by an ice cap, whilst the drier central and eastern

areas developed smaller individual ice caps or glaciers at higher elevations (Golledge, 2008).

6.4.2 Glacial-climate relationships in the Romanian Carpathians

The temperate climate of the Romanian Carpathians is wetter and colder than other areas at similar latitudes as they are influenced by both the western dominant winds and the dry continental climate from the east. In addition, the Retezat Mountains are influenced by air masses from the Mediterranean Sea.

The past changes in the North Atlantic Ocean were also an important control on eastern European climate during the last glaciation. However, in spite of the largely simultaneous climatic patterns across Europe, the relative magnitude and spatial variability of glacial events may have differed (Golledge et al., 2008), with the North Atlantic climate signal likely diminished, or transmitted more slowly, towards the south and east of the European continent. Although responding to the same North Atlantic stimulus, the location of the Carpathians in the transition area between the western oceanic climate and the continental east resulted in different local climatic responses.

Although the glaciations were different in extent, the Carpathians and other mountain areas further east experienced similar climatic conditions. The restricted amounts of precipitation in Eastern Europe and western Russia resulted in smaller ice fields than occurred in north-western Europe during the Devensian glaciations. However, the cold temperatures experienced in these high elevated Eastern European areas were the main controlling factor for glacier extent (Sheinkman & Barashkova, 1991). Growing continentality eastwards caused the glaciers of the Ural, Caucasus and Retezat Mountains to reach their greatest extent before the global LGM (Mangerud et al., 2008; Reuther et al., 2007).

During the LGM, the Romanian Carpathians were located at the southern periphery of the NW European ice sheet. A more limited expansion of ice, in the form of mountain glaciers at high elevations, occurred here at this time. The climatic gradients were likely different than at present as the presence of the large ice sheet in the NW part of Europe would have repositioned the dominant western winds to lower latitudes. The cold and dry climate of NW Europe at that time would likely have led to depressed temperatures emanating from

an expanded Polar High (to include the Siberian High) and to produce a westerly moving cold air stream over eastern Europe (Tarasov et al., 1999). For example, the cold environment east of the Rodna Mountains prevented the establishment of trees at Mitoc (Romania) and Coșăuți (Moldova) during the global LGM (Willis & Andel, 2004).

In the SW part of the Romanian Carpathians, conditions would have been slightly different, due to its location closer to the influence of the Mediterranean Sea and sea level fluctuations and associated temperature changes would have impacted on atmospheric moisture, influencing glacier dynamics.

During the last glacial episodes, major sea level fluctuations occurred in the Mediterranean Sea and in the connected marine basins (Lambeck & Purcell, 2005). Generally, high water levels in the Black Sea occurred during the wet deglaciation periods, whilst low sea level characterized the dry periods of the early interglacials (Chepalyga, 1984). During the global LGM (26-21 ka), the Black Sea was 110 m lower than today (Aksu et al., 2002). According to Ryan et al. (2003), the sea level drop in the Bosphorus and Dardanelles Straits isolated the Marmara Sea. Disconnected from the Mediterranean Sea, the Black Sea (= Euxenic Lake) became freshened by continental rivers and subsequently by meltwater from the disintegrating Eurasian ice sheet (Mikolajewicz, 2011; Ryan et al., 1997, 2003), delivering excess water over the sill points towards the Mediterranean (Dawson, 1992; Major et al., 2006; Lericolais et al., 2007). The available marine records in the Black Sea area supports a very cold and arid climate with reduced precipitation and low evaporation rates during this period, especially in the northern and western parts (Buynevich, 2011; Atanassova, 2005; Kwiecien et al., 2009). However, a colder and wetter climate than today was experienced by mountain areas located further south and south-westwards (Mudie et al., 2002; Sarikaya et al., 2008).

6.5 Comparison in the context of global climate records

The spatial difference in the ice extent in the Monadhliath and the Rodna Mountains is supported by the difference in the chronological framework of the Devensian glaciation. This refers to the length of time needed for both areas to respond to the same dominant stimulus, i.e. the North Atlantic ocean, set against local influencing factors which increase in importance with distance away from the main influential factor. The European records

show a wide variety of regional and local responses combined with the general atmospheric circulation responsible for the distribution of precipitation and temperature. The spatial diversity fits very well with a more limited extent of the ice towards south and south-eastern Europe in the Late Devensian. A weakening of the driving Atlantic influence towards the east is certainly apparent during the LGM (Tarasov et al., 1999) and the past glacier fluctuations in Northern Romania are one of the indicators that argue against an entirely synchronous climatic ice response during the Devensian glaciation.

6.5.1 Middle Devensian (60-30 ka)

The transition from the Early to Middle Devensian period took place in cold climatic conditions, as suggested by the isotopic record of speleothems between ~ 67-58 ka in the south-western Romania (Constantin et al., 2007). The Scandinavian ice sheet spread southwards to the latitude of Denmark at ca. 55 ka and then retreated, leaving a small ice cap over Scandinavia by 50 ka (Siegert et al., 2001; Svendsen et al., 2004; Wohlfarth et al., 2008). Details of the ice advance are still debated with Houmark-Nielsen (2010) suggesting that between 54-46 ka lobes of the SIS had advanced in the south-western Baltic, corresponding to the warming and increased precipitation during the Dansgaard-Oeschger oscillation 14-13.

The decrease in the global ice volume at ca. 50 ka led to an increase in the atmospheric moisture budget in southern and south-eastern Europe (Florineth & Schlüchter, 2000). As the moisture increased, it is possible that the Romanian glaciers were already advancing at a time when the ice masses in the NW Europe were still retreating. The build up and maintenance of mountain glaciers did not depend only on global conditions (i.e. increasing temperature), but they were more influenced by the local relief (Gillespie & Molnar, 1995). The glaciers in the Vosges and Jura Mountains and the Massif Central advanced towards their maximum extent during the Middle Devensian, but restricted southerly moist airflows in the Alps accounted for only small glacier advances at higher altitudes (van Husen, 1997; Florineth & Schlüchter, 2000). These earlier maximum expanses of ice before the global LGM may have been influenced by the increased amount of western precipitation and gradual global cooling which led to lower range of valley glaciers at an earlier time than the global LGM. The glacial record in the Rodna Mountains also indicates a significant lowering of the glacier equilibrium line altitude and glacier expansion towards their

maximum ice advance. It has previously been suggested that the glacial maximum extent was not synchronous everywhere, especially between continental glaciation and high altitude glaciers (Gillespie and Molnar, 1995; Reuther et al., 2007).

Glacier advance and preservation for few millennia in the Rodna Mountains was also enhanced by the eastern cold and dry climate associated with the Siberian anticyclone. Cold periods were recorded in speleothems in the Tatra Mountains at ca. 55 ka and 40-35 ka (Bogdan & Leszek, 1999), and reduced precipitation was received on the eastern side of the Scandinavian Ice Sheet between 47-37 ka (Houmark-Nielsen, 2010).

The location of the Polar Front over southern latitudes caused a slow retreat of ice masses across Europe. According to Florineth & Schlüchter (1998), the Scandinavian ice sheet retreat was driven by arid conditions rather than warming of the climate. The dry conditions over other areas of Europe were also not suitable for preserving ice masses and led to a similar retreat of glaciers in the NW Iberia, the Vosges and Pyrenees Mountains in a cold, but dry, climate (Jalut, 1992, 2010; Seret et al., 1992).

The timing and the rate of ice growth in the Rodna Mountains is unknown, however, the glaciers were retreating from their maximum position at ca. 37 ka at a time when the British ice sheet was advancing across the ice-free Scottish lowlands (Hubbard, 1999; Bradwell et al., 2008b). According to Blaauw et al. (2009), a more rapid atmospheric transmission of the climatic signal between the North Atlantic and the European continent would have probably led to nearly synchronous events within the Northern Hemisphere. However, the earlier LGM in the Romanian Carpathians and other parts of Europe (e.g. NW Iberia, Pyrenees, Cantabrian Mountains) might suggest a faster response of areas located further south or east (Ehlers & Gibbard, 2004; Jalut et al., 1992, 2010). Being much smaller in size than the north-western and central European ice masses, the mountain glaciers in Romania responded quicker to the oscillations in the temperature and precipitation regimes, similar to the Mediterranean region (Gillespie & Molnar, 1995; Florineth & Schlüchter, 1998; Hughes & Woodward, 2008).

6.5.2 Global LGM (30-19 ka)

The glacial retreat from a maximum position in the Rodna Mountains was probably continued by precipitation reductions during Heinrich event 3 (31 ka) and increasingly more arid conditions linked to the gradual development of the Scandinavian Ice Sheet (30-27 ka; Houmark-Nielsen, 2008) which coalesced with the BIIS (30-25 ka; Bradwell et al., 2008b), partially contributing to a considerable sea level drop of 120-150 m (Lambeck & Chapell, 2001). The growth of these ice sheets may have starved of moisture the rest of the European continent as the global LGM approached (Boulton et al., 2004). The reduction in sea surface temperature (SST), enhanced by the movement of the polar front to southerly latitudes in the North Atlantic (~40°N), would have led to cooling and formation of a more extensive sea ice cover, with subsequent low levels of evaporation (Penaud et al., 2009; Kjellström et al., 2010). The global cooling of the climate was amplified as a result of winds blowing over the sea ice, leading to decreases in atmospheric water vapour and cold winters in central and northern Europe (Clark et al., 1999; Pinot et al., 1999; Florineth & Schlüchter, 2000). For example, the limited precipitation forced the ice in the Bavarian Forest to melt back at ca. 32 ka (Raab & Völkel, 2003) which is coeval with the very cold climate of the eastern Alps after 31 ka, constraining ice in high topographical locations towards the LGM (van Husen, 1997). The glaciers in the Rodna Mountains gradually retreated, at a time when the European ice sheet was reaching its maximum extent and the moisture availability in the atmosphere was minimal (26-21 ka; Peltier & Fairbanks, 2006). This is consistent with the observations that deglaciation in a cold climate is possible when the atmosphere is starved of precipitation (Sutherland, 1994).

Before the LGM, the circulation patterns were probably similar to today and moist air was delivered by westerly air flow from the North Atlantic and south/south-westerly air flow from the Mediterranean region (Florineth & Schlüchter, 2000). However, during the last glaciation, the atmospheric circulation responsible for non-synchronous events across Europe differed from that of today (Tarasov et al., 1999). The cold environment in the North Atlantic and the ice presence in Europe interfered with the atmospheric circulation, constraining the climate over the European continent (Pinot et al., 1999). The slowing down of the North Atlantic Ocean circulation, the SST decrease and the slower hydrological cycle between the oceanic and the cold terrestrial surface led to diminished moisture across Europe (Tarasov et al., 1999). However, Pinot et al. (1999) proposed that this would have only a partial effect over southern Europe, especially eastwards (Kuhlemann et al., 2008). The presence of the much larger ice sheet in the NW Europe and

the smaller extent of ice masses further south and east, and the changes in vegetation patterns across the European continent with ice free areas covered by tundra and polar desert in the north and semi desert steppe in the south (Tzedakis et al., 1999, 2002) all support the variability in the transmission of the climate signals during the Late Devensian glaciation.

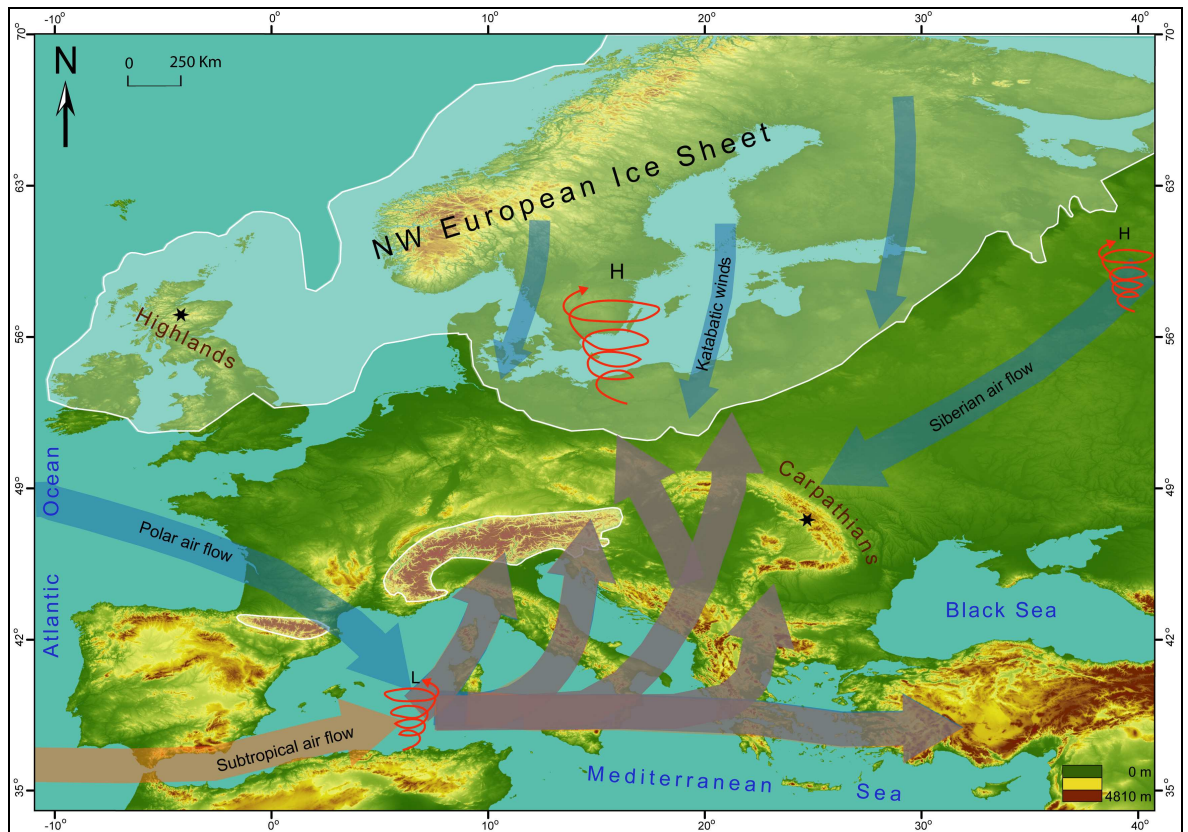


Figure 6.1. Atmospheric circulation pattern during the Last Glacial Maximum in Europe modified from Florineth & Schlüchter (2000) and Kuhlemann et al. (2009). Ice limits drawn according to Svendsen et al. (2004) and Bradwell et al. (2008b). Digital elevation model from SRTM (NASA, 2004).

The variability of the climatic conditions across Europe also suggests influences from different atmospheric factors. The presence of a massive northern ice sheet would have had a great effect on European climate. Katabatic winds drained off the ice sheet resulting in a cold, dense air at low elevations in ice-free areas (Figure 6.1), with reduced precipitation especially in Central and eastern Europe during the maximum extent of the European ice sheet (Harrison et al., 1996; Florineth & Schlüchter, 1998; Siegert & Marsiat, 2001). Because of these cold and arid conditions, glacier advance in the Vosges Mountains, the Pyrenees and the Massif Central was more restricted during the global LGM than during their maximum extent in the wetter conditions of the preceding Late Middle Devensian period (Florineth & Schlüchter, 2000; Ehlers & Gibbard, 2004). Moreover, southward winds blowing towards the equator are deflected to the right in the Northern Hemisphere,

thus increasing the cold westerly airflow towards the Carpathians (Figure 6.1). The temperatures at high latitudes in the areas adjacent to the ice sheet were also decreased by a greater continental albedo of the ice surface which increased the temperature gradient from high to low latitudes, implicitly strengthening the western air flows (Harrison et al., 1992; Clark et al., 1999). This cold effect would be stronger in the surrounding areas of the European ice sheet than around the smaller ice fields across Europe and especially in winter when the temperature gradients were greater (Tarasov et al., 1999).

A north-easterly anticyclonic wind system from the European ice sheet (Figure 6.1) would have deflected or presented a barrier to moisture-bearing winds from the west, enhancing the cold and dry climate over much of central, eastern and south-eastern Europe (Harrison et al., 1992, 1996; Florineth & Schlüchter, 1998; Ruddiman, 2001; Kjellström et al., 2010).

The southern displacement of the polar front steepened the north-south temperature gradient across the Atlantic Ocean between mid- and low-latitudes, resulting in an increase in eastern cold and dry air flows in winter, especially in northern and central Europe (Harrison et al., 1992; Florineth & Schlüchter, 2000; Kwiecien et al., 2009). The rain-bearing western winds were forced towards the southern edge of the European ice sheet, explaining the repeated advances in the south as opposed to retreats in the northern parts (Dawson, 1992; Ruddiman, 2001). Model simulations of the LGM sea climate suggest that cold and wet airflows from the Atlantic contributed to increased summer cooling in the southern Europe and the Mediterranean (Kwiecien et al., 2009; Mikolajewicz, 2011). The glacier advances in the Alps varied due to wet winds from west and south/south west, with an increase of the southerly cold and dry winds towards the eastern Alps and the Pannonian Basin (Ivy-Ochs et al., 1996; van Husen, 1997, Florineth & Schlüchter, 2000). Polar air flowing between the Pyrenees and the Alps combined with subtropical air from NW Africa created cyclones in the western Mediterranean (Figure 6.1). The strengthened moisture bearing jet stream from southern France continued eastward across the Mediterranean, splitting and diverging north-northeast towards the south-eastern Alps and further north over Albania, towards Ukraine supplying moisture to the Fennoscandian ice sheet (Rohling et al., 1998; Tarasov et al., 1999; Florineth & Schlüchter, 2000; Kuhlemann et al., 2009). This is consistent with reconstructions in the Tatra Mountains where southern atmospheric circulation prevailed during the LGM (Zasadni, 2009). Another branch from the Mediterranean air masses continued eastwards (Figure 6.1), supplying moisture and bringing cold temperatures to western and southern Turkey (Sarıkaya et al., 2008).

Peyron et al. (1998) and Harrison et al. (1996) argue for a colder and wetter climate in the Mediterranean than in the north of Europe, but with a strong winter precipitation gradient eastwards limiting the effect on the south-east part of Europe. This agrees well with the reconstructed environment in the Albanian Alps (Kuhleemann et al., 2009). Again, simulations in southern Spain suggest cold and wet conditions but rather dry in central Italy (Harrison et al., 1996). However, ample evidence suggests that the last humid and cold climate in the Mediterranean occurred at ca. 30-25 ka, before the severe cold and dry environment of the LGM, which did not allow major glacial advances in the Mediterranean mountains (Tzedakis, 1999, 2007; Hughes et al., 2007; Hughes and Woodward, 2008).

It appears that dry conditions characterized the SW part of the Carpathians during the LGM as glaciers were already retreating towards higher catchments (Reuther et al., 2007). The evidence found in this study further north in the Rodna Mountains, is consistent with recent climatic models that suggest dry conditions over eastern Europe and northern and mid-latitude Russia during the global LGM (Tarasov et al., 1999). Located between the NE and E air flows from the Mediterranean Sea (Figure 6.1), the Rodna Mountains do not appear to be affected by the moist air flows. It is possible that the moist air flow from the Mediterranean region caused the glacier advance (M2) in the Retezat Mountains (Reuther et al., 2007), creating a föhn effect on the northern part of these mountains. Thus only a dry air stream reached the Rodna Mountains. The aridity recorded in the Rodna Mountains and the restricted glacier extent was also due to the local interaction with the dry continental climate of eastern Europe. The lack of western moisture would have required exceptionally low summer temperatures to sustain the glaciers throughout the global LGM. Low summer temperatures could have been the result of the strengthened Siberian High which spread intense cold and dry air westwards (Figure 6.1) (Nesje et al., 2000). Smaller glaciers were also reconstructed in the northern Urals during the LGM, emphasizing the north-eastwards extension of dry and cold conditions (Mangerud et al., 2008). While climate is the most important factor in ice masses dynamics, the high accumulation areas in the Rodna Mountains were also contributing to the preservation of the glaciers and their subsequent slow retreat. This reflects the sensitivity of high mountain glaciers to the local conditions (Reichert et al., 2001).

In contrast, Tarasov et al. (1999) suggested that during the global LGM the area around the Black Sea was characterized by somewhat wetter conditions than the present climate. An increase in the moisture budget in the northern and eastern Mediterranean is supported by lake level records and climate modelling (Prentice et al., 1992; Harrison et al., 1996). This

moisture could have been supplied by the eastward flow of air masses from the western Mediterranean.

The atmospheric circulation patterns discussed above are reflected in loess deposition across Europe (Figure 6.2). The loess in central Europe is mainly attributed to winds blowing from the front of the ice sheet (Goudie, 1983). However, eastern Europe has extensive and thick covers of loess which are likely to have been deposited in a similar way by the north-easterly anticyclonic winds blowing from the Eurasian ice sheet during the LGM (Dawson, 1992). Loess deposition eastwards and southwards of the Carpathians arch (40 000 km²) has been the subject of several works (Gherghina et al., 2006 & reference therein; Timar et al., 2010).

6.5.3 LGM deglaciation (21-15 ka)

Deglaciation of the ice masses in Europe were essentially characterised by an oscillating glacial retreat. The climate fluctuated repeatedly from warm to cold during the Lateglacial and the changes were mostly in phase across the European continent. Ice sheets and glaciers shrank from their maximum volumes shortly after 19 ka because of rapid sea level rise (Yokoyama et al., 2000; Lambeck & Chappell, 2001). A fast response to the changes in the North Atlantic region occurred in Scotland and NW Europe as the western maritime lobes of the European ice sheet were affected first (Rinterknecht et al., 2006). The evidence in the Rodna Mountains suggests a slow and continuous retreat of ice towards the higher ground between 18-15 ka and there is no indication of a re-advance during the Lateglacial. The likely slower response of the Rodna glaciers to the warming of the North Atlantic was the result of the reduced importance of maritime conditions towards the east and a colder and drier continental eastern Europe.

The northward retreat of the polar front and warmer temperatures over the continent led to the initial melting of the European ice sheet and other ice masses in Europe. It took 5-6 ka for the ice sheet to melt back between the LGM limits and the Baltic (Kalm, 2010). The early deglaciation and the high amount of fresh water and icebergs discharged into the Atlantic are thought to have affected the formation of NADW, causing the polar front to move southwards again (Penaud et al., 2009). However, the ice sheets and glaciers continued to retreat as a response to the cold and arid conditions in Europe (Raven, 2001;

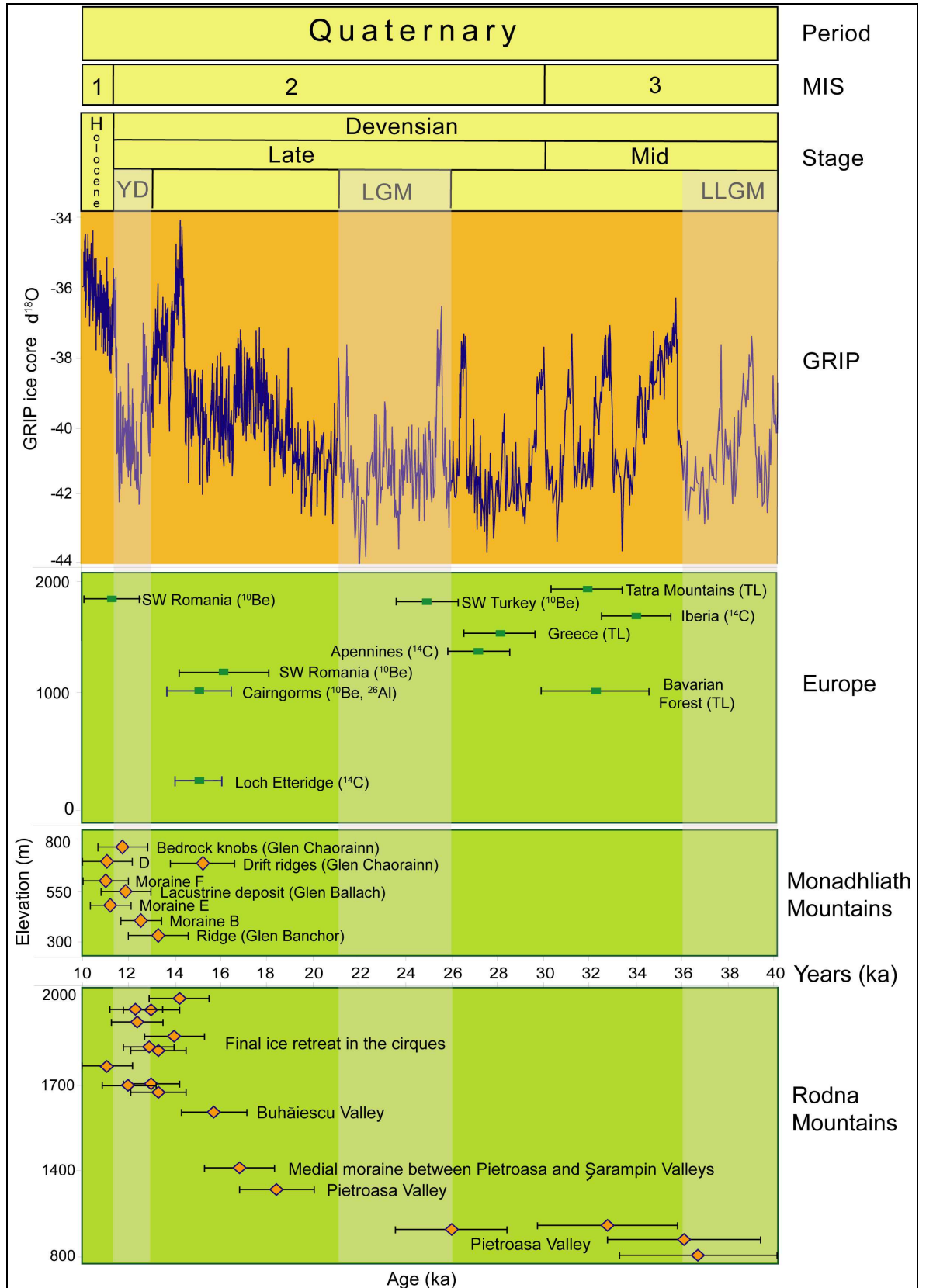


Figure 6.3. Late Quaternary chronostratigraphy (Monadhliath & Rodna Mountains) and their correlation with Marine Isotope Stages and Greenland ice core data (NGRIP dating group, 2008) and other European dates. The last local maximum glaciation (LLGM) after 40 ka is also shown.

Rinterknecht et al., 2006). Ice free areas were common in the Alps and Turkey around 17.7 ka and 17.3 ka, again because of cold and very dry climatic conditions.

In contrast, the increase in the precipitation regimes across Europe caused by the melting ice, led to readvances of valley glaciers in the southern part of the Romanian Carpathians (Reuther et al., 2007). This was likely to happen in the area closest to the Black, Marmara, and the Mediterranean seas which act, even at present, as moisture sources for this part of the Carpathians (Ono et al., 2004; Reuther et al., 2007). A similar readvance occurred at ca. 15.8 ka in the Alps after the initial deglaciation (Ivy-Ochs et al., 2004). Readvances in southern (16.8 ka) and north-western (16.1 ka) Turkey occurred in similar conditions as a result of the H1 cold event (Sarıkaya et al., 2008; Zahno et al., 2010; Hughes & Woodward 2008). The increase in freshwater and sediment in the Black Sea from the northern areas occurred after ca. 16 ka when the European climate became warmer (Kwiecien et al., 2009).

The sea level rise also caused a punctuated retreat of the BIIS as evidenced by offshore glacial landforms, retreating to the coastline by ~16 ka (Bradwell et al., 2008b; Hubbard et al., 2009). Terrestrial geomorphological features suggest a rapid retreat of ice, marked by stillstands and short readvances (Young, 1974; Brazier et al., 1998; Merritt, 1998; Golledge, 2002). Deglaciation in the Monadhliath Mountains occurred at ca. 15.1 ka, at similar times as the nearby Loch Etteridge and the Cairngorms (Walker, 1975; Phillips et al., 2006).

6.5.4 Lateglacial (14.7-12.9 ka)

The retreat of the European ice sheet and changes in vegetation from semi-arid to temperate species (Feurdean & Bennike, 2004; Hubbard et al., 2009) is consistent with the increased warmth and atmospheric moisture budget throughout Europe after the H1 event. The Bølling-Allerød warming resulted in the massive retreat of the European ice sheet to near interglacial conditions (14.6 ka; Rinterknecht et al., 2006). The eastern part of Scotland was deglaciated before ca. 14.5 ka but readvances occurred at ca. 14 ka in the NW areas (Ballantyne, 2010). Similarly, the upper valleys in the Rodna Mountains were ice free by 14 ka (this study) after a warming phase in the north and west part of Romania (Wohlfarth et al., 2001; Tămaş et al., 2005). The Older Dryas cold event (14.5-13.7 ka) at the beginning of the Bølling-Allerød warming led to short oscillations of the glaciers

margins in Scotland (Golledge et al., 2008) and vegetation suffered a brief decline in tree populations in Romania (Björkman et al., 2002; Feurdean et al., 2007). Favourable conditions existed in the NW part of Scotland for ice to be maintained even after 14 ka (Sutherland, 1984; Bradwell, 2008a; Lukas & Bradwell, 2010). A distinct deglaciation from a readvance was also recorded at 13.3 ka in north-western Turkey (Zahno et al., 2010).

6.5.5 Younger Dryas (12.9-11.7 ka)

The rise in SST in the North Atlantic during the Bølling-Allerød was interrupted by the repositioning of the Polar Front southwards resulting in an abrupt cooling event across Europe known as the Younger Dryas (Ruddiman & McIntyre, 1981; Harrison et al., 1992; Humlum, 1997; Golledge, 2008).

In the Rodna Mountains and the Monadhliath Mountains, the short and abrupt phase of distinct climate cooling of the Younger Dryas (12.8-11.7; Rasmussen et al., 2006; Lowe et al., 2008) was characterized by the preservation of existing ice or possibly small ice readvances (Figure 6.3). The deglaciation chronology presented in this study supports regional synchronism of glacial dynamics in the Scottish Highlands, along the Carpathians and further north in the Ukraine (Rinterknecht et al., submitted). Outside of the glaciated areas the cooling event is recorded in oxygen isotope records from speleothems in western Romania and the gradual expansion of open vegetation and barren areas (Björkman et al., 2002, 2003; Feurdean and Bennike, 2004; Tămaş et al., 2005).

Younger Dryas glaciers in southern Turkey and the Alps deglaciated at ca 11.5 ka (Zahno et al., 2010; Ivy-Ochs et al., 2006, 2008). Further north, deglaciation from the Younger Dryas limits occurred at 13.5-10.9 ka in Finland (Rinterknecht et al., 2006). The similarity in the response of ice masses in NW Europe, the Mediterranean region and eastern Europe suggest synchronicity of climatic forcing during the Younger Dryas stadial.

Interestingly, the similarities between the two regions in this study show no spatial diminution of the climatic signal as occurred during the LGM (Beaulieu et al., 1994), but rather a simple, synchronous transmission towards southern and eastern Europe. Furthermore, the consistency between the data here and the Greenland ice core records

(Bond et al., 1997; Björck et al., 1998) suggests that the transmission of the climatic signal from the North Atlantic region was smoother and faster than in previous stadial and interstadial episodes. The suggestion is that this synchronicity resulted from the absence of the large European ice sheet and the more northern position of the oceanic polar front in the North Atlantic, which allowed stronger and colder westerly winds to penetrate across Europe (Brauer et al., 2008).

The most marked precipitation and temperature decline during the Younger Dryas occurred in the north-western European countries, as evidenced by larger ice caps and glaciers. Generally, a steep west-east precipitation gradient was recorded from NW to SE Europe (Harrison et al. 1992; Renssen et al., 2001), which emphasises the diminished role of the ice masses themselves in exerting a control over the regional climate, and certainly less than that of the previous glacial advances. The Younger Dryas glaciers did slightly modify the local climate by decreasing the temperatures in the adjacent ice free areas and creating a pronounced periglacial regime (Ballantyne et al., 2007). The Younger Dryas was terminated by a rapid increase in atmospheric temperature and moisture at ca. 11.5 ka resulting in the deglaciation of the two study areas, and the replacement of open vegetation by trees (Feurdean et al., 2007).

The hypothesis presented here is that the Rodna Mountains glaciers did not disappear completely before the Younger Dryas stadial which occurred simultaneously across Europe. According to Birks et al. (1994), the Bølling-Allerød period was cool and wet which allowed for the glaciers to survive, even at low elevations. This is supported by climatic reconstruction in NW Scotland, where glaciers were preserved in favourable locations (Bradwell et al., 2008a). It is likely that glaciers in western Scotland started to build up much earlier than the general accepted onset date (12.9 ka) for YD glaciation, due to the atmospheric moisture availability during the preceding interstadial when the sea was ice free, combined with gradual northern hemisphere cooling (Bradwell et al., 2008a; Lukas & Bradwell, 2010). Thus their maximum limits were reached during the extremely cold stadial, enhanced by lower summer SST and a more widespread sea ice cover (Lohne et al., 2007). As sea ice is a strong and rapid cause for atmospheric cooling, oceanic eastward winds would have amplified Europe's cold climate (Brauer et al., 2008). It is well known that during the Heinrich events polar waters entered the Western Mediterranean contributing to decreases in SST and implicitly lowered evaporation. This is reflected in the dry environments of southern and eastern Europe at these times (Tzedakis, 2010).

6.6 Equilibrium Line Altitudes (ELA)

Detailed geomorphological mapping of the glacial landforms in the Monadhliath Mountains in Scotland and Rodna Mountains in Romania allowed reconstruction of the ice mass responses to changes in temperature and precipitation regimes. The ELA reconstructions presented in this study can be compared with published and dated ELA reconstructions from other European sites (Figure 6.4).

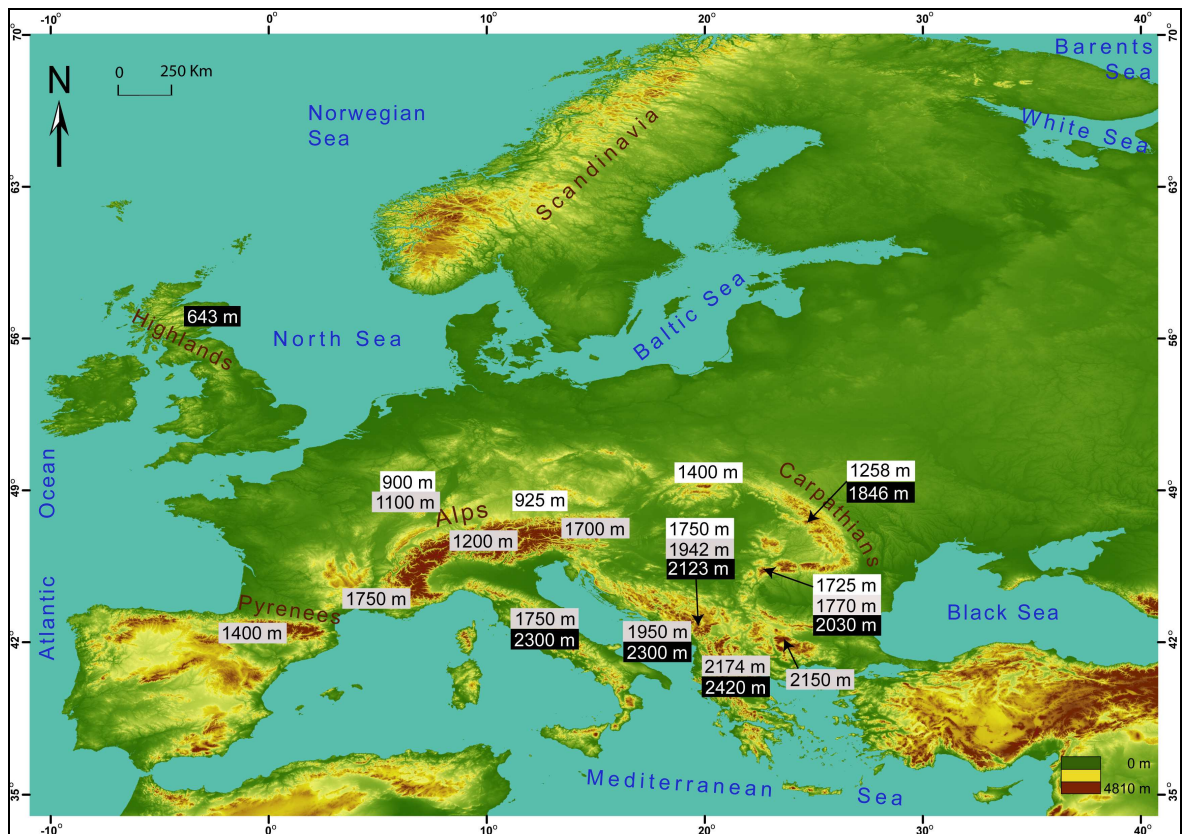


Figure 6.4. Equilibrium Line Altitudes in Europe (white box = LLGM, grey box = global LGM; black box = YD) (SRTM from NASA, 2004).

LLGM. Prior to 32 ka, during the most extensive glacial event, the ELA in the Vosges Mountains was estimated at 900 m (Mercier & Jeser, 2004) and in the Bavarian Forest at 925-1050 m (Raab & Völkel, 2003). East of this area the ELA increases to 1258-1336 m in northern Romania (this study) and 1750 m in the Albanian Alps (Milicojević et al., 2008). The difference in glacial extent between the western areas of Europe and those located further east shows a distinct increase in the elevation of the ELA. Due to different dynamics of the atmosphere, the Rodna Mountains were subjected to higher amounts of western and north-western precipitation than during the global LGM which led to a greater development of glaciers.

The Carpathian range shows a south-north ELA gradient from the Retezat Mountains in SW Romania (1725 m; Urdea & Reuther, 2009), towards the Rodna Mountains (1258 m) and further north to the Tatra Mountains (1400 m; Zasadni, 2009). This is consistent with the hypothesis that the cold climate from the east and north-east, much harsher during the Devensian glacial advances, combined with precipitation, caused a lower ELA earlier in comparison with other European glacial advances.

LGM. During the maximum extent of global ice, the ELA increases from the central Alps (1200-1500 m; Ivy-Ochs et al., 2006) to the Eastern Alps (1700-1800 m; van Husen, 1997). The ELA estimations in the Carpathians at the time of the global LGM supports the west-east gradient of precipitation in Europe as the ELA in the Retezat Mountains was estimated at 1770 m (Reuther et al., 2007). This west-east ELA gradient indicates that geographic location plays an important role in glacier extent. The larger ice masses in western Europe strongly suggest wetter local conditions as a result of the more pronounced westerly airstream.

The reconstructed ELAs across the Mediterranean region indicate a similar west-east gradient from the Pyrenees (1400 m; Calvet, 2004), Vosges Mountains (1100 m; Mercier & Jeser, 2004), French Alps (1750 m; Cossart et al., 2010), the Apennines (1750 m; Giraudi & Frezzotti, 1997), the Šara Range (1950 - 2150 m; Kuhlemann et al., 2009), the Albanian Alps (1942 m; Milicojević et al., 2008), northern Greece (2174 m; Hughes & Braithwaite, 2008) to the Rila Mountains (2150-2250 m; Zhelezov, 2010). The west-east increase in ELA elevation across the Mediterranean is supported by the same west-east gradient of precipitation during the winter season at the time of maximum glacier extent, indicating drier conditions further eastward (Kuhlemann et al., 2009).

YD. Similar differences in the ELA pattern are found across Europe during the YD cold stadial. The ELA in the Retezat Mountains was estimated to have been located at 2030 m, which indicates lower precipitation and higher ablation possibly due to the Mediterranean influence compared with the more northern Rodna Mountains (1846 m), where a colder climate prevailed during the YD. An even higher ELA was estimated in the Albanian Alps at 2123 m (Milivojević et al., 2008), at 2300 m in the Šara Range (Kuhlemann et al., 2009) and in Greece at 2420 m (Hughes & Braithwaite, 2008). In the two study areas, Monadhliath and Rodna Mountains, similar ELA trends can be observed. The calculated ELA for the main YD glaciers in the Monadhliath valleys ranged from 643 m to 809 m from west to east, while the moraines in the Rodna Mountains indicate a west-east ELA

increase between 1846 m and 1935 m, supporting the strong west-east climatic gradient across Europe.

Overall, the regional differences in the ELA reconstructions across Europe appear to be mainly due to the location of the glaciated area in relation to the dominant palaeo-wind direction. The north-western countries received more precipitation as they are closer to the Atlantic Ocean and precipitation had an important role in controlling the ELA changes during the last glacial episodes. Hence the rapid changes in glacial extent and dynamics of the western ice masses. The high altitudes of the accumulation areas in eastern Europe, combined with the dry and cold winds from the stronger Siberian anticyclone during glacial episodes, resulted in less extensive glaciers.

A significant factor to take into account is topography which may also have been responsible for some of the apparent local differences across the study areas. Local topography provides the conditions for snow accumulation, especially from wind-drifting of snow. Variations of the ELA values in each of the study areas are also related to the differences between altitude and size of the accumulation area and the shape and aspect of each cirque, resulting in ELA gradients from west to east during the last three major ice advances (LLGM, LGM and YD).

6.7 Summary

Numerous studies have shown that terrestrial Europe had a clear response to the changes in the North Atlantic circulation and the subsequent weakening of oceanic transport of heat to higher latitudes. However, the amplitude of the response was recorded in different ways across the continent. The highest climatic sensitivity occurs in areas closer to the North Atlantic where glaciers advanced more, forming massive ice sheets that subsequently influenced the global sea level and conditioned the climate. Further south and east, smaller glaciers advanced from high mountain environments towards the lower valleys. In spite of the coupled ocean-ice-atmosphere-biosphere system, the insights gathered from various proxy records support a strong temporal variability across the Northern Hemisphere in terms of maximum cold and aridity and maximum ice volume at various sites. The results presented in this thesis indicate dissimilarities in terms of driving forces and magnitude of changes during stadials.

The European atmospheric disturbances during the Middle Devensian (=MIS 3) are less known than the subsequent LGM climate. A warmer climate and increased atmospheric moisture during MIS 3 led to the maximum expansion of ice in areas located further south and east of the retreating Scandinavian ice sheet. There are an increasing number of European areas where climate reconstructions indicate that the ice masses were at their maximum extension during MIS 3. The glacial record in the Romanian Carpathians supports this discrepancy in the glacial dynamics across the continent, emphasizing that the regional climate may be the controlling factor but the glacial response may be influenced by the local conditions. The warming of the European continent was counteracted by the cold Siberian airflows which allowed the glaciers in mountain regions to reach their maximum position during the middle part of the last glacial cycle.

Large scale reorganisations of oceanic and atmospheric circulation in the North Atlantic Ocean resulted in renewed cooling over Europe during the LGM. Fluctuations of the Polar Front triggered changes in the transmission of the climatic signal from the high latitudes towards the mid latitudes. The main climatic characteristics of the LGM were the high amplitude north-south temperature gradient caused by the more southerly repositioning of the Polar Front and a west-east precipitation gradient from the Atlantic Ocean towards eastern and southeastern Europe. The continuous retreat of ice in the Romanian

Carpathians, even during the LGM, was caused by moisture starvation of the area due to the build up of the NW European ice sheet (including the BIIS).

A more restricted glaciation during the Younger Dryas stadial led to more or less synchronous events across the Northern Hemisphere. The more northern position of the Polar Front allowed the wet and cold westerly winds to reach all areas, from the Scottish Highlands to the Romanian Carpathians, at similar times. It was a faster and more rapid transmission of the climatic signal from the North Atlantic region. However, there was a similar west-east precipitation gradient as smaller ice fields were formed towards southern and south-eastern areas.

Chapter 7

Conclusions

7.1 Conclusions

This thesis has constrained the spatial and temporal extent of glaciations in two areas of Europe: the Monadhliath Mountains in Scotland and the Rodna Mountains in Romania. Surface exposure ages in this study are the first direct dating obtained in both study areas and provided significant information on the timing of Devensian glacial events. The reconstructed palaeoenvironments improve our understanding of European atmospheric circulation at the end of the last glaciation.

- Mapping of the glacial erosional and depositional landforms in the south-eastern Monadhliath Mountains has allowed identification of two phases of glaciation. The ^{10}Be exposure ages indicate deglaciation of the Last Devensian ice sheet at 15.1 ka (n = 2). Moraines in three Monadhliath cirques were deposited between 11.8 ka and 9.8 ka (470 – 600 m) suggesting that a glacial readvance occurred during the Younger Dryas stadial (n = 9). A plateau ice field fed the cirque glaciers contributing to this readvance, especially in the western valleys.
- Geomorphological mapping has established the extent and pattern of glaciation in the northwest part of the Rodna Mountains. During the last local glacial maximum, ice reached lower elevations than had been previously suggested, as boulders were abandoned between 37.2 – 26.6 ka at an elevation of ~700 m (n = 4). The retreat of ice towards higher ground during the Lateglacial occurred between 18.1 – 13.2 ka (1100 – 1800 m altitude) based on erratics and bedrock samples (n = 27). The final deglaciation took place in the cirques at 12.5 - 11.2 ka (n = 8).
- There is a spatial and temporal difference in the advance and retreat pattern between the Scottish Highlands and the Northern Romanian Carpathians. Located in the NW part of Europe, Scotland was influenced by wetter and colder conditions from the North Atlantic region which resulted in the build-up of the large BIIS, leaving a significant imprint on the landscape. During this time, outside the European ice sheet limits smaller ice advances occurred. As the amount of glacial modification to landscape is proportional to ice thickness and topographical constraints, the small mountain glaciers in the Romanian Carpathians have left a limited geomorphological record.

- The maximum advance of the European ice sheet during the last glacial cycle did not occur synchronously with the Last Local Glacial Maximum (LLGM) inferred from other areas in Europe. As part of the British-Irish ice sheet, the Monadhliath Mountains were deglaciated at ca. 15 ka, at similar times as the rest of the north-west European regions. However, the last local maximum glaciation in the Romanian Carpathians was asynchronous to global climate records, as deglaciation in the Rodna Mountains occurred before ca. 37 ka, implying an earlier LLGM. This earlier maximum advance of ice indicates that the responses to the climatic oscillations in the North Atlantic region were very different across the continent.
- The palaeoenvironmental context which caused the temporal and spatial difference in the build up of the last continental ice sheets and mountain glaciers can be understood only through reconstructing the past atmospheric circulation patterns. At the maximum extent of the European ice sheet, the polar front was probably located in a more southern location. The combination of the polar front and the subtropical air flows from NW Africa may have triggered cyclones in the western Mediterranean. A strengthened moisture bearing jet stream could have continued eastward across the Mediterranean, splitting and diverging north-northeast and supplying moisture to various parts of Europe. However, the branch flowing towards Romania would not deliver moisture to the Rodna Mountains because of blocking by the eastern Siberian high pressure system and the very cold and dry conditions associated with that system.
- The cooling during the Younger Dryas stadial was more likely synchronous across the European continent due to a more northerly position of the oceanic polar front in the North Atlantic region, which allowed for stronger moisture-bearing winds from the west to reach most of Europe at the same time. Winds blowing over sea ice in Greenland and the North Atlantic region augmented the increased cooling over the whole continent.
- The strong west-east precipitation gradient between Scotland and Romania during the last glacial advances is supported by the ELA reconstructions in both study areas. Northwestern Europe received more precipitation as it is located closer to the Atlantic Ocean. This indicates that precipitation had an important role in controlling ELA changes. Temperature acted as the main atmospheric control

which sustained the glaciers in high elevated areas located further away from the Atlantic.

7.2 Future considerations

The research described in this PhD thesis represents a significant contribution towards establishing the environmental conditions in Europe during the last glacial cycle. This study has established a good chronology for the Scottish Highlands and Northern Romanian Carpathians and the most likely scenario for the atmospheric circulation during the maximum extent of ice sheets and glaciers.

Until recently, past climatic changes were thought to occur as a response to a smooth atmospheric forcing. However, new evidence from various European locations has gradually changed this view. The interlocking climate systems that drive glacier change is complex and further in-depth investigations into the climatic response are needed.

Although the changes in the North Atlantic have triggered climatic fluctuations from north-western to south-eastern Europe, different magnitudes of climate change occurred in response to interaction with the easterly airflows from central Asia acting together with local factors. The complexities and uncertainties in the transmission of climate signals highlight the need for more palaeoenvironmental studies to provide a clearer picture of the atmospheric circulation spanning high latitude maritime climates and lower latitude continental climates. This thesis has established that the past atmospheric circulation in Europe was different than of today, its distinctive dynamics in the Romanian Carpathians generated by the location at the bifurcation of several climatic influences: oceanic (W), Mediterranean (SW) and continental (E).

The Carpathians are also located mid-way between the most responsive area to climate oscillations in the North Atlantic (Scotland) and the least responsive area to the same stimulus (continental Asia) and they can provide important information in understanding modes of operation of climate across substantial distances. At present, the main difficulty lies in a lack of sufficient records of glacial extent and timing in the southern Romanian Carpathians, and the next step is to improve the long-term glacial chronology in more Romanian mountains. Establishing the glacial history over the whole Carpathians chain

would allow the identification of the strongest influencing factors and their role in the regional distribution of temperature and precipitation. The comparison with other neighbouring areas, such as Ural, Caucasus, Turkey, Ukraine, could be used to understand wider issues of glacier–climate relationships.

These reconstructions and comparisons are critical for providing the boundary constraints for future numerical simulations which can be used to address a series of key questions, in order to clarify the climatic changes that induced the past cyclical growth and decay of glaciers, their long-term behaviour, the pattern and geographical extent of ice build-up and the asynchronous timing of maximum ice extent in this part of Europe. More empirical data against which to test climate models is required to increase confidence in the capability of the models predicting future climate changes and their impacts.

Appendixes

Appendix A

Terrestrial in situ cosmogenic ^{10}Be

Laboratory Procedure

Introduction

This is the procedure for preparing very pure quartz separates. Most silicate minerals dissolve faster than quartz in diluted HF and can be etched away to leave a very pure quartz residue. Some quartz is lost - usually ~10% of coarse-grained fractions (500-850 μ) and up to 20-30% of fine-grained fractions (250-500 μ). It is difficult to get good yields from this procedure using grain sizes <250 μ .

Some minerals will not dissolve (e.g. garnet, zircon, rutile, ilmenite). Fortunately, except for garnet, these are trace constituents of most rocks. Muscovite is the only other common mineral that causes problems. It dissolves at about the same rate as quartz, so the procedure won't concentrate quartz relative to muscovite.

An initial heavy liquid separation will remove garnet and muscovite (as well as most other mafic silicates and oxide minerals), if present. However, not all rocks need to be processed in heavy liquids before HF treatment. Small amounts of zircon, ilmenite, etc. in the final sample do not cause problems in the Al-Be extraction chemistry.

The HF leach has the added advantage of dissolving the outermost shell of the quartz grains, as well as etching cracks, where any contamination by meteoric ^{10}Be would be concentrated.

Crush and sieve

Notes: This process is used for surface samples and cobbles from gravel pits. For sand samples, dry the sample in the oven overnight before sieving it - crushing is not necessary. Separate surface samples into two batches before crushing. Samples from gravel pits should be split after crushing and/or sieving. One of these "splits" can be saved as insurance against mistakes. Weigh each clast from cobble gravel pit samples before crushing, and record their masses.

1. Select two sieves and clean them thoroughly with a brush and a dissecting needle. The goal is to eliminate polymineralic grains, so the coarser sieve should have openings somewhat smaller than the average crystal size in the rock. Use a 0.5 or

- 0.25 mm screen for the finer sieve. For coarse granite samples. The ideal grain size is 0.25-0.50mm.
2. Clean the jaw crusher and pulverizer thoroughly with a wire brush. Be sure to clean the catch trays for both the crusher and the pulverizer.
 3. Set the crusher jaws about half a centimeter apart. Make sure that the catch tray is in place. Crush the sample and pass it through the sieves. Put a magazine or piece of wood over the top of the crusher so that sample material does not fly out and hit you.
 4. Sieve the sample to remove the grain size you want. Crushing the sample again will crush the grain size you want. This will reduce the amount of the grain size fraction you want.
 5. Reset the crusher jaws so that they are two or three millimeters apart. Collect the material from the upper sieve and crush it again, then pass it through the sieves.
 6. Set the pulverizer discs about two millimeters apart. Pass the sample through it, a few grams at a time, and pour it through the sieves. Again, make sure that the catcher tray is in place before pouring in the sample.
 7. Repeat the last step two more times, each time passing the result through the sieves and putting only the too-coarse fraction back into the pulverizer.
 8. Reset the pulverizer discs to be about a millimeter apart. Pass the sample through the pulverizer and pour it through the sieves.
 9. Repeat the last step two more times, each time passing the result through the sieves and putting only the too-coarse fraction back into the pulverizer.
 10. Reset the pulverizer discs to be very close together. Pass the sample through the pulverizer and pour it through the sieves.
 11. Repeat the last step two more times, each time passing the result through the sieves and putting only the too-coarse fraction back into the pulverizer.
 12. There should only be a few grams of sediment remaining on the coarser sieve. These grains will be mostly flakes of feldspar and mica. Pour these into a sample bag over a clean tray and label the bag with the sample name and the grain size.
 13. Pour the desired grain size fraction into another sample bag. Again, label the bag with the sample name and the grain size.
 14. Also pour the fine fraction into a third sample bag, and label the bag.

Rinse fines

1. Write the sample name on a baking tray.

2. Pour the sample into the tray slowly.
3. Add enough water to fill the tray about two-thirds full. Pour off the water.
4. Repeat the last step (as many as 10 times) until the decanted water is clear.

Quartz cleaning procedure

Pre-treatment

- (1) Pour about 60 grams of sample into a glass beaker.
- (2) Wash the sample with water to remove the remaining fines.
- (3) Under the fume hood and wearing gloves add enough aqua regia to cover the sample.
- (4) Place the beaker on a hotplate on low setting and cover it with a watch glass. Stir the sample; if gas evolves after stirring be very careful with heating applied to sample as gas may get trapped in sample's layers having an "explosive" effect. Leave the sample overnight.
- (5) The next day stir the sample. If solution gets yellower and grains lighter go to step 6; if not heat the sample longer and at a slightly higher temperature. Bubbles will evolve.
- (6) Cool the beaker and carefully pour the acid into the hazardous waste container without losing sample.
- (7) Rinse the sample several times with water and discard the liquid into the hazardous waste container. After thorough rinsing, solution should be clearer and pH ~5.2.
- (8) Once the sample is clean, dry it in the drying oven.
- (9) Once samples are dry bag them up.

Acid neutralization

Notes: Mix the sodium hydroxide solution several hours before you will need it. When sodium hydroxide dissolves in water, it releases a lot of heat. If you pour hot sodium hydroxide solution into a waste acid carboy, you will breathe the acid vapour. If you can see vapour coming out of the waste acid carboy when you take off the lid, or if the waste

acid carboy feels very hot, stop! Put the lid loosely on the carboy, put the carboy in the hood, and come back a few hours later.

1. Put the empty sodium hydroxide carboy in or near the fume hood.
2. Put the sodium hydroxide bucket in or near the fume hood, and ~20 scoops of sodium hydroxide flakes into the carboy. Add ~10 L water to the carboy, stir by shaking the carboy in a circular motion, wait several hours.
3. Put the waste acid carboy in the sink. Add a bit of pH paper to make sure that the waste is acidic.
4. Give the cap of the sodium hydroxide carboy about half a turn to the left, counterclockwise. Otherwise, sodium hydroxide solution will run down the outside of the carboy when you try to pour from it.
5. Turn the waste acid carboy so that you can clearly see the graduations on its side. Pour in about half a liter of sodium hydroxide solution for HCl/HNO₃. For neutralizing HF/HNO₃, use less than 100ml the first pour.
6. Replace the lid on the waste acid carboy and rock it in a circle for at least a minute.
7. Check the pH.
8. Repeat steps 7 through 9 until the pH becomes 7. If the pH becomes too basic, add some waste acid until it reaches 7.
9. Turn on tap water and pour the neutralized acid down the drain, and then clean off the outside of the waste carboy.
10. Let the tap run for about five minutes to flush any neutralized acid that may be left in the drain.

Rinse and dry

Notes: Make sure that there is a good supply of sodium hydroxide solution and plenty of room in the waste acid carboy, before beginning. Do not pour the aqua regia mixture into the hydrofluoric acid waste carboy. The first few steps should be done in or near a fume hood.

1. Put the waste acid carboy into the fume hood and lower the glass to working height.
2. Decant the acid from the 4 L beaker into the waste acid carboy.
3. Add DI to the beaker, being careful to suspend all the grains, and decant the water into the waste carboy. To avoid contaminating the sample, do not touch the rim or inside of the beaker.

4. Repeat the last step at least three more times, or until the decanted water is not obviously yellow.
5. Remove the beaker from the fume hood and put it in a sink with a DI tap. The decanted water in the remaining rinses can be poured down the drain.
6. Rinse the sample with deionized water at least fifteen, and possibly more than twenty repetitions will be needed.
7. Transfer the sample to a 1 L beaker and put it in the oven to dry.
8. Neutralize the acid in the waste carboy with sodium hydroxide.

Magnetic separation

1. This step can either be done before or after the initial roller leaching. If there is not much sample material it is best to do magnetic separation after the initial leach. This is because the quartz grains will become detached from the host mineral during the physical and chemical abrasion of the roller leach.
2. Pour the dried sample through a funnel stuck between the arms of a powerful magnet before passing it through the magnetic separator. Save the magnetite grains in a sample bag. Label the bag with the sample name, the grain size, and the word "magnetic."
3. Clean the magnetic separator with the wet/dry vacuum. Pay special attention to the loading hopper, the loaf pan trays, and the brush under the wheel. Vacuum first, and then blow out the brush and the gap between the magnet and the wheel.
4. Turn on the magnet and the wheel. The magnet should have a current of about 4.0.
5. The magnetic grains will come out of the two chutes on the left, while the non-magnetic grains will come out of the rightmost chute. Place two loaf pans to catch the magnetic and non-magnetic grains separately.
6. Turn on the vibrating hopper. Adjust the flap between the two chutes on the bottom right so that the nonmagnetic grains go into the rightmost chute only. Use the plastic shield to prevent grains from flying out of the separator.
7. Pour the magnetic grains into the sample bag. Save the nonmagnetic grains in a bag labeled with the sample name and the words "Leached in aqua regia; nonmagnetic."

Heavy liquids separation

You need...

1. 250 ml separatory funnels
 2. Ring stands
 3. LST density 2.7
 4. Recovery dish
 5. Recovery flask
 6. Coffee filters
 7. Pure water
 8. Hot plate
 9. 1L beakers
 10. Squeeze bottle
 11. Millipore filtering system
-
1. Put a separation funnel in the wire ring over a flask with a ceramic filter funnel. Arrange a coffee filter in the filter funnel to catch the drippings from the separation funnel. Make sure the stopcock of the separation funnel is closed. Pour in enough heavy liquid of the appropriate density to fill the funnel to the "Mexico" mark, or about two-thirds of the way from the stopcock to the widest part of the funnel.
 2. Pour ~60 grams of sample material into separatory funnel containing 2.7 density heavy liquid.
 3. Let the funnel sit until any grains which are falling through the sediment-free heavy liquid near the bottom of the funnel have settled. This may take fifteen minutes to several hours. The smaller the grain size, the longer this step will take.
 4. Turn the stopcock 90 degrees, so the handle is inline with the discharge spout of the funnel. The heavy minerals will pass through the stopcock and collect on the coffee filter. When draining the heavy minerals, close the stopcock quickly as soon as the heavy minerals are discharged so as not to lose too much heavy liquid. The more liquid there is in the separatory funnel, the easier the minerals separate. Do this several times or until no more heavy minerals settle.
 5. Add 15 drops of water to the heavy liquid and cap tightly. To do this, use a squirt bottle and squirt water on the cap of the separatory funnel. Let the drops form on the cap, and as they fall off, count and record on the side of the glass funnel. Shake

the funnel vigorously a few times over a catch basin. Keep a tally on the funnel of how many drops you have added and how many times you shake it.

6. NOTE: Be sure to loosen the cap in the separatory funnel. Failure to loosen the cap after shaking will result in the cap being “glued” in by the dried heavy liquid. In this case, add a few drops of water around the rim of the cap where it touches the separatory funnel. Do not push on the cap or pry on it any way, the funnel may break! Let the water do the job. Only try to twist the cap.
7. Repeat steps 3 and 4 with the 15 drops of water. At this point most of the heavy minerals have fallen out. Add more drops of water 2 or 3 at a time and shake. Drain as necessary. At this point quartz with inclusions will be separated. When the quartz sinks the lighter minerals will float on top of the solution
8. Rinse the coffee filter with pure water and save it, with the heavy minerals. Replace it with another filter.
9. Drain the quartz separate into the clean coffee filter, being careful not to drain the lighter minerals. This step may take several tries. Give the quartz enough time to re-settle before draining more. Rinse the quartz with plenty of water to remove all the heavy liquid.

Place quartz in a clean PP bottle in preparation for ultra sonic leach. Be sure to label the cap and bottle.

HF leaching

- (1) Using 500ml bottles designated for HF leaching transfer up to 60 g of sample per bottle. Weight the bottle before the transfer; tare the bottle’s weight and weight again after samples’ transfer -to monitor samples’ mass loss.
- (2) Under the fume hood make up a less concentrated solution of HF + HNO₃. All leaches except the last one are prepared with RO water, the last one with MQ water.
- (3) Fill the sample bottle with the solution to within 2 cm of the top.
- (4) Gently squeeze the bottle before capping. This gives the contents room to expand when the bottle heats up. Also, loss of vacuum will alert you to the possibility that the bottle has leaked. Check that the bottle is tightly sealed and holding its slight vacuum.

- (5) In the fume hood, gently invert it 3-4 times to mix the contents.
- (6) Mark the bottle to indicate how many times it has been processed.
- (7) Place the bottle in the ultrasonic bath for 72 hours applying heat and ultrasound 3 times per day for a period of 99' each time. Mix the contents of the bottle several times during sonication.

After the first 3-days, change the solution as follows:

- (8) Cool the bottles (if they are warm).
- (9) In the fume hood, uncap the bottle and discard the solution into the HF waste container. Be careful not to pour out the sample.
- (10) Rinse the remaining grains thoroughly with 2 changes of RO water; decanting off the rinse water into the waste acid container while any clay or fine, milky fluoride precipitate is still suspended, but after "fine sand"-sized grains have settled. Don't worry about losing some of the very fine grains, unless the sample is unusually small.
- (11) Add the HF + HNO₃ solution to the bottle just like in the first treatment and repeat the 3-day processing for a second time.

After the second 3-days, check the appearance of the sample as follows:

Pure quartz samples have a uniform appearance and do not cake on the floor of the bottle. Impure samples usually appear speckled and may contain a cloudy fluoride precipitate.

If the sample does not appear pure, repeat the HF leaching for another 3-day period with HF + HNO₃ in RO water.

Sample recovery

After the last leach (in MQ water) has been carried out in a pure quartz sample cool the bottle.

- (1) In the fume hood, uncap the bottle and discard the solution into the HF waste container.

- (2) Rinse with at least 3 changes of MilliQ as above. Try to rinse away any trace of milky fluoride. The rinse water must be clear (and absolutely free of residual HF).
- (3) Dry in the oven.
- (4) Cool the samples and transfer them - with the help of funnels - to a labelled ziplock bag. Weight the bag before and after sample's transfer and record the weight of sample and number of leaches carried out.

Aluminium Determination from a Mineral Aliquot (MA)

To assess the purity of the quartz we determine the aluminium content of the cleaned separate. It is essential to obtain the lowest possible Al concentration. The higher the Al concentration, the lower the $^{26}\text{Al}/^{27}\text{Al}$ ratio for measurement, the fewer ^{26}Al nuclides counted and the worse the counting statistics. The Al concentration should preferably be in the range 10 - 100 ppm. A higher concentration generally (though not always) indicates the presence of an impurity such as feldspar, muscovite or an insoluble fluoride residue from the quartz clean-up (e.g. Na_3AlF_6).

Procedure

Static charge should always be removed before weighing.

1. Label and weigh a Teflon vial and lid on the 4-figure balance. Record the tare weight on the sample data sheet. Using a stainless steel spatula, transfer few g of the sample into the vial. Replace the lid and record the weight. The amount of sample is not too critical, but its weight must be recorded accurately. Be careful when replacing the lid, as static charge may cause small grains to jump up onto the lid or out of the vial. Clean the spatula with a kimwipe (+ethanol) before using it for the next sample.
2. When all the samples have been weighed into vials, open the vials in a fume hood and add few ml of conc. HF and few drops of diluted H_2SO_4 to each.
3. In the fume hood, place the open vials on the edge of the hotplate at low setting for 8 hours (overnight). Keep track of which lid belongs to which vial. The quartz will dissolve as the solution slowly evaporates. After total dissolution has been achieved,

- increase the heat to fume off HF/ H₂SO₄. Do not overheat the small flat-bottomed vials, as solutions will boil and damage the hotplate surface. Tilting the hotplate a few degrees by propping up the front will ensure that the solid fluorides crystallise as a small clump in one "corner" of the vial.
4. Once all the HF/ H₂SO₄ has evaporated, the residue should be a dry, brown speck, containing a few hundred µg total of Al, Fe and Ti fluorides. If any quartz remains (usually only if the original sample was very coarse-grained), **cool the vials** and repeat the procedure with further HF and H₂SO₄ solutions.
 5. Cool the vials. Dissolve the dry residue in diluted HNO₃ and HCl if sample will be analysed by AAS. If sample will be analysed by ICP-OES dissolve in diluted HNO₃. Use the Eppendorf 1-5 ml adjustable pipettor and the attachment dedicated to diluted HNO₃. Cap the vials with their original caps and leave to stand a few hours. The fluorides should dissolve totally to give a clear (or perhaps faintly green) solution.
 6. Invert the capped vials a few times to homogenise the solutions, then weigh and record the vial + solution weights. Decant the solutions into labelled centrifuge tubes and send them off for analysis.
 7. The expected concentration of Al in pure quartz is <100 ppm.

Carrier Addition and Sample Digestion

Our aim is to extract Beryllium from the quartz sample and to measure the ¹⁰Be/⁹Be ratio using AMS. However, Be is a very rare element in quartz. Therefore it is necessary to spike the sample with a known quantity of ⁹Be. The aim of spiking is that we can trace the movement of the Be through the processing and that the very low concentrations of naturally occurring Be will follow the same path as the added Be. Also need to end up with enough Be to generate an ion beam in the AMS. Obviously we do not want to introduce ¹⁰Be to the sample since this is the nuclide we are trying to measure. For this reason we have Be carrier solutions with known concentrations of ⁹Be. It is critical that a low-level carrier is used for samples with potentially low levels of ⁹Be.

Procedure

Sample weighing

1. Label, remove static (by wrapping bottle in foil paper or using the anti static cathode) and weigh a clean FEP Teflon bottle (bottle + lid). Make sure to use a bottle large enough to contain the HF addition. Record the tare weight on the sample data sheet. Transfer the sample to the bottle. This is best done with the help of a funnel (one per sample). It helps to reduce static if bottle is wrapped in foil paper when transferring the sample. Some grains will charge and cling to the bottle walls. No problem. Cap the bottle.
2. Remove static and re-weigh. Subtract the bottle tare to determine the sample weight.

Be carrier addition

1. Take the current Be carrier bottle, invert it a few times to homogenize the solution. Be sure drops of condensation around the lid are mixed in. Remove static (by wrapping bottle in foil paper or using the anti static cathode) and weigh it. Record the initial weight in the blank sample log sheet (and if possible, confirm that it equals the final weight from its last use).
2. Load the 1000 μ l Eppendorf pipette with a clean tip and uptake the Be carrier. Be sure the tip does not touch anything while handling the pipette. If the tip does touch something, discard it and take another.
3. Start the Be carrier addition with the blank sample of the batch. Open the sample bottle.
4. Tare the balance to zero. Remove the carrier, open it and pipette carrier into the sample bottle. Eject the carrier smoothly, being sure not to leave a drop in the tip. If this happens, uptake MQ water and dispense over the sample to ensure all carrier is added. Don't allow the tip to touch the sample bottle. Recap the carrier bottle as quickly as possible, remove static and re-weigh it. The balance will read the weight removed. Record the weight and the Be concentration of the carrier. Calculate the Be added.
5. Repeat the process from point 3 until Be carrier is added to all samples.

6. At the end of each session tare the balance to zero and record the final weight of the carrier bottle in the blank log sheet for cross-checking. Check that the cap is screwed on firmly and seal it with parafilm.

Sample digestion

1. In fume hood, wearing gloves and goggles, add HF (c) to each sample bottle. Also add HF (c) to the blank bottle.
2. Cap the bottle, tighten the lid down, then back it off ~1/4 turn. The bottle must not be gas-tight (check by squeezing it gently).
3. Once the reaction has subsided (usually 1-2 hours), the bottles can be placed around the edges of the hotplate set on a low temperature. They only need very gentle warming to ensure overnight dissolution. From this point on, they can also be swirled occasionally to mix HF down into the dense H_2SiF_6 forming around the quartz grains.
4. Once all the quartz has been dissolved turn off the hotplate and cool the bottles to room temperature. The time required for dissolution varies depending on sample. 30 g of pure quartz may take up to 3 days; 60 g may take 4 days. If solution seems to be saturated (dissolution goes very slowly) add more HF (c) to sample.
5. Tighten the caps, being wary of any droplets of condensation inside the screw threads that might be squeezed out onto the surface of the bottle.

Splitting for Aluminium Determination

Accelerator mass spectrometry does not provide absolute values of nuclide concentrations in the sample. Rather AMS provides a ratio between the cosmogenic nuclide and the stable nuclide occurring in the sample but not produced by cosmic ray interaction. For example, AMS gives us the $^{26}\text{Al}/^{27}\text{Al}$ ratio, where ^{26}Al is the cosmogenic nuclide and ^{27}Al the stable, native aluminium in the sample. Therefore, to determine the actual concentration of cosmogenic ^{26}Al in the sample we need to know the ^{27}Al concentration in the sample. Because cosmogenic ^{26}Al is so rare we can estimate the stable ^{27}Al concentration by measuring the total Al in the sample solution (parent solution). Total Al in an aliquot of the parent solution is measured by ICP.

Procedure

1. Homogenize the solutions by swirling and inverting the bottles to mix in HF condensed around the top of the bottle. Total sample Al concentrations will be determined from splits (aliquots) of these solutions, so they must be thoroughly mixed.
2. Weigh the bottles. For all but the smallest samples it will be necessary to use the top-loading balance. Subtract the bottle tare weight and calculate the total solution weight.
3. For each sample calculate the expected Al concentration (ppm) of the parent solution and use this to calculate the amount of parent solution required to obtain a 10ml solution with 3ppm Al.
4. For each sample, take a Teflon vial. Label, remove static, weigh the vial and record the weight on the sample data sheet.
5. In the fume hood; open the vials; open the sample bottle. Using a pipette transfer the calculated amount of parent solution into each vial. Remember you are transferring HF.
6. Without rushing, but as quickly as possible, close the vials. Weigh them and record the weights. Calculate the weight of each split.
7. After splitting each sample, the aliquots can be dried down to remove HF in preparation for ICP-OES analysis. Transfer aliquots back to the fume hood, taking care not to splash liquid into the lids of the vials. Add few drops of H_2SO_4 to each and dry on the

hotplate. A small dot of liquid or a precipitate of Fe-Al-Be-Ti alkali salts should appear in the base of each vial after evaporation.

7. Cool the vials. Dissolve the dry residue in diluted HNO₃. Use the Eppendorf 1-50 ml adjustable pipettor and the attachment dedicated to diluted HNO₃. Cap the vials with their original caps and leave to stand a few hours. The fluorides should dissolve totally to give a clear (or perhaps faintly green) solution.
8. Weigh and record the vial + solution weights.
9. Invert the capped vials a few times to homogenise the solutions, decant them into labelled centrifuge tubes and store in designated drawer. Prior to ICP-OES analysis an aliquot of this solution will be taken out and Y will be added as IS. This solution will be analysed by ICP-OES to determine [Al].

Parent Solution Dry Down and Chloride Conversion

Successive evaporation and re-dissolution eliminates fluoride (as HF) almost entirely. Fe, Ti, Al, Be, alkalis etc. should be left as chloride salts ready for anion exchange clean-up. The final solution will generally be coloured a deep yellow-green by FeCl₃. By the end of this procedure, however, some samples may have thrown a fine, powdery, white precipitate that will not re-dissolve. This is TiO₂. No Al or Be is co-precipitated with the Ti, which should be removed by centrifuging before moving on to the anion exchange columns.

Procedure

1. Carefully transfer the parent solution to a clean and labelled Teflon beaker.
2. Rinse the bottle with a few ml of MilliQ and add the rinsate to the beaker. Take care not to let any sample solution splash back onto the MQ wash bottle.
3. Using separate disposable transfer pipettes add few ml of diluted HCl and few ml of diluted HNO₃ to each beaker.
4. Switch the water pump on to allow water to recirculate through the system. Place the beakers on the hotplate and dry overnight. For <100 ml, the beakers will dry down in

12 - 15 hours. Larger solution volumes may take a bit longer. When drying large volumes droplets will condense on the rim of beakers, do not worry they will dry off. When dry, there will be a thin covering of white to gray-green fluoride salts on the floor of the beaker.

Fuming sulphuric

1. Transfer the sample (centrifuge if necessary) to the Pt crucible using a disposable transfer pipette
2. Rinse sample container with HCl (centrifuge if necessary) and transfer to Pt crucible using the same pipette. Heat the Pt crucible to a temperature sufficient for sulphuric acid to evaporate (whitish fumes). The boiling point of sulphuric acid is 338 °C.
3. Once the sulphuric acid is gone, cool the sample.
4. Dissolve the sample in HCl; leave standing for one hour and transfer to centrifuge tube.
5. Rinse the Pt crucible with HCl and transfer to centrifuge tube. Repeat this step if necessary.
6. Clean the Pt crucible.

To convert the residue to chloride form...

5. Take the beakers off the hotplate and cool them. Using a disposable pipette, add diluted HCl. The cake should mostly re-dissolve instantaneously, and in most cases will go back into solution entirely after warming on the hotplate.
6. Return the beakers to the hotplate and dry again.
7. Cool and repeat the HCl addition.
8. Dry again, cool and re-dissolve a third time, then take down as close to dryness as possible. Try to avoid complete drying at the end of this step, to make it easy to get the sample back into solution for anion exchange. Don't worry if drying is unavoidable, however.
9. Add diluted HCl to each sample container. Swirl the liquid to pick up and dissolve the entire sample from the floor of the container. Leave standing overnight. Do not warm to promote dissolution - evaporation will change the acid strength.

10. After standing overnight (or at least a few hours) transfer each sample to a labelled centrifuge tube -using a clean disposable pipette for each sample. Add diluted HCl to each sample container and rinse. Swirl to pick up any remaining droplets of the original sample solution. Pick the rinse solution up and add to their appropriate centrifuge tube. If necessary – presence of TiO_2 (smoky white insoluble material) or other insoluble particulates - solutions will have to be centrifuged before running them through the columns. Spin the tubes at maximum speed for 10 minutes and keep centrifuge tube with residue material until results are obtained. The pipettes used for each sample should be reserved (in the original sample containers) for loading onto columns. If sample is fully dissolved, centrifugation is not necessary. The samples can be stored indefinitely in centrifuge tubes.

Ion Exchange

Anion exchange columns are used to separate remaining impurities such as Fe and Ti from the sample. In strong HCl, Fe(III) forms a range of anionic Cl^- complexes (FeCl_4^- , FeCl_5^{2-} and FeCl_6^{3-}), which bind tightly to the anion exchange resin. These can be seen as a brown stain in the top few mm of the resin. Al and Be do not form strong Cl^- complexes and wash through the column as HCl is added. Titanium is a bit more problematic; Ti (IV) forms TiCl_6^{2-} , which binds, but some Ti always seems to remain cationic, form neutral species or revert to Ti(III), which doesn't form strong Cl^- complexes. Ti is seldom 100% stripped from the Al + Be fraction. Al and Be are split and Ti is further removed using cation exchange columns.

Procedure for Anion Exchange Chromatography

- (1) Load a column stand with ion exchange columns. Place a plastic container underneath.
- (2) Squirt some alcohol (ethanol, isopropanol) into each to wet the frit (to eliminate trapped air).
- (3) Using AG-1 X8 200-400# anion resin from stock soaking in diluted HCl, pipette a very loose slurry into each column (use a disposable pipette). The aim is to block

the column and back up a head of acid so that the resin bed can be built up from suspension. This prevents trapping of air bubbles.

- (4) Now continue slurring resin into the columns to build the resin beds. If too much resin is added, a long pasteur pipette can be used to adjust the volume. Once the resin has compacted to the correct height, allow the supernatant to drain through.
- (5) Wash the resin with few ml of diluted HCl. Allow the wash solution to drain through the resin bed.
- (6) Condition the resin with few ml of diluted HCl. Add the first ml by running drops down the column walls - try to keep the top surface of the resin bed flat to ensure uniform flow through the column when the sample is added. The resin will darken and shrink as it adjusts to the higher acid strength (it may not be noticeable).
- (7) Take a batch of Teflon vials and label them with sample ID.
- (8) Once the HCl conditioning solutions have drained, carefully remove the plastic container from beneath the columns and replace them with Teflon vials. The HCl in the container should be disposed in the acid waste container.
- (9) Using separate disposable pipette for each sample (those centrifuged will already have one), load the sample solutions onto the columns. Drip the solution down the column wall, reaching as far as possible into the column with the pipette. Do NOT pour the sample into the column. Try to transfer the sample quantitatively. Try not to disrupt the top surface of the resin. Return each pipette to its sample container.
- (10) Allow the loading solution to drain fully into the resin.
- (11) Elute Al + Be from the columns by adding few ml of diluted HCl. The first ml should be added carefully from a disposable pipette so as not to disrupt the top of the resin bed. Allow to drain through before adding the remaining solution.
- (12) Once Al + Be have been eluted, remove the vials and replace them with labelled disposable centrifuge tubes.
- (13) If bulk Al removal is required continue with steps 16 and 17 and proceed with the Al/Be fraction as indicated in the bulk Al removal section.

- (14) If bulk Al removal is not required, add few drops of diluted H_2O_2 to each Teflon vial. Change of colour to yellow-orange indicates the presence of Ti in the fraction. Note changes to monitor fractions during following sample prep steps.
- (15) If BULK Al removal is not required, add few ml of diluted H_2SO_4 with a trace of H_2O_2 to each Teflon vial and dry on the hotplate overnight. Dry to avoid boiling the sample. After dry down, proceed with the Al/Be fraction as indicated in the section.
- (16) Wash Fe + Ti off the resin with MQ water. Rinse out and discard the sample and dispensing pipettes. Rinse out and wash the sample transfer containers.
- (17) Rinse out resin and clean the columns.

To convert the residue to sulphate form

Once the samples have dried down they may turn an alarming dark-brown to black colour. This is due to chary reaction products formed from organics which bled from the anion resin. Don't worry, it will disappear gradually over the next few steps.

- (18) Cool the vials. Add few drops of diluted H_2O_2 . Add few ml of MilliQ water containing a trace of H_2SO_4 . The cakes will begin to dissolve, taking on an amber/gold color if Ti is present. Reheat the vials. The black chary material will disperse and disappear (do not worry if it does not happen straight away; the heat applied will help the dispersion).
- (19) Dry the samples down again. The H_2O_2 oxidises the organics. It also indicates the presence of Ti in the sample by turning the solution yellow-orange. The darker the colour, the more Ti is present.
- (20) Cool the vials and repeat the H_2O_2 /MilliQ water addition, and dry the samples a second time. At the end of this procedure, the samples should end up either as compact white cakes; small, syrupy droplets of involatile H_2SO_4 or orange/yellow syrupy cakes. If they remain chary or discolored, repeat the peroxide/water addition and dry them down as many times as necessary.
- (21) Take the sample up (as a cake or 1-2 drops) in few ml of diluted H_2O containing a trace of H_2SO_4 . Add few drops of diluted H_2O_2 . Leave overnight.
- (22) If samples do not dissolve completely after leaving overnight warm them a little.

Don't risk evaporating too much water – keeping the acid strength low for column loading gives a sharper elution and cleaner Ti-Be cut.

(23) Transfer sample to a labelled centrifuge tube. Add a further ml of diluted H_2SO_4 with a trace of H_2O_2 to the sample containers and rinse. Swirl to pick up any remaining droplets of the original sample solution. Pick the rinse solution up and add to their appropriate centrifuge tubes. If necessary (dissolution is not complete) centrifuge sample and keep centrifuge tube with residue material until results are obtained. If sample is fully dissolved centrifugation is not necessary. The samples can be stored indefinitely in centrifuge tubes.

(24) Samples are now ready for cation exchange to remove Ti and to split Be and Al into separate fractions.

Procedure for Cation Exchange Chromatography

(1) Load a column stand with ion exchange columns. Place a plastic container underneath.

(2) Squirt some alcohol (ethanol, isopropanol, whatever is on hand) into each to wet the frit.

(3) Using AG 50W - X8 200-400# cation resin from stock soaking in diluted HCl, pipette a very loose slurry into each column (use a disposable pipette). The aim is to block the column and back up a head of acid so that the resin bed can be built up from suspension. This prevents trapping of air bubbles.

(4) Now continue slurring resin into the columns to build the resin beds. If too much resin is added, a long pasteur pipette can be used to adjust the volume. If too thick a slurry is added and bubbles get trapped in the bed, the column must be emptied and re-packed. Bubbles will channel flow through the column and ruin the separation. Once the resin has compacted to the correct height, allow the supernatant to drain through.

(5) Strip the columns twice with few ml of diluted HCl of different concentration.

(6) Condition the columns with few ml of diluted H_2SO_4 (with a trace of H_2O_2).

- (7) Once the H_2SO_4 conditioning solutions have drained, carefully remove the plastic beaker from beneath the columns and replace them with labelled disposable centrifuge tubes to collect the Ti fraction.
- (8) Using separate disposable pipettes for each, load the sample solutions onto the columns. Drip the solution down the column wall, reaching as far as possible into the column with the pipette. Do not pour the sample into the column. Try to transfer the sample quantitatively. Try not to disrupt the top surface of the resin. Return each pipette to its sample container.
- (9) Allow the loading solution to drain fully into the resin. If present, Ti will have formed an orange band at the top of the column.
- (10) Add few ml of diluted H_2SO_4 with a trace of H_2O_2 to the columns but pipetting the first ml to avoid disturbing the resin. Allow to drain through before adding the remaining solution and watch the band of Ti move down the column.
- (11) If not all Ti has been eluted, the elutant are yellow and/or an orange band will be present in the resin. In all cases (all Ti has been eluted or not) add few further mls of diluted H_2SO_4 with a trace of H_2O_2 . If not all Ti is eluted make a note of the sample and Ti will be separated from fraction by precipitating it at pH 4.
- (12) Replace the centrifuge tubes with labelled Teflon vials to collect the Be fraction.
- (13) Elute Be from the columns by adding few ml of diluted HCl. The first few ml should be added carefully from a disposable pipette so as not to disrupt the top of the resin bed.
- (14) Once the columns have drained replace the vials with labelled centrifuge tubes (use the tubes that will fit in the centrifuge) to collect Al.
- (15) Add few drops of diluted HNO_3 (to dry off Boron, more drops may cause static problems) to the Teflon vials. Dry them down overnight.
- (16) Elute Al from the columns by adding few ml of diluted HCl. The first few ml should be added carefully from a disposable pipette so as not to disrupt the top of the resin bed. Once the columns have drained cap the tubes and store them until hydroxide precipitation.
- (17) Clean the columns.

Precipitation as Hydroxides

Be fraction

1. Once the Be solutions have dried down (near dryness as possible), cool the vials. There should only be a small white dot or small drop in the bottom of the vials.
2. Add diluted HNO_3 to the vials. The Be should dissolve readily. If it doesn't, you can heat the vials to assist dissolution.
3. Transfer the solutions to labelled centrifuge tubes.
4. Add another HNO_3 to the vials, swirl it around and transfer the rinse solution to the appropriate tube.
5. If Ti is present in sample use less concentrated NH_4OH solutions to bring pH up to 4. Ti will precipitate as hydroxide whilst Be will remain in solution. Centrifuge the solutions. Decant and collect supernatant (Be fraction) in centrifuge tubes. Precipitate is Ti hydroxide.
6. Using the NH_4OH solutions, bring Be solutions in the centrifuge tubes to pH 8 (8-8.5) to precipitate Be as a hydroxide. Addition of ammonium hydroxide may have to be drop by drop with pH checks in-between. Leave the tubes standing for a few hours.
7. Centrifuge the solutions.
8. Decant and discard the supernatant into the acid waste tank.
9. Rinse the samples with MilliQ water and few drops of NH_4OH added to the centrifuge tubes.
10. Disperse the samples by vortexing (until precipitate is re-dissolved).
11. Centrifuge again.
12. Decant and discard the supernatant into the acid waste tank.
13. Repeat the MilliQ + NH_4OH rinse three times (in total).

Drying and Oxidation

1. Carefully open the centrifuge tubes containing the Be hydroxides and lie them on a kimwipe in the drying oven. It helps to put a folded kimwipe under the **open ends** to keep them slightly elevated. Keep track of which lid belongs to which tube. Cover the tubes with a kimwipe and dry overnight.
2. When dry, cap the centrifuge tubes with their respective lids and let them cool.
3. Weigh a cleaned quartz crucible and lid to 4 decimal places. Place the crucible into the perspex holder. On a piece of paper write down the relative positions of the quartz crucibles and the Sample ID of the sample which will be transferred into them.
4. For Be hydroxides: In the Be box, wearing a new pair of gloves, and a face mask, pour the small pellet of dried Be hydroxide over a clean weighing paper and transfer it to the quartz crucible. Use the help of a spatula if the pellet does not come off the walls of the centrifuge tube easily. If you experience problems with static electricity; use the anti-static device or wrap tubes with foil paper. Pour the pellet over a clean weighing paper and transfer it to the quartz crucible. Cover the quartz crucible with its respective quartz lid. Place the crucibles in their position in the Perspex holder. Avoid sample cross contamination.

Mixing and pressing unknown BeO samples

1. Place a clean cathode inside the anvil assembly.
2. Weigh the required amount of Nb powder needed for the sample. Half of a weighing paper can be used for this purpose and can be re-used to weigh Nb for the following samples until it becomes difficult to remove the Nb from it.
3. Record the weight in a piece of paper.
4. Remove the sample (crucible and lid) from stand using the tweezers. Pass it through the antistatic cathode and place on top of the weighing paper.
5. Take the weighing paper containing the Nb to the box and place on a secure place.
6. Take a quartz pestle and make a “skirt” using the square pieces of foil paper. Leave carefully beside the acrylic stand and remember to avoid cross-contamination.
7. Remove the quartz lid and set aside.
8. Add the Nb powder to the BeO sample.

9. Grind and try to homogenise the mixture, in the middle of this process you can put the lid on and pass through the anti-static device again.
10. Once the mixture looks homogenised transfer directly to the cathode (placed inside the anvil assembly) with the help of the tweezers.
11. Tap the anvil assembly gently to allow the mixture to funnel through to the cathode.
12. Transfer the anvil assembly to the press. It is vital to support the assembly – holding all parts together- when transferring it for pressing; otherwise the sample may be lost.
13. Bring the needle down and apply ~125-150psi Pressure once the needle is inside the cathode, turn anvil assembly 180 degrees and repeat. Do not apply excessive pressure as the cathode can be damaged as a consequence, making its removal from the assembly very difficult. Release needle holding the anvil assembly down.
14. Bring the anvil assembly down to acrylic stand, open the assembly and remove the cathode with the help of the spanner.
15. Place cathode in the appropriate labelled eppendorf vial.
16. If there are no traces of BeO in the quartz lid, it can be clean and re-use again but only keep the lid if you are absolutely sure that there are no traces of BeO; if in doubt, throw it away in the BeO waste bag.
17. The quartz crucible should be disposed of in the BeO waste bag. Wipe all devices used with alcohol a couple of times, the first wipe should go into the BeO waste bag.
18. Weigh the paper used for weighing the Nb and calculate how much Nb was added to the sample and record this weight in the table.
19. Repeat the process for the following sample. Once all samples are pressed place them in a labelled bag and store them inside the cabinet until they are submitted to the AMS for analysis.

Appendix B

Sample details

Monadliath Mountains

1. Field and laboratory information

No	Lab ID	Latitude (degrees)	Longitude (degrees E)	Elevation (m)	Sample thickness (cm)	Shielding factor	Quartz mass (g)	Spike mass (μg)
1	GB07-01	57.0884	-4.2314	600	6	0.9945	24.779	243.05
2	GB07-02	57.0884	-4.2314	579	2	0.9945	27.001	242.9
3	GB07-03	57.0805	-4.2332	528	3	0.9980	31.093	242.7
4	GB07-04	57.0805	-4.2332	528	3	0.9949	26.609	242.48
5	GB07-05	57.0567	-4.0567	362	3	0.9990	26.174	233.5
6	GB07-06	57.0557	-4.2220	362	3	0.9990	25.897	242.91
7	GB07-07	57.0794	-4.2558	655	3	0.9938	26.125	233.5
8	GB07-08	57.0794	-4.2558	655	3	0.9938	26.365	236.7
9	GB08-12	57.0854	-4.2306	520	3	0.9963	23.768	235.7
10	GB08-13	57.0853	-4.2298	520	3	0.9963	23.986	235.1
11	GB08-22	57.0643	-4.2394	470	4	0.9974	24.218	245.8
12	GB09-23	57.1194	-4.1671	755	4	0.9852	21.432	233.9
13	GB09-24	57.1196	-4.1668	755	3	0.9872	20.733	242.2
14	GB09-25	57.1158	-4.1548	646	2	0.9898	21.783	233.7
15	GB09-26	57.1154	-4.1549	641	2	0.9959	25.327	238.2
16	GB09-27	57.1147	-4.1555	634	3	0.9959	26.465	238.9

2. AMS measurement ratios and ^{10}Be concentration

No	Cathode no	$^{10}\text{Be}/^9\text{Be}$ ($\times 10^{-15}$)	error ($\times 10^{-15}$)	Be^{10}/Be procedural blank ($\times 10^{-15}$)	error ($\times 10^{-15}$)	N^{10} ($\times 10^4$ atom g^{-1})	N^{10} error	STD
1	b2833	137.75	4.03	7.5389	2.384	85346	3215	NIST_30600
2	b2836	154.49	4.49	7.5389	2.384	88337	3191	NIST_30600
3	b2625	195.00	5.21	4.93	0.88	99139	3478	NIST_30600
4	b2837	158.87	4.87	7.5389	2.384	92151	3895	NIST_30600
5	b3091	171.77	4.26	8.564	8.439	97292	6023	NIST_30600
6	b2626	156.00	4.50	4.93	0.88	94688	3553	NIST_30600
7	b3092	171.59	4.50	8.564	8.439	97367	6096	NIST_30600
8	b3152	181.01	3.98	6.4582	0.9136	104717	3322	NIST_30600
9	b3153	150.18	3.30	6.4582	0.9136	95238	3093	NIST_30600
10	b3154	145.07	3.34	6.4582	0.9136	90786	3035	NIST_30600
11	b3677	139.70	3.48	3.369	0.6689	92461	3141	NIST_30600
12	b3680	179.40	6.20	3.369	0.6689	128375	5292	NIST_30600
13	b3681	150.20	3.77	3.369	0.6689	114618	3880	NIST_30600
14	b3682	216.3	5.15	3.369	0.6689	152652	4877	NIST_30600
15	b3683	216.30	5.15	3.369	0.6689	133819	4275	NIST_30600
16	b3684	183.10	4.50	3.369	0.6689	108415	3566	NIST_30600

Rodna Mountains

1. Field and laboratory information

No	Lab ID	Latitude (degrees)	Longitude (degrees E)	Elevation (m)	Sample thickness (cm)	Shielding factor	Quartz mass (g)	Spike mass (mg)
1	RD01	47.6209	24.6525	1108	3	0.9895	25.28	302.37
2	RD02	47.6055	24.6408	1669	5	0.9454	31.055	248.46
3	RD03	47.6055	24.6408	1669	2	0.9454	27.285	242.82
4	RD04	47.6055	24.6408	1669	3	0.9454	28.956	244.26
5	RD05	47.6031	24.6396	1753	5	0.9058	24.367	243.99
6	RD06	47.6032	24.6390	1767	2	0.9330	25.858	243.54
7	RD07	47.6032	24.6390	1767	2	0.9330	24.244	243.87
8	RD08	47.6028	24.6484	1801	4	0.9599	24.659	246.03
9	RD09	47.6028	24.6484	1801	4	0.9599	27.025	233.6
10	RD10	47.6028	24.6484	1801	2	0.9599	25.115	234.08
11	RD11	47.6016	24.6503	1794	3	0.9679	27.347	235.5
12	RD12	47.6017	24.6502	1898	2	0.9178	26.727	239.1
13	RD13	47.5767	24.6485	1819	2	0.9937	25.227	235.9
14	RD14	47.5756	24.6379	1971	4	0.9932	25.104	236.1
15	RD15	47.5729	24.6528	1943	4	0.9988	23.136	235.9
16	RD16	47.5843	24.6492	1688	2	0.9683	24.286	237.7
17	RD17	47.5832	24.6557	1636	3	0.9872	26.489	236.5
18	RD18	47.5849	24.6527	1706	3	0.9834	24.85	233.6
19	RD19	47.5851	24.6523	1718	1	0.9834	23.016	231.3
20	RD20	47.5855	24.6511	1741	2	0.9834	23.305	236.3
21	RD21	47.5851	24.6450	1864	5	0.9685	21.901	234.1
22	RD22	47.5855	24.6455	1847	3	0.9685	24.472	234.8
23	RD23	47.5861	24.6457	1842	4	0.9685	24.974	234
24	RD24	47.5861	24.6446	1847	2	0.9580	26.566	236.3
25	RD25	47.5861	24.6446	1847	4	0.9580	24.703	237.9
26	RD26	47.5810	24.6401	1904	3	0.9984	23.58	234.6
27	RD27	47.6385	24.6628	868	4	0.9984	24.556	236.7
28	RD28	47.6286	24.6548	970	5	0.9952	22.038	234.8
29	RD29	47.6214	24.6481	1116	3	0.9931	26.255	233.4
30	RD30	47.6134	24.6492	1379	4	0.9841	25.118	234.1
31	RD31	47.6143	24.6492	1344	2	0.9864	25.662	234.8
32	RD32	47.6172	24.6502	1237	2	0.9882	26.206	234.8
33	RD33	47.6196	24.6512	1170	4	0.9897	24.389	235.6
34	RD34	47.6155	24.6495	1245	1.5	0.9881	23.735	234.5
35	RD35	47.5802	24.6397	1865	3	0.9818	25.799	235.2
36	RD36	47.5798	24.6385	1918	2.5	0.9818	25.918	235.5
37	RD37	47.5791	24.6357	1957	2.5	0.9655	26.318	233.6
38	RD38	47.5787	24.6353	1973	2.5	0.9737	26.801	238.6
39	RD39	47.5776	24.6360	1979	2	0.9857	26.395	236.5
40	RD40	47.5969	24.6442	1908	3	0.7314	25.194	236.4
41	RD41	47.5969	24.6442	1908	3	0.7116	26.514	239.4
42	RD49	47.6282	24.6517	999	2.5	0.9951	46.698	223.5
43	RD50	47.6276	24.6566	969	2.5	0.9945	32.277	223.9

Rodna Mountains

2. AMS measurement ratios and ^{10}Be concentration

No	Cathode no	$^{10}\text{Be}/^9\text{Be}$ ($\times 10^{-15}$)	error ($\times 10^{-15}$)	Be^{10}/Be procedural blank ($\times 10^{-15}$)	error ($\times 10^{-15}$)	N10 ($\times 10^4$ atom g ⁻¹)	N10 error	STD
1	b3094	203.76	4.23	6.3497	1.64	157781	4961	NIST_30600
2	b3097	432.20	8.74	6.3497	1.64	227669	6654	NIST_30600
3	b3098	412.30	7.72	6.3497	1.64	241410	6819	NIST_30600
4	b3099	390.51	7.82	6.3497	1.64	216545	6329	NIST_30600
5	b3100	169.15	4.53	6.3497	1.64	108930	4014	NIST_30600
6	b3101	363.96	7.18	6.3497	1.64	225065	6553	NIST_30600
7	b3103	346.01	6.14	6.3497	1.64	228308	6357	NIST_30600
8	b3104	368.50	8.69	6.3497	1.64	241448	7710	NIST_30600
9	b3105	481.14	9.60	6.3497	1.64	274240	7930	NIST_30600
10	b3106	454.77	9.20	6.3497	1.64	279279	8161	NIST_30600
11	b3109	501.95	9.34	6.3497	1.64	285190	7969	NIST_30600
12	b3110	465.63	7.43	6.3497	1.64	274555	7217	NIST_30600
13	b3137	511.85	10.90	6.4582	0.9136	315800	9384	NIST_30600
14	b3111	563.36	11.14	6.3497	1.64	350057	10031	NIST_30600
15	b3139	3243.60	64.31	6.4582	0.9136	2205584	62237	NIST_30600
16	b3112	411.01	7.79	6.3497	1.64	264659	7518	NIST_30600
17	b3113	513.35	8.06	6.3497	1.64	302480	7873	NIST_30600
18	b3140	409.42	8.15	6.4582	0.9136	253124	7312	NIST_30600
19	b3116	331.16	6.61	9.2359	1.173	216183	6377	NIST_30600
20	b3117	428.19	8.17	9.2359	1.173	283859	8093	NIST_30600
21	b3141	375.90	7.58	6.4582	0.9136	263880	7694	NIST_30600
22	b3118	448.30	8.82	9.2359	1.173	281500	8127	NIST_30600
23	b3121	445.73	8.42	9.2359	1.173	273293	7743	NIST_30600
24	b3122	625.70	10.49	9.2359	1.173	366410	9749	NIST_30600
25	b3142	425.64	8.74	6.4582	0.9136	269755	7906	NIST_30600
26	b3145	483.20	9.10	6.4582	0.9136	316949	8872	NIST_30600
27	b3146	606.34	12.08	6.4582	0.9136	386392	11060	NIST_30600
28	b3123	583.60	11.58	9.2359	1.173	408917	11758	NIST_30600
29	b3124	403.50	7.45	9.2359	1.173	234206	6595	NIST_30600
30	b3125	271.37	5.78	9.2359	1.173	163253	5040	NIST_30600
31	b3147	446.96	8.32	6.4582	0.9136	269325	7517	NIST_30600
32	b3148	379.27	7.33	6.4582	0.9136	223208	6374	NIST_30600
33	b3149	342.64	7.62	6.4582	0.9136	217009	6679	NIST_30600
34	b3151	380.68	5.86	6.4582	0.9136	247061	6413	NIST_30600
35	b3127	533.19	11.06	9.2359	1.173	319190	9408	NIST_30600
36	b3128	499.51	10.01	9.2359	1.173	297681	8640	NIST_30600
37	b3129	500.08	8.95	9.2359	1.173	291129	8013	NIST_30600
38	b3130	551.76	10.95	9.2359	1.173	322746	9295	NIST_30600
39	b3133	572.82	11.62	9.2359	1.173	337435	9814	NIST_30600
40	b3134	279.77	5.67	9.2359	1.173	169627	5097	NIST_30600
41	b3135	273.78	5.11	9.2359	1.173	159613	4625	NIST_30600
42	b3969	1220.30	0.23	2.8987	0.5798	389346	7811	NIST_30600
43	b3970	658.32	16.15	2.8987	0.5798	303811	9673	NIST_30600

Appendix C

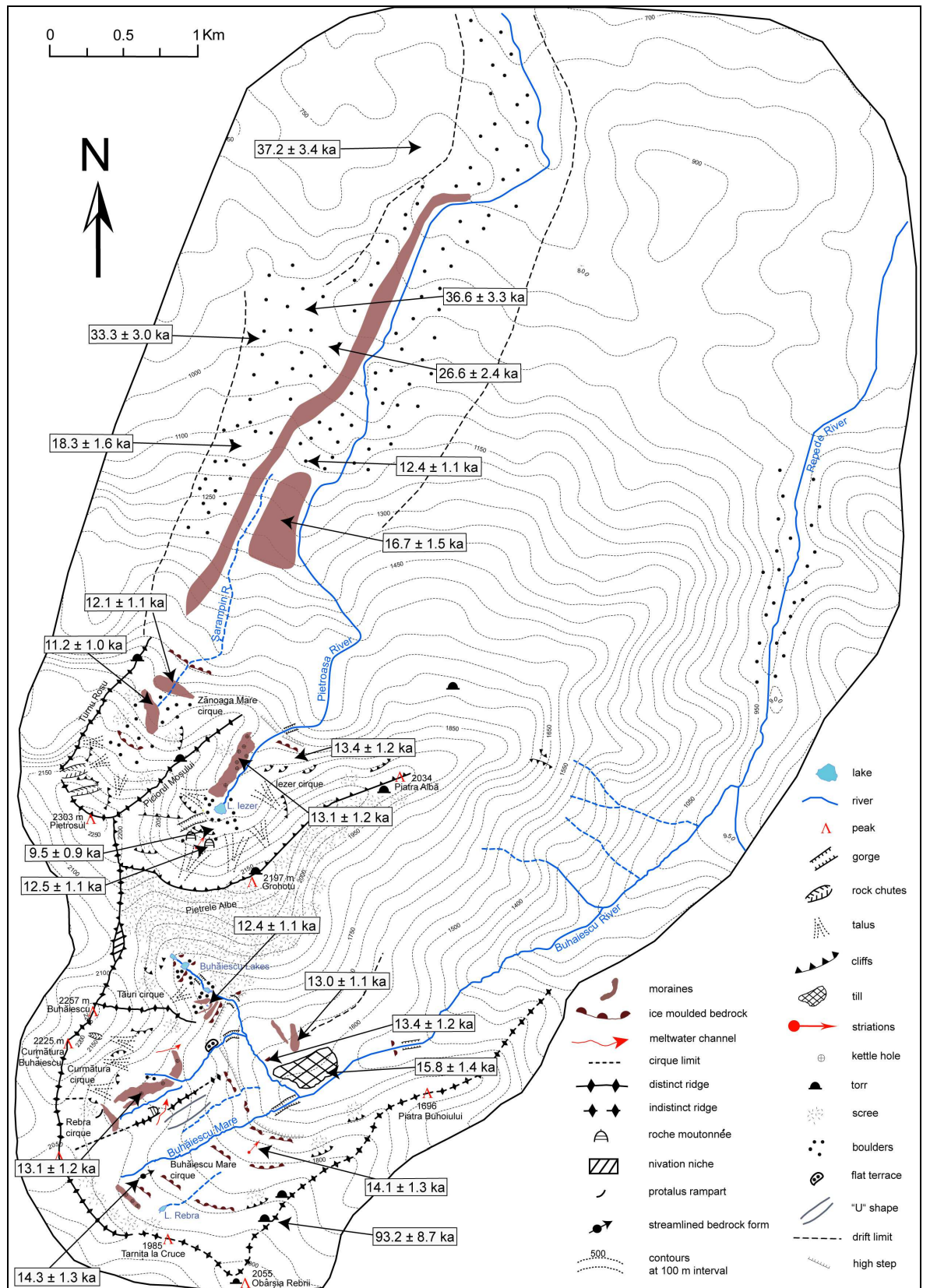
Maps

Monadhliath Mountains

Surface exposure ages plotted on the geomorphological map

Rodna Mountains

Surface exposure ages plotted on the geomorphological map



References

- Academia Republicii Socialiste România. 1979. Atlasul Republicii Socialiste România. *Editura Academiei Republicii Socialiste România*, București.
- Aksu, A.E., Hiscott, R.N., Kaminski, M.A., Mudie, P.J., Gillespie, H., Abrajano, T. & Yasar, D. 2002. Last glacial-Holocene Paleooceanography of the Black Sea and Marmara Sea: stable isotopic, foraminiferal and coccolith evidence. *Marine Geology* **190**, 119-149.
- Allen, R., Siebert, M.J., Payne, A.J. 2008. Reconstructing glacier-based climates of LGM Europe and Russia –Part 2: A dataset of LGM precipitation/temperature relations derived from degree-day modelling of palaeoglaciators. *Clim. Past.* **4**, 249–263.
- Alley, R.B. 2000. The Younger Dryas cold interval as viewed from central Greenland. *Quaternary Science Reviews* **19**, 213–226.
- Andersen, B.G. & Mangerud, J. 1989. The last interglacial-glacial cycle in Fennoscandia. *Quaternary International* **3/4**, 21-29.
- Astakhov, V.I. 1997. Late Glacial Events in the Central Russian Arctic. *Quaternary International* **41**, 42, 17–26.
- Atanassova, J. 2005. Palaeoecological setting of the western Black Sea area during the last 15000 years. *The Holocene* **15**, 4, 576–584.
- Athanasu, S. 1899. Morphologische Skizze der Nordmoldauer Karpathen, Bull. Soc. Șt. București, t. VII, nr. 3, p. 232-277.
- Atkinson, T.C., Briffa K.C., Coope, G.R. 1987. Seasonal temperatures in Britain during the past 22,000 years, reconstructed using beetle remains. *Nature* **325**, 587-592.
- Auton, C.A. 1998. Aspects of the Quaternary geology of 1:50,000 Sheet 74W (Tomatin). *British Geological Survey*, Technical Report WA/98/21.
- Balco, G., & Schaefer, J. M. 2006. Cosmogenic-nuclide and varve chronologies for the deglaciation of southern New England. *Quaternary Geochronology* **1**, p. 15-28.
- Balco, B., Stone, J., Lifton N., Dunai, T. 2008. A simple, internally consistent, and easily accessible means of calculating surface exposure ages and erosion rates from Be-10 and Al-26 measurements. *Quat. Geochronology* **3**, pp. 174–195.
- Balco, G., Briner, J., Finkel, R.C., Rayburn, J.A., Ridge, J.C., Schaefer, J.M. 2009. Regional beryllium-10 production rate calibration for late-glacial northeastern North America. *Quaternary Geochronology* **4**, p. 93–107.
- Ballantyne, C.K. 1986. Landslides and slope failures in Scotland: a review. *Scottish Geographical Magazine* **102**, 3, p. 134-150.
- Ballantyne, C.K. 1989. The Loch Lomond Readvance in the Isle of Skye, Scotland: Glacier reconstruction and palaeoclimatic implications. *Journal of Quaternary science* **4**, 95-108.
- Ballantyne, C.K. 2002. The Loch Lomond Readvance on the Isle of Mull, Scotland: glacier reconstruction and palaeoclimatic implications. *Journal of Quaternary Science* **17**, 759–771.
- Ballantyne, C.K. 2010. Extent and deglacial chronology of the last British–Irish Ice Sheet: implications of exposure dating using cosmogenic isotopes. *Journal of Quaternary Science*, **25**, 515-534.
- Ballantyne, C.K. & Kirkbride, M.P., 1987. Rockfall activity in upland Britain during the Loch Lomond Stadial. *Scottish Geographical Journal* **153**, 86-92.
- Ballantyne, C. K., Hall, A. M., Phillips, W., Binnie, S. & Kubik, P. W. 2007. Age and significance of former low-altitude corrie glaciers on Hoy, Orkney Islands. *Scottish Journal of Geology* **43**, 2, 107-114.
- Barrow, G., Hinxman, L.W. & Craig, E.H.C. 1913. The geology of upper Strathspey, Gaick and the Forest of Atholl. *Memoir of the Geological Survey of Scotland*, Edinburgh.
- Beaulieu, J.L. de, Richard, H., Ruffaldi, P., Clerc, J. 1994. History of vegetation, climate and human action in the French Alps and the Jura over the last 15 000 years. *Dissertationes Botanicae*, **234**, pp. 253–276.
- Benn, D.I. 1997. Glacier fluctuations in Western Scotland. *Quaternary International* **38-39**, 137-147.
- Benn, D.I. & Ballantyne, K.C. 2005. Paleoclimatic reconstruction from Loch Lomond Readvance glaciers in the West Drumochter Hills, Scotland. *Journal of Quaternary Science* **20**, 577-592.
- Benn, D.I. & Evans, D.J.A. 1998. Glaciers and glaciation. *Edward Arnold*, London, p. 734.
- Benn D., I. & Gemmell A.M.D. 1997. Calculating equilibrium line altitudes of former glaciers. *Glacial geology and geomorphology*. *Glacial Geology and Geomorphology*, <http://ggg.qub.ac.uk/ggg/>.
- Benn, D.I., Kirkbride, M.P., Owen, L.A. and Brazier, V. 2005. Glaciated Valley Landsystems. In *Glacial landsystems*, Evans D.J.A. (ed), Arnold, London, 372-405.
- Benn, D.I., Lowe, J.J. and Walker, M.J.C. 1992. Glacier response to climate change during the Loch Lomond Stadial and early Flandrian: Geomorphological and palynological evidence from the Isle of Skye, Scotland. *Journal of Quaternary Science* **7**, 125 – 144.
- Bennett, M. R. & Boulton, G. S. 1993. Deglaciation of the Younger Dryas or Loch Lomond Stadial ice-field in the northern Highlands, Scotland. *Journal of Quaternary Science* **8**, 133-145.
- Bennett, M.R. & Glasser, N.F. 1991. The glacial landforms of Glen Geusachan, Cairngorms: A Reinterpretation. *Scottish Geographical Journal* **107**, 116 - 123.
- Berner, U. & Streif, H. 2000. Klimafakten, Der Rückblick - Ein Schlüssel für die Zukunft: Stuttgart: E. Schweizerbartsche Verlagsbuchhandlung, Science Publishers.

- de Beaulieu, J.-L., Richard, H., Ruffaldi, P., & Clerc, J. 1994. History of vegetation, climate and human action in the French Alps and the Jura over the last 15 000 years. *Dissertationes Botanicae* **234**, pp. 253–276.
- Bierman, P.R., Caffee, M.W., Davis, P.T., Marsella, K., Pavich, M., Colgan, P., Mickelson, D. 2002. Rates and timing of earth surface processes from in situ-produced cosmogenic Be-10, Beryllium: Mineralogy, Petrology, and Geochemistry. *Series: Reviews in Mineralogy and Geochemistry* **50** in: E.S. Grew (Ed), Mineralogical Society of America, Washington, DC, pp. 147–205.
- Bigg, G.R, Jickells TD, Liss, P.S., 2003: The role of the oceans in climate. *International Journal of Climatology* **23**, 10, 1127-1159.
- Birks, H.H., Paus, A., Svendsen, J.-I., Alm, T., Mangerud, J. & Landvik, J.Y. 1994. Late Weichselian environmental changes in Norway, including Svalbard. *Journal of Quaternary Science* **9**, 133–45.
- Björck, S., Walker, M. J. C., Cwynar, L. C., Johnsen, S., Knudsen, K. L., Lowe, J. J., Wohlfarth, B., & INTIMATE Members. 1998. An event stratigraphy for the Last Termination in the North Atlantic region based on the Greenland ice-core record: a proposal by the INTIMATE group. *Journal of Quaternary Science* **13**, 283–292.
- Björckman, L., Feurdean, A., Cinthio, K., Wohlfarth, B., Possnert, G. 2002. Lateglacial and early Holocene vegetation development in the Gutâiului Mountains, NW Romania. *Quaternary Science Reviews* **21**, 1039–1059.
- Björckman, L., Feurdean, A. & Wohlfarth, B. 2003. Lateglacial and Holocene forest dynamics at Steregoiu in the Gutâiului Mountains, NW Romania. *Review of Palaeobotany and Palynology* **124**, 79–111.
- Blaauw, M., Wohlfarth, B., Christen, J. A., Ampel, L., Veres, D., Hughen, K. A., Preusser, F. & Svensson, A. 2009. Were last glacial climate events simultaneous between Greenland and France? A quantitative comparison using non-tuned chronologies. *J. Quaternary Science* **25**, 1047.
- Bleahu, M. 1957. Forme periglaciare și glaciare în Munții Maramureșului, Comunicare la Sesiunea Științifică a Universității București.
- Bogdan, G. & Leszek, L. 1999. Glaciokarst of subalpine and alpine zone of the Mala laka Valley, Tatra Mts., Poland. *Acta carsologica* **28**, 1, 71-86.
- Bond, G. C., & Lotti, R. 1995. Iceberg discharges into the North Atlantic on millennial time scales During the Last Glaciation, *Science*, **267**, 1005-1010.
- Bond, G., Showers, W., Cheseby, M., Lotti, R., Almasi, P., de Menocal, P., Priore, P., Cullen, H., Hajdas, I., & Bonani, G. 1997. A pervasive millennial-scale cycle in North Atlantic Holocene and Glacial climates. *Science* **278**, 1257-1266.
- Boston, C., Lukas, S., Carr, S. 2011. Evidence for a Younger Dryas Plateau Icefield in the Monadhliath Mountains, Scotland: implications for regional palaeo-climate reconstructions. Poster abstract. INQUA 2011, Bern, Switzerland.
- Boulton, G.S., Jones, A.S., Clayton, L.M., Kenning, M.J. 1977. A British ice sheet model and patterns of glacial erosion and deposition in Britain. In Shotton, F.W. *British Quaternary Studies: recent advances*. Clarendon Press, Oxford, 231-246.
- Boulton, G.S., Smith, G.D., Jones, A.S. and Newsome, J., 1985. Glacial geology and glaciology of the Last mid-latitude ice sheets. *Journal of the Geological Society*, **142**, p. 447-474.
- Boulton, G.S., Dongelmans, P., Punkari, M. & Broadgate, M., 2001. Palaeoglaciology of an ice sheet through a glacial cycle: the European ice sheet through the Weichselian. *Quaternary Science Reviews* **20**, 591-625.
- Boulton, G.S., Dongelmans, P., Punkari, M., Broadgate, M., 2004. Evidence of European ice sheet fluctuation during the last glacial cycle. In: Ehlers, J., Gibbard, P.L. (Eds.), *Quaternary Glaciations, Extent and Chronology*, P. I: Europe. Elsevier, Amsterdam, pp. 441-460.
- Braconnot, P., Hourdin, F., Bony, S., Dufresne, J.L., Grandpeix, J.Y., Marti, O. 2007. Impact of different convective cloud schemes on the simulation of the tropical seasonal cycle in a coupled ocean-atmosphere Model. *Climate Dynamics* **29**, 5, 501-520.
- Bradwell, T., Fabel, D., Stoker, M., Mathers, H., McHargue, L. and Howe, J. 2008a. Ice caps existed throughout the Lateglacial Interstadial in northern Scotland. *Journal of Quaternary Science* **23**, 401–407.
- Bradwell, T., Stoker, M.S., Golledge, N.R., Wilson, C., Merritt, J., Long, D., Everest, J.D., Hestvik, O., Stevenson, A., Hubbard, A., Finlayson, A., Mathers, H., 2008b. The northern sector of the last British ice sheet : maximum extent and demise. *Earth Science Reviews* **88**, 207–226.
- Brauer, A., Endres, C., Günter, C., Litt, T., Stebich, M., Negendank, J.F.V. 1999. High resolution sediment and vegetation responses to Younger Dryas climate change in varved lake sediments from Meerfelder Maar, Germany. *Quaternary Science. Reviews* **18**, 3, 321–329.
- Brauer, A., Haug, G.H., Dulski, P., Sigman, D.M., Negendank, J.F.W. 2008. An abrupt wind shift in western Europe at the onset of the Younger Dryas cold period. *Nature Geoscience* **1**, 520–523.
- Brazier, V, Kirkbride, M.P. & Gordon, J.E. 1998. Active ice sheet deglaciation and ice-dammed lakes in the northern Cairngorm Mountains, Scotland. *Boreas* **27**, 297-310.
- Broecker, W.S., Peteet, D.M. & Rind, D. 1985. Does the ocean-atmosphere system have more than one stable mode of operation? *Nature* **315**, 21-26.

- Broecker, W.S. 2006. Abrupt climate change revisited. *Global and Planetary Change* **54**, 211–215.
- Brooks, S. J. & Birks, H.J.B. 2000. Chironomid-inferred Late-glacial air temperatures at Whitrig Bog, southeast Scotland. *Journal of Quaternary Science* **15**, 759–764.
- Buynevich, I.V. 2011. Geology and geoarchaeology of the Black Sea Region: beyond the flood hypothesis. Boulder, Colo. : Geological Society of America, 196 pages.
- Calvet, M. 2004. The Quaternary glaciation of the Pyrenees. In: Ehlers, J., Gibbard, P.L. (Eds.), *Quaternary Glaciations—Extent and Chronology*. Elsevier, Amsterdam, pp. 119–128.
- Carr, S.J. 2001. A glaciological approach for the discrimination of Loch Lomond Stadial glacial landforms in the Brecon Beacons, South Wales. *Proceedings of the Geologists' Association* **112**, 253–262.
- Cârciumaru, M., 1980. Mediul geografic în pleistocenul superior și culturile paleolitice din România. Editura Academiei Republicii Socialiste România, București, p 268.
- Cerling, T.E., Craig, H., 1994. Geomorphology and in-situ cosmogenic isotopes. *Annual Reviews of Earth and Planetary Sciences* **22**, 273–317.
- CERN. 2003. Developments at the Gran Sasso laboratory. BUL-NA-2003-081. www.cdsweb.cern.ch/record/627596.
- Charlesworth JK., 1956. Lateglacial history of the Highlands and islands of Scotland. *Transactions of the Royal Society of Edinburgh* **62**, 769–928.
- Chepalyga, A.L. 1984. Inland sea basins. In: Velichko, A.A. (Ed.), *Late Quaternary Environments of the Soviet Union*. University of Minnesota Press, Minneapolis, MN, pp. 229–246.
- Child, D., Elliott, G., Mifsud, C., Smith, A.M., Fink, D., 2000. Sample processing for earth science studies at ANTARES. *Nuclear Instruments and Methods in Physics Research Section B: Beam Interactions with Materials and Atoms* **172**, 856e860.
- Chmeleff, J., von Blanckenburg, F., Kossert, K., Jakob, D. 2010. Determination of the ^{10}Be half-life by multicollector ICP-MS and liquid scintillation counting. - *Nuclear Instruments and Methods in Physics Research / B*, **263**, 2, 192–199
- Clapperton, C.M., Gunson, A.R. and Sugden, D.E. 1975. Loch Lomond Readvance in the eastern Cairngorms. *Nature* **253**, 710–12.
- Clapperton, C. M. 1997. Greenland ice cores and North Atlantic sediments: implications for the last glaciation in Scotland. In; Gordon, J. E. (ed), *Reflections on the ice age in Scotland: an update on Quaternary Studies*. Scottish Association of Geography Teachers and Scottish Natural Heritage, p 45–58.
- Clark, P.U, Alley, R.B., Pollard, D. 1999. Northern Hemisphere ice-sheet interactions on global climate change. *Science* **286**, 1104–1111.
- Clark, P., Pisias, N.G., Stocker, T.F. & Weaver, A.J. 2002. The role of the thermohaline circulation in Abrupt climate change. *Nature* **415**, pages 863–869.
- Clark, C., Evans, D., Khatwa, A., Bradwell, T., Jordan, C., Marsh, S., Mitchell, W. & Bateman, M. 2004. Map and GIS database of glacial landforms and features related to the last British Ice Sheet. *Boreas* **33**: 4, 359 - 375.
- Coldea, G. 1990. Munții Rodnei. Studiu geobotanic, *Edit. Academiei Române*, București, 183 p.
- Constantin, S., Bojar, A.M., Lauritzen, S.E., Lundberg, J. 2007. Holocene and Late Pleistocene climate in the sub-Mediterranean continental environment: A speleothem record from Poleva Cave (Southern Carpathians, Romania). *Palaeogeography, Palaeoclimatology, Palaeoecology* **243**, 322–338.
- Coope, G.R., Lemdahl, G., Lowe, J.J., Walking, A. 1998. Temperature gradients in Northern Europe during the last Glacial-Interglacial Transition (14–9 14Cka BP) interpreted from coleopteran assemblages. *J. of Quaternary Science* **13**, 419–433.
- Cossart, E., Fort, M., Bourles, D., Carcaillet, J., Perrier, R., Siame, L. & Braucher, R. 2010. Climatic significance of glacier retreat and rockglaciers re-assessed in the light of cosmogenic dating and weathering rind thickness in Clarée valley (Briançonnais, French Alps). *Catena* **80**, pp. 204–219.
- Czirbusz, G. 1896. Hegyen-völgön. A Radnai havasokon, Erdély, t. V, fasc. 10–12.
- Davis, R.J. & Schaefer, O.A. 1955. Chlorine-36 in nature. *Annals New York Academy of Science* **62**, 105–122.
- Dayton, N. 2006. An assessment and evaluation of herbivore impacts on blanket bog habitat in the Monadhliath Special Areas of Conservation. Scottish Natural Heritage Commissioned Report No.165.
- Dawson, A. 1992. *Ice age Earth. Late Quaternary geology and climate*. London, Routledge.
- Desilets, D. & Zreda, M. 2003. Spatial and temporal distribution of secondary cosmic-ray nucleon intensities and applications to in situ cosmogenic dating. *Earth Planet. Sci. Lett.* **206** 21–42.
- Desilets, D.M. 2005. *Cosmogenic nuclides as a surface exposure dating tool: improved altitude/latitude scaling factors for production rates*. Ph.D. dissertation, Department of Hydrology and Water Resources, The University of Arizona, Tuscon, Arizona.
- Desilets, D., Zreda, M. and Prabu, T., 2006. Extended scaling factors for in situ cosmogenic nuclides: New measurements at low latitude. *Earth Planet. Sci. Lett.* **246**, 265–276.
- Dansgaard, W., Johnson, S.J., Clausen, H.B., Dahl-Jensen, D., Gundenstrup, N.S., Hammer, C.U., Hvidberg, C.S., Steffensen, J.P. and Sveinbjörnsdottir, A.E. 1993 Evidence for general instability of past climate from a 250-kyr ice-core record. *Nature* **364**, 218–20.

- Dolvik, T., Hjelle, T., Mangerud, J., Matiouchkov, A., 2002. Weichselian glaciations in the Polar Ural Mountains. Quaternary Environment of the Eurasian North (QUEEN), sixth workshop, Spiez Switzerland. European Science Foundation, Abstract volume, p. 11.
- Donisa, N. 2005. Restoration forest habitata from Pietrosul Rodnei biosphere Reserve, LIFE-NATURE Project, Bucharest.
- Dzierżek, J. & Zreda, M. 2007. Timing and style of deglaciation of north-eastern Poland from cosmogenic ^{36}Cl dating of glacial and glaciofluvial deposits. *Geological Quarterly* **51**, 2, 203-216.
- Dyke, A.S., Andrews, J.T., Clark, P.U., England, J.H., Miller, G.H., Shaw, J., Veillette, J.J. 2002. The Laurentide and Innuitian ice sheets during the Last Glacial Maximum. *Quaternary Science Reviews* **21**, 9–13.
- Dunai, T.J. 2000. Scaling factors for production rates of in situ produced cosmogenic nuclides: a critical reevaluation *Earth and Planetary Science Letters* **176**, 157-169.
- Dunai, T.J. 2001. Influence of secular variation of the geomagnetic field on production rates of in situ produced cosmogenic nuclides. *Earth and Planetary Science Letters* **193**, 1-2, 197-212.
- Dunai, Tibor J. 2010. Cosmogenic Nuclides: Principles, Concepts and Applications in the Earth Surface Sciences. Cambridge, MA: Cambridge University Press.
- Dunne, J., Elmore, D., Muzikar, P. 1999. Scaling factors for the rates of production of cosmogenic nuclides for geometric shielding and attenuation at depth on sloped surfaces. *Geomorphology* **27**, 3–11.
- Ehlers, J., & Gibbard, P.L. 2004. Quaternary glaciations—Extent and chronology, Part II: North America. *Developments in Quaternary Science*: Amsterdam, Elsevier, 440p.
- Evans, D. J. A., Rea, B. R., Hansom, J. D. and Whalley, W. B. 2002. Geomorphology and style of plateau icefield deglaciation in fjord terrains: the example of Troms-Finnmark, north Norway. *Journal of Quaternary Science* **17**, 221–239.
- Everest, J.D. & Gollledge, N.R. 2004. Dating deglaciation in Strath spey and the Cairngorm Mountains. In *The Quaternary of the Central Grampian Highlands: Field Guide*, Lukas S, Meritt JW, Mitchell WA (eds). *Quaternary Research Association*, London, 50-57.
- Fabel, D. Stroeven, A.P., Harbor, J., Kleman, J., Elmore, D. & Fink, D. 2002. Landscape preservation under ice sheets. *Earth and Planetary Science Letters* **201**, 397-406.
- Fărcaș, S., de Beaulieu, J.L., Reille, M., Coldea, G., Diaconeasa, B., Goeury, C., Goslar, T., Jull, T. 1999. First ^{14}C dating of Late Glacial and Holocene pollen sequences from the Romanian Carpathians. *Comptes Rendues de l'Académie des Sciences de Paris, Sciences de la Vie* **322**, 799– 807.
- Feurdean, A. 2005. Holocene forest dynamics in northwestern Romania. *The Holocene* **15**, 435-446.
- Feurdean, A. & Bennike, O. 2004. Late Quaternary palaeoecological and paleoclimatological reconstruction in the Gutâiului Mountains, NW Romania. *Journal of Quaternary Science* **19**, 809-827.
- Feurdean, A., Tâmaș, T., Tanțău, I., Fărcaș, S. 2011. Elevational variation in the biotic response to repeated climate changes in the Carpathians as revealed by the pollen records. *Journal of Biogeography*, DOI: 10.1111/j.1365-2699.2011.02605.x
- Feurdean, A., Wohlfarth, B., Björkman, L., Tanțău, I., Bennike, O., Willis, K.J., Farcas, S., Robertsson, A.M. 2007. The influence of refugial population on Lateglacial and early Holocene vegetational changes in Romania. *Review of Palaeobotany and Palynology* **145**, 305-320.
- Finlayson, A.G. 2006. Glacial Geomorphology of the Creag Meagaidh Massif, Western Grampian Highlands: implications for Local Glaciation and Palaeoclimate during the Loch Lomond Stadial. *Scottish Geographical Journal* **122**, 293-307.
- Finlayson, A.G. 2008. The northern Creag Meagaidh massif: geomorphology and glacier modelling. In *The Quaternary of Glen Roy and vicinity. Field guide*. Palmer, AP, Lowe, JJ, Rose, J. (eds).
- Finlayson, A.G., Gollledge, N.R., Bradwell, T. and Fabel, D. 2011. Evolution of a Lateglacial mountain icecap in northern Scotland. *Boreas*, **40**, pp. 536-554.
- Florineth, D. & Schlüchter, C. 1998. Reconstructing Last Glacial Maximum (LGM) ice surface geometry and flowlines in the Central Swiss Alps. *Eclogae geologicae Helvetiae* **91**, 391–407.
- Florineth D, Schlüchter C. 2000. Alpine evidence for atmospheric circulation patterns in Europe during the Last Glacial Maximum. *Quaternary Research* **54**: 295 - 308.
- Freeman S., Bishop, P., Bryant C., Cook G., Fallick A., Harkness D., Metcalfe S., Scott M., Scott R., Summerfield M. 2004. New environmental sciences AMS laboratory in Scotland. *Nucl. Instr. and Meth. in Phys. Res. B: Beam Interactions with Materials and Atom.*, **223–224** 31–34.
- Freeman, S., Bishop, P., Bryant, C., Cook, G., Dougans, D., Ertunc, T., Fallick, A., Ganeshram, R., Maden, C., Naysmith, P., Schnabel, C., Scott, M., Summerfield, M. and Xu, S. 2007. The SUERC AMS laboratory after 3 years. *Nuclear Instruments and Methods in Physics Research Section B: Beam Interactions with Materials and Atoms* **259**, 1, pp. 66-70.
- García-Ruiz, J.M., Valéro-Garcés, B.L., Martí-Bono, C., González-Sampériz, 2003. Asynchronicity of maximum glacier advances in the central Spanish Pyrenees. *Journal of Quaternary Science* **18** (1), 61–72.
- Gherghina, Alina, Grecu, Florina, Coteț, Valentina. 2006. The loess from Romania in the Romanian specialists' vision, In: Factori și procese în zona temperată. Symposium Proceedings Ed. Universității "Al. I. Cuza" Iași, vol. **5**, pp. 103–116.
- Gibbons, W., Moreno, T., (eds.). 2002. The Geology of Spain. London (The Geological Society). 649 p.

- Gillespie, A., & P. Molnar, Asynchronous maximum advances of mountain and continental glaciers, *Rev. Geophys.* **33**, 311-364, 1995.
- Giraudi, C. & Frezzotti, M. 1997. Late Pleistocene glacial events in the central Apennines, Italy. *Quaternary Research* **48**, 280-290.
- Gellatly, A.F, Whalley W.B., Gordon J.E., Hansom J.D., Twigg D.S. 1989. Recent glacial history and climatic change, Bergsfjord, Troms-Finnmark, Norway. *Norsk geogr. Tidsskr.* **43**, 19-30.
- Gobejshvili R. 2004. Late Pleistocene (Würmian) glaciation of the Caucasus. In: Ehlers J., Gibbard P.L. (eds) *Quaternary Glaciations. Extent and Chronology. Part I: Europe*. Elsevier Science, Amsterdam 129-134.
- Golledge, N.R. 2002. Glaci-tectonic deformation of proglacial lake sediments in the Cairngorm Mountains. *Scottish Geographical Journal* **38**, 127-136.
- Golledge, N.R. 2006. The Loch Lomond Stadial Glaciation South of Rannoch Moor: New Evidence and Palaeoglaciological Insights *Scottish Geographical Journal*. Vol. **122**, 326 – 343.
- Golledge, N.R. 2007. Sedimentology, stratigraphy, and glacier dynamics western Scottish Highland. *Quaternary Research* **68**, 79–95.
- Golledge, N.R. 2008. Glacial geology and glaciology of the Younger Dryas ice cap in Scotland. Ph.D. thesis. University of Edinburgh, Edinburgh.
- Golledge, N.R. & Hubbard, A. 2005. Evaluating YD glacier reconstructions in part of the western Scottish Highlands: a combined empirical and theoretical approach. *Boreas* **34**, 274–286.
- Golledge, N.R., Hubbard, A., Sugden, D.E., 2008. High-resolution numerical model of YD glaciation in Scotland. *Quaternary Science Reviews* **9-10**, 888-904.
- Gordon J.E. and Sutherland D.G. 1993. *Quaternary of Scotland*, **6**, Chapman & Hall, London.
- Gordon, J.E., Whalley, W.B., Gellatly, A.F. 1995. Fluctuations of glaciers in Lyngsdalen, Troms, Norway, during the 20th century. *Zeitschrift für Gletscherkunde und Glazialgeologie* **31**, 125-134.
- Gosse, J.C. & Phillips, F.M. 2001. Terrestrial in situ cosmogenic nuclides: theory and application. *Quaternary Science Reviews* **20**, 1475-1560.
- Goudie, A. 1983. *Environmental Change* (2nd Ed.). New York, NY: Oxford University Press, 118-169.
- Granger, D.E. & Muzikar, P.F. 2001. Dating sediment burial with in situ-produced cosmogenic nuclides: Theory, techniques, and limitations. *Earth and Planetary Science Letters* **188**, 1-2, pp 269-281.
- Gray, J.M. 1995, In Gordon, J.E. 1997. Reflections on the ice age in Scotland. The Scottish Association of Geography Teachers and Scottish Natural Heritage.
- Gyte, J.N. 2004. Late-glacial landforms and climate change in the Monadhliath Mountains, Scotland. *Unpublished undergraduate thesis*, University of Edinburgh.
- Hall, A.M. & Glasser, N.F. 2003. Reconstructing former glacial basal thermal regimes in a landscape of selective linear erosion: Glen Avon, Cairngorm Mountains, Scotland. *Boreas* **32**, 191-207.
- Harrison, S.P., Prentice, I.C., Bartlein, P.J. 1992. Influence of insolation and glaciation on atmospheric circulation in the North Atlantic sector: implications of general circulation model experiments for the late Quaternary climatology of Europe. *Quaternary Science Reviews* **11**, pp 283-300.
- Harrison, S.P., Yu, G. & Tarasov, P.E. 1996. Late Quaternary lake-level record from Northern Eurasia. *Quaternary Research* **45**, pp. 138–159.
- Haselock, P.J., Winchester, J.A. & Whittles, K.H. 1982. The stratigraphy and structure of the southern Monadhliath Mountains between Loch Killin and upper Glen Roy. *Scottish Journal of Geology* **18**, 275-290.
- Haase, D., Fink, J., Haase, G., Ruske, R., Pecsí, M., Richter, H., Altermann, M., Jäger, K.D. 2007. Loess in Europe - its spatial distribution based on a European Loess Map, scale 1:2,500,000. *Quaternary Science Reviews* **26**, 9-10, pp. 1301-1312
- Hormes, A, Ivy-Ochs, S., Kubik, P., Ferrelly, L., Michetti, A.M. 2007. ¹⁰Be exposure ages of a rock avalanche and a late glacial moraine in Alta Valtellina, Italian Alps. *Quaternary International*.
- Houmark-Nielsen, M. 2008. Testing OSL failures against a regional Weichselian glaciation chronology from southern Scandinavia. *Boreas* **37**, pp. 660–677.
- Houmark-Nielsen, M. 2010. Extent, age and dynamics of Marine Isotope Stage 3 glaciations in the south-western Baltic Basin. *Boreas* **39**, pp. 343–359.
- Houmark-Nielsen, M., Jakobsson, M., Kuzmina, S., Larsen, E., Lunkka, J. P., Lyså, A., Mangerud, J., Möller, P., Saarnisto, M., Schirrmeyer, L., Sher, S. V., Siegert, M. J. & Svendsen, J. I. 2004. The periglacial climate and environment in northern Eurasia during the Last Glaciation. *Quaternary Science Reviews* **23**, 1333–1357.
- Hubbard, A. 1999. High-resolution Modelling of the Advance of the YD Ice Sheet and *imts* Climate in Scotland. *Quaternary Research* **52**, 27-43.
- Hubbard, A., Bradwell, T., Golledge, N., Hall, A., Patton, H., Sugden, D., Cooper, R., Stoker, M. 2009. Dynamic cycles, ice streams and their impact on the extent, chronology and deglaciation of the British–Irish ice sheet. *Quaternary Science Reviews* **28**, 758–776.
- Hubberten, H.W., Andreev, A., Astakhov, V.I., Demidov, I., Dowdeswell, J.A., Henriksen, M., Hjort, C., Houmark-Nielsen, M., Jakobsson, M., Kuzmina, S., Larsen, E., Lunkka, J.P., Lyså, A., Mangerud, J., Möller, P., Saarnisto, M., Schirrmeyer, L., Sher, A.V., Siegert, C., Siegert M.J. & Svendsen, J.I., 2004:

- The periglacial climate and environment in northern Eurasia during the last glaciation (LGM). *Quaternary Science Reviews* **23**, 1333-1357.
- Hughes, P.D., Woodward, J.C. & Gibbard, P.L. 2006. Late Pleistocene glaciers and climate in the Mediterranean region. *Global and Planetary Change* **46**, 83-98.
- Hughes, P.D., Woodward, J.C. & Gibbard, P.L. 2007. Middle Pleistocene cold stage climates in the Mediterranean: New evidence from the glacial record. *Earth and Planetary Science Letters* **253**, 50-56.
- Hughes, P.D. & Braithwaite, R.J. 2008. Application of a degree-day model to reconstruct Pleistocene glacial climates. *Quaternary Research* **69**, 110-116.
- Hughes, P.D. & Woodward, J.C. 2008. Timing of glaciation in the Mediterranean mountains during the last cold stage. *Journal of Quaternary Science* **23**, 575-588.
- Humlum, O. 1997. Younger Dryas glaciation in Söderåsen, South Sweden: an analysis of meteorologic and topographic controls. *Geogr. Ann.* **79** A, 1-2, p 1-15.
- Ivy-Ochs, S., Schäfer J., Kubik P.W., Synal H.-A., Schlüchter, C. 2004. The timing of deglaciation on the northern Alpine foreland (Switzerland). *Eclogae Geologicae Helveticae* **97**, 47-55.
- Ivy-Ochs, S., Schlüchter, C., Kubik, P.W., Synal, H.-A., Kerschner, H., 1996. The exposure age of an Egesen moraine at Julier Pass, Switzerland, measured with the cosmogenic radionuclides ^{10}Be , ^{26}Al and ^{36}Cl . *Eclogae Geologicae Helveticae* **89**, 1049-1063.
- Ivy-Ochs, S., Kerschner, H., Reuther, A.U., Maisch, M., Sailer, R., Schaefer, J., Kubik, P.W., Synal, H.-A. & C. Schlüchter. 2006. The timing of glaciations in the European Alps based on surface exposure dating with cosmogenic ^{10}Be , ^{26}Al , ^{36}Cl , and ^{21}Ne . In: Siame, L.L., Bourlés, D.L., and Brown, E.T. (eds.): Application of cosmogenic nuclides to the study of Earth surface processes: The practice and the potential: Geological Society of America Special Paper 415, 43-60.
- Ivy-Ochs, S., Kerschner, H., Reuther, A., Preusser, F., Heine, K., Maisch, M., Kubik, P.W., Schlüchter C. 2008. Chronology of the last glacial cycle in the European Alps. *Journal of Quaternary Science* **23**, 559-573.
- Jacobi, R. M., Rose, J., Macleod, A., & Higham, T. F. G. 2009. Revised radiocarbon ages on woolly rhinoceros (*Coelodonta antiquitatis*) from western central Scotland: significance for timing the extinction of woolly rhinoceros in Britain and the onset of the LGM in central Scotland. *Quaternary Science Reviews* **28**, 25-26, 2551-2556.
- Jalut, G., Montserrat-Martí, J., Fontugne, M., Delibrias, G., Vilaplana, J.M., Julià, R., 1992. Glacial to Interglacial vegetation changes in the northern and southern Pyrénées: deglaciation, vegetation cover and chronology. *Quaternary Science Reviews* **11**, 449-480.
- Jalut, G., Turu i Michels, V., Dedoubat, J.J., Otto, T., Ezquerra, J., Fontugne, M., Belet, J.M., Bonnet, L., García de Celis, A., Redondo-Vega, J.M., Vidal-Romaní, J.R. & Santos, L. 2010. Palaeoenvironment studies in NW Iberia (Cantabrian range): Vegetation history and synthetic approach of the last deglaciation phases in the western Mediterranean. *Palaeogeogr., Palaeoclimatol., Palaeoecol.* **297**, 2, pages 330-350.
- Jarman, D. 2006. Large rock slope failures in the Highlands of Scotland: characterisation, causes and spatial distribution. *Engineering Geology* **83**, pp. 161-182.
- Johnsen, S. J., Dahl-Jensen, D., Gundestrup, N., Steffensen, J. P., Clausen, H. B., Miller, H., Masson-Delmotte, V., Sveinbjörnsdóttir, A. E. and White, J. 2001. Oxygen isotope and palaeotemperature records from six Greenland ice-core stations: Camp Century, Dye-3, GRIP, GISP2, Renland and NorthGRIP. *Journal of Quaternary Science.*, **Vol. 16**, pp. 299-307.
- Kalm, V. 2010. Ice-flow pattern and extent of the last Scandinavian ice sheet southeast of the Baltic Sea. *Quaternary Science Reviews*. doi:10.1016/j.quascirev.2010.01.019.
- Kaplin, P.A., Selivanov, A.O. 2004. Lateglacial and Holocene sea level changes in semi-enclosed seas of North Eurasia: examples from the contrasting Black and White Seas. *Paleogeography, Paleoclimatology, Paleoecology* **209**, 19-36.
- Kjellström, E., Brandefelt, J., Näslund, J.-O., Smith, B., Strandberg, G., Voelker, A.H.L. & Wohlfarth, B. 2010. Simulated climate conditions in Europe during the Marine Isotope Stage 3 stadial. *Boreas* **39**, 436-456.
- Kräutner, T. 1930. Die Spuren der Eiszeit in den Ost- und Süd-Karpathen. Geologisch-morphologische Studie, Verhandl. und Mitt. des Siebenbürg. Vereins für Naturwissenschaften zu Hermannstadt, LXXIX-LXXX Band, Jahrgang 1929-1930, pp. 10-85.
- Klein, J., Giegengack, R., Middleton, R., Sharma, P., Underwood, J.R., Weeks, R.A. 1986. Revealing histories of exposure using in situ produced ^{26}Al and ^{10}Be in Libyan Desert Glass. *Radiocarbon* **28** (2A), 547-555.
- Kohl, C.P. and Nishiizumi, K. 1992. Chemical isolation of quartz for measurement of in situ-produced cosmogenic nuclides. *Geochimica et Cosmochimica Acta*, **56**, 3586-3587.
- Korschinek, G., Bergmaier, A., Dillmann, I., Faestermann, T., Gerstmann, U., Knie, K., von Gostomski, C.L., Maiti, M., Poutivtsev, M., Remmert, A., Rugel, G., Wallner, A. 2009. Determination of the ^{10}Be Half-life by HI-ERD and Liquid Scintillation Counting, Goldschmidt, Davos, p. A658.
- Kubik, P.W., Ivy-Ochs, S., Masarik, J., Frank, M., and Schlüchter, C. 1998. ^{10}Be and ^{26}Al production rates

- deduced from an instantaneous event within the dendro-calibration curve, the landslide of Köfels, Ötz Valley, Austria. *Earth Planet. Sci. Lett.* **161**, 231–241.
- Kuhlemann, J., Krumrei, I., Rohling E., Kubik, P., Ivy-Ochs S. & Kucera, M., 2008. Regional synthesis of Mediterranean atmospheric circulation during the Last Glacial Maximum. *Science*, 321, 1338–1340.
- Kuhlemann, J., Milivojević, M., Krumrei, I., Kubik, P.W. 2009. Last glaciation of the Šara range (Balkan peninsula): Increasing dryness from the LGM to the Holocene. *Austrian Journal of Earth Sciences* **102**, 146–158.
- Kwiecien, O., Arz, H.W., Lamy, F., Plessen, B., Bahr, A. & Haug, G.H. 2009. North Atlantic control on precipitation pattern in the eastern Mediterranean/Black Sea region during the last glacial. *Quat. Res.* **71**, pp. 375–384.
- Lal, D., Arnold, J.R. & Honda, M. 1960. *Phys. Rev.* **118**, 1626.
- Lal, D., Peters, B., 1967. Cosmic ray produced radioactivity on the earth. In: Sitte, K. (Ed.), *Handbuch der Physik*. Springer, Berlin, pp. 551–612.
- Lal, D., 1988. In situ-produced cosmogenic isotopes in terrestrial rocks. *Ann. Rev. Earth Planet. Sci.* 16 355–388.
- Lal, D., 1991. Cosmic ray labeling of erosion surfaces: in situ nuclide production rates and erosion rates. *Earth and Planetary Science Letters* **104**, 424–439.
- Lal D. 2000. Cosmogenic nuclide production rate systematics in terrestrial materials; present knowledge, needs and future action for improvement. *Nuclear Instruments and Methods in Physics Research B* **172**: 772–81.
- Lal, D., 2007. Recycling of cosmogenic nuclides after their removal from the atmosphere; special case of appreciable transport of ¹⁰Be to polar regions by aeolian dust. *Earth Planet. Sci. Lett.* **264**, 177–187.
- Layos, V. 1927. A Radi keleti felének glacialis jelensegei, Foldrajazi kozlemeneyek, T. LV, Budapest.
- Lambeck, K. & Chappell, J. 2001. Sea level change through the last glacial cycle: *Science* **292**, no. 5517, p. 679–686.
- Lambeck, K., Purcell, A. 2005. Sea-level change in the Mediterranean Sea since the LGM: model predictions for tectonically stable areas. *Quaternary Science Reviews* **24**, 1969–1988.
- Lambeck, K., Yokoyama, Y., Johnston P. & Purcell, A. 2000. *Earth and Planetary Science Letters*, **181**, 4, p. 513–527.
- Lambeck, K. & Purcell, A. 2005. Sea-level change in the Mediterranean Sea since the LGM: model predictions for tectonically stable areas. *Quaternary Science Reviews* **24**, 1969–1988.
- Lambert, R.St.J., Holland, J.G. & Winchester. J.A. 1982. A geochemical comparison of the Dalradian Leven Schists and the Grampian Division Monadhliath Schists of Scotland. *Journal of the Geological Society* **139**, p. 71–84.
- Larsen, E. & Mangerud, J. 1981. Erosion rate of a Younger Dryas cirque glacier at Kråkenes, western Norway. *Annals of Glaciology* **2**, 153–158.
- Lauritzen, S.-E. & Onac, B.P., 1995. Uranium series dating of some Speleothems from Romania. *Theoretical and Applied Karstology* **8**, 25–36.
- Lehmann, P.W. 1885. Die Südkarpathen zwischen Retjezat und Königstein, *Zeitschr. d. Geseellschaft f. Erdkunde Berlin*, t. XX, p. 325–336, 346–364.
- Lehmann, P.W. 1891. Der ehemalige Gletscher des Lalatales im Rodnaergebirge, *Petermanns Mitteilungen*, t. XXXVII, pp. 98–99.
- Lericolais, G., Popescu, I., Guichard, F., Popescu, S.M. & Manolakakis, L. 2007. Water-level fluctuations in the Black Sea since the Last Glacial Maximum, V. Yanko-Hombach, A.S. Gilbert, N. Panin, P.M. Dolukhanov (Editors), *The Black Sea Flood Question: Changes in Coastline, Climate, and Human Settlement*, pp. 437–452.
- Li, J.L., Waliser, D.E., Jiang, J.H., Wu, D.L., Read, W., Waters, J.W., Tompkins, A.M., Donner, L.J., Chern, J.D., Tao, W.K., Atlas, R., Gu, Y., Liou, K.N., Genio, A. Del, Khairoutdinov, M. and Gettelman, A. 2005. Comparisons of EOS MLS cloud ice measurements with ECMWF analyses and GCM simulations Initial results. *Geophys. Res. Lett.* **32**, L18710.
- Lifton, N. 2008. In situ cosmogenic C-14 from surfaces at secular equilibrium, *Geochim. Cosmochim. Acta* **72** A552.
- Lifton, N., Bieber, J.W., Clem, J. M., Duldig, M. L., Evenson, P., Humble, J.E. and Pyle, R., 2005. Addressing solar modulation and long-term uncertainties in scaling secondary cosmic rays for in situ cosmogenic nuclide applications, *Earth Planet. Sci. Lett.* **239** 140–161.
- Lifton, N., Bieber, J.W., Clem, J.M., Duldig, M.L., Evenson, P., Humble, J.E. & Pyle, R., 2005. Addressing solar modulation and long-term uncertainties in scaling secondary cosmic rays for in situ cosmogenic nuclide applications. *Earth Planet. Sci. Lett.* **239** 140–161.
- Lindner L., Dzierżek J., Nitychoruk, J. 1990. Question of the age and glaciers limit during the Last Glaciation (Vistulian) in the Polish Tatra Mts (in Polish with English summary). *Geol. Quart.* **34**, 2, 339–354.
- Lindner L., Dzierżek J., Marciniak B., Nitychoruk J. 2003. Outline of Quaternary glaciations in the Tatra Mts.: their development, age and limits. *Geol. Quart.* **47**, 3, 269–280. Warszawa.

- Lohne, Ø., Bondevik, S., Mangerud, J., Svendsen, J.I. 2007. Sea-level fluctuations imply that the Younger Dryas ice-sheet expansion in western Norway commenced during the Allerød. *Quaternary Science Reviews* **26**, 2128–2151.
- Lotter, A.F., Ammann, B., Beer, J., Hajdas I. and Sturm, M. 1992. A step towards an absolute time-scale for The Late-Glacial: Annually laminated sediments from Soppensee (Switzerland). In Bard, E. and Broecker, W. S., eds., *The Last Deglaciation. Absolute and Radiocarbon Chronologies*. NATO ASI Series I. Berlin, Springer-Verlag, 45-68.
- Lowe, J.J. and Walker, M.J.C. 1976. *Nature* **264**, 632–633.
- Lowe, J.J., Rasmussen, S.O., Björk, S., Hoek, W.J., Steffensen, J.P., Walker, M.J.C., Yu, Z.C., INTIMATE Group. 2008. Synchronisation of palaeoenvironmental events in the North Atlantic region during the Last Termination: a revised protocol recommended by the INTIMATE group. *Quaternary Science Reviews* **27**, 6–17.
- Lukas, S. and Benn, D.I. 2006. Retreat Dynamics of YD Glaciers in the far NW Scottish Highlands Reconstructed from Moraine Sequences, *Scottish Geographical Journal* **122**, 308 – 325.
- Lukas, S., Bradwell, T., 2010. Reconstruction of a lateglacial (Younger Dryas) mountain ice field in Sutherland, NW Scotland, and its palaeoclimatic implications. *Journal of Quaternary Science* **25**, 567-580.
- Lundqvist, J. 1986. Stratigraphy of the central area of the Scandinavian glaciation. *Quaternary Sciences Reviews*, **5**, 251-268.
- Major, C.O., Goldstein, S.L., Ryan, W.B.F., Lericolais, G., Piotrowski, A.M., Hajdas, I., 2006. The co-evolution of Black Sea level and composition through the last deglaciation and its paleoclimatic significance. *Quaternary Science Reviews* **25**, 2031–2047.
- Manley, G. 1959. The Late-glacial climate of N.W. England. *Liverpool Manchester Geol. J.* **3**, 185– 217.
- Mangerud, J., 1991. The Scandinavian ice sheet through the last interglacial/glacial cycle. In: Frenzel, B. ed., *Klimageschichtliche Probleme der letzten 130, 000 Jahre*. Stuttgart/New York, G. Fischer, 307-330.
- Mangerud, J. 2004. Ice sheet limits on Norway and the Norwegian continental shelf. In Ehlers, J. & Gibbard, P. (eds.): *Quaternary Glaciations - Extent and Chronology*, pp 271-294, Vol. **1** Europe, Elsevier, Amsterdam.
- Mangerud, J., Gosse, J., Matiouchkov, A. & Dolvik, T. 2008. Glaciers in the Polar Urals, Russia, were not much larger during the Last Global Glacial Maximum than today. *Quaternary Science Reviews* **27**, 1047-1057.
- Marjanac, L. and Marjanac, T., 2004. Glacial history of the Croatian Adriatic and Coastal Dinarides. In: J. Ehlers and P.L. Gibbard (eds.), *Quaternary Glaciations – Extent and Chronology. Part I: Europe*. Elsevier, Amsterdam, pp. 19-26.
- Marks, L., 2002. Last Glacial Maximum in Poland. *Quaternary Science Reviews* **21**, 103–110.
- Marks, L., 2010. Timing of the Late Vistulian (Weichselian) glacial phases in Poland, *Quaternary Science Reviews*, 1-8, doi:10.1016/j.quascirev.2010.08.008.
- Martonne, Emm. de. 1924. Excursion géographiques de l'Insti tut de Géographie de l'Université de Cluj en 1921. Résultats scientifiques, Lucr. Inst. de Geogr. al Univ. din Cluj, vol. I, pp. 43-211.
- Masarik, J., Reedy, R.C., 1995. Terrestrial cosmogenic-nuclide production systematics calculated from numerical simulations. *Earth and Planetary Science Letters* **136**, 381-395.
- Masarik, J., Frank, M., Schäfer, J.M. and Wieler, R., 2001. 800 kyr calibration of in-situ cosmogenic nuclide production for geomagnetic field intensity variations, *Geochim. Cosmochim. Acta* **65**, 2995–3003.
- Masarik, J. & R. Wieler, R. 2003. Production rates of cosmogenic nuclides in boulders. *Earth and Planetary Science Letters* **216**, pp. 201–208.
- Mândrescu, M., Evans, I.S. and Cox, N.J. 2010. Climatic implications of cirque distribution in the Romanian Carpathians: palaeowind directions during glacial periods. *J. Quaternary Science* **24**, 0, pp 1–14.
- McDougall, D. A. 2001. The geomorphological impact of Loch Lomond (Younger Dryas) Stadial plateau icefields in the central Lake District, northwest England. *Journal of Quaternary Science* **16**, 531–543.
- Mercier, J.-L. & Jeser, N. 2004. The glacial history of the Vosges Mountains. In: Ehlers, J., Gibbard, P.L. P.L. (Eds.), *Quaternary Glaciations, Extent and Chronology, P. I: Europe*. Elsevier, Amsterdam. 113-118.
- Merritt, J.W. 1998. The Quaternary geology of the Dalwhinnie District. *BGS technical report WA/99/14R* Met Office. 2009. UK overview. www.metoffice.gov.uk
- Met Office. 2011. National Meteorological Library and Archive. Fact sheet No. 4 – Climate of the UK.
- Mikolajewicz, U. 2011. Modeling Mediterranean Ocean climate of the Last Glacial Maximum. *Climate of the Past* **7**, 161–180.
- Milivojević, M., Menković, L., and Čalić, J., 2008. Pleistocene glacial relief of the central part of Mt. Prokletije (Albanian Alps). *Quaternary International* **190**, 112-122.
- Mitchell, W.A. 1996. Significance of snowblowing in the generation of Loch Lomond Stadial (Younger Dryas) glaciers in the Western Pennines, northern England. *Journal of Quaternary Science* **11**, 233-248.
- Mitchell W.A. and Merritt J.W. 2004. The glacial geomorphology of the Upper Garry and northern side of Loch Rannoch. In *The Quaternary of the Central Grampian Highlands: Field Guide*, Lukas S, Merritt, J. W., Mitchell WA (eds). *Quaternary Research Association*, London, 190-199.
- Morariu, T. 1940. Contribuțiuni la glaciațiunea din Munții Rodnei. *Rev. geografică română*, an. III, fasc I,

- pp. 60-72.
- Morariu, T. 1981. Le relief glaciaire des Carpates Orientales de Roumanie, Rech. *Géographique a Strasbourg*, nr. 16-17, pp. 67-69.
- Mudie, P.J., Rochon, A., Aksu, A.E., Gillespie, H., 2002. Dinoflagellate cysts, freshwater algae and fungal spores as salinity indicators in Late Quaternary cores from Marmara and Black seas. *Mar. Geol.* **190**, 203–231.
- Munteanu-Murgoci, G. 1898. Les Serpentes d'Urde, Muntiu, et Găuri, Annal. Mus. Géol., Bucharest, t. LXVIII, vol. II, pp. 54-185.
- Nesje, A., Lie, Ø. and Dahl, S. O. 2000. Is the North Atlantic Oscillation reflected in Scandinavian glacier mass balance records? *J. Quaternary Sci.* **15**, pp. 587–601.
- Niederman, S. 2002. Cosmic-ray-produced noble gases in terrestrial rocks: Dating tools for surface processes. In: Porcelli, D., Ballantine, C., Wieler, R. (Eds.). Noble Gases in Geochemistry and Cosmochemistry. *Mineral. Soc. of Amer.* **47**, 731–784.
- Nishiizumi, K., Winterer, E. L., Kohl, C. P., Lal, D., Arnold, J. R., Klein, J. and Middleton, R. 1989. Cosmic ray production rates of ^{10}Be and ^{26}Al in quartz from glacially polished rocks. *J. Geophys. Research* **94**, 17907-17915.
- Nishiizumi, K., Finkel, R.C., Klein, J., Kohl, C.P., 1996. Cosmogenic production of ^7Be and ^{10}Be in water targets. *Journal of Geophysical Research* **101**, 22,225-22,232.
- Nishiizumi, K., Imamura, M., Caffee, M. W., Southon, J. R., Finkel, R. C., & McAninch, J. 2007. Absolute calibration of ^{10}Be AMS standards. *Nuclear Instruments and Methods in Physics Research Section B: Beam Interactions with Materials and Atoms* **258**, 403-413.
- Oerlemans, J. 2005. Extracting a Climate Signal from 169 Glacier Records. *Science* **308**, 5722: 675- 677.
- Onac, B.P., Lauritzen, S.E. 1996. The climate of the last 150,000 years recorded in Speleothems: Preliminary results from North-Western Romania. *Theoretical and Applied Karstology* **9**, 9–21.
- Ono, Y., Shulmeister, J., Lehmkuhl, F., Asahi, K., Aoki, T., 2004. Timings and causes of glacial advances across the PEP-II transect (East-Asia to Antarctica) during the last glaciation cycle. *Quaternary International* **118–119**, 55–68.
- Ono, Y., Aoki, T., Hasegawa, H., Dali, L. 2005. Mountain glaciation in Japan and Taiwan at the global Last Glacial Maximum. *Quaternary International* **138–139**, 79–92.
- Osmaston, H. 2005. Estimates of glacier equilibrium line altitudes by the Area x Altitude, the Area x Altitude Balance Ratio and the Area x Altitude Balance Index methods and their validation. *Quaternary International* **22**, 31, pp 138–139.
- Paneth, F. A. , Reasbeck, P. & Mayne, K. I. 1952. *Geochim. et Cosmochim. Acta*, **2**, 300.
- Parcul Național Munții Rodnei (PNMR), (2006), *Planul de management al Parcului National Muntii Rodnei Rezervatie a Biosferei*. Inclusiv habitatul refăcut prin Proiectul LIFE-Natura.
- Payne, A. and Sugden, D.E. 1990. Topography and Ice Sheet Growth. *Earth Surface Processes and Landforms* **15**, 625-639.
- Pawłowski, St. 1936. Les Karpates á l'époque glaciaire, C.R. Congr. Intern. Géogr., Varsovie (1934), Travaux de la section II, vol. II, pp.89-141.
- Peacock, J.D. 1970. Glacial geology of the Lochy–Spean area. *Bull. geol. Surv. Gt. Br* **31**, 185–98.
- Peach, B.N. & Horne, J. 1930. Chapter on the geology of Scotland. Oxford University Press, London, p. 232.
- Peltier, W.R. and Fairbanks, R.G., 2006. Global glacial ice volume and Last Glacial Maximum duration from an extended Barbados sea level record. *Quaternary Science Reviews*, **25**, 3322-3337.
- Peltier, W.R., Vettoretti, G., & Stastna, M. 2006. Atlantic meridional overturning and climate response to Arctic Ocean freshening: *Geophysical Research Letters* **33**, doi:10.1029/2005GL025251.
- Penaud, A., Eynaud, F., Turon, J. L., Zaragosi, S., Malaizé, B., Toucanne, S., and Bourillet, J. F. 2009. What forced the collapse of European ice sheets during the last two glacial periods (150 ka B.P. and 18 ka cal B.P.). Palynological evidence, *Palaeogeogr. Palaeocl.* **281**, 66–78.
- Petculescu, A. & Samson, P.M., 2001. Aspecte climatice ale ultimului ciclu glaciari, bazate pe asociațiile de micromamifere din carstul Dobrogei Centrale. *EcoCarst* p 2.
- Peyron, O., Guiot, J., Cheddadi, R., Tarasov, P., Reille, M., de Beaulieu, Bottema, S., and Andrieu, V. 1998. Climatic reconstruction in Europe for 18 000 yr B.P. from pollen data, *Quaternary Res.* **49**, 183–196.
- Phillips W.M., Hall A.M., Mottram R., Fifield L.K., Sugden D.E. 2006. Cosmogenic ^{10}Be and ^{26}Al exposure ages of tors and erratics, Cairngorm Mountains, Scotland: Timescales for the development of a classic landscape of selective linear glacial erosion, *Geomorphology* **73**, 222– 245.
- Pigati, J.S., and Lifton, N.A., 2004, Geomagnetic effects on time-integrated cosmogenic nuclide production with emphasis on in-situ ^{14}C and ^{10}Be . *Earth and Planetary Science Letters* **226**, 193-205.
- Pinot, S., Ramstein, G., Harrison, S.P., Prentice, I.C., Guiot, J., Stute, M., Joussaume, S. & PMIP-participating-groups. 1999. Tropical paleoclimates at the Last Glacial Maximum: comparison of Paleoclimate Modeling Intercomparison Project (PMIP) simulations and paleodata". *Climate Dynamics* **15**, 11: 857–874.
- Porter, S.C. 1975. Equilibrium line altitudes of late Quaternary glaciers in the Southern Alps, New Zealand. *Quaternary Research* **5**: 27-47.
- Porter, S. 2001. Snowline depression in the tropics during the Last Glaciation. *Quaternary Science Reviews*

- 20, 1067–1091.
- Prentice, I.C., Cramer, W., Harrison, S.P., Leemans, R., Monserud, R.A., Solomon, A.M. 1992. A global biome model based on plant physiology and dominance, soil properties and climate. *J Biogeogr* **19**, 117–134.
- Punkari, M., 1984. The relations between glacial dynamics and tills in the eastern part of the Baltic Shield *Striae* **20**, 49–54.
- Punkari, M. & Forsström, L. 1995. Glacial flow systems in the zone of confluence between the Scandinavian and Novaya Zemlya ice sheets, *Quaternary Science Reviews* Vol. **14**, pp. 5894XT3, 1995.
- Purves, S.R., Mackaness, W.A. and Sugden, D.E., 1999. An approach to modelling the impact of snow drift on glaciation in the Cairngorm Mountains, Scotland. *Journal of Quaternary Science* **14**, 4, 313–321.
- Putnam, A.E., Schaefer, J., Barrell, D.J.A., Vendergoes, M., Denton, G.H., Kaplan, M.R., Finkel, R.C., Schwartz, R., Goehring, B., Kelley, S.E., 2010. In situ cosmogenic ¹⁰Be production-rate calibration from the 728 Southern Alps, New Zealand. *Quaternary Geochronology* **5**, pp. 392–409.
- Raab, T., Völkel, J. 2003. Late Pleistocene glaciation of the Kleiner Arbersee area in the Bavarian Forest, south Germany. *Quaternary Science Reviews* **22**, 581–593.
- Rahmstorf, S. 2003. Thermohaline circulation: The current climate. *Nature* **421**, 699.
- Rasmussen, S.O., Andersen, K.K., Svensson, A.M., Steffensen, J.P., Vinther, B.M., Clausen, H.B., Siggaard-Andersen, M.-L., Johnsen, S.J., Larsen, L.B., Dahl-Jensen, D., Bigler, M., Rothlisberger, R., Fischer, H., Goto-Azuma, K., Hansson, M.E., and Ruth, U. 2006. A new Greenland ice core chronology for the last glacial termination, *J. Geophys. Res.*, 111, D06102.
- Raven, J.A. & Edwards, D. 2001. Roots: evolutionary origins and biogeochemical significance. *J. Exp. Bot.* **52**, 381.
- Rădulescu, C., Samson, P.M., 1992. Chronologie et paléoclimatologie de trois grottes des Carpates Orientales (Roumanie) d'après les mammifères. 1 Micrommifères. *Travaux d'Institute de Spéologie Émile Racovița* **31**, 95–104.
- Reichert, B. K., Bengtsson, L. & Oerlemans, J. 2001. Mid-latitude forcing mechanisms for glacier mass balance investigated using general circulation models *J. Climate* **14**, 3767–3784.
- Reitner, J. 2007. Glacial dynamics at the beginning of Termination I in the Eastern Alps and their stratigraphic implications. *Quaternary International* **164–165**, 64–84.
- Renssen, H., Goosse, H., Fichefet, T., Campin, J.-M. 2001. The 8.2 kyr BP event simulated by a global atmosphere–sea-ice–ocean model. *Geophys Res Lett* **28**, 567–570.
- Reuther, A.U., Urdea, P., Geiger, C., Ivy-Ochs, S., Niller, H.P., Kubik, P.W., Heine, K. 2007. Late Pleistocene glacial chronology of the Pietrele Valley, Retezat Mountains, Southern Carpathians constrained by ¹⁰Be exposure ages and pedological investigations. *Quaternary International*, 164–165, pp. 151–169.
- Rinterknecht, V., Matoshko, A., Gorokhovich, Y., Fabel, D., Xu, S. Submitted. Expression of the Younger Dryas cold event in the Carpathian Mountains, Ukraine.
- Rinterknecht, V.R., Clark, P.U., Raisbeck, G.M., Yiou, F., Bitinas, A., Brook, E.J., Marks, L., Zelcs, V., Lunkka, J.-P., Pavlovskaya, I.E., Piotrowski, J.A., Raukas, A., 2006. The last deglaciation of the southeastern sector of Scandinavian ice sheet. *Science* **311**, 1449–1452.
- Rinterknecht, V.R., Marks, L., Piotrowski, J.A., Raisbeck, G.M., Yiou, F., Brook, E.J., Clark, P.U. 2005. Cosmogenic ¹⁰Be ages on the Pomeranian moraine, Poland. *Boreas* **34**, 186–191.
- Rinterknecht, V.R., Pavlovskaya, I.E., Clark, P.U., Raisbeck, G.M., Yiou, F., Brook, E.J. 2007. Timing of the last deglaciation in Belarus. *Boreas* **36**, 307–313.
- Rinterknecht, V.R., Bitinas, A., Clark, P.U., Raisbeck, G.M., Yiou, F., Brook, E.J. 2008. Timing of the last deglaciation in Lithuania. *Boreas* **37**, 426–433.
- Rohling, E.J., Hayes, A., Rijk, D., Kroon, D., Zachariasse, W.J. & Eisma, D. 1998. Abrupt cold spells in the northwest Mediterranean. *Paleoceanography* **13**, 316–322.
- Rohling, E.J., Mayewski, P.A. and Challenor, P. 2003. On the timing and mechanism of millennial-scale climate variability during the last glacial cycle. *Climate Dynamics* **20**, 2–3, 257–267.
- Romer, E. Epoka lodowa na Swidowcu., *Rozprawy Ak. Um., Krakow.*, A 46 6 (1906), pp. 11–80 Seria III.
- Ruddiman, W.F. 2001. *Earth's Climate: Past and Future*. W. H. Freeman and Sons, New York.
- Ruddiman, W.F., & McIntyre, A. 1981. The North Atlantic during the last deglaciation. *Palaeogeography, Palaeoclimatology, Palaeoecology*, **35**, 145–214.
- Ryan, W.B.F., Pitman, W.C., Major, C.O., Shimkus, K., Moskalenko, V., Jones, G., Dimitrov, P., Gorur, N., Sakinc, M. & Yuce, H. 1997. An abrupt drowning of the Black Sea shelf. *Marine Geology* **138**, 119–126.
- Ryan, W.B.F., Major, C.O., Lericolais, G., Goldstein, S.L., 2003. Catastrophic flooding of the Black Sea. *Annual Reviews of Earth and Planetary Sciences* **31**, 525–554.
- Sarıkaya MA, Zreda M, Çiner A, Zweck C. 2008. Cold and wet Last Glacial Maximum on Mount Sandras, SW Turkey, inferred from cosmogenic dating and glacier modelling. *Quaternary Science Reviews* **27**, 769–780.
- Sánchez, M.J., Arquer, P.F. 2002. New radiometric and geomorphologic evidences of a last glacial maximum older than 18 ka in SW European mountains: the example of Redes Natural Park (Cantabrian Mountains, NW Spain). *Geodinamica Acta* **15**, 93–101.

- Sârcu, I. 1963. Le probleme de la glaciation quaternaire dans les montagnes du Maramureş, Anal. şt. Univ. „Al. I. Cuza” Iaşi, (Serie nouă), sect. II (Şt. nat.) b. Geologie-Geografie, t. IX, pp. 125-134.
- Sârcu, I. 1978. Munţii Rodnei. Studiu morfogeografic, *Ed. Academiei*, Bucureşti, 112.
- Sawicki, L. 1909. A Biharhegység eljegesedésének kérdéséhez, *Földrajzi Közle- mények*, t. XXXVII, nr. 10, pp. 316-325.
- Sawicki, L. 1911. Die glazialen Züge der Rodnaer Alpen und der Marmaroscher Karpaten, *Mitt. d. k. k. Geogr. Gesellschaft in Wien*, t. X-XI, pp. 510-571.
- Sawicki, L. 1912. Les etudes glaciaire dans les Karpates. Aperçu historique et critique, *Ann. de Geographie*, Paris, vol. **XXI**, p. 230-250.
- Sârcu, I. 1978. Munţii Rodnei. Studiu morfogeografic, *Ed. Academiei*, Bucureşti, p. 112.
- Seret, G., Guiot, J., Wansard, G., de Beaulieu, J.L., & Reille, M. 1992. Tentative palaeoclimatic reconstruction linking pollen and sedimentology in La Grande Pile (Vosges, France). *Quaternary Science Reviews* **11**, 425–430.
- Schaefer, J.M., & Lifton, N. 2007. Cosmogenic nuclide dating; methods. In *Encyclopedia of Quaternary Science*. Edited by S.A. Elias. Elsevier, Amsterdam, Netherlands..pp. 412-419.
- Sheinkman, V.S. & Barashkova, N.K. 1991. The Pleistocene glaciation of Siberian mountains and atmospheric circulation. In: *Glaciers-Ocean-Atmosphere Interactions* (Proceedings of the International Symposium held at St Petersburg, September 1990). IAHS Publ. no. 208, 1991.
- Siegert, M.J., Dowdeswell, J.A., Hald, M. & Svendsen, J.I.. 2001a. Modelling the Eurasian ice sheet through a full (Weichselian) glacial cycle. *Global and Planetary Change* **31**, 367-385.
- Siegert, M.J. & Marsiat, I., 2001b. "Numerical modelling of LGM climate in the Eurasian High Arctic". *Quaternary Science Reviews* **20**, 15, 1595-1605.
- Sissons, J.B. 1967. The evolution of Scotland's scenery. *Oliver and Boyd*, Edinburgh.
- Sissons, J.B. 1973. A Late-glacial ice cap in the central Grampians, Scotland. *Transactions of the Institute of British Geographers* **62**, 95-114
- Sissons, J.B. 1974. The Quaternary in Scotland: a review. *Scottish Journal of Geology* **10**, 311-337.
- Sissons, J. B. and Sutherland, D.G. 1976. Climatic inferences from former glaciers in the south-east Grampian Highlands, *Scotland. J. Glaciol.* **17**, 325 346.
- Sissons, J.B. 1978. The parallel roads of Glen Roy and adjacent glens, Scotland. *Boreas*, Vol. **7**, pp. 229-244.
- Sissons, J.B. 1979a. Palaeoclimatic inferences from former glaciers in Scotland and the Lake District. *Nature* **278**, 518-521.
- Sissons, J.B. 1979b. The Loch Lomond Stadial in the British Isles. *Nature* **280**, 199-203.
- Sissons J.B. 1980. The Loch Lomond Advance in the Lake District, northern England. *Transactions of the Royal Society of Edinburgh: Earth Sciences* **71**, 13–27.
- Sissons, J.B., Walker, M.J.C. 1974. Lateglacial site in the Central Grampian Highlands. *Nature* **249**, 822-824.
- Stone J.O., Ballantyne C.K., Fifield K.L. 1998. Exposure dating and validation of periglacial weathering limits, northwest Scotland. *Geology* **26**, 587–590.
- Stone, J.O. 2000. Air pressure and cosmogenic isotope production. *Journal of geophysical research* **105**, No. B10, pages 23,753-23,759.
- Straus, L.G. 1992. Iberia before the Iberians: the Stoneage Prehistory of Cantabrian Spain, University of New Mexico Press, Albuquerque, USA.
- Sugden, D.E. 1968. The selectivity of glacial erosion in the Cairngorm Mountains, Scotland. *Transactions of the Institute of British Geographers* **45**, 79–92.
- Sugden D.E. 1970. Landforms of deglaciation in the Cairngorm Mountains, Scotland. *Transactions of the Institute of British Geography* **51**, 201-219.
- Svendsen, J., Alexanderson, H., Astakhov, V., Demidov, I., Dowdeswell, J., Funder, S., Gataullin, V., Henriksen, M., Hjort, C., Houmark-Nielsen, M., Hubberten, H., Ingólfson, O., Jakobsson, M., Kjær, K., Larsen, E., Lokrantz, H., Lunkka, J., Lyså, A., Mangerud, J., Matiouchkov, A., Murray, A., Möller, P., Niessen, F., Nikolskaya, O., Polyak, P., Saarnisto, M., Siegert, C., Siegert, M., Spielhagen, R., & Stein, R. 2004. Late Quaternary ice sheet history of Northern Eurasia. *Quaternary Science Reviews* **23**, 1229-1271.
- Sutherland, D. 1984. The Quaternary deposits and landforms of Scotland and the neighbouring shelves. *Quaternary Science Reviews* **3**, 157-234.
- Szadeczky, G. 1905. Bericht über die im Jahre 1905 Bihargebirge vorgenommenenn geologischen Aufnahmen, *Jahresb. d Ung. Geol. Anstalt*, pp. 144-170.
- Szadeczky, G. 1906. Glecsernyomok a Biharhegységben, *Földrajzi Közlemenyek*, t. XXXIV, nr. **8**, pp. 299-304.
- Tarasov, P.E., Peyron, O., Guiot, J., Brewer, S., Volkova, V.S., Bezusko, L.G., Dorofeyuk, N.I., Kvavadze, E.V., Osipova, I.M., Panova, N.K. 1999. Last Glacial Maximum climate of the former Soviet Union and Mongolia reconstructed from pollen and macrofossil data. *Climate Dynamics* **15**, 227–240.
- Tămaş, T., Causse, C. 2000/2001. U-Th TIMS chronology of two stalagmites from V11 Cave, Bihor Mountains, Romania. *Theoretical and Applied Karstology* **13** and **14**, 25–32.
- Tămaş, T., Onac, B.P. & Bojar, A.V. 2005. Lateglacial-Middle Holocene stable isotope records in two coeval stalagmites from the Bihor Mountains, NW Romania. *Geological Quarterly* **49**, 2, 185–194.

- Terhürne-Berson, R. 2005. Changing distribution patterns of selected conifers in the Quaternary of Europe caused by climatic variations. Doctoral thesis.
- Thorp, P.W. 1984. Glacial geomorphology of part of the western Grampians with specific reference to the limits of the Loch Lomond Advance. *Unpublished Ph.D thesis*, City of London Polytecnic.
- Thorp, P.W. 1986. A mountain icefield of Loch Lomond Stadial age, western Grampians, Scotland. *Boreas* **15**, 83-97.
- Thorp, P.W. 1987. Late Devensian ice sheet in the western Grampians, Scotland. *Journal of Quaternary Science* **2**, 103–112.
- Timar, A., Vandenberghe, D., Panaiotu, E.C., Panaiotu, C.G., Necula, C., Cosma, C. & van den Haute, P. 2010. Optical dating of Romanian loess using fine-grained quartz. *Quaternary Geochronology* **5**, 2-3, 143-148.
- Trelea, M. 2008. Reconstruction of the YD glaciation in the Monadhliath Mountains. MSc thesis, University of Edinburgh. Edinburgh.
- Tzedakis, P.C. 1999. The last climatic cycle at Kopais, central Greece. *Journal of the Geological Society* **156**, 425–434.
- Tzedakis, P.C. 2010. The MIS 11-MIS 1 analogy, southern European vegetation, atmospheric methane and the 'early anthropogenic hypothesis'. *J. Clim Past* **6**, 2, 131-144.
- Tzedakis, P.C, Lawson, I.T., Frogley, M.R., Hewitt, G.M., Preece, R.C. 2002. Buffered tree population changes in a Quaternary refugium: evolutionary implications. *Science* **297**, 2044–2047.
- Tzedakis, P.C. 2007. Seven ambiguities in the Mediterranean palaeoenvironmental narrative. *Quaternary Science Reviews* **26**, 2042–2066.
- Urdea, P. & Reuther, A.U. 2009. Some new data concerning the Quaternary glaciation in the Romanian Carpathians. *Geographica Pannonica* **13**, Issue 2, 41-52.
- van Husen, D. 1997. LGM and Late Glacial fluctuations in the Eastern Alps. *Quaternary International* Vols **38/39**, pp. 109-118, 1997.
- Walker, M.J.C. 1975. A pollen diagram from the pass of Drumochter, Central Grampians Highlands, Scotland. Volume Eastern Grampian Mountains Site: Loch Etteridge (GCR ID: 2103): *Quaternary of Scotland* Chapter **9**, Geological Conservation Review.
- Whalley, W.B., Gordon, J.E., Gellatly, A.F. and Hansom, J.D. 1995. Plateau and valley glaciers in north Norway: responses to climate over the last 100 years. *Zeitschrift für Gletscherkunde und Glazial geologie* **31**, 115-124.
- Willenbring, J.K., von Blanckenburg, F. 2010. Meteoric cosmogenic Beryllium-10 adsorbed to river sediment and soil: applications for Earth-surface dynamics. *Earth Science Reviews* **98**, 105–122.
- Williams, M., Dunkerley, D., De Deckker, P., Kershaw, P. and Chappell, J. 1998. Quaternary Environments, 2nd Edition, Arnold, London, 1998, 329 pages.
- Willis, K.J. and van Andel, T.H. 2004. Trees or no trees? The environments of central and eastern Europe during the Last Glaciation. *Quaternary Science Reviews* **23**, 2369-2387.
- Wohlfarth B., Hannon G., Feurdean A., Ghergari L., Onac B.P. & Possnert, G. 2001. Reconstruction of climatic and environmental changes in NW Romania during the early part of the last deglaciation (15,000–13,600 cal years BP). *Quaternary Science Reviews* **20**, 1897–1914.
- Wohlfarth, B., Björck, S., Funder, S., Houmark-Nielsen, M., Ingólfsson, O., Lunkka, J.P., Mangerud, J., Saarnisto, M., Vorren, T. Quaternary of Norden. // Episodes. - 2008 (31) : 1, s. 73-81.
- Woodward, J.C., Macklin, M.G., Smith, G.R. 2004. Pleistocene glaciation in the mountains of Greece. In Ehlers, J. & Gibbard, P. (eds.): *Quaternary Glaciations - Extent and Chronology*, pp 271-294, Vol. **1** Europe, Elsevier, Amsterdam.
- Wunsch, C. 2006. Abrupt climate change: An alternative view. *Quaternary Research* **65**, 191-203.
- Yokoyama, Y., Lambeck, K., De Deckker, P., Johnston, P., & Fifield, L.K. 2000. Timing of the Last Glacial Maximum from observed sea-level minima. *Nature* **406**, 713-716.
- Young, J.A.T. 1974. Ice wastage in Glenmore, upper Spey Valley, Inverness-shire. *Scottish Journal of Geology* **10**, 147-157.
- Young, J.A.T. 1978. The Landforms of Upper Strathspey. *Scottish Geographical Magazine* **94**, 76 – 94.
- Zahno C., Akçar N., Yavuz V., Kubik P.W., Schlüchter C. 2010. Chronology of Late Pleistocene glacier variations at the Uludağ Mountain, NW Turkey. *Quaternary Science Reviews* **29**, 1173–1187.
- Zasadni, J. 2009. Critical remarks on reconstruction of surface geometry of glaciers in the Polish High Tatra Mts. *Prz. Geol.* **57**, 7, 607–613.
- Zapalowicz, H. 1886. Geologische Skizze des östlichen Teiles der Pokutisch-Marmaroscher Grenzkarpathen Verhandl. k. k. Geol. Reichsanstalt., XXXVI, pp. 361-594.
- Zhelezov, G. 2010. Sustainable development in mountain regions: Southeastern Europe. Springer Science and Business Media. 291 pages.
- Zreda, M.G., Phillips, F.M., Elmore, D., Kubik, P.W., Sharma, P., Dorn, R.I., 1991. Cosmogenic ³⁶Cl production in terrestrial rocks. *Earth and Planetary Science Letters* **105**, 94-109.